Structure Function and Properties of Copper-containing Proteins: Hemocyanins and Superoxide Dismutase

Struktur, Funktion und Eigenschaften von kupferhaltigen Proteinen: Hämocyanine und Superoxiddismutasen

DISSERTATION

der Fakultät für Chemie und Pharmazie

der Eberhard-Karls-Universität Tübingen

zur Erlangung des Grades eines Doktors

der Naturwissenschaften

2005

vorgelegt von

Aleksandar Dolashki

Tag der mündlichen Prüfung:	01.August 2005
Dekan:	Prof. Dr. Stefan Laufer
1. Berichterstatter:	Prof. Dr. Dr. h. c. mult. W.Voelter
2. Berichterstatter:	Prof. Dr. U. Weser

Die vorliegende Arbeit wurde unter der Anleitung von Herrn Prof. Dr. Dr. h. c. mult. W. Voelter in der Zeit von Februar 2002 bis Dezember 2004 an der Abteilung fur Physikalische Biochemie des Physiologisch-chemischen Institutes der Eberhard Karls-Universität Tübingen angefertigt.

Part of this work was already published:

Dolashka-Angelova, P., Beltramini, M., **Dolashki, A.**, Salvato, B., Hristova, R., Voelter, W. (2001) Carbohydrate composition of *Carcinus aestuarii* hemocyanin. Arch. Bioch. Biophys. 389, 153-158

Dolashka-Angelova, P., Beck, A., **Dolashki, A.**, Beltramini, M., Stevanovic, S., Salvato, B. and Voelter, W. (2003) Characterization of the carbohydrate moieties of the functional unit RvH1-a of *Rapana venosa* haemocyanin using HPLC/electrospray ionization MS and glycosidase digestion. Biochem. J. 374, 185-192.

Dolashka-Angelova, P., Schwarz, H., **Dolashki, A.**, Beltramini, M., Salvato, B., Schick, M., Saeed, M. and Voelter, W. (2003) Characterization of the reassociation and oligomeric stability of *Rapana venosa* hemocyanin (RvH) and its structural subunits. Biochim. Biophys. Acta 1646, 77-85.

Dolashka-Angelova, P., Beck, A., **Dolashki, A.**, Beltramini, M., Stevanovic, S., Salvato, B., Hristova, R., Velkova, L., Voelter, W. (2004) Carbohydrate moieties of molluscan *Rapana venosa* hemocyanin. Micron 35, 101–104.

Dolashka-Angelova, P., Stevanovic, S., **Dolashki, A.**, Angelova, M., Serkedjieva, J., Krumova, E., Pashova, S., Zacharieva, S., and Voelter, W. (2004) Structural and functional analysis of glycosylated Cu/Zn-superoxide dismutase from the fungal strain *Humicola lutea* 103. Biochem. Biophys. Res. Commun. 317, 1006–1016.

Dolashka-Angelova, P., **Dolashki, A.**, Stevanovic, S., Hristova, R., Atanasov, B., Nicolov, P. and Voelter, W. (2005) Structure and stability of arthropodan hemocyanin *Limulus polyphemus*. Accepted in Spectrochim. Acta.

Dolashka-Angelova, P., **Dolashki, A.**, Savvides, S. N., Hristova, R., Beeumen, J. Van, Voelter, W., Devreese, B., Weser, U., Di Muro, P., Salvato, B. and Stevanovic, S., (2005) Structure of hemocyanin subunit CaeSS2 of the crustacean mediterranean crab *Carcinus aestuarii*. Accepted in J. Biochemistry.

Dolashki, A., Stevanovic, S., Hristova R., Atanasov B., Voelter, W. and Dolashka-Angelova P. Conformational stability of arthropodan hemocyanin *Limulus polyphemus.* In preparation.

Velkova, L., **Dolashki, A.**, Schwarz, H., Stevanovic, S., Hristova, R., Voelter, W. and Dolashka-Angelova, P. Structure and oligomeric stability of hemocyanin isolated from the garden snail *Helix vulgaris*. In preparation

Dolashki, A., Hristova R., Rao, G.S., Betzel, C., Atanasov, B., Voelter, W., Stevanovic, S. and Dolashka-Angelova P. Conformational stability of *Humicola lutea* superoxide dismutase. In preparation.

Dedicated to

the moments of encouragements

Acknowledgments

I would like to express my sincere gratitude and appreciation to my supervisor Prof. Dr. Dr. h. c. mult. Wolfgang Voelter for his guidance, continued interest and inspiration throughout the course of this work.

I am most grateful to the DLR and NATO for providing me scholarships for my Ph.D. research.

I am also whole heartily thankful to Prof. Stefan Stefanovic, Prof. Hans-Georg Rammensee (Department of Immunology, Institute for Cell Biology, University of Tübingen, Germany), Prof. Benedetto Salvato (Department of Biology, University of Padua, Italy), Assoc. Prof. Pavlina Dolashka-Angelova, Maria Angelova (Bulgarian Academy of Science, Sofia, Bulgaria), Dr. Heinz Schwarz (Max Planck Institut für Entwicklungsbiologie, Tübingen, Germany), Prof. Josef Van Beeumen and Prof. Bart Devreese (Laboratory of Protein Biochemistry and Protein Engineering, Ghent University, Belgium), Prof. Jurgen Markl (Institute of Zoology, Johannes Gutenberg University Mainz, Germany), and Prof. Heinz Decker (Institute of Molecular Biophysic, Johannes Gutenberg University Mainz, Germany), Prof. Dr. U. Weser (Physiologisch-chemisches Institut der Universität Tubingen) for their support and help to conduct some part of this thesis.

I am indebted to my parents (Dr. Pavlina Dolashka and Konstantin Dolashki, Sofia, Bulgaria) for their love, constant care and encouragement during the course of my research.

I wish to express my thanks to my colleagues and friends especially for providing me a charming company at Tübingen University and for their support and stimulating discussions, Dr. Wieland Stock, Miriam Fecker, Dr. Alexander Beck, Dr. Roland Wacker, Dr. Syed Tasadaque, Dr. Muhammad Saeed, Dr. Rumyana Hristova and Dr. Ludmila Velkova.

Contents

1. Introduction 1

1.1 Metalloproteins (Copper-containing proteins: Hemocyanins and SODs) 1
1.1.1 Oxygen-transporting proteins 1
1.1.2 Hemocyanins 2
1.1.2.1 Occurrence of hemocyanins 2
1.1.2.2 Active site of hemocyanins 2
1.1.2.3 Evolution of different cooper centres in arthropodan and molluscan hemocyanins and their relationship to tyrosinases 5
1.1.2.4 Arthropodan hemocyanins 6
1.1.2.4.1 Origin and structure of arthropodan hemocyanins 6
1.1.2.4.2 Formation of arthropodan hemocyanin multimers 8
1.1.2.4.3 Evolution of arthropodan hemocyanins 9
1.1.2.4.4 Hemocyanin subunit diversity in Chelicerata species 11
1.1.2.4.5 The hemocyanins of the Myriapoda species 12
1.1.2.4.6 Hemocyanin evolution in Crustacea species 13
1.1.2.5 Molluscan hemocyanins 14
1.1.2.5.1 Classes of molluscs 14
1.1.2.5.2 Evolution of molluscan hemocyanins as deduced from DNA sequencing 16
1.1.2.5.3 Model building of a molluscan hemocyanin from X-ray solution scattering 19
1.1.2.6 Studies of structure of hemocyanins by three-dimensional transmission electron microscopy 20
1.1.2.7 Electron microscopy studies of hemocyanins 22
1.1.2.8 Glycosilation of hemocyanins 23
1.1.3 Superoxide dismutases (SODs) 25
1.1.3.1 Manganese superoxide dismutase (Mn-SOD) 27
1.1.3.2 Copper, zinc superoxide dismutase (Cu/Zn-SOD) 28
1.1.3.3 Extracellular superoxide dismutase (EC-SOD) 30
1.1.3.4 Nickel superoxide dismutase (Ni-SOD) 31
1.2 Objects of our investigation 31
1.2.1 Marine snail *Rapana venosa* 31
1.2.2 Garden snail *Helix vulgaris* 32
1.2.3 Green crab *Carcinus aestuarii* 33
1.2.4 Horseshoe crab *Limulus polyphemus* 33
1.3 Methods and techniques 34
1.3.1 Matrix-assisted laser desorption/ionisation (MALDI) mass spectrometry 34
1.3.2 Sequence analysis. Edman degradation 37
1.3.3 Circular dichroism spectroscopy 38
1.3.3.1 Circular dichroism data analysis 41
1.3.4 Fluorescence spectroscopy 43
1.3.4.1 Excitation and fluorescence emission spectra 44

2. Aim of this study 47

3. Materials and Methods 48

3.1 Materials 48

3.1.1 Chemicals 48
3.1.2 Enzymes and proteins 49
3.1.3 Tests, kits and other materials 51
3.1.4 Equipment 51
3.1.4.1 Chromatography columns 51
3.1.4.2 HPLC/FPLC 52
3.1.4.3 Lyophylisation 52
3.1.4.4 Matrix-assisted laser desorption/ionization (MALDI) mass spectrometry 52
3.1.4.5 Sequence analysis 52
3.1.4.6 Circular dichroism 53
3.1.4.7 UV-spectroscopy 53
3.1.4.8 Fluorescence spectroscopy 53
3.1.4.9 Electron microscopy 53
3.2 Methods 53
3.2.1 Preparation of *Rapana venosa* hemocyanin and its structural subunits 53
3.2.2 PAGE and SDS polyacrylamide gel electrophoresis 54
3.2.3 Amino acid sequence of RvH1 and RvH2 54
3.2.4 Dissociation-reassociation of the hemocyanin subunits RvH1 and RvH2 54
3.2.5 Electron microscopy (EM) 55
3.2.6 Isolation of functional unit RvH1-a from the structural subunit RvH1 of *Rapana venosa* hemocyanin 55
3.2.7 Preparation of copper-free hemocyanin from functional unit RvH1-a 56
3.2.8 Carbohydrate determination and protein digestion of functional unit RvH1-a 56
3.2.9 Glycoprotein/peptide-staining of functional unit RvH1-a on silica-gel plates 57
3.2.10 Amino acid sequence analysis of functional unit RvH1-a 57
3.2.11 Enzymatic digestions of glycopeptides 1 and 2 of functional unit RvH1-a and glycopeptide 3 of functional unit RvH1-f 57
3.2.12 MALDI-MS analysis of glycopeptides 1 and 2 of functional unit RvH1-a and glycopeptide 3 of functional unit RvH1-f 58
3.2.13 Electrospray ionization mass spectrometry on glycopeptides 1 and 2 of functional unit RvH1-a and glycopeptide 3 of functional unit RvH1-f 58
3.2.14 Capillary electrophoresis on glycopeptides 1 and 2 of functional unit RvH1-a and glycopeptide 3 of functional unit RvH1-f 58
3.2.15 Isolation of *Carcinus aestuarii* Hc and its structural subunit 2 (CaeSS2) 59
3.2.16 Modification of CaeSS2 by reduction and S-pyridylethylation 59
3.2.17 Enzymatic hydrolysis of CaeSS2 structural subunit 60
3.2.18 Mass spectroscopic analysis of glycopeptides 61
3.2.19 Amino acid sequence determination of glycopeptides 61
3.2.20 Fluorescence spectroscopy of glycopeptides 61
3.2.21 Purification of the native proteins and the structural subunits 62
3.2.22 UV spectroscopy of arthropodan hemocyanin *Limulus polyphemus* (LpH) 62
3.2.23 Fluorescence spectroscopy of arthropodan hemocyanin *L. polyphemus* 63
3.2.23.1 pH stability of arthropodan hemocyanin *Limulus polyphemus* 64
3.2.23.2 Denaturation in Gdn.HCl water solutions of arthropodan LpH 64
3.2.23.3 Quenching of the tryptophan emission of arthropodan LpH 64
3.2.24 CD spectroscopy of arthropodan hemocyanin *Limulus polyphemus* 65
3.2.24.1 Temperature and pH stability of arthropodan Hc *Limulus polyphemus* 65
3.2.24.2 Denaturation by guanidinium hydrochloride (Gdn.HCl) of arthropodan hemocyanin *Limulus polyphemus* 65
3.2.25 Preparation and analysis of glycopeptides of *Carcinus aestuarii* hemocyanin 66
3.2.25.1 Enzymatic digestion of CaeSS2 66
3.2.25.2 Automated amino acid sequence analysis of CaeSS2 67

3.2.25.3 Treatment of glycopeptides with α-N-acetylgalactosaminidase and Peptide N Glycosidase F (PNGase-F) 67
3.2.26 Culture conditions of fungal strain *Humicola lutea* 103 68
3.2.27 Analytical methods for measurement the activity of superoxide dismutase 69
3.2.28 SOD antibodies against *Humicola lutea* Cu/Zn-superoxide dismutase 69
3.2.29 Western-blotting analysis of *Humicola lutea* Cu/Zn-superoxide dismutase 70
3.2.30 Measurement of protein carbonyl content 70
3.2.31 Purification of *Humicola lutea* Cu/Zn-superoxide dismutase 70
3.2.32 Pyridylethylation of *Humicola lutea* Cu/Zn-superoxide dismutase 71
3.2.33 Enzymatic digestions of *Humicola lutea* Cu/Zn-superoxide dismutase 71
3.2.34 Mass spectrometric analysis of *H*. *lutea* Cu/Zn-superoxide dismutase 72
3.2.35 Amino acid sequence determination of *Humicola lutea* Cu/Zn-SOD 73
3.2.36 Glycoprotein/peptide staining of *H. lutea* Cu/Zn-superoxide dismutase on a silica-gel plates 73
3.2.37 Enzymatic deglycosylation of *Humicola lutea* Cu/Zn-superoxide dismutase 73
3.2.38 Dithiothreitol (DTT) titration of *Humicola lutea* Cu/Zn-superoxide dismutase 73
3.2.39 Effect of glycosylated and non-glycosylated SODs on influenza-induced pneumonitis in mice 74
3.2.40 Ethical aspects 74
3.2.41 Virus infection and effect of glycosylated and non-glycosylated SODs 74
3.2.42 Experimental design to study the effect of glycosylated and non-glycosylated SOD in influenza-induced pneumonitis 75

4. Results and Discussion 76

4.1 Isolation, structure and investigation on selected hemocyanins 76
4.1.1 Oligomeric stability of *Rapana venosa* hemocyanin (RvH) and its structural subunits 76
4.1.1.1 Isolation of *Rapana venosa* molluscan hemocyanins and separation of structural subunits 76
4.1.1.2 Gallery of electron micrographs of native, dissociated and reassociated *Rapana venosa* hemocyanin 77
4.1.1.3 Gallery of electron micrographs of the oligomerization dynamics of structural subunit RvH1 80
4.1.1.4 Studies on the stability of RvH1 multidecamers and tubules at different pH values 82
4.1.1.5 Gallery of electron micrographs on the oligomerization dynamics of structural subunit RvH2 83
4.1.1.6 Studies on the stability of RvH2 multidecamers and tubules at different pH values 85
4.1.1.7 Fluorescence intensity at 600 nm of purified RvH1 and RvH2 didecamers in stabilizing buffer 86
4.1.2 Oligomeric stability of *Helix vulgaris* hemocyanin (HvH) 86
4.1.3 Isolation of functional units of the structural subunits RvH1 and RvH2 and N-terminal sequence determination after depolymerisation with $ZnCl_2$ and proteolytic enzymes 87
4.1.4 Characterization of the carbohydrate moieties of *Rapana venosa* hemocyanin using HPLC/electrospray ionization mass spectrometry and glycosidase digestions 89
4.1.4.1 Isolation of glycopeptides from the functional unit RvH1-a 89
4.1.4.2 Sequencing of glycopeptides from the functional unit RvH1-a 91

4.1.4.3 Composition of the carbohydrate portion of glycopeptide 1 (Glp 1) of functional unit RvH1-a 92
4.1.4.4 Carbohydrate content of glycopeptide 2 (Glp 2) of functional unit RvH1-a and glycopeptide 3 (Glp 3) of functional unit RvH1-f 96
4.1.5 Structure and stability of arthropodan hemocyanin *Limulus polyphemus* 100
4.1.5.1 Isolation of structural subunits of *Limulus polyphemus* hemocyanin 100
4.1.5.2 Fluorescence properties of native molecule and structural subunits of LpH 104
4.1.5.2.1 Fluorescence lifetime of native molecule of *Limulus polyphemus* Hc 107
4.1.5.2.2 Denaturation with Gdn.HCl of native molecule of *L. polyphemus* Hc 109
4.1.5.2.3 Effect of pH on the stability of native molecule of *L. polyphemus* Hc 114
4.1.5.3 Circular dichroism properties of native molecule of *L. polyphemus* Hc 119
4.1.5.3.1 Temperature denaturation of native molecule of *L. polyphemus* Hc 119
4.1.5.3.2 Effect of pH on the stability of native molecule of *L. polyphemus* Hc 122
4.1.5.3.3 Denaturation of native LpH with guanidine hydrochloride (Gnd.HCl) 124
4.1.6 Structure of *Carcinus aestuarii* structural subunit 2 (CaeSS2) 128
4.1.6.1 Fragmentation and purification of peptides from subunit CaeSS2 129
4.1.6.2 Primary structure of *Carcinus aestuarii* structural subunit 2 (CaeSS2) 133
4.1.6.3 Fluorescence properties of *Carcinus aestuarii* subunit 2 (CaeSS2) 137
4.1.7 Carbohydrate composition of *Carcinus aestuarii* (Ca) hemocyanin 141
4.1.7.1 Carbohydrate content of *Carcinus aestuarii* structural subunit 2 (CaeSS2) 141
4.1.7.2 Tryptic digestion of *Carcinus aestuarii* structural subunit 2 (CaeSS2) 142
4.1.7.3 MALDI-MS of glycopeptides 1, 2, 3 and 4 of CaeSS2 before and after treatment with specific glycosidases 143
4.1.7.4 Suggested structure of the carbohydrate chains of glycopeptides 1,2,3 and 4 of CaeSS2 146
4.2 Isolation, structure and biological investigation on fungal Cu/Zn superoxide dismutase 148
4.2.1 Structural and functional analysis of glycosylated Cu/Zn-superoxide dismutase from the fungal strain *Humicola lutea* 103 (HL-SOD), cultivited under copper stress conditions 148
4.2.1.1 Response of *Humicola lutea* cells to Cu^{2+} stress 149
4.2.1.2 Amino acid sequence determination of HL Cu/Zn-superoxide dismutase 151
4.2.1.3 MALDI-TOF analysis of the glycopeptide of HL-SOD and yeast SOD 157
4.2.1.4 Protective effect of HL-SOD 158

5. Conclusion 159

6. References 163

7.Appendix 188

List of abbreviations

Amino acids

A	Ala	Alanine
C	Cys	Cysteine
D	Asp	Aspartic Acid
E	Glu	Glutamic Acid
F	Phe	Phenylalanine
G	Gly	Glycine
H	His	Histidine
I	Ile	Isoleucine
K	Lys	Lysine
L	Leu	Leucine
M	Met	Methionine
N	Asn	Asparagine
P	Pro	Proline
Q	Gln	Glutamine
R	Arg	Arginine
S	Ser	Serine
T	Thr	Threonine
V	Val	Valine
W	Trp	Tryptophan
Y	Tyr	Tyrosine

Common terms

Å	Angstrom
aa	Amino acids
Aa6	*Androctonus australis* subunit
AcH	*Aplysia californica* hemocyanin
BAS	Bulgarian Academy of Sciences
Bs	*Buthus sindicus*
°C	Degree Celsius
Ca	*Carcinus aestuarii*
CaeSS2	*Carcinus aestuarii* structural subunit 2
ca.	Circa
cDNA	Complementary DNA

CD	Circular dichroism
Cm6	*Cancer magister* subunit
Da	Dalton
DNA	Deoxyribonucleic acid
DTT	Dithiothreitol
Ece	*Euripelma californica* subunit
EDTA	Ethylenediaminetetraacetic acid
e.g.	For example
EM	Electron microscope
EC-SOD	Extracellular SOD
Fig.	Figure
FU	Functional unit
FUs	Functional units
GalNAc	*N*-acetyl-D-galactosamine
Glp	Glycopeptide
h	Hours
Hc	Hemocyanin
Hcs	Hemocyanins
HL	*Humicula lutea*
HL-SOD	*Humicula lutea* superoxide dismutase
Ha	*Homarus americanus*
HpH	*Helix pomatia* hemocyanin
HPLC	High pressure liquid chromatography
HtH	*Haliotis tuberculata* hemocyanin
IC	Internal conversion
ISC	Intersystem crossing
kDa	KiloDalton
kg	Kilogram
KLH	Keyhole limpet hemocyanin
λ	Wavelength
LcH	*Lepidochitona cinerea* hemocyanin
LpH	*Limulus polyphemus* hemocyanin
MALDI	Matrix-assisted laser desorption/ionization
MALDI-MS	Matrix-assisted laser desorption/ionization mass spectrometry
Man	D-mannose

mg	Milligram
ml	Millimeter
mM	Millimole
Ms	*Maia squinado*
Mw	Molecular weight
n.d.	No data
nm	Nanometre
NnH	*Nucula nucleus* hemocyanin
NMR	Nuclear magnetic resonance
NpH	*Nautilus pompilius* hemocyanin
OdH	*Octopus dofleini* hemocyanin
PAGE	Polyacrlamide gel electrophoresis
Pi	*Panulirus interruptus*
pmole	Picomole
PNGase-F	Peptide: N-Glycosidase F
PTH	Phenylthiohydantoin
Pv	*Palinurus vulgaris*
ROS	Reactive oxygen species
RtH	*Rapana thomasiana* hemocyanin
S	Singlet state
s	Second
SAXS	Small angle X-ray scattering
SB	Stabilizing buffer
SDS	Sodium dodecylsulfate
SOD	Superoxide dismutase
SoH	*Sepia officinalis* hemocyanin
SS	Structural subunit
τ	Lifetime
T	Temperature
TEM	Transmission electron microscopy
TEMED	Tetramethylethylenediamine
TOF	Time-of-flight
Tris	Tris-(hydroxymethyl)-aminomethane
UV	Ultraviolet
UV/Vis	Ultraviolet/visible

1. Introduction

1.1 Metalloproteins (Copper-containing proteins: Hemocyanins and SODs)

Metalloproteins possess one or more metal ions, essential for their structure and function. Many proteins contain metal in the active site with different functions. This thesis presents studies on two classes of metalloproteins: hemocyanins and Cu/Zn superoxide dismutase. Hemocyanins of arthropods [Burmester, 2001] and molluscs belong to the hemocyanin/hexamerin/phenoloxidase superfamily; they probably evolved independently from a common ancestral non-hemocyanin protein.

1.1.1 Oxygen transporting proteins

In response to the need for an efficient carrier that enhances the oxygen transport capacity of the body fluid, many animals evolved respiratory proteins, as represented by hemoglobins, hemerythrins, and hemocyanins **(Figure. 1)**.

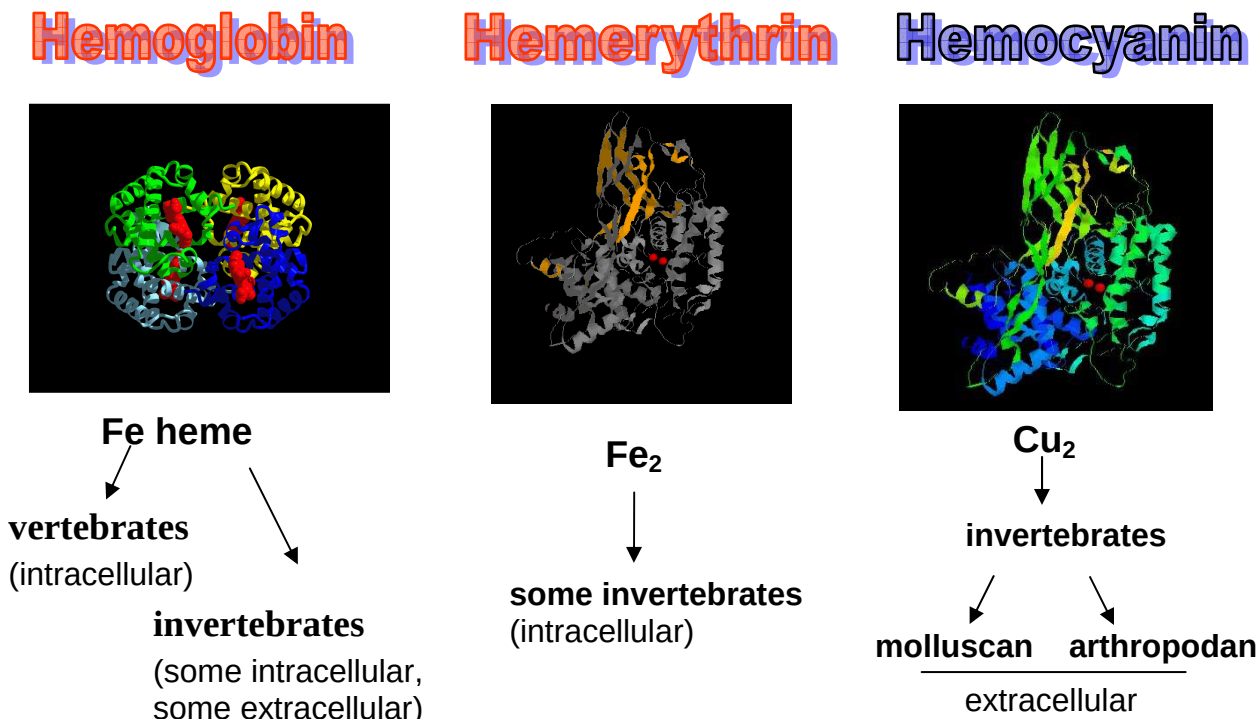

Figure 1. Different types of oxygen-transporting proteins (Hemoglobin** [Shen et al., 1993] **and Hemerythrin** [Holmes et al., 1991] **with iron metal ions in the active site or Hemocyanin** [Makino, 1985] **with two copper ions in the active site).

The delivery of oxygen within the animal's body is an essential process that is accomplished by three different types of metal-containing proteins: hemoglobins, hemerythrins and hemocyanins. Iron ions are used in the active sites of hemoglobins and hemerythrins, whereas copper ions are characteristic for hemocyanins which in their oxygenated state are blue. While hemoglobins are widespread throughout the animal kingdom, hemerythrins and hemocyanins are restricted to only a few phyla [Vinogradov, 1985; Terwilliger, 1998*;* Kurtz, 1999].

1.1.2 Hemocyanins

1.1.2.1 Occurrence of hemocyanins

Hemocyanins are large proteins that may assemble to complexes of up to several million Daltons. These copper proteins only occur in the body fluid of some arthropodan and molluscan species, dissolved in the circulating fluid, the hemolymph, that is pumped by the heart [Markl and Decker, 1992*;* van Holde and Miller, 1995]. Hemocyanins are found in various arthropods such as crabs, lobsters, scorpions, spiders and centipedes as well as in molluscs like snails, whelks, octopus, squids, limpets, sea cucumbers and conches.

1.1.2.2 Active site of hemocyanins

The biological function of these proteins is related to their capacity of reversibly binding molecular oxygen at an active site containing a binuclear copper centre. The protein exists in two different forms: deoxy-Hc, containing a [Cu(I)Cu(I)] copper pair, and oxy-Hc. The copper complex in the latter form is currently formulated as [Cu(II)O_2^{2-} Cu(II)], reflecting an electron transfer from Cu (I) to dioxygen [Solomon, 1978; Solomon et al., 1992; **Figure 2**].

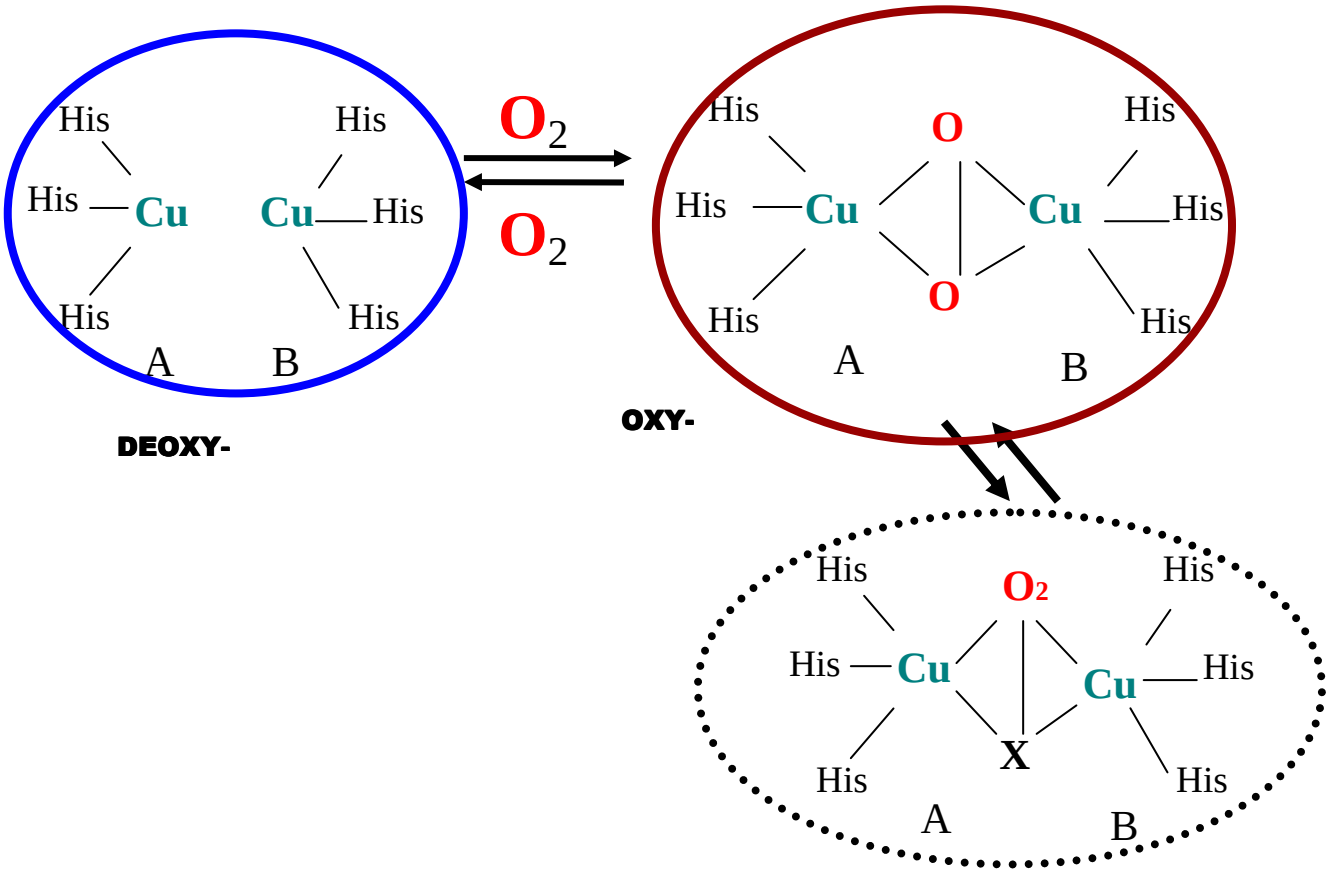

Figure 2. Oxy-form (containing [Cu(II)O_2^{2-} Cu(II)] complex) and deoxy-form (containing a [Cu(I)Cu(I)] copper pair) of the oxygen-binding active site in hemocyanins. *Each cooper ion is bound with three histidine residues [Solomon, 1978].*

The X-ray crystallographic studies of deoxy-Hc from *Panulirus interruptus* [Volbeda and Hol, 1989] and the deoxy and oxy- forms of *Limulus polyphemus* [Hazes et al., 1993; Magnus et al, 1994; Shrive et al., 1999] have elicited a detailed picture from the active site of proteins.

The crystal structures, available for a 50 kDa subunit OdH-g from molluscan Hcs *Octopus dofleini* [Cuff et al., 1998], *Rapana thomasiana* [Stoeva et al., 1998], arthropodan Hcs *Panulirus interruptus* [Volbeda and Hol, 1989] and for subunit II of *Limulus polyphemus* [Hazes et al., 1993], allow a comparison of Hcs from these two phyla **(Figure 3)**.

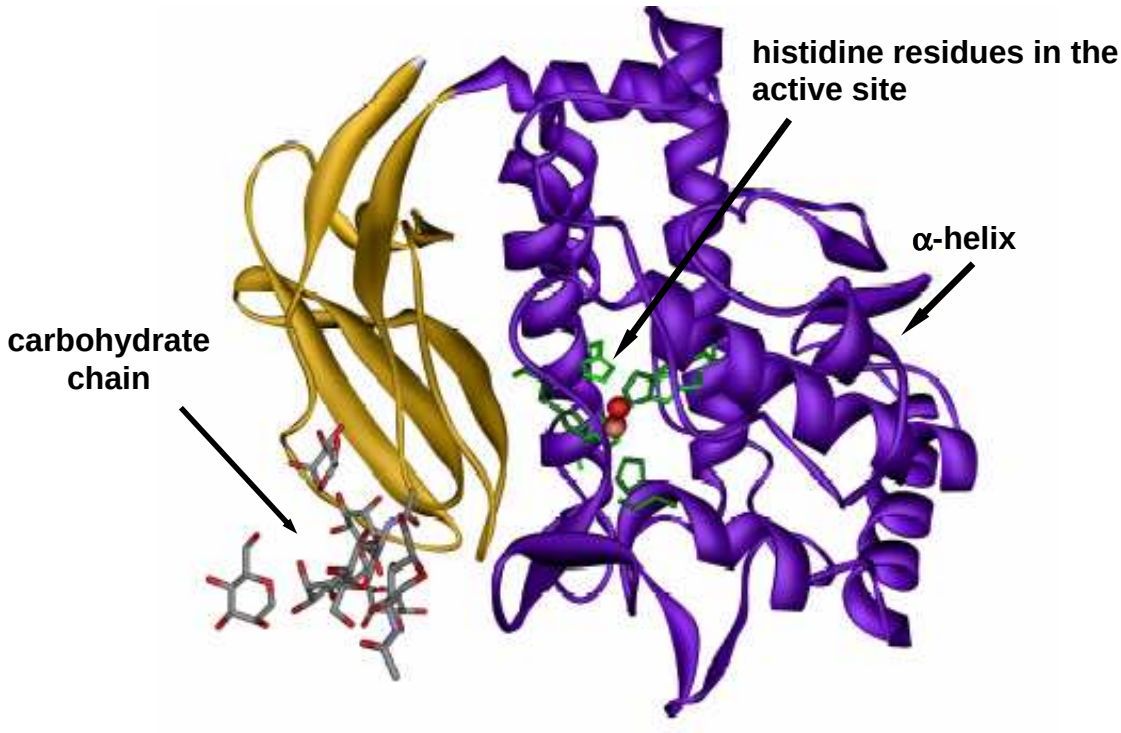

Figure 3. X-ray structure of functional unit (FU) g of molluscan Hc Octopus dofleini. *Two copper ions labeled CuA and CuB (in red) and histidine residues (in green) are part of the active site [Cuff et al., 1998].*

In arthropodan and molluscan hemocyanins, the two copper ion in the active site, labeled CuA and CuB [Ling et al., 1994], are not equivalent and are likely to play a different role in the biological function. The CuA copper(II) centre that seems to be more accessible to the solvent in the binuclear site controls the reactivity of the site, while the second copper (II) centre (CuB) plays a complex role in controlling the local conformation and electrostatic effects in the oxygenation cycle.

The active site is deeply buried within the protein matrix and a number of hydrophobic residues, including tryptophans, are involved in the active site pocket. It was proposed that such residues may contribute to stabilize the hydrophobic core of the protein **(Figure 4).**

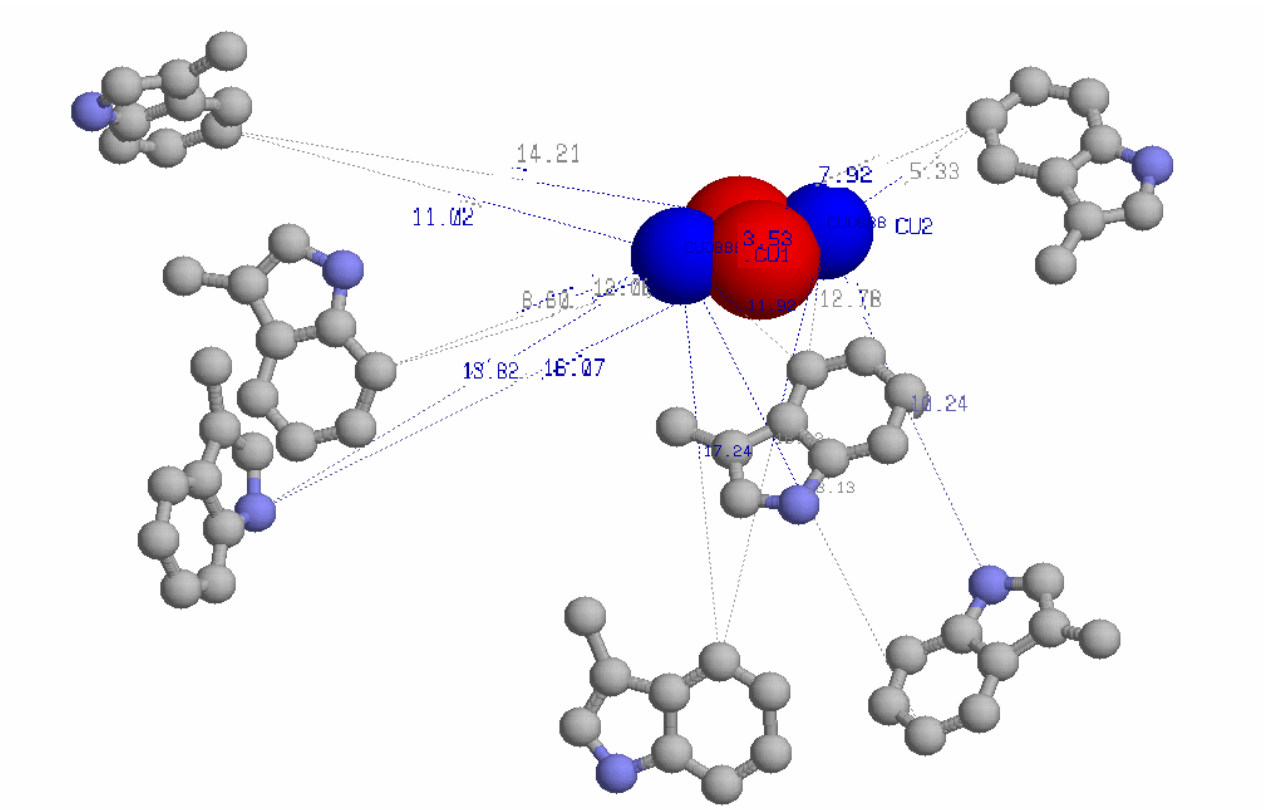

Figure 4. Active site of FU g of molluscan Hc Octopus dofleini. *Eight tryptophan residues are buried in the molecule [Cuff et al., 1998].*

1.1.2.3 Evolution of different copper centres in arthropodan and molluscan hemocyanins and their relationship to tyrosinases

There are fundamental differences in the constitution of the native hemocyanins of the two phyla [e.g. Markl and Decker, 1992*;* van Holde and Miller, 1995; van Holde et al., 2001]. Statistical analyses have demonstrated that even the sequence similarities between the molluscan and arthropodan hemocyanin superfamily are not significant [Burmester, 2001]. Thus the molluscan and arthropodan hemocyanins emerged independently, most likely from existing copper-proteins [Burmester, 2001; van Holde et al., 2001]. The molluscan hemocyanins share significant sequence similarities with the tyrosinases found in many bacteria, fungi, plants, and animals [Drexel et al., 1987*;* Muller et al., 1988*;* Markl and Decker, 1992*;* Cuff et al., 1998; Burmester, 2001; Lieb et al., 2001] suggesting that these tyrosinases and the molluscan hemocyanins represent an ancient protein superfamily most probably already present in the stem line of all living cells [van Gelder et al., 1997] **(Figure 5).**

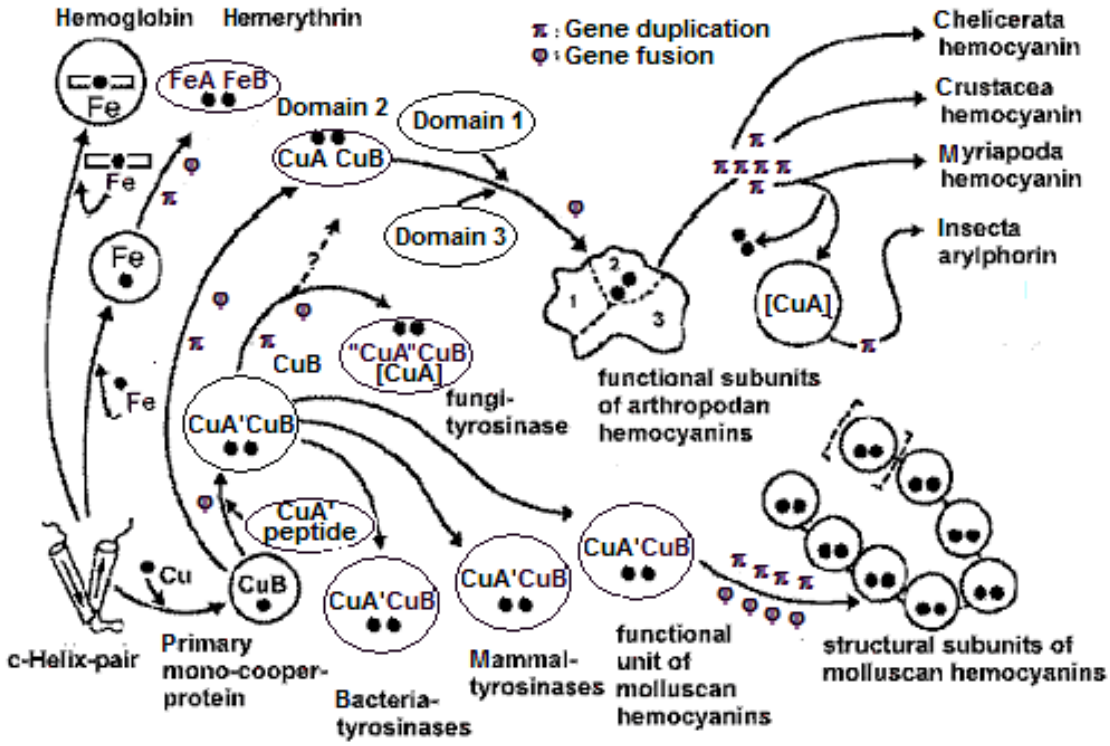

Figure 5. Hypothetic representation of relationships between hemoglobins, hemerythrins and hemocyanins*. Evolution of different cooper centres in arthropodan and molluscan hemocyanins and their relationships to tyrosinases [van Gelder et al., 1997].*

1.1.2.4 Arthropodan hemocyanins

1.1.2.4.1 Origin and structure of arthropodan hemocyanins

Hemocyanins have been identified from all arthropodan subphyla. They are present in the last common ancestors of Chelicerata, Crustacea, Myriapoda and Insecta [Markl and Decker, 1992*;* van Holde and Miller, 1995; Burmester, 2001]*.* It is noteworthy that many arthropods, e.g. the chironomid mosquitoes or the branchiopod crustaceans [Weber and Vinogradov, 2001] apparently lost their hemocyanins later in evolution and recruited intracellular globins for this task. The arthropod hemocyanin superfamily includes other classes of proteins that share significant sequence similarities, but serve distinct functions [Beintema et al., 1994*;* Burmester and Scheller, 1996*;* Burmester, 2001; van Holde and Miller, 1982; Ellerton et al., *1983;* Linzen et al., 1985; Salvato and Beltramini, 1990*;* Markl and Decker, 1992*;* van Holde and Miller, 1995]. Markl and co-workers [Markl, 1986; Markl et al., 1986] have carried out an immunological approach to elucidate hemocyanin

relationship and evolution within the Crustacea and Chelicerata family. *Maia squinado* and *Limulus polyphemus* belong to the Chelicerata family, while *Homarus americanus*, *Carcinus aestuarii* and *Panulirus interruptus* to the Crustacea family **(Figure 6).**

Figure 6. a) Maia squinado, *an example of the Chelicerata family.*

Figure 6. b) Homarus americanus, *an example of the Crustacea family.*

Figure 6. c) Panulirus interruptus, *an example of Crustacea family.*

1.1.2.4.2 Formation of arthropodan hemocyanin multimers

The most ancient hemocyanin was likely to be a hexamer [Jaenicke and Decker, 2003]. Arthropodan hemocyanins either form hexamers or multi-hexamers of six similar or identical subunits, each of which may bind one oxygen molecule [Markl and Decker, 1992; van Holde and Miller, 1995] **(Figure 7).**

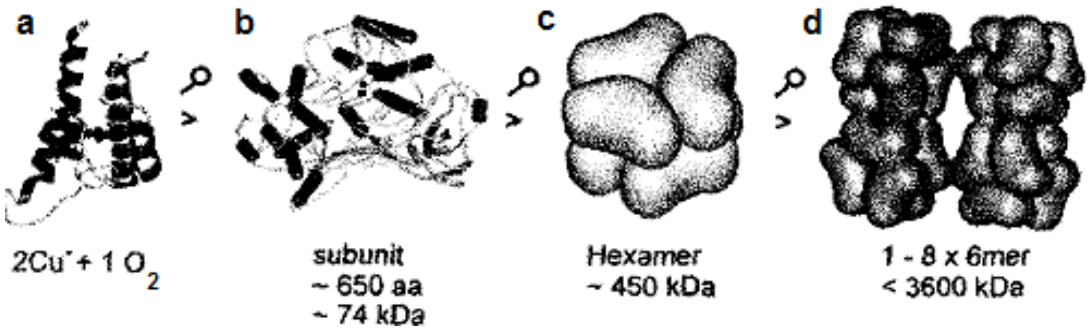

Figure 7. Structure of arthropod hemocyanin. a) *O_2-binding site;* ***b)*** *subunit containing 650 aa (amino acid residues);* ***c)*** *simplified hexamer structure;* ***d)*** *simplified multi-hexamer (arachnid 4x6 hemocyanin) [Markl and Decker, 1992].*

A typical arthropodan hemocyanin subunit consists of about 630-660 amino acids (ca. 70-80 kDa protein) which are divided into three structural domains [Gaykema et al., 1984*;* Volbeda and Hoi, 1989] **(Figure 8).** The first domain comprises the N-terminal 150-180 amino acids and is formed mainly by α-helices that build a super-secondary structure of a stable helical bundle. The second domain (about 220 amino acid residues) contains the two copper-binding sites, CuA and CuB, each of which consists of two α-helices with three histidine residues that coordinate the copper ions. The third domain (about 260 amino acid residues) is mainly built by β-sheets that form the super-secondary structure. X-ray structures of the hemocyanin subunits or hexamers have been resolved from *Panulirus inlerruptus* [Gaykema et al., 1984*;* Volbeda and Hol, 1989] and *Limulus polyphemus* [Hazes et al., 1993].

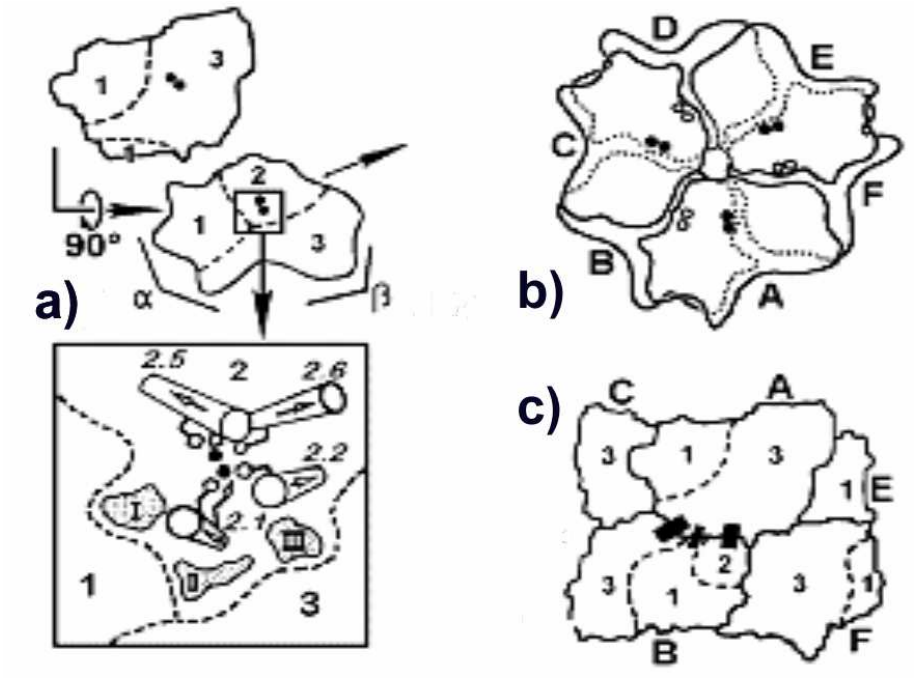

Figure 8. Structure of arthropodan hemocyanin. a) *Ventral- and dorsal view of the subunit; orbital and black dots: cooper atoms; dotted lines: boundaries between the structural domains 1 - 3; α: rich α-helical region; β: rich β-sheet region; close-up view of the active centre: 2.1, 2.2, 2.5, 2.6: the 4 antiparallel, on cooper bond participating α-helices; I - III: enclosed water;* ***b)*** *The hemocyanin model composed of 6 (A, B, C, D, E, F) structural subunits;* ***c)*** *View of the hexamers in vertical to threefold rotation of axis; "narrow" contact regions between the functional subunits are marked as black rectangles (■) [Volbeda and Hol, 1989].*

1.1.2.4.3 Evolution of arthropodan hemocyanins

The evolution of distinct hemocyanin subunits, as well as the formation of multihexamers, has occurred independently within the arthropod subphyla. One of the most striking feature of the arthropod hemocyanins is their enormous subunit diversity [Markl, 1986] which is in contrast to the vertebrate hemoglobins [e.g. Dickerson and Geis, 1983]. However, the distinct hemocyanin subunit types are not orthologous among the subphyla, but evolved independently. The mode of assembly of the hexamers to higher quaternary structures also differs markedly among, and even within, the arthropod subphyla [Markl, 1986*;* Markl and Decker, 1992]. Thus, the evolution of the distinct subunits that occur in the Crustacea, Chelicerata and probably also the Myriapoda from a single hemocyanin subunit type clearly occurred independently [Markl, 1986*;* Burmester, 2001] **(Figure 9)**.

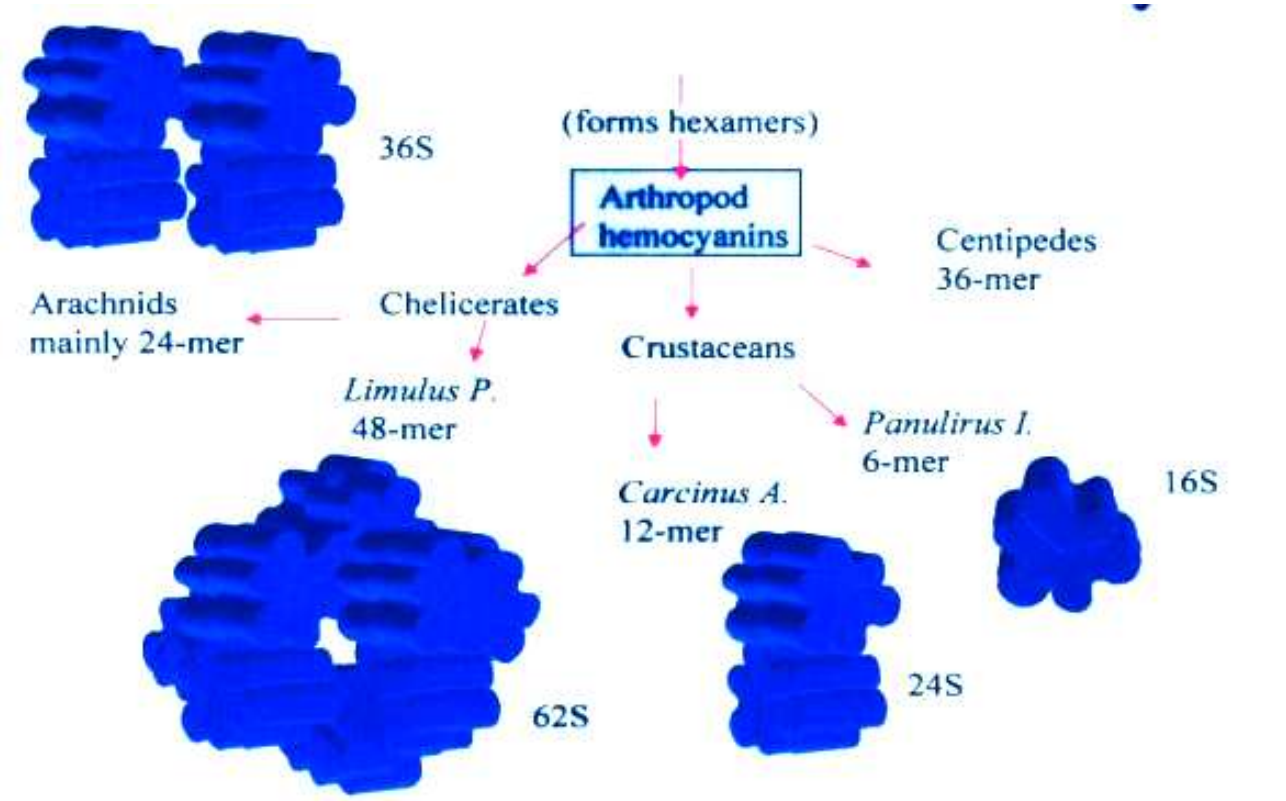

***Figure 9. Simplified quaternary structures of different arthropodan hemocyanins. Crustaceans**: **a)** 6-mer (1x6) hemocyanin found in many arthropod taxa (e.g. Panulirus interruptus); **b)** (2x6) hemocyanin (e.g. Homarus americanus, Carcinus aestuarii); **Chelicerates: a)** 24-mer (4x6) Arachnids hemocyanin (e.g. Eurypelma californicum) and **b)** 48-mer (8x6) hemocyanin of the Xiphosura (e.g. Limulus polyphemus); **Myriapoda** hemocyanin: 36-mer (6x6) Centipedes hemocyanin (e.g. Scutigera coleoptratd). **S**: sedimentation coefficient. This figure is taken from poster session [Dolashka, 2003].*

Also, the formation of the multi-hexamers, which may aggregate up to 8x6-mers, occurred convergently, probably in response to osmotic requirements [Markl, 1986; Markl and Decker, 1992]. Subunit evolution is strikingly different in Chelicerata, Myriapoda, and Crustacea [Markl, 1986; Burmester, 2001, 2002] **(Table 1)**.

Table 1. Structure and properties of arthropodan hemocyanins.

Main function	Occurrence	Number of hexamers	Copper content	Protein chain length (aa)
Oxygen transport	Chelicerata	1-8x6	yes	630
	Crustacea	1-4x6	yes	660
	Myriapoda	6x6	yes	640
	Insecta	n.d.	yes	650

Within the Chelicerata, the xiphosuran hemocyanins are 8x6-mers, while most arachnids are composed of 4x6-mers, formed from seven distinct subunit types [Voit et al., 2000; Averdam et al., 2003]. Some modern spiders, however, have 1x6 or 2x6 hemocyanins built of fewer subunit types [Ballweber et al., 2002]. The myriapod-typical 6x6-mer hemocyanin and at least some distinct subunits emerged before the separation of Chilopoda and Diplopoda [Kusche and Burmester, 2001; Kusche et al., 2003a]. Crustacean hemocyanins are highly variable in quaternary structures and subunit compositions which also may alter in response to environmental changes. Three evolutionary distinct subunit types (a–g) have been identified in Decapoda [Markl, 1986; Kusche et al., 2003b].

1.1.2.4.4 Hemocyanin subunit diversity in Chelicerata species

In the chelicerates, hemocyanins have been found in many spiders (Arachnida), scorpions and horseshoe crabs (Xiphosura) [Markl, 1986; Markl et al., 1986]. The scorpions and most arachnids possess a typical 24-mer (4x6) hemocyanin, the Xiphosura 48-mers (8x6). The hemocyanins of the Chelicerata are very often multimers of hexamers that are formed by different subunits that occupy distinct positions in the native oligomer (Markl and Decker 1992). Up to eight distinct subunit types (a-h) may occur in the different chelicerate classes. The eighth subunit type (h), which is most likely a variant of the a-type, is only present in the scorpions, while the others (a-g) are homologous among the Arachnida, Xiphosura and scorpions [Markl, 1986]. For example, the 24mer (4x6) hemocyanin of the tarantula *Eurypelma californicum* is composed of seven different subunits (EcaHcA–EcaHcG). The different hemocyanin subunits have distinct physic-chemical properties and sequences, but similar oxygen-binding behaviour [Decker et al., 1979; Markl et al., 1981a]. Several subunits have been sequenced on the protein level of Xiphosura (horseshoe crabs) *Limulus polyphemus* and *Tachypleus tridentatus* [Linzen et al., 1985; Nakashima et al., 1986] and the scorpion *Androctonus australis* [Buzy et at.,

1995], and the North American tarantula *Eurypelma californicum* [Schartau et al., 1983; Schneider et al., 1983]. In addition, the cDNA sequences of all seven subunits (a-g) *of E. califomicum* [Voit and Schneider, 1986; Voit and Feldmaier-Fuchs, 1990; Voit et al., 2000], as well as the gene of subunit *e* of the same species [Voll and Voit, 1990] are known. Comparison of the sequences confirms the earlier immunological classification of the different subunits [Markl, 1986; Voit et al., 2000; Burmester, 2001], The chelicerate hemocyanins are very conserved proteins. The subunit sequences share about 53-64% of the amino acids. There is, however, strong evidence that the *E. californicum* subunits b and c, responsible for the interhexamer contact, are closely related.

1.1.2.4.5 The hemocyanins of the Myriapoda species

Such proteins occur in the Spirostreptidae (Diplopoda) as well [Jaenicke et al., 1999; Kusche and Burmester, 2001]. Although information concerning the minor myriapod taxa (Symphyla and Pauropoda) is still missing, these findings suggest that oxygen-transporting hemocyanins may be rather widespread within this taxa. The hemocyanins of the Spirostreptidae and Scutigeramorpha form quaternary structures of 6x6 subunits. While the arrangement of the hexamers within the chelicerate and crustacean hemocyanins is variable [Markl, 1986; Markl et al., 1986; Markl and Decker, 1992], this unique 36-mer hemocyanin is a common feature of the Diplopoda and Chilopoda. However, recent data show that the centipede *Lithobius forficatus* possesses a simple 6-mer hemocyanin, suggesting that different quaternary structures may also occur in the myriapodan hemocyanins. A hemocyanin subunit sequence from *Spirostreptus spider*. and two subunit sequences from *S. coleoptrata* have been determined [Kusche and Burmester, 2001b; K. Kusche, W. Gebauer, and T. Burmester, unpublished results]. The dipolopod and chilopod hemocyanins share about 50% of their amino acids.

1.1.2.4.6 Hemocyanin evolution in the Crustacea species

Hemocyanins are present in the malacostracan Crustacea, including Hoplocarida (mantis shrimps etc.), Eucarida (Decapoda) and Pericarida (Isopoda, Amphipoda, Mysidacea and Euphausiacea) [Mangum, 1983; Markl, 1986]. In the haemocytes of Remipedia, large crystals have been detected that resemble those of *Limulus polyphemus* 8x6 hemocyanin [Yager, 1991].

Within the Malacostraca, there is little information on hemocyanin subunit composition of the Hoplocaridae and Pericaridae [Mangum, 1983]. These species mostly possess hexameric hemocyanins (1x6), although in the mantis shrimp *Squilla mantis* (Hoplocaridae) a unique 2x6-mer has been observed [Bijiholt and van Bruggen, 1986]. The eucarid taxa of the Isopoda and Euphausicea have 1x6 hemocyanins which are composed of immunological identical subunits [Markl, 1986]. However, recent data suggest multiple subunit types also exist in amphipodan and isopodan species [Hodgson and Spicer, 2001]. Most hemocyanins of the Decapoda are either hexamers or dihexamers [Markl, 1986; Markl et al., 1986; Markl and Decker, 1992], although there is at least one exception: on thalassinid shrimp *Callianassa califomiensis* possesses a 4x6 hemocyanin [Miller et al., 1977]. Subunit composition and evolution of the decapod hemocyanin-hexamer differ strikingly from those of Chelicerata [Markl, 1986, Markl, et al., 1986; Burmester, 2001]. While the structure of the chelicerate hemocyanins is highly conserved, there is much more variability in terms of subunit organisation in Crustacea [Markl, 1986; Markl et al., 1986; Stocker et al., 1988; Mangum and Joy, 1997]. Some subunits may be expressed only in certain developmental stages or under specific physiological conditions [Markl and Decker, 1992; Durstewitz and Terwilliger, 1997; Terwilliger, 1998]. This has never been observed in chelicerates or myriapodas.

Immunological studies have demonstrated three types of subunits to occur in Decapoda (α, β, and γ); [Markl, 1986; Markl et al., 1986]. The seven known crustacean subunits form two distinct clades, representing the α (HamHcA, PinHcA, PinHcB, PvuHc)

and γ (PinHcC, PvaHc, CamHc6) types, while β-type amino acid sequences are still unknown.

The rate of amino acid replacement in the crustacean hemocyanins is about two times higher than that of chelicerate proteins [Burmester, 2001]. The γ- subunits evolved about 25% faster than the α-subunits, consistent with the proposed central role in the crustacean hemocyanins of the latter [Kusche and Burmester, 2001a].

1.1.2.5 Molluscan hemocyanins

The word "mollusk" derives from Latin *mollis* meaning "soft," just as the term "malacology," The study of mollusks, is derived from the Greek word for soft, *malakos*. In the early 1800s, Baron Georges Cuvier realized that gastropods, bivalves, scaphopods, and cephalopods belonged in one group, but he included barnacles and brachiopods in the Mollusca, which have since been removed.

1.1.2.5.1. Classes of molluscs

The living molluscs are divided into seven classes, Aplacophora, Monoplacophora, Polyplacophora, Gastropoda, Bivalvia, Scaphopoda and Cephalopoda**.** Members of the first three groups are rarely observed **(Table 2)**. All molluscs are characterised by having soft, unsegmented bodies, which in many species are protected by a hard shell. The length of all 600 species ranges from 10 mm for male argonauts to 20 m for giant squids.

Table 2. Classes of molluscan hemocyanins

Class	Examples	Number of species
Bivalvia(also Pelecypoda)	clams, oysters, scallops, mussels	8,000
Scaphopoda	tusk shells, dentalium	350
Gastropoda	snails and slugs, limpets, sea hares, sea butterfly	40,000
Cephalopoda	squids, octopuses, nautilus, cuttlefish, all marine	650

Some members of molluscs are shown in **Figure 10**.

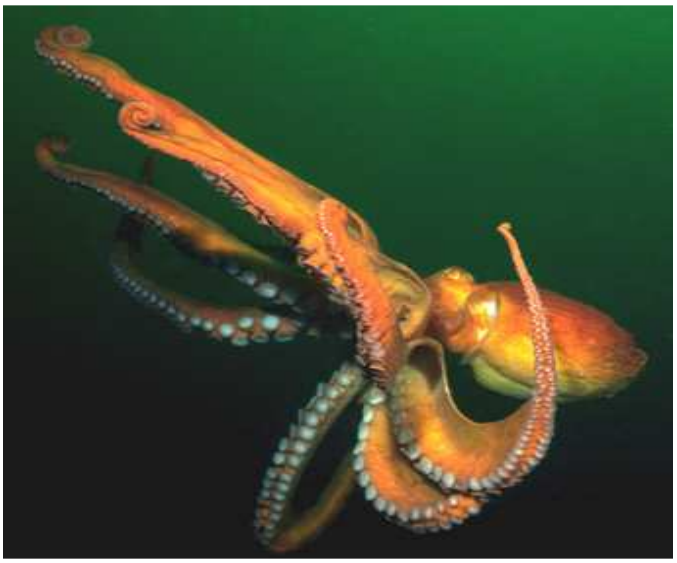

Figure 10. a) The cephalopods include the most intelligent animals among the invertebrates, e.g. octopus Octopus dofleini.

Figure 10. b) The European abalone Haliotis tuberculata is a member of the Archaeogastropoda.

Figure 10. c) Californian giant keyhole limpet (KL) Megathura crenulata, a marine gastropod.

The structure of molluscan hemocyanins is shown in **Figure 11**.

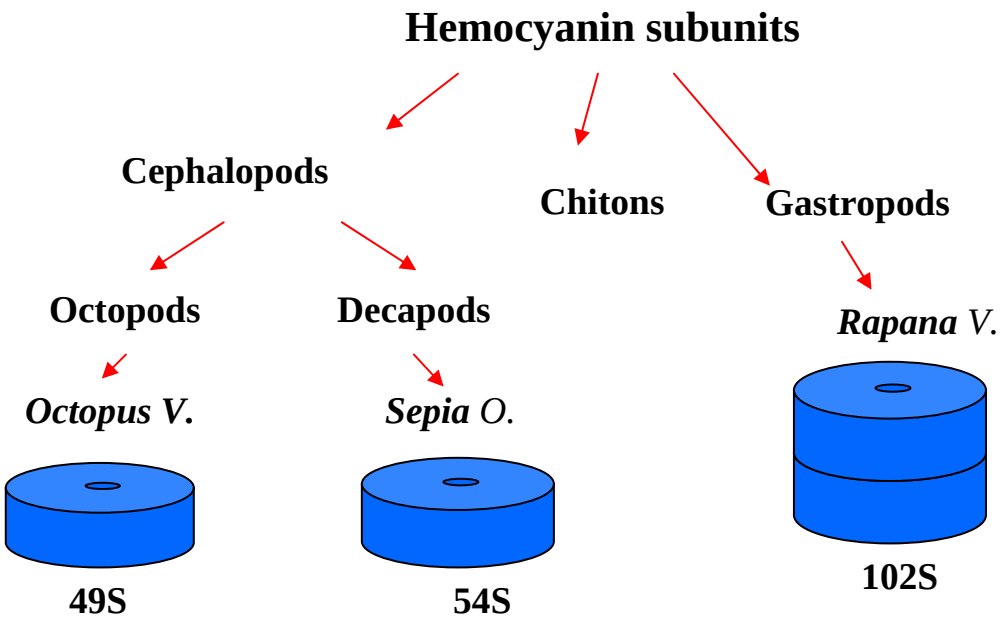

Figure 11. Structure of molluscan hemocyanins: Cephalopod *(Octopods and Decapods) hemocyanins are decamers with a molecular mass of about 4x10^6 Da,* ***Gastropods*** *hemocyanin are didecamers with a molecular mass of about 9x10^6 Da,* ***Chitons*** *are decamers. S- sedimentation coefficient. This figure is taken from poster session [Dolashka, 2003].*

Gastropods have a single-valved shell which is usually spirally coiled and is reduced or absent in slugs and semi-slugs. They are one of the few groups of organisms well-represented in marine, fresh water, and terrestrial habitats. There are about 60,000 species. Size ranges from 0.5 millimeters to 0.75 meters.

Bivalves have two valves connected by a flexible ligament. Most bivalves are filter feeders. There are about 10,000 living species of bivalves in marine and fresh water habitats worldwide. Size ranges from 0.5 millimeters to 1.3 meters.

1.1.2.5.2 Evolution of molluscan hemocyanins as deduced from DNA sequencing

Molluscan hemocyanins are huge cylindrical assemblies composed of a 350–400 kDa polypeptide subunits, subdivided into 7 or 8 covalently-linked functional units (FUs, termed a to h) of *ca*. 50 kDa [for details, see Meissner et al., 2000] **(Figure 12).**

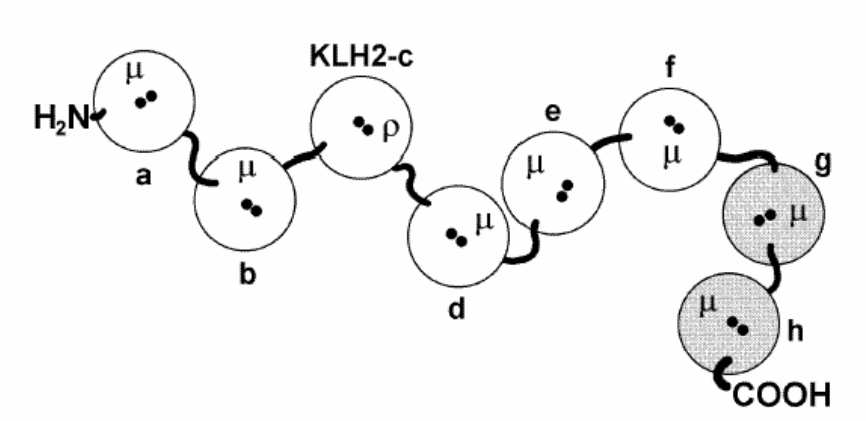

Figure 12. Conformation of structural subunit 2 of keyhole limpet hemocyanin (KLH2) Megathura crenulata. *Eight functional units (a-h) with Mw about 5x10^4 Da costitute the structural subunit. Black dots – cooper ions in the active sites;* ***H_2N****- N-terminal;* ***COOH*** *– C-terminal; ρ: O-glycans; μ: N-glycans [Gebauer et al., 1999].*

Each FU is able to reversibly bind a dioxygen molecule. This study is based on the sequence information of 13 hemocyanins from four different animal classes of the phylum Mollusca.

Several of the molluscs studied exhibit two rather different hemocyanin isoforms, structural subunits which almost certainly originated from duplication of a single eight-FU gene. From the phylogenetic tree's sequence alignment in **Figure 13** it is very clear that these duplication events occurred several times independently, because NnH1/NnH2 (*Nucula nucleus* hemocyanin) on the one hand and HtH1/HtH2 (*Haliotis tuberculata* hemocyanin) /KLH1/KLH2 (Keyhole limpet hemocyanin *Megathura crenulata*) on the other are members of two different branches. A third branch is formed by RtH2-e, indicating that duplication yielding the isoform pair RtH1/RtH2 occurred independently [Gebauer et al., 1999]. The common ancestor of the two vetigastropods *Haliotis* and *Megathura* already possessed the two hemocyanin isoforms. In contrast, the common clade of the opisthobranch gastropod *Aplysia* and the pulmonate gastropod *Helix* branched off well before this vetigastropod gene duplication event; therefore, the various FUs of *Aplysia* are as distant to HtH1/KLH1 as they are to HtH2/KLH2. Another clade is apparently represented by the neogastropod *Rapana thomasiana*.

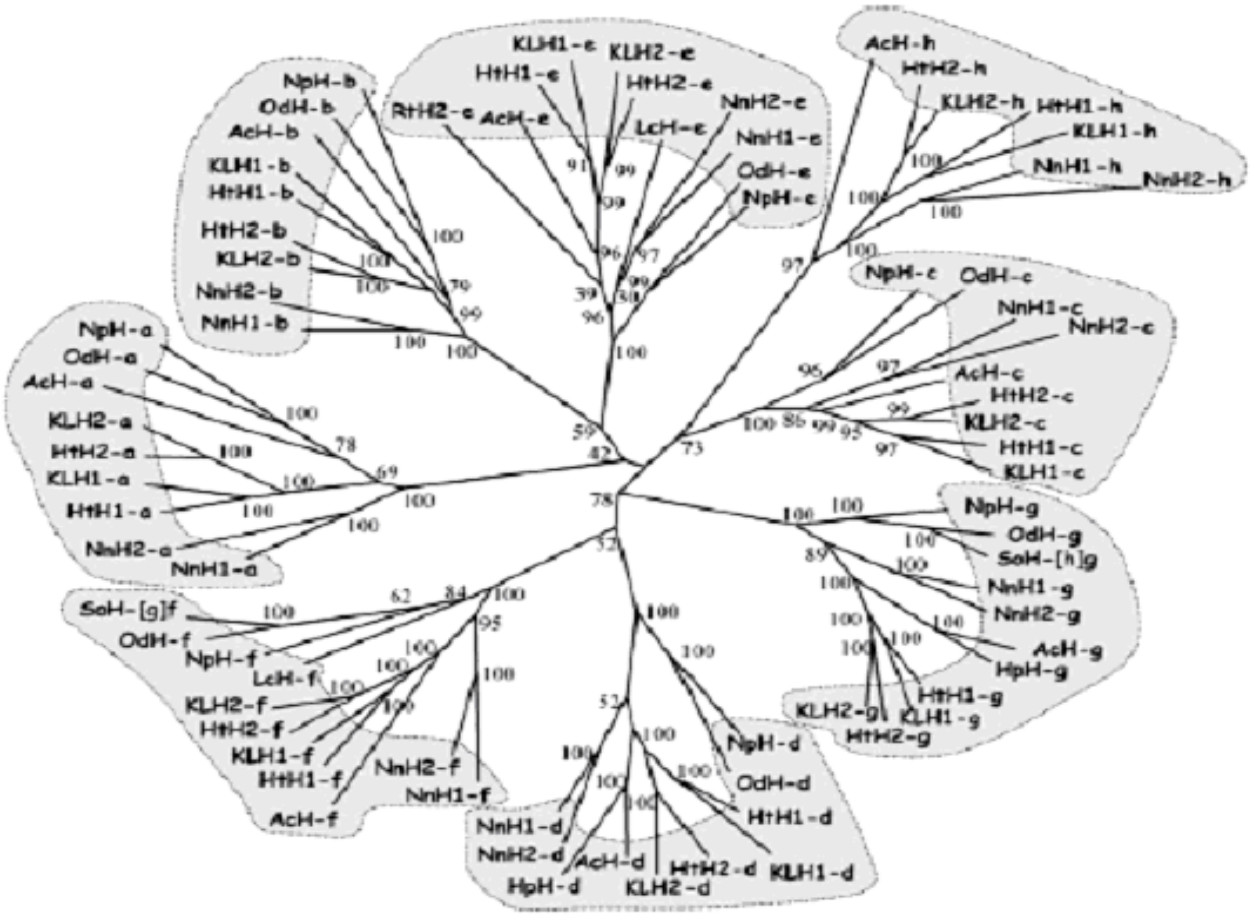

Figure 13. Radial phylogenetic tree of molluscan hemocyanins*. This unrooted tree is based on a program CLUSTALW amino acid sequence alignment. Note that FUs occupying the same position within the polypeptide chain (and identified by the letters a to h) form a common branch within this tree, together yielding eight different branches. Sequence data from the following hemocyanins were used: HtH1, HtH2 from Haliotis tuberculata [Lieb et al., 2000, 2001a; Altenhein et al., 2002]; KLH1, KLH2 from Megathura crenulata [Streit et al., 2003]; AcH from Aplysia californica [Boisgue´rin et al., 2003], RtH2 from Rapana thomasiana [Stoeva et al., 2002], HpH from Helix pomatia [Drexel et al., 1987]; NnH1, NnH2 from Nucula nucleus [Bergmann et al., 2003], NpH from Nautilus pompilius [Bergmann et al., 2003], SoH from Sepia officinalis [Beuerlein et al., 2003], OdH from Octopus dofleini [Miller et al., 1998; Lieb et al., 2001a]; LcH from Lepidochitona cinerea [Lieb et al., 2001b].This figure is taken from [Lieb et al., 2004].*

As deduced from bootstrapping, phylogenetic trees calculated from the currently available molluscan hemocyanin sequences are very robust within the gastropods and cephalopods, respectively. Therefore, the exceptionally long hemocyanin sequences appear to be highly efficient characters which are useful to unravel deep phylogenies within each of the molluscan classes, i.e. events that occurred 500–200 million years ago.

All three cephalopod hemocyanins lack FU-h also at the gene level; this seems indeed to be a synapomorphy of the cephalopods and underlines the classical concept of their monophyly. The available information from the three cephalopod hemocyanin genes shows that in *Nautilus* internal introns are lacking which probably reflects a very primordial situation in this living fossil. *Octopus* and *Sepia* show common as well as specific internal introns; consequently, within the *Octopus Sepia* clade the pattern of internal introns changed much more recently than within the Vetigastropoda. In *Sepia*, an additional FU evolved which was an early observation [Avissar et al., 1986].

1.1.2.5.3 Model building of a molluscan hemocyanin from X-ray solution scattering

Molluscan hemocyanins are proteins of a truly enormous size. Because of this, determination of their quaternary structure at high resolution can not easily be obtained by standard methods such as X-ray crystallography and NMR. Therefore, several low-resolution techniques were used to understand the hemocyanin structure. A model of the *Rapana venosa* hemocyanin has been obtained from a template model and small angle X-ray scattering (SAXS) data **(Figure 14**) [Micetic and Salvato, 2004].

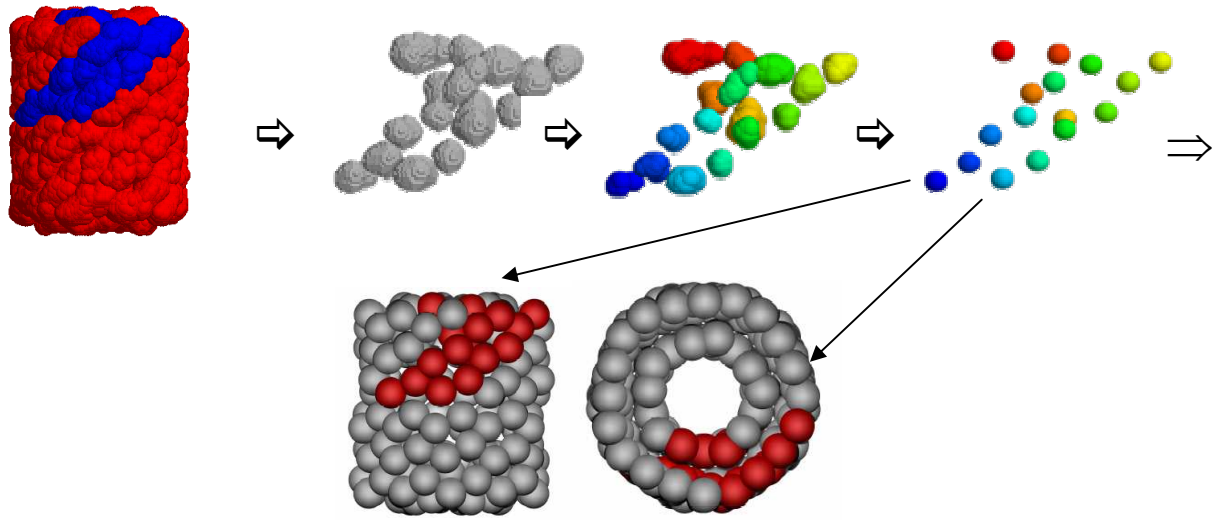

Figure 14. Template model building of Rapana venosa hemocyanin*. Increasing the probe radius to 12.8 Å (top row) produced a cavity with 16 distinct lobes. The mean of the centers of probe spheres in each lobe gave the coordinates of the initial model (longitudinal (bottom left) and axial (bottom right) view) [Micetic and Salvato, 2004].*

The template model was built from the electron density of the closely related *Haliotis tuberculata* hemocyanin and a computer program was written to fit this model to the SAXS data using the simulated annealing algorithm **(Figure 15).**

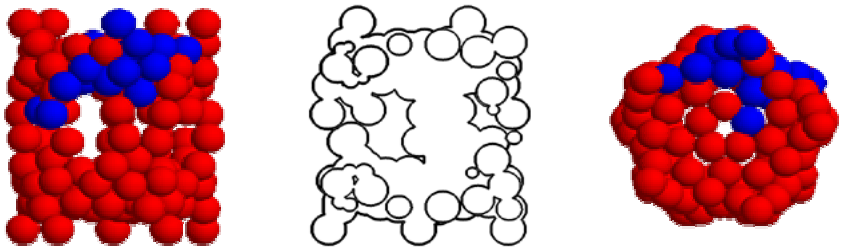

Figure 15. Best final fit model of Rapana venosa hemocyanin, longitudinal (left) and axial (right) view. *The radius in the final model was 26.5 Å [Micetic and Salvato, 2004].*

1.1.2.6 Studies of structure of hemocyanins by three-dimensional transmission electron microscopy

Three-dimensional transmission electron microscopy (3-D cryo-TEM) of frozen-hydrated proteins can now yield reconstructions well below the 1 nm resolution level. The 3-D cryo-TEM reconstructions of the didecamer (2x10-mer) hemocyanin molecules from the giant keyhole limpet *Megathura crenulata* [Orlova et al., 1997] and the European abalone *Haliotis tuberculata* have been studied [Meissner et al., 2000] as well as the hemocyanin subunit dimer from the polyplacophoran *Acanthochiton fascicularis*. It could be shown that 1 didecamer from *H. tuberculata* (HtH1) has a hollow cylindrical quaternary structure, consisting of an outer wall and two pentameric internal collar complexes **(Figure 16a)**. Each of the collar complexes contains a more central “arc” component and a peripheral “collar” ring. The repeating unit of HtH1 quaternary structure is a subunit dimer **(Figure 16b)**, assembled from two copies of the 400 kDa subunit; this dimer assembly was structurally defined three decades ago [Siezen and van Bruggen, 1974] and has been confirmed by the present reconstruction. Within the dimer, the two subunits are thought to be in an anti-parallel arrangement; however, in a manner which is not yet fully understood: the two C-terminal parts of the subunit are folded internally into a parallel arrangement, to then form the collar complex.

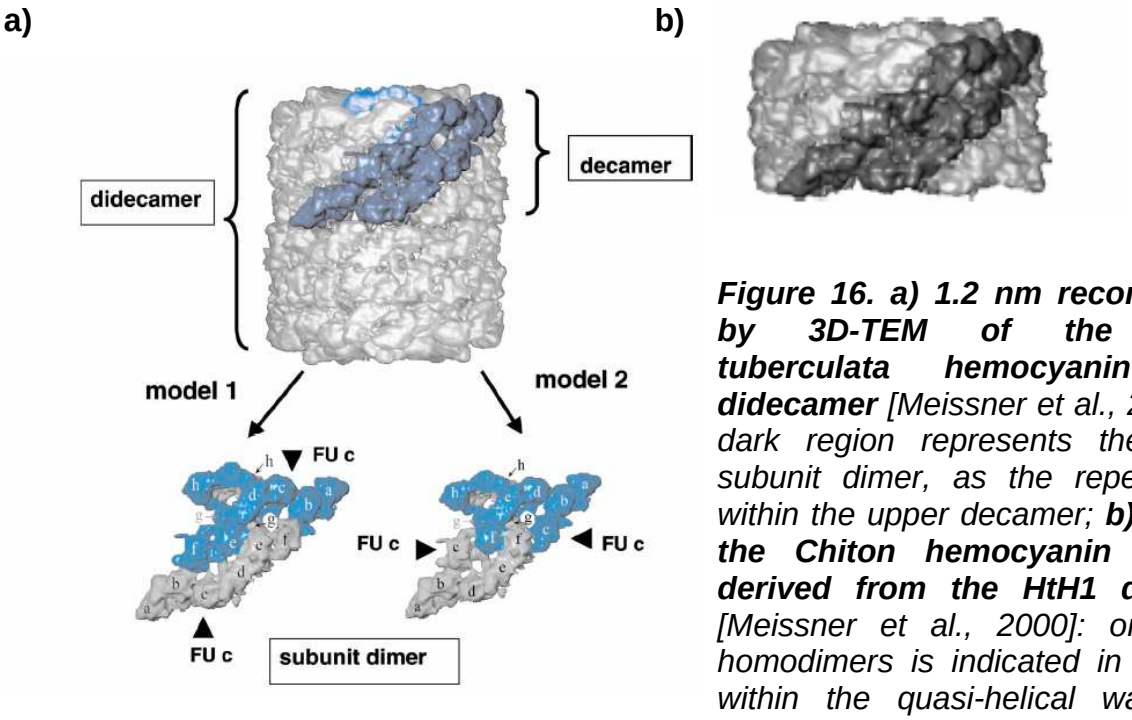

Figure 16. a) 1.2 nm reconstruction by 3D-TEM of the Haliotis tuberculata hemocyanin (HtH1) didecamer *[Meissner et al., 2000]. The dark region represents the putative subunit dimer, as the repeating unit within the upper decamer;* ***b) Model of the Chiton hemocyanin decamer, derived from the HtH1 didecamer*** *[Meissner et al., 2000]: one of the homodimers is indicated in dark grey within the quasi-helical wall of the molecule [Harris et al., 2003].*

The 3-D reconstruction from cryo-TEM images of the giant keyhole limpet hemolymph protein megathurin was obtained. Megathurin is a 2x5-mer of a 35000 kDa subunit; its dimensions are 14 nm x 5 nm with a central channel of 2 nm in diameter. Using the 3-D reconstruction of isolated subunit dimers purified from *Acanthochiton fascicularis* hemocyanin, following dissociation and reassociation [Harris et al., 2003]. It has been found that this particular dimer is more stable than those prepared from the subunits of other molluscan species.

The 3D-TEM has been studied for the 1x6-mer arthropodan Hc of the spiny lobster *Panulirus elephas* and compared with the available X-ray data from a different, though closely related, spiny lobster 1x6-mer hemocyanin [Meissner et al., 2003].

Figure. 17 a and **b** show the 0.32 nm X-ray structure of spiny lobster (*Panulirus interruptus*) 1x6-mer hemocyanin [Gaykema et al., 1986] which was successfully fitted into the 0.8 nm 3-D cryo-TEM reconstruction of spiny lobster (*Palinurus elephas*) 1x6-mer hemocyanin [Meissner et al., 2003].

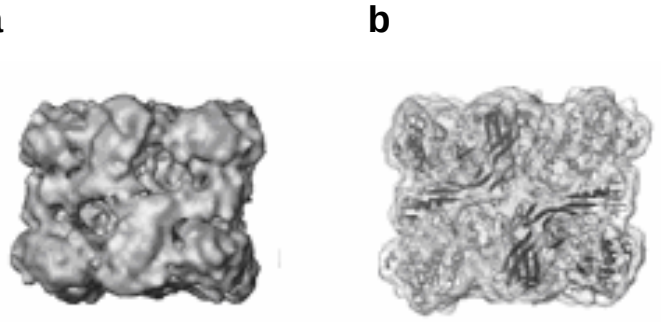

Figure 17. a) 3D-TEM reconstruction of the 1x6-mer hemocyanin from the spiny lobster Palinurus elephas *[Meissner et al., 2003] at a resolution of 0.8 nm;* ***b) X-ray structure of 1x6-mer hemocyanin from the spiny lobster Panulirus interruptus*** *[Gaykema et al., 1986] at a resolution 0.32 nm.*

This combination can now be applied as the basic module to analyze higher order arthropodan hemocyanins as well as oxy- and deoxy- forms [De Haas et al., 1993].

1.1.2.7 Electron microscopy studies of hemocyanins

Electron microscopy has been used for several studies on the structure of hemocyanins. The 3D-structure of *Sepia officinalis* hemocyanin was studied by immunoelectron microscopy [Boisset, N. and Mouche, F. 2000] and the oligomerization states and polymerization properties of keyhole limpet hemocyanin (KLH, from *Megathura crenulata*) [Gebauer et al., 1994; Harris et al., 1993; Harris et al., 1995a; Harris et al., 1995b]. KLH1 apparently exists as a stable didecamer with random clusters of didecamers, whereas KLH2 exists as decamers, didecamers and multidecamers of varying length [Harris and Markl, 1999; Harris et al., 1998; Harris et al., 1997; Gebauer et al., 1999]. *Haliotis tuberculata* [Keller et al., 1999] and *Helix pomatia* [van Breemen et al., 1979] were investigated using transmission and immunoelectron microscopy [Harris and Markl, 1999; Harris et al., 1998].

Aplysia californica hemocyanin has been also electron-microscopically studied [Bevelaqua et al., 1975; Herskovits and Hamilton, 1991] and the presence of di- and multidecamers were found that the latter can be exceptionally long **(Figure. 18)**.

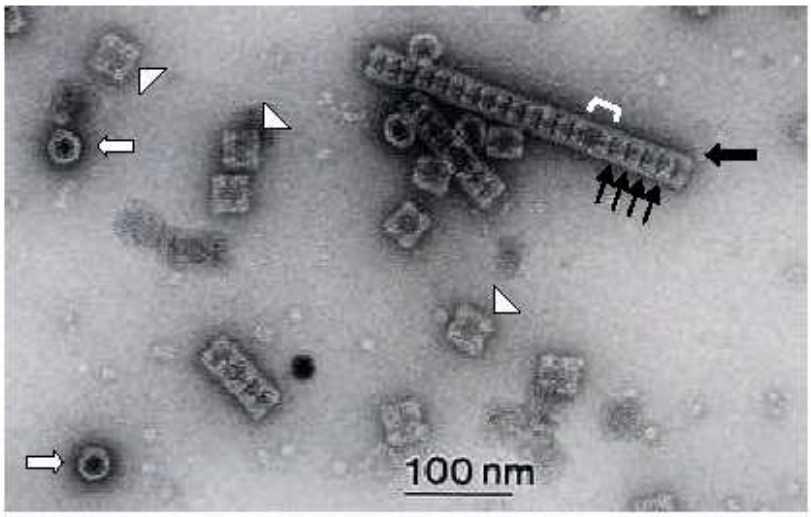

Figure 18. Electron microscopy of negatively stained Aplysia californica hemocyanin *(AcH) showing didecamers in side view (white arrowheads) and top view (white arrows), and multidecamers of varying length (large black arrow). Note that multidecamers consist of a central didecamer (white bracket) to which single decamers (small black arrows) are attached. The bar represents 100 nm [Lieb et al., 2004].*

Compared to other gastropod hemocyanins capable for multidecamer formation under native conditions, in KLH2 and RvH1 these structures can be extremely long [Gebauer et al., 1994; Dolashka-Angelova et al., 2003]. A similar capacity for the formation of very long multidecamers is observed in *Aplysia* [Herskovits et al., 1995]. So far, sequence alignments have given no clue towards an explanation why certain gastropod hemocyanins form very long multidecamers, others form very short ones and again others are restricted to didecamers, or just decamers, as in the Chitons. Strictly, didecameric hemocyanins are expressed in pulmonates, and pulmonate hemocyanins such as those from *Helix pomatia* and *Lymnea stagnalis* are heavily glycosylated [Hall et al., 1977]. HtH1, which is also inefficient to form multidecamers at least in buffers simulating native conditions, shows a larger number of potential N-glycosylation sites than HtH2. In this context, it is interesting to note that *Aplysia californica* hemocyanin (AcH) contains only seven potential N-glycosylation sites: two in AcH-e and one each in AcH-a, AcH-d, AcH-f, AcH-g, and AcH-h **(Figure 19)**.

1.1.2.8 Glycosylation of hemocyanins

Most Hcs are glycoproteins, although there are large differences in their carbohydrate contents and their monosaccharide composition, and both, O-linked and N-

linked oligosaccharides were identified. The monosaccharide compositions and the carbohydrate contents of Hcs from various arthropodan species usually range between 0.1 and 2%, and D-mannose (Man) and *N*-acetyl-D-galactosamine (GalNAc) are the most abundant residues [Van Kuik et al., 1990; Markl et al., 1976]. For the Hc from the centipede *Scutigera coleoptrata*, an exceptionally high carbohydrate content (4.9%) was found [Waxman, 1975]. Carbohydrate contents of molluscan Hcs have been studied from proteins isolated from the terrestrial snail *Helix pomatia* [Lommerse et al., 1975], the fresh water snail *Lymnaea stagnalis* [Hall et al., 1977], the marine gastropod *Rapana thomasiana* [Stoeva, 1995] and the keyhole limpet *Megathura crenulata* [Stoeva et al., 1999]. A relatively high carbohydrate content, between 2 and 9% (w/w), is typical for these molluscan Hcs, and as monosaccharides xylose, fucose (Fuc), 3-*O*-methyl-D-galactose (3MeGal), Mannose, D-galactose (Gal), GalNAc and *N*-acetyl-D-glucosamine (GlcNAc) were determined. The carbohydrate moiety of molluscan Hcs has recently received particular interest for their immunostimulatory properties [Harris and Markl, 2000].

Studies on *Lymnea stagnalis* hemocyanin and KLH show the existence of a variety of glycan side chains [Hall et al., 1977; Kurokawa et al., 2002], and in case of KLH it has been demonstrated that most of the FUs are indeed glycosylated [Stoeva et al., 1999]. It was suggested that in *Aplysia* hemocyanin most, if not all potential sites also carry N-linked glycans **(Figure 19)**. This modification would slightly increase the molecular mass of AcH (from 387 kDa for the “naked” polypeptide to *ca.* 400 kDa). In *Haliotis*, *Megathura* and *Octopus*, potential N-glycosylation sites are missing in case of FU-c, which agrees with the result from *Aplysia* hemocyanin. There is evidence for O-linked sugar components in KLH2-c [Stoeva et al., 1999], which has still to be investigated for AcH-c. HtH1-h has two potential N-glycosylation sites in quite unusual positions **(Figure 19)**. Both sites are localized on the same face which in all other FUs, including HtH2-h, is not N-glycosylated. It has therefore been speculated that this putative glycosylation might help to inhibit multidecamers formation in HtH1, whereas its absence allows multidecamers

formation in HtH2 [Lieb et al., 2000]. AcH also lacks such a site, which would fit the hypothesis **(Figure 19)**.

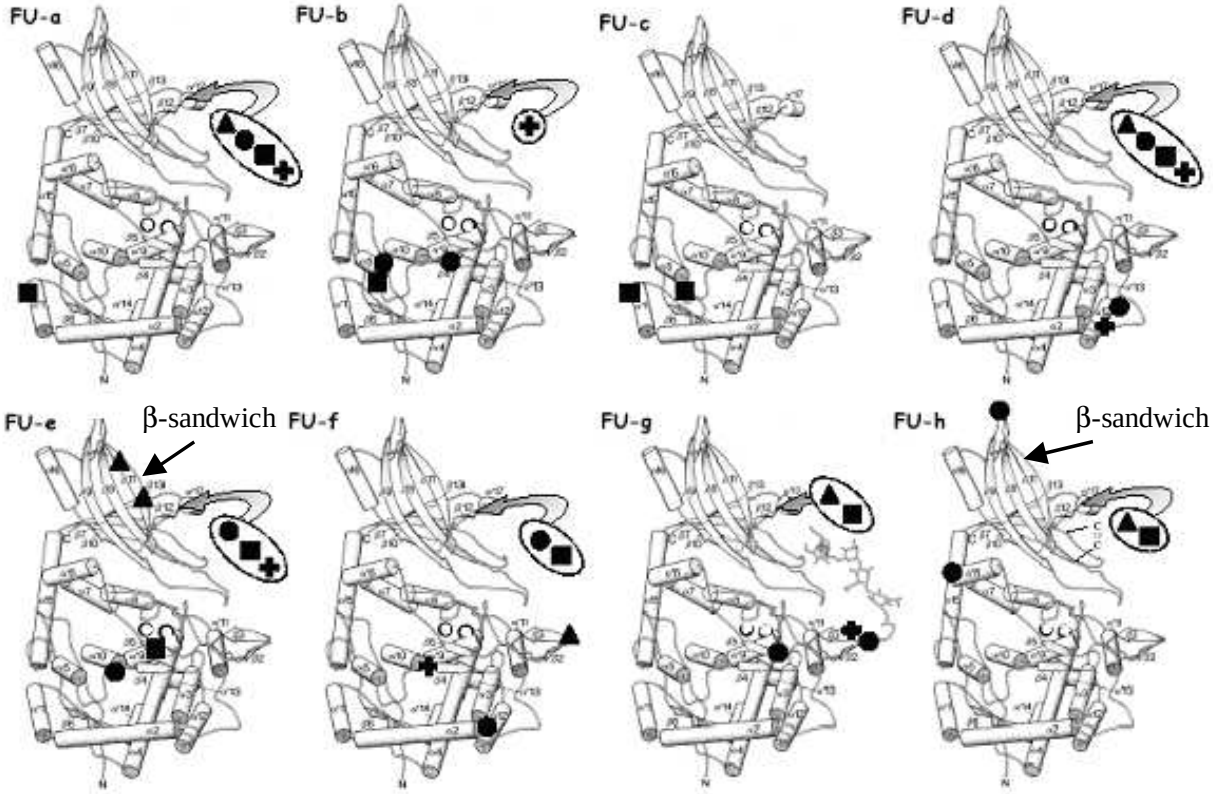

Figure 19. Projection of potential N-glycosylation sites of Aplysia californica (AcH) (▲) in comparison to Haliotis tuberculata* hemocyanin (*HtH1) (●), (HtH2) (■) and Octopus dofleini* hemocyanin (*OdH) (+) into the X-ray structure of OdH-g [Cuff et al. 1998] assigned to the different FUs (a,b,c,d,e,f,g,h). *Five FUs of AcH possess a single N-glycosylation site; both positions could allow a sugar side chain in a topology comparable to that found in OdH-g [Keller et al., 1999; Lieb et al., 1999]. In contrast, the two potential N-glycosylation sites in AcH-e are unique. Note that neither of the AcH FUs has a potential N-glycosylation site in other positions of the core domain, in contrast to various FUs of the other molluscan hemocyanins. Interestingly, within the ß-sandwich only HtH1-h (one site) and AcH-e (2 sites) possess additional glycosylation sites. The sum of all N-glycosylation sites shows that at least one sugar side chain might be present on each FU, with the exception of AcH-b and FU-c of several species [Lieb et al.,2004].*

1.1.3 Superoxide dismutases (SODs)

Aerobic metabolism entails the production of reactive oxygen species (ROS) such as the superoxide anion radical (O_2^-), H_2O_2 and the hydroxyl radical. These ROS can cause wide-ranging damage to the living cell through their detrimental effects on key

macromolecules. Oxygen toxicity results, when the level of ROS exceeds the capacity of the cell's defense, i.e. an oxidative stress occurs. There is no doubt that ROS reactions are implicated in the pathology of over 50 human diseases (neurodegenerative, cardiovascular, brain and lung diseases, arteriosclerosis, viral infection, etc.). Much of the experimental evidence accumulated in recent years suggests a role for ROS in tumor initiation, promotion and progression.

Superoxide dismutases (SODs) are metalloenzymes, involved in the physiological response to oxygen toxicity by their ability to catalyze the dismutation of superoxide anion to molecular oxygen and H_2O_2 [Fridovich, 1995] **(Figure 20)**.

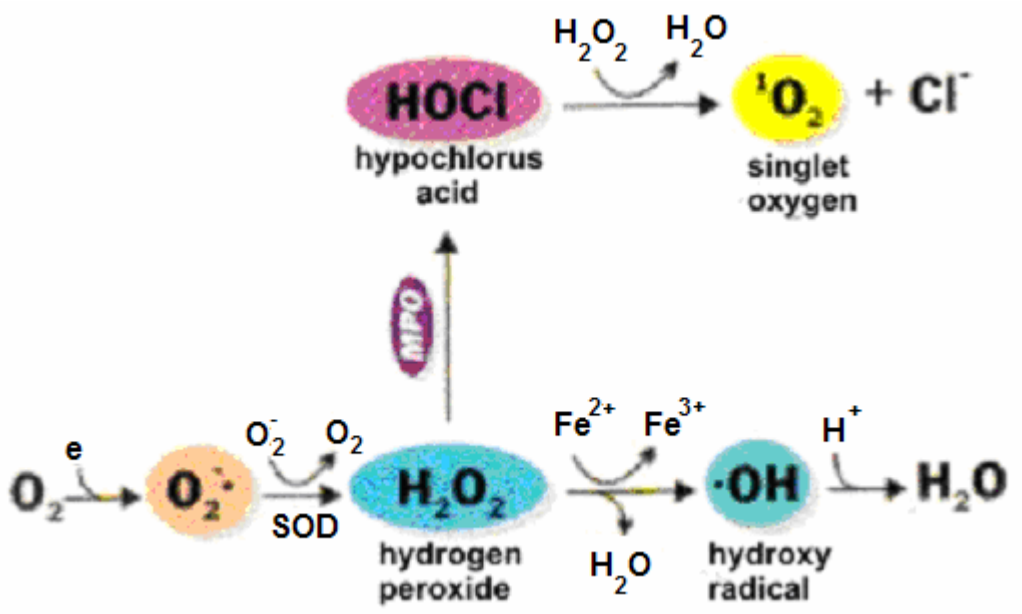

Figure 20. The active oxygen system*. Molecular oxygen is reduced to water in four single-electron steps, where MPO is myeloperoxidase and SOD is superoxide dismutase.*

Reduction of nonradical forms of oxygen is a "forbidden" process and thus usually involves spin-orbit coupling by a heavy metal or a halide atom or excitation to singlet state. An example is Fenton's reaction, the reduction of peroxide to water and a hydroxyl radical by ferrous iron. Hydroxyl radical is one of the most powerful oxidizing agents known. Simply put, reducing agents act as prooxidants by reducing nonradical forms of oxygen to radical forms, usually with heavy atom involvement. Similarly, they can act as

antioxidants by reducing radical forms of oxygen, by terminating radical chain reactions or by, for example, reducing hydroperoxides. This dual property can be of great significance. For example, in humans uric acid is probably the primary extracellular antioxidant. On the other hand, a Fenton-type reaction of phagocytized urate with granulocyte-produced peroxide may contribute to the etiology of gout.

Four classes of SOD have been identified, containing either binuclear Cu/Zn or mononuclear Fe, Mn or Ni cofactors [M. Whittaker and J. W. Whittaker, 1998]. Fe-SODs and Mn-SODs show homology and possess identical metal chelating residues at the active site, sharing substantial sequence and three-dimensional structural homology, while the other superoxide dismutases are structurally unrelated. In humans, there are three forms of SOD: cytosolic Cu/Zn-SOD, mitochondrial Mn-SOD, and extracellular-SOD (EC-SOD) [Majima et al., 1998]. SOD catalyses the dismutation of O_2^- by successive oxidation and reduction of the transition metal ion at the active site in a Ping Pong type mechanism with remarkably high reaction rates [Hsieh et al., 1998].

Where are all these SODs present?

- Cu/ZnSOD is found in Eukarya as a cytosolic and extracellular enzyme and in Bacteria as a periplasmic enzyme.
- Mn-SOD is present in mitochondria of eukaryotic aerobes, in cytosol of Bacteria and Archaea and in chloroplasts of plants.
- Fe-SOD is present in the cytosol of Bacteria, Archaea and plants;Ni-SOD in Bacteria as cytosolic enzyme.
- EC-SOD has been isolated first from mammalian sources and then from pathogenic bacteria where it appears to be a pathogenicity factor.

1.1.3.1 Manganese superoxide dismutase (Mn-SOD)

Mn-SOD is a homotetramer (96 kDa) containing one manganese atom per subunit

that cycles from Mn (III) to Mn (II) and back to Mn (III) during the two step dismutation of superoxide. The respiratory chain in mitochondria is a major source of oxygen radicals. Mn-SOD is a nuclear-encoded primary antioxidant enzyme removing superoxide radicals [Guan et al., 1998]. Mn-SOD is a biological important enzyme [Majima et al., 1998].

1.1.3.2 Copper, zinc superoxide dismutase (Cu/Zn-SOD)

Cu/Zn-SOD is another class of enzymes conserved throughout evolution which usually has two identical subunits of about 32 kDa, each containing a metal cluster, the active site, constituted of a copper and a zinc atom bridged by a common ligand His 61 [Banci et al., 1998] **(Figure 21)**.

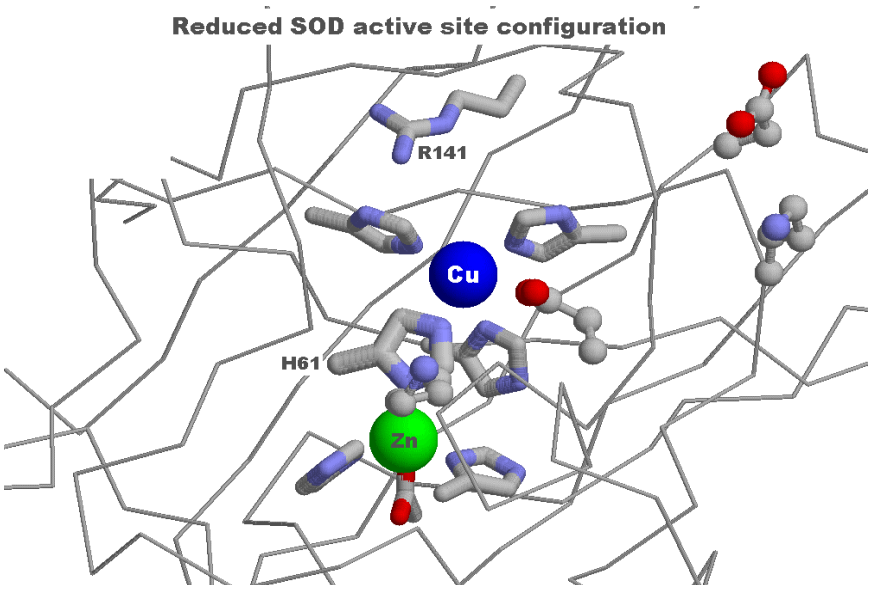

Figure 21. Active site of human Cu/Zn-SOD. *Each monomer binds one copper and one zinc atom via 1 aspartic acid residue and 6 histidine residues, bridged by a common ligand His 61 [Banci et al., 1998].*

The great interest on this enzyme lately is the result of its important physiological role in primary cellular defence against active oxygen species and its 3D-structure concerning structure-function relationships of SODs from pro- and eukaryotes which

contribute to the understanding of the molecular evolution of this enzyme family and the therapeutic application of SOD as an antioxidant.

Research investigations suggest that SOD is an extremely potent antioxidant, probably the most important enzyme in our body for the control of free radicals, keeping our cell membranes intact. Human clinical studies of SOD are still at an early stage, but many scientists [Maxwell and Stojanov, 1996; Kherer, 1993; Trotti, 1997; Sabitha and Shyamaladevi, 1999; Mates, and Sanchez-Jimenez, 1999; Sikka 2001; Bilodeau et al., 2002] claim that SOD:

- reduces the aging process;
- shows effects in treating Alzheimer's disease, musculoskeletal inflammation and osteoarthritis, severe skin diseases and radiation damage either from prolonged sun exposure or due to radiation treatment;
- mitigates cardiovascular and lung failure, and reduces intensive care treatment and inflammation;
- protects against free radical damage, reducing injuries of brain and other organs caused by reperfusion or oxygen deprivation, reduces blood pressure and increased cranial pressure after trauma;
- reduces oncogenesis, tumor promotion, tumor invasiveness and cytotoxic and cardiotoxic effects of anticancer drugs or improves mammalian spermatozoa functions during liquid storage and cryopreservation.

Considerable experimental evidences have accumulated that application of SOD might be beneficial for the treatment of postischemic reperfusion injury [Rios et al., 1999], rheumatoid and osteoarthritis [Kakimoto et al., 1993], brain trauma [Yunoki et al., 1997], and influenza-induced lung pneumonitis [Sidwell et al., 1996]. SODs have been proposed to be clinically useful for a wide variety of applications including prevention of oncogenesis, tumor promotion, tumor invasiveness [Kherer, 1993] and reduction of the

cytotoxic and cardiotoxic effects of anticancer drugs [Trotti, 1997; Sabitha and Shyamaladevi, 1999].

Whereas Mn-SOD was found in all tumors, and the ratio between the activities of Cu/Zn-SOD and Mn-SOD was not different from that of the normal tissues, tumors posses less Cu/Zn-SOD than the more metabolically active tissues [Westman et al., 1981]. Cu/Zn-SOD is believed to play a major role in the first line of antioxidant defence by catalyzing the dismutation of superoxide anion radicals, to form hydrogen peroxide and molecular oxygen.

The fungal strain *Humicola lutea* 103 produces a naturally glycosylated Cu/Zn-SOD. Maximum enzyme productivity of SOD was approximately $300x10^3$ U(kg.wet biomass)$^{-1}$. The novel enzyme was purified to electrophoretic homogeneity. The molecular mass of *H. lutea* Cu/Zn-SOD was calculated to be 31870 Da for the native molecule and 15936 Da for the structural subunits. The N-terminal sequence revealed a high degree of structural homology with Cu/Zn-SOD from other prokaryotic and eukaryotic sources. *H. lutea* Cu/Zn-SOD was used in an *in vivo* model for the demonstration of its protective effect against myeloid Graffi tumour in hamsters. Comparative studies revealed that the enzyme (i) elongated the latent time for tumour appearance, (ii) inhibited tumour growth in the early stage of tumour progression (73–75% at day 10), and (iii) increased the mean survival time of Graffi-tumour-bearing hamsters. Moreover, the fungal Cu/Zn-SOD exhibited a strong protective effect on experimental influenza virus infection in mice. The survival rate increased markedly, the time of survival rose by 5 days, and the protective index reached 86%. The *H. lutea* SOD protected mice from mortality more efficiently compared to the selective antiviral drug ribavirin and to commercial bovine SOD.

1.1.3.3 Extracellular superoxide dismutase (EC-SOD)

EC-SOD is a secretory, tetrameric, Cu/Zn containig glycoprotein (with a high affinity to certain glycosaminogycans, such as heparin and heparan sulfate) found in the

interstitial spaces of tissues and also in extracellular fluids, accounting for the majority of the SOD activity of plasma, lymph, and synovial fluid [Adachi and Wang, 1998]. EC-SOD is not induced by its substrate or other oxidants (xanthine oxidase plus hypoxanthine, paraquat, pyrogallol, alpha-naphthoflavone, hydroquinone, catechol, Fe^{2+} ions, Cu^{2+} ions, buthionine sulphoximine, diethylmalate, *t*-butyl hydroperoxide, cumene hydroperoxide, selenite, citiolone and high oxygen partial pressure) and its regulation in mammalian tissues primarily occurs in a manner coordinated by cytokines rather than as a response of individual cells to oxidants [Buschfort et al., 1997].

1.1.3.4 Nickel superoxide dismutase (Ni-SOD)

Ni-SOD has been purified from the cytosolic fraction of *Streptomyces coelicolor*. It is composed of four identical subunits of 13.4 kDa, stable at pH 4.0-8.0, and up to 70 degrees Celsius. It is inhibited by cyanide and H_2O_2, but minor by the presence of azide. The amino acid composition is different from iron, manganese and copper, zinc SODs. The apoenzyme has no ability to mediate the conversion of superoxide anion to hydrogen peroxide, strongly indicating that Ni^{III} plays a main role for the activity [Young et al., 1996].

1.2 Objects of our investigation

1.2.1 Marine snail *Rapana venosa*

Rapana thomasiana (gastropod) **(Figure 22)** is a marine snail, originally found along the coasts of China and Japan. Fifty years ago this species was transferred to the West coast of the Black Sea, where it adapted. The hemocyanin of the marine gastropod mollusc *Rapana thomasiana* (rename *Rapana venosa*) was collected from animals living on the west cost of the Black Sea and characterized for its biochemical and functional properties.

Figure 22. Shell of the marine snail Rapana venosa *collected from animals living on the west cost of the Black Sea.*

1.2.2 Garden snail *Helix vulgaris*

Snails are fresh water or marine or terrestrial gastropod molluscs usually having an external enclosing spiral shell. There are several kinds of Helix snails: *Helix pomatia* (one of the chief edible snails), *Helix aspersa* (brown snail and serious garden pest having a brown shell with paler zigzag markings), garden snail (any of several inedible snails of the genus Helix; often destructive pests). *Helix vulgaris* is a brown garden snail originally found on the north coast of Black Sea.

Figure 23. Shell of garden snail Helix vulgaris *collected from animals living in Bulgaria.*

1.2.3 *Green crab Carcinus aestuarii*

Carcinus maenas (rename *Carcinus aestuarii*), commonly referred to as the European green crab, is a portunid crab native to northern European coastal waters. In the early 1800's it appeared on the East Coast of the United States. Later, in the 1900's, *C. maenas* successfully invaded the southern coast of mainland Australia and just recently (about 10 years ago) colonized the island state of Tasmania. Green crabs are known to be voracious predators, preferring bivalves and other infaunal organisms, but are also known to prey on other species of crab. *Carcinus maenas* inhabit a wide variety of habitats and environmental conditions and appear to be responsible for broadscale changes in invertebrate communities, including commercially important species. In addition, green crabs may have a myriad of effects in vertebrate and invertebrate populations.

***Figure 24. European green crab (Carcinus aestuarii)**, is a portunid crab native to northern European coastal waters.*

1.2.4 Horseshoe crab *Limulus polyphemus*

The horseshoe crab, *Limulus polyphemus*, is more closely related to chelicerates such as spiders, scorpions, ticks and mites than it is to true crabs and other crustaceans. Horseshoe crabs are considered to be "living fossils" that have evolved little in the past 250 million years. *Limulus* is an ancient genus which has probably existed since the Silurian period (440 to 410 million years ago), and shows little morphological change from

the now extinct genus *Paleolimulus* that lived about 200 million years ago. *Limulus polyphemus* is believed to be the closest living relative of trilobites [Shuster, 1982]. Like all chelicerates, members of the order Xiphosura have a two-part body consisting of a prosoma or head region and an opisthosoma, or abdominal region. The prosoma contains 6 pairs of legs, all of which bear claws except the last pair. The prosoma also contains 2 types of eyes: 2 compound eyes, or ommatidia, are located on either side of the head and 2 simple eyes, or ocelli, are located in the center of the head. The opisthosoma contains an additional 6 pairs of appendages which aid in respiration, reproduction, and locomotion.

Figure 25. Horseshoe crab Limulus polyphemus *have a two-part body consisting of a prosoma, or head region and an opisthosoma, or abdominal region.*

1.3 Methods and techniques

1.3.1 Matrix-assisted laser desorption/ionization (MALDI) mass spectrometry

MALDI-MS is a powerful and versatile new tool for the study of proteins and the required instrumentation is significantly simpler than conventional mass spectrometers. This relative simplicity makes the technique potentially accessible to many biologists. The extent to which MALDI-MS will impact on biological research will depend, to a large degree, both on the production of effective commercial instrumentation and on the development of methods for making MS easily accessible to biologists [Beavis and Chait, 1994].

The mechanism of MALDI is not totally understood, but it is believed to work along the following lines **(Figure 26):**

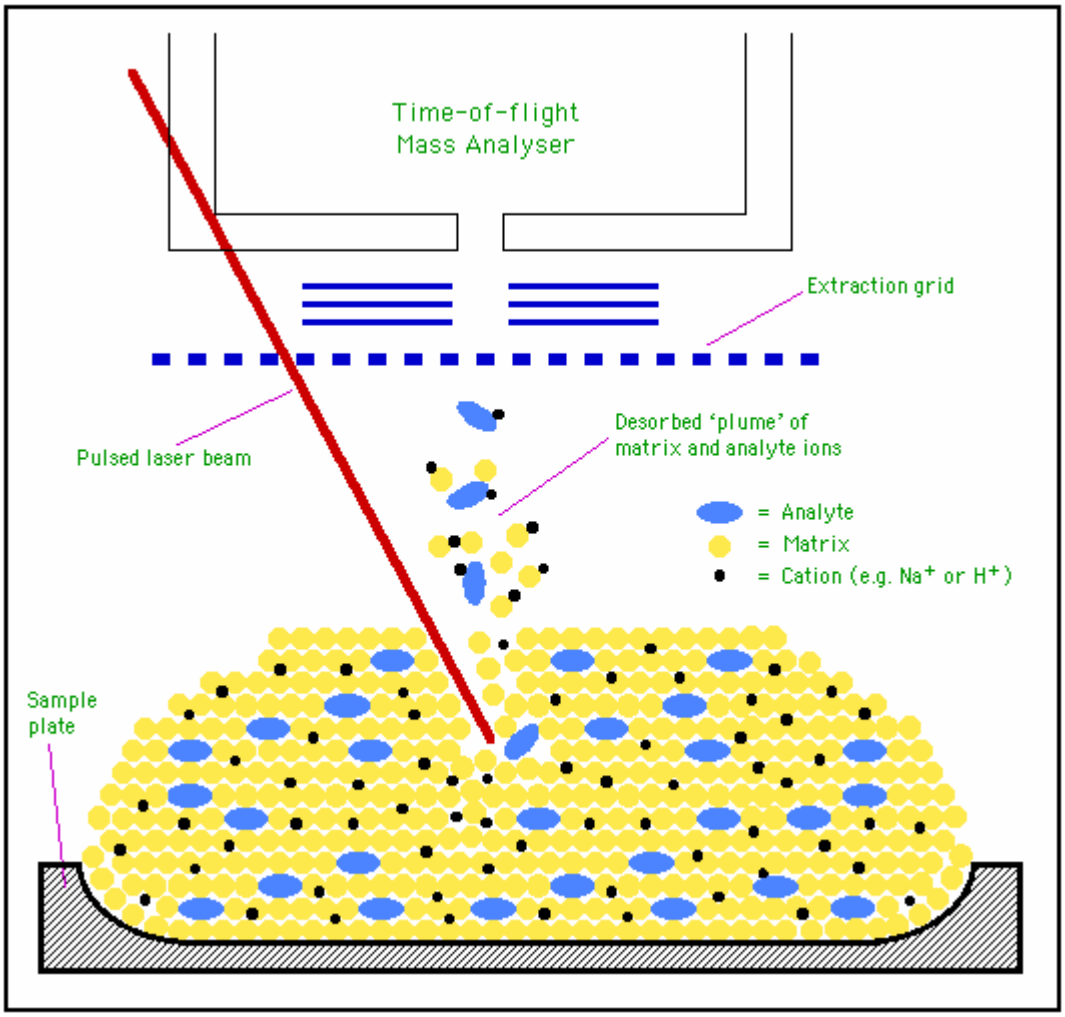

Figure 26. Schematic of Matrix-assisted laser desorption/ionization (MALDI) mass spectrometry *[Paul Gates, 2000].*

(i) The Formation of a solid solution. The analyte molecules are distributed throughout the matrix so that they are completely isolated from one other. This is necessary if the matrix is to form a homogenous 'solid solution' (any liquid solvent(s) used in preparation of the solution are removed when the mixture is dried before analysis).

(ii) Matrix Excitation. Some of the laser energy incident on the solid solution is absorbed by the matrix, causing rapid vibrational excitation, bringing about localized disintegration of the solid solution, forming clusters made up of a single analyte molecule surrounded by

neutral and excited matrix molecules. The matrix molecules evaporate away from these clusters to leave the excited analyte molecule.

(iii) Analyte Ionization. The analyte molecules can become ionized by simple protonation by the photo-excited matrix, leading to the formation of the typical $[M+X]^+$ type species (where X= H, Li, Na, K, etc.). Some multiply charged species, dimers and trimers can also be formed. Negative ions are formed from reactions involving deprotonation of the analyte by the matrix to form $[M-H]^-$ and from interactions with photoelectrons to form the $[M]^-$ radical molecular ions. These ionization reactions occur in the first tens of nanoseconds after irradiance, and within the initial desorbing matrix/analyte cloud. It is in this way that the characteristic MALDI spectra are created, typically giving large signals for species of the type $[NM+X]^{n+}$ (N * n) [Paul Gates, 2000].

MALDI-MS is versatile and effective for the analysis of peptides and proteins because of the special properties and capabilities of the technique. Some of these capabilities and properties are listed below [Beavis and Chait, 1994].

- Biological samples can be examined without extensive purification.
- Common biochemical additives such as buffers, salts, glycerol, chelating agents, chaotropic agents, certain detergents, etc. do not interfere with the analysis.
- Most classes of proteins can be examined, provided that the protein can be dissolved in appropriate solvents.
- Posttranslationally modified proteins can be measured.
- Useful mass spectra can be obtained from complex mixtures of peptides and proteins.
- Proteins with masses ranging to greater than 100 kDa can be analyzed.
- The total amount of protein required for an analysis is usually in the range 1 - 10 pmole.
- Protein molecular masses can be determined with mass accuracies as high as 1 part in 10,000.
- Complete analyses can be made in a matter of minutes.

1.3.2 Sequence analysis. Edman Degradation

Pehr Edman devised a method for labelling the amino-terminal residue and cleaving it from the peptide without disrupting the peptide bonds between the other amino acid residues. The Edman degradation sequentially removes one residue at a time from the amino end of a peptide [Berg et al., 2002] **(Figure 27)**:

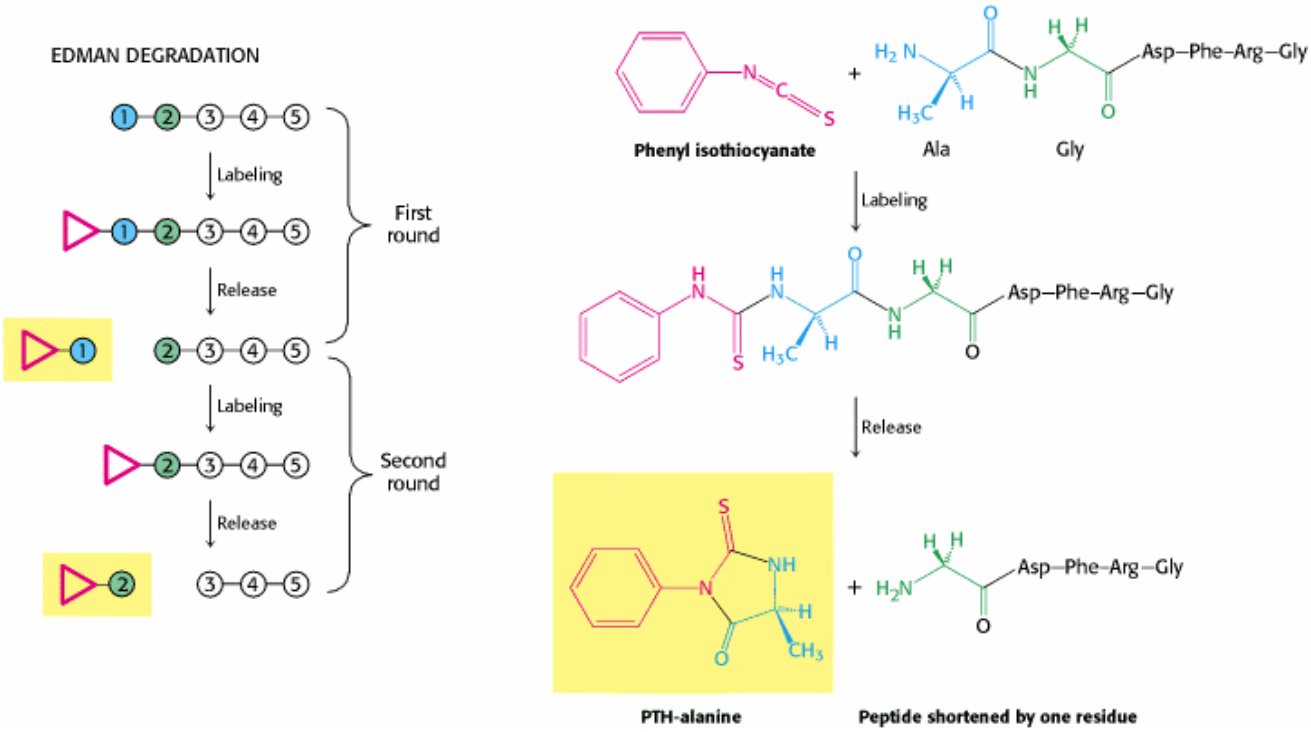

Figure 27. The Edman Degradation. *The labeled amino-terminal residue (PTH-alanine in the first round) can be released without hydrolyzing the rest of the peptide. Hence, the amino-terminal residue of the shortened peptide (Gly-Asp-Phe-Arg-Gly) can be determined in the second round. Three more rounds of the Edman degradation reveal the complete sequence of the original peptide [Berg et al., 2002].*

Phenyl isothiocyanate reacts with the uncharged terminal amino group of the peptide to form a phenylthiocarbamoyl derivative. Then, under mildly acidic conditions, a cyclic derivative of the terminal amino acid is liberated, which leaves an intact peptide shortened by one amino acid. The cyclic compound is a phenylthiohydantoin (PTH)-amino acid, which can be identified by chromatographic procedures. The Edman procedure can then be repeated on the shortened peptide, yielding another PTH-amino acid, which can again

be identified by chromatography. Three more rounds of the Edman degradation will reveal the complete sequence of the original peptide pentapeptide.

The development of automated sequencers has markedly decreased the time required to determine protein sequences. One cycle of the Edman degradation—the cleavage of an amino acid from a peptide and its identification—is carried out in less than 1 hour [Berg et al., 2002].

1.3.3 Circular dichroism spectroscopy

The phenomenon of circular dichroism is very sensitive to the secondary structure of polypeptides and proteins. Circular dichroism (CD) spectroscopy is a form of light absorption spectroscopy that measures the difference in absorbance of right- and left-circularly polarized light (rather than the commonly used absorbance of isotropic light) by a substance.

$$CD = A_L - A_R$$

CD is particularly useful for studying chiral molecules, by which we mean ones that cannot be superposed on their mirror images. It has been shown that CD spectra between 260 and approximately 180 nm can be analyzed for the different secondary structural types: alpha helix, antiparallel beta sheet, turn, and other **(Figure 28)**.

Distinctive CD spectra have been described for pure conformations such as the α helix, β sheets (with different ones sometimes being given for parallel and anti-parallel sheets), β-turns, and also the random coil. At least in principal, the CD spectrum of a native protein is then the sum of the appropriate percentages of each component spectrum.

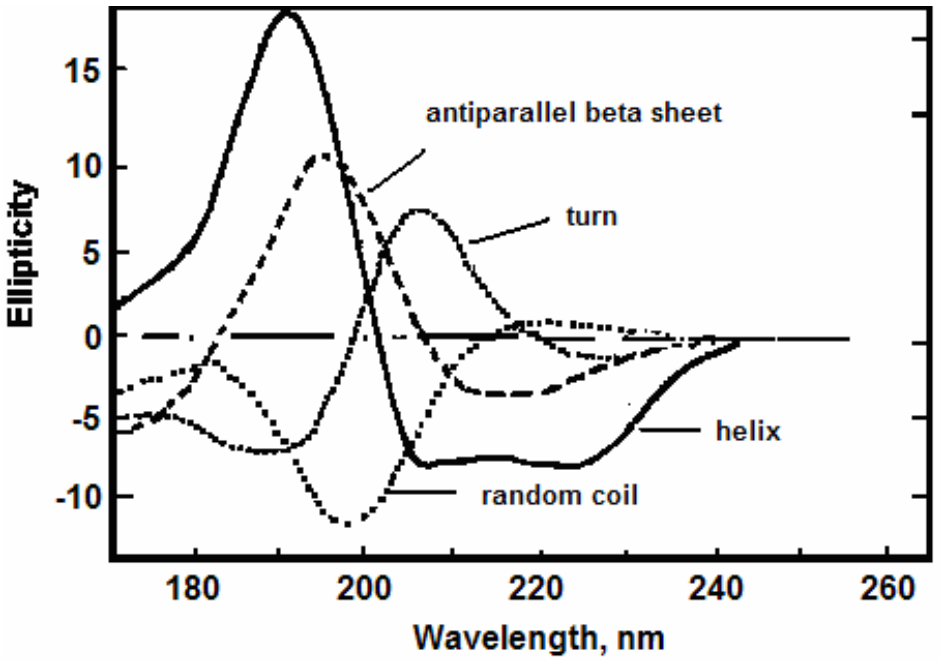

Figure 28. The different secondary structural types: alpha helix *with negative peak and separate maxima of similar magnitude at 222 nm and 208 nm and positive peak at 190 nm;* ***antiparallel beta sheet*** *with a negative band at about 216 nm and a positive band of magnitude near 195 nm;* ***random coil*** *with negativ peak at about 200nm and positive peak at 220nm.*

α - helix

The α helix is the dominant secondary structure in many proteins and on average accounts for about one-third of the residues in globular proteins. The CD spectra of α helices are characterized by a negative peak with separate maxima of similar magnitude at 222 nm and 208 nm.

β - sheet

The CD characterization of β sheets has proven to be more difficult than that of α helices due to the practical reason that they are less soluble in solvents with a good UV transmission and due to the intrinsic reason that they are generally structurally less well definded: they may be parallel or anti-parallel and of varying lengths and widths.

The general characteristics of β sheets CD may be taken to be a negative band at about 216 nm and a positive band of magnitude near 195 nm.

β - turn

The label β-turn is usually used to include all possible turns that occur, not simply the ones that enable a single strand to become an antiparallel β sheet.

Modern secondary structure determination by CD are reported to achieve accuracies of 0.97 for helices, 0.75 for beta sheet, 0.50 for turns, and 0.89 for other structure types [Manavalan and Johnson, 1987].

The differential absorption of radiation polarized in two directions as a function of frequency is called dichroism. When applied to plane polarized light, this is called linear dichroism; for circularly polarized light, circular dichroism. We can think of linear polarized light as the result of two equal amplitudes of opposite circular polarization. After passing through an optically active sample, circularly polarized light will be changed in two aspects.

Linear dichroism is the difference in absorption of light linearly polarized parallel and perpendicular to an oriented axis:

$$LD = A_{\parallel} - A_{\perp}$$

Linear dichroism is used with systems that are either intrinsically oriented or are oriented during the experiment.

Using CD, these different transitions are more clearly evident (no one has had success predicting secondary structure content from simple UV spectra). Exciton splitting of the p → p* transition results in the negative band at 208 and positive band at 192. The three aromatic side chains that occur in proteins (phenyl group of Phe, phenolic group of Tyr, and indole group of Trp) also have absorption bands in the ultraviolet spectrum. However in proteins, the contributions to the CD spectra in the near UV (where secondary structural information is located) is usually negligible. The disulfide group is an inherently asymmetric chromophore as it prefers a gauche conformation with css = xb1 90xb0 , corresponding to a right- or left-handed helical sense and can lead to a broad CD

absorption around 250 nm. Aromatic residues, if unusually abundant, can have significant effects on the CD spectra in the region < 230 nm complicating analysis.

CD is now a routine tool in many laboratories. There are many advantages of CD as a probe of biological molecules.

- The experiments are simple and quick to perform.
- CD is uniquely sensitive to the asymmetry of a system, and as the increasing emphasis on developing enantiomerically pure drugs shows, asymmetry can be a key feature of the interaction of a drug with its receptor.
- CD experiments deal with solution phases. This is important for biological systems because the crystallization process can change the structure of a molecule.
- CD experiments require significantly lower concentrations that are appropriate for nuclear magnetic resonance (NMR). This means, CD not only requires less sample, but it can be used for systems where the concentrations required for NMR may change the system entirely.

1.3.3.1 Circular dichroism data analysis

The essential features of a CD spectropolarimeter are a source of (more or less) monochromatic left and right circularly polarized light and means of detecting the difference in absorbance of the two polarizations of light. The normal method of achieving these requirements, because the CD of molecules is generally quite weak, is to implement a polarization phase-modulator technique.

Most CD spectropolarimeters, although they measure differential absorbance, produce a CD spectrum in units of ellipticity θ, in millidegrees versus λ, rather than ΔA versus λ. The conversion between these two is:

$$CD = A\ (absorbance\ units) = CD = A_L - A_R$$

$$\theta_r = \frac{2.303}{4}.\left(A_L - A_R\right).\left[rad\right] \quad (1)$$

which can be easily converted into degrees

$$\theta_d = \frac{2.303}{4}.\left(A_L - A_R\right).\frac{180}{\pi}.\left[\deg\right] \quad (2)$$

To be able to compare these ellipticity values we need to convert into a normalized value. The unit most commonly used in protein and peptide work is the mean molar ellipticity per residue. We need to consider path length *l*, concentration *c*, molecular weight *M* and number of residues

$$\theta_{mr} = \theta_d.\frac{M}{c.l.n_r} \quad (3)$$

in proper units (CD spectroscopists use decimol)

$$\theta_{mrd} = \frac{\theta_{mr}}{10}\left[\deg.\frac{g}{dmol}.\frac{cm^3}{g}.\frac{1}{cm}.\frac{1}{residue}\right] \quad (4)$$

which finally reduces to

$$\theta_{mrd} = \frac{\theta_{mr}}{10}\left[\frac{\deg.cm^2}{dmol.residue}\right] \quad (5)$$

The values for mean molar ellipticity per residue are usually in the 10.000's

Like the other forms of absorption spectroscopy (UV/Vis, IR, etc.), CD is particularly powerful in monitoring conformational changes. In the region of 230-178 nm, one expects to observe effects of backbone conformational changes while CD effects at longer wavelengths (>230 nm) should isolate aromatic chromophore contributions.

1.3.4 Fluorescence spectroscopy

Absorption spectroscopy (nonfluorescent compounds) and fluorometry allows investigation of a number of molecular properties. These include fluorescence emission and excitation spectra, and associated with these spectra the intensity, shape peak position (wavelength), loss of energy, fluorescence lifetime, fluorescence quantum yield, and fluorescence polarization. In many cases any one or a combination of these properties of a fluorescent molecule allows its direct analysis.

The fluorescences of aromatic amino acids have been of much analytical interest. All of these acids show two absorption bands in the UV region. The higher wavelength absorption bands are ca. 280 nm for tryptophan, 277 nm for tyrosine, and 258 nm for phenylalanine. The fluorescence is at ca. 348 nm for tryptophan, 303 nm for tyrosine, and 282 nm for phenylalanine. Among these, tryptophan has the largest molar absorptivity and, hence, the fluorescence observed in proteins is dominated by this type of amino acid. The fluorescence of the residues of aromatic amino acids present in almost all proteins and fluorescent coenzymes, including flavines and nicotinamide, or of fluorescent molecules introduced in biomolecules as probes allow direct analysis.

The mechanisms by which electronically excited molecules come to ground state are given by the Jablonski diagram as shown in **Figure 29**. The absorption of a photon takes the molecule from ground state (singlet state, S0) to either first excited state (singlet state S1) or second excited state (S2). Then the excited molecule relaxes to the lowest vibronic level of the first excited state through internal conversion (IC). Now it can relax from the singlet excited state to the ground state *via* three mechanisms. Firstly, by emitting a photon (radiative process), secondly without emitting a photon (nonradiative mechanim) and thirdly shifting to a triplet state (T1) by intersystem crossing (ISC) which is also a nonradiative process. The transition from triplet (T1) to ground singlet state is forbidden and hence is a very slow process relative to florescence. Emission from T1 is called phosphorescence, and generally is shifted to longer wavelengths relative to the

fluorescence. Also the excited state S1 can be deactivated by a quenching reaction in which a quencher Q quenches the excited state of the fluorophore S1 through an excited state reaction.

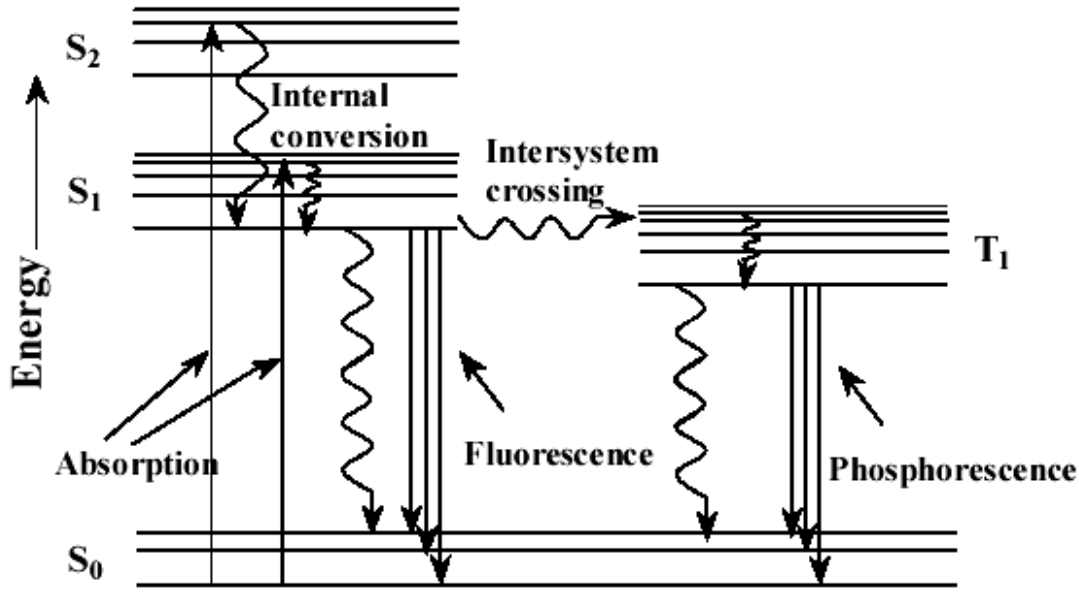

Figure 29. Jablonski diagram showing the energy levels and various processes in an electronically excited molecule.

Fluorescence spectroscopy is a powerful research tool for the investigation of excited-state molecular behaviour. Such information is rather difficult to obtain and the procedures are expensive. Direct analysis of the fluorescent species allows an estimation of a number of important properties including lifetime, dipole moment, binding, size, diffusion, interaction with the surrounding environment, and, hence, knowledge about the microscopic environment.

1.3.4.1 Excitation and fluorescence emission spectra

The fluorescence from a molecule can be represented in two different ways: (a) by plotting the fluorescence emission probability (or signal intensity) upon excitation at a fixed wavelength [normally the peak (excitation) wavelength] or (b) by plotting the fluorescence intensity at a fixed emission wavelength with variable (excitation)

wavelength. Each of these above approaches results in two different types of spectra, that is, the fluorescence emission spectrum wherein the wavelength distribution of the emitted radiation from an excited molecule is seen, and the excitation spectrum wherein the fluorescence distribution at various excitation wavelengths is observed. In practice, a fluorescence spectrum is recorded by irradiating the sample with a fixed wavelength and scanning all the emission wavelengths, while the excitation spectrum is obtained by keeping the emission wavelength constant and scanning the excitation wavelengths. Both types of spectra are normally presented on a wavelength scale calibrated in nanometers (nm).

Fluorescence quantum yields are determined by the following equation:

$$Q_x = Q_{st}\left(\frac{F_x}{A_x}\right)\left(\frac{A_{st}}{F_{st}}\right)\left(\frac{\lambda_x}{\lambda_{st}}\right) \quad (6)$$

where Q_x, F_x and A_x are the emission quantum yield, the emission intensity at wavelength λ and the absorbance at the excitation wavelength, respectively, for the protein sample; Q_{st}, F_{st} and A_{st} are the same parameters for the reference standard. N-acetyltryptophanamide (Ac-Trp-NH_2) with a quantum yield of 0.13 was chosen as a standard.

The efficiency e of the tyrosine-to-tryptophan energy transfer was calculated using the relationship:

$$Q = Q_{Trp}\left[\, f_{Trp}(\lambda) + e.f_{Tyr}(\lambda)\right] \quad (7)$$

where Q is the fluorescence quantum yield of the protein sample at the excitation wavelength, Q_{trp} is the fluorescence quantum yield of the tryptophyl residues in the protein molecule after excitation at 300 nm and $f_{Trp}(\lambda)$ and $f_{Tyr}(\lambda)$ are the fractional absorptions of tryptophan and tyrosine, respectively, at the excitation wavelength λ, calculated from their molar ratio in the protein.

The results of the quenching reactions between the excited tryptophyl side chains and acrylamide were analyzed according to the Stern-Volmer equation :

$$\frac{F_0}{F} = 1 + K_{sv}[X] \quad (8)$$

where F_0 and F are the fluorescence intensities at an appropriate emission wavelength in the absence and presence of quencher, K_{sv} is the quenching constant and [X] the quencher concentration. The inner filter effect due to acrylamide was corrected by the factor:

$$Y = \frac{anti\log\ (Abs_{exc} + Abs_{emiss})}{2} \quad (9)$$

where Abs_{exc} and Abs_{emiss} are the absorbance at the excitation and emission wavelength respectively.

2. Aim of this study

The purpose of this thesis was to study the structure and properties of the metal - containing proteins, hemocyanins and superoxide dismutase. Both proteins contain a copper ion in their active site and are useful in immunotherapy of various diseases.

The structure of hemocyanins from different species was studied: molluscan hemocyanin of *Rapana venosa* and the arthropodan hemocyanins from Chelicerata *Limulus polyphemus* and Crustacea *Carcinus aestuarii* and their structures were compared with those of other molluscs and arthropods. The thesis describes in detail the amino acid sequence and carbohydrate structure of a structural subunit 2 of *Carcinus aestuarii* hemocyanin and of functional units RvH1-a and RvH1-f of *Rapana venosa* hemocyanin in order to get more insight into structure-function relationships of these respiratory proteins.

Several spectroscopic methods, such as fluorescence spectroscopy and circular dichroism were used to study the unfolding of these hemocyanin at different temperatures, pH values and also at different concentrations of guanidine hydrochloride and urea.

Furthermore the complete amino acid sequences of *Humicola lutea* superoxide dismutase and its carbohydrate side chain were determined as well as its potential application in medicine.

3. Materials and Methods

3.1 Materials

3.1.1 Chemicals

Acetic acid	Merck, Darmstadt
Acetonitrile	Merck, Darmstadt
Ammonium bicarbonate	Merck, Darmstadt
Calcium chloride	Serva, Heidelberg
Comassie Brillant Blue R-250	Serva, Heidelberg
Copper sulfate	Merck, Darmstadt
α-Cyano-4-hydroxycinnamic acid	Sigma, Deisenhofen
2,5-Dihydroxybenzoic acid	Sigma, Deisenhofen
2,4-Dinitrophenylhydrazine (DNPH)	Sigma, Deisenhofen
Disodium hydrogen phosphate	Merck, Darmstadt
EDTA (ethylenediaminetetraacetate)	Merck, Darmstadt
Formic acid	Merck, Darmstadt
Glacial acetic acid	Merck, Darmstadt
Glycine	Merck, Darmstadt
Guanidine hydrochloride	Serva, Heidelberg
Hydroxylamine hydrochloride	Serva, Heidelberg
Magnesium chloride	Merck, Darmstadt
β-Mercaptoethanol	Sigma, Deisenhofen
Methanol	Merck, Darmstadt
N-acetyltryptophan amide	Sigma, München
Nitro blue tetrazolium (NBT)	Boehringer, Mannheim
PMSF (phenylmethanesulfonyl fluoride)	Sigma, Deisenhofen
Phosphate-buffered saline (PBS)	Boehringer, Mannheim

Physiological saline (PBS)	Boehringer, Mannheim
Potassium chloride	Merck, Darmstadt
Potassium cyanide	Merck, Darmstadt
Ribavirin	Sigma, Deisenhofen
Sodium bicarbonate	Sigma, Deisenhofen
Sodium dodecylsulfate (SDS)	Bio-Rad, Munich
Sodium chloride	Merck, Darmstadt
Sodium citrate	Merck, Darmstadt
Sodium hydroxide	Merck, Darmstadt
Sodium phosphate	Merck, Darmstadt
Sucrose	Merck, Darmstadt
TFA trifluoroacetic acid	Merck, Darmstadt
Tris	Merck, Darmstadt
Uranyl acetate	Merck, Darmstadt
Urea	Merck, Darmstadt
4-Vinylpyridine	Sigma, München

3.1.2 Enzymes and proteins

β1-2,3,4,6-N-Acetylglucosaminidase	Sigma, Deisenhofen
Beer agar	BAS, Sofia, Bulgaria
Bovine insulin	Sigma, Deisenhofen
Bovine pancreas	Sigma, Deisenhofen
Bovine serum albumin	Sigma, Deisenhofen
Carboanhydrase	Sigma, Deisenhofen
Carcinus aestuarii Hemocyanin	University Padova, Italy
Catalase	Sigma, Deisenhofen

Chymotrypsin	Boehringer, Mannheim
Cooper zinc superoxide dismutase	BAS, Sofia
Crystalline bovine albumin	Sigma, Deisenhofen
Egg albumin	Sigma, Deisenhofen
β-Galactosidase	Boehringer, Mannheim
β1-3,4,6-Galactosidase	Sigma, Deisenhofen
Glucose-6-phosphate-dehydrogenase (G6PD)	Sigma, Deisenhofen
Homarus americanus hemocyanin	University Padova (Italy)
Immunoglobulin G (IgG)	Applied Biosystems, Weiterstadt
Limulus polyphemus hemocyanin	Sigma, Deisenhofen
Lysozyme	Seikagaku, Japan
Lysyl endopeptidase	Sigma, Deisenhofen
Maia squinado hemocyanin	University Padova (Italy)
Manganese superoxide dismutase	BAS, Sofia, Bulgaria
α1-2,3,6-Mannosidase	Sigma, Deisenhofen
α1-2,3-Mannosidase	Sigma, Deisenhofen
Megathura crenulata hemocyanin	Biosyn, Fellbach
Neuraminidase	BAS, Sofia, Bulgaria
Palinurus vulgaris hemocyanin	Sigma, Deisenhofen
Rapana venosa hemocyanin	BAS, Sofia, Bulgaria
Phosphorylase b	BAS, Sofia, Bulgaria
PNGase F, peptide N-glycosidase F	Roche, Mannheim
Trypsin	Sigma, Deisenhofen

3.1.3 Tests, kits and other materials

BioFocus 3000 CE instrument	Bio-Rad, Munich
Protran nitrocellulose membranes (0.45 μm)	Schleicher + Schuell, Dassel
Whatman № 4 filter	Clifton, USA
Speed vacuum evaporator	Savant, New York, USA
Harvard syringe pump (5 μl/min)	Harvard, USA
Ultracentrifuge Mod L50 at 18 000 xg	Hettich, Tuttlingen
Fused silica capillary 50 cm x 50 μm (I.D.)	Grom, Herrenberg
Nitrogen-filled flash lamp	Bio-Rad, Munich
Pulsed liquid sequencer Model 473 A	Applied Biosystems, Weiterstadt
Shaker (220 rpm)	Bohemia, NY, USA
Petri dishes	BAS, Sofia, Bulgaria
Semidry electroblotter	Jancos, Denmark
Orcinol/H_2SO_4 test	Calbiochem, Schwalbach
Bovine testes	BAS, Sofia, Bulgaria
Humicula lutea 103 fungal strain	BAS, Sofia, Bulgaria
Mice	BAS, Sofia, Bulgaria
Rabbits	BAS, Sofia, Bulgaria

3.1.4 Equipment

3.1.4.1 Chromatography columns

Aquapore RP-300 column (2.1x30 mm)	Applied Biosystems, Weiterstadt
DEAE cellulose - 52 column (3.5x10 cm)	Serva, Heidelberg
Diethylaminoethyl cellulose (DEAE)	Roth, Karlsruhe
HiLoad 26/10 Sepharose Q	Applied Biosystems, Weiterstadt
LiChrospher 60 RP column (250x4 mm)	Applied Biosystems, Weiterstadt

Mono Q 10/10 (100x3.6 mm)	Pharmacia, Uppsala, Sweden
Nucleosyl 100 RP-18 column (250x10 mm)	Machery-Nagel, Dueren
Resource Q 6 ml column	Pharmacia, Uppsala, Sweden
Sephadex G-150 column	Pharmacia, Freiburg
Superdex 300 (2x30 cm)	Pharmacia, Freiburg

3.1.4.2 HPLC/FPLC

FPLC Mono Q system	Pharmacia, Uppsala, Sweden
FPLC Resource 6 ml column	Pharmacia, Uppsala, Sweden
HPLC system	Macherey-Nagel, Dueren
HPLC system 2200	LKB Bromma, Bromma, Sweden
HPLC system BT8000	Biotronik, Maintal

3.1.4.3 Lyophylisation

LOC-1-Lyophilisator	Christ, Osterode/Harz

3.1.4.4 Matrix-assisted laser desorption/ionization (MALDI) mass spectrometry

Electrospray ionization mass spectrometer	Shimadzu Europe, Duisburg
Kratos Kompact MALDI III	Shimadzu Europe, Duisburg
Voyager	PerSeptive Biosystems, Wiesbaden
Triple quadrupole mass spectrometer	Finnigan MAT, Bremen

3.1.4.5 Sequence analysis

Pulsed Liquid Protein Sequencer 494A	Applied Biosystems, Weiterstadt

3.1. 4.6 Circular dichroism

J-720 spectropolarimeter	Jasco, Tokyo, Japan
Thermostat model RTE-110	Neslab, Newington, USA
Digital programming controller	Neslab, Newington, USA

3.1.4.7 UV-Spectroscopy

UVIKON spectrophotometer, model 930	Kontron Instruments, Eching

3.1.4.8 Fluorescence spectroscopy

Fluorescence spectrometer LS 50	Perkin Elmer, Ueberlingen
System PRA 2000 spectrofluorimeter	Perkin Elmer, Ueberlingen

3.1.4.9 Electron microscopy

Philips CM 10 TEM	Philips, Eindhoven, Holland

3.2 Methods

3.2.1. Preparation of *Rapana venosa* hemocyanin and its structural subunits.

Rapana venosa hemocyanin was isolated from marine snails, living in the Black Sea. Hemolymph was centrifuged at 5000 xg at 4℃, and PMSF (phenylmethanesulfonyl fluoride) was added to inhibit proteases. The clear, deep blue supernatant was dialyzed over night against 10 mM Tris/HCl buffer (pH 7.0**)** containing 20 mM $CaCl_2$ and then the hemocyanin was separated from the hemolymph by ultracentrifugation (Spinco-Beckman Mod L50) at 18 000 xg for 4 h. Native Hc was purified from the hemolymph of *Rapana venosa* Hc, as described previously [Boteva et al., 1991]. Before use, the protein, stored at -20℃ in the presence of 18% sucrose, was dialyzed at 4℃ against the desired buffer. Dissociation of native Hc was achieved by dialyzing the protein against 0.13 M glycine/NaOH buffer, pH 9.6, and RvH1 and RvH2 were purified by means of an ion-

exchange HiLoad 26/10 Sepharose Q high performance column using a FPLC system. Elution was performed with eluent A (50 mM Tris/HCl buffer, pH 8.5, containing 10 mM EDTA) and eluent B (1 M NaCl in buffer A) with a non-linear gradient program: 0% B for 10 min, then 0-100% B in 80 min at a flow rate of 7 $ml.min^{-1}$. Two electrophoreticallly pure structural subunits were isolated.

3.2.2 PAGE and SDS polyacrylamide gel electrophoresis.

SDS polyacrylamide gel electrophoresis was carried out as described by Laemmli [Laemmli, 1970] using a 10% gel and Comassie Brillant Blue as stainer. The samples were run at 23℃ with a current of 60 mA. The molec ular masses were calculated by comparison with a standard protein mixture containing: a) lysozym (14 kDa), carboanhydrase (29 kDa), egg albumin (45 kDa), bovine serum albumin (66 kDa) and phosphorylase b (97.4 kDa).

3.2.3 Amino acid sequence of RvH1 and RvH2

Each subunit was further purified on a HPLC Nucleosil RP C18 column using 0.1% TFA in H_2O as loading buffer and 0.085%TFA (eluent A), 80% acetonitrile in H_2O and 0.05 % TFA as eluting solution (eluent B). The following conditions were used: 10% B for 10 min followed by 10-100% B within 70 min at a flow rate of 1 $ml.min^{-1}$. Peak fractions were dried and after dissolving in 40% methanol, 1% formic acid, they were subjected to automated Edman N-terminal sequencing (Procise 494A Pulsed Liquid Protein Sequencer, Applied Biosystems GmbH, Weiterstadt, Germany).

3.2.4 Dissociation-reassociation of the hemocyanin subunits RvH1 and RvH2

The dissociation and reassociation behaviour of RvH and its two isoforms RvH1 and RvH2 were studied by electron microscopy. For EM studies, samples of native RvH were dialyzed against 50 mM Tris/HCl stabilizing buffer (SB), pH 7.0, containing different

concentrations (10 and 100 mM) of, both, $CaCl_2$ and $MgCl_2$. The dissociation of the native molecule into its structural subunits RvH1 and RvH2 was performed by overnight dialysis at 4℃ against 0.13 M Gly/NaOH buffer, pH 9.6. Reas sociation of the isoforms from the fully dissociated state at pH 9.6 was achieved by dialysis against the stabilizing buffer (50 mM Tris, pH 7.0, containing either 10 or 100 mM of, both, $CaCl_2$ and $MgCl_2$) at 4℃. After several days or weeks, the samples were taken for negative staining for EM studies. The stability of the multidecameric forms of RvH1 and RvH2 were investigated after dialysis of the proteins against the same buffer, but with different pH values (pH 7.0, 8.6, 9.2 and 9.6).

3.2.5 Electron microscopy (EM)

Studies of EM specimens were performed using a Philips CM 10 electron microscope with a 30 mm objective aperture. Samples were adsorbed for 60 s to a glow-discharged pistoform/carbon-coated support film, washed three times with droplets of distilled water to remove buffer salts and then negatively stained with 1% uranyl acetate. Electron micrographs were routinely recorded at an instrumental magnification of 52 000.

3.2.6 Isolation of the functional unit RvH1-a from the structural subunit RvH1 of Rapana venosa hemocyanin

Native Hc was purified from the hemolymph of *Rapana venosa* Hc as described previously [Dolashka et al., 1996; Dolashka-Angelova et al., 2000; Boteva et al., 1991]. Subunit RvH1, previously referred to as RHSS1, was eluted as the first peak from an ion-exchange chromatography column in 50 mM Tris/HCl buffer, pH 8.2, with a 0-0.5 M NaCl gradient. Then, 200 mg of the subunit were treated with trypsin (trypsin-Hc ratio 1:400) for 1 h at room temperature in 20 mM NH_4HCO_3 buffer, pH 8.2. The tryptic hydrolysate was separated on a Sephadex G-150 column, eluted with the same buffer at a flow rate of 1ml.min^{-1}. The last eluting peak fraction, containing RvH1-a, was loaded on a Mono Q

10/10 column (FPLC), equilibrated with 50 mM Tris/HCl buffer, pH 8.2, and the FU was eluted with a linear gradient (0-0.5 M NaCl in 60 min) at a flow rate of 1 ml.min^{-1} and desalted on a Sephadex G-25 column with water.

3.2.7 Preparation of copper-free hemocyanin from functional unit RvH1-a

To prepare the starting material, suitable for glycopeptide analysis, the apo-protein was prepared. Lyophilized portions of RvH1-a were dialyzed over night against 50 mM Tris/HCl buffer, pH 8.2, containing 10 mM KCN, with three changes of buffer.

3.2.8 Carbohydrate determination and protein digestion of functional unit RvH1-a

8 mg of RvH1-a were dissolved in 1 ml of 40 mM Tris/HCl buffer, pH 8.6, containing 6 M guanidine-HCl and 0.2 M EDTA. To cleave the disulphide bonds, 20 µl of a β-mercaptoethanol solution was added with stirring. After heating at 50℃ for 4 h, 3 µl of 4-vinylpyridine was added and the reaction mixture allowed to stand for 3 h at room temperature. The reaction was terminated by the addition of 50 µl of 2.0 M acetic acid. The sample was dissolved in 200 µl of 0.1 M ammonium bicarbonate buffer, pH 9.0, and 50 µl of the trypsin solution (bovine pancreas, Hc-trypsin ratio 50:1) was added and the reaction mixture incubated at room temperature for 3 h. The glycopeptide mixture was separated on a Superdex 300 gel filtration column (2x30 cm), and the fractions were eluted with water at a flow rate of 1 ml.min^{-1}. Each chromatographic peak fraction was checked for carbohydrates using the orcinol/H_2SO_4 test [Dolashka-Angelova et al., 2001; Francois et al., 1962]. The only peak fraction giving a positive reaction was further fractionated by reverse phase HPLC using a Nucleosil 7 C18 column (250x10 mm; Macherey-Nagel, Düren, Germany). For elution, a linear gradient of 5% A (0.1% TFA in water) and 100% B (0.085% TFA in acetonitrile) within 70 min at a flow rate of 1ml.min^{-1} was used. The HPLC fractions, detected at a wavelength of λ=206 nm, were collected,

lyophilized and analyzed for carbohydrates with 0.1% orcinol in 20% H_2SO_4 on silica-gel plates.

3.2.9 Glycoprotein/peptide-staining of functional unit RvH1-a on silica-gel plates

The lyophilized peptides were dissolved in water. 2-4 µl of their solutions transferred to the plate, taking care to restrict the size of the spot to 2-3 mm in diameter, and air dried. The plate was sprayed with orcinol/H_2SO_4 and heated for 20 min at 100°C [Francois et al., 1962].

3.2.10 Amino acid sequence analysis of functional unit RvH1-a

Amino acid sequence analysis was performed from the peptides that were positive in the orcinol test. The fractions were dried and after dissolving in 40% methanol, 1% formic acid, subjected to automated Edman N-terminal sequencing (Procise 494A Pulsed Liquid Protein Sequencer, Applied Biosystems GmbH, Weiterstadt, Germany).

3.2.11 Enzymatic digestions of glycopeptides 1 and 2 of functional unit RvH1-a and glycopeptide 3 of functional unit RvH1-f

The fractions giving a positive test for carbohydrates, covering an amino acid sequence fragment Asn-X-Ser/Thr, were N-deglycosylated by PNGase-F from *Flavobacterium meningosepticum* (Calbiochem). The glycopeptides were dissolved in 50 mM Tris/HCl buffer, pH 7.0, and 5 µl PNGase-F (1,5 $U.ml^{-1}$) were added [Settineri and Burlingame, 1997; His et al., 1991]. After 24 h incubation time at room temperature the samples were analyzed by MALDI-MS as described below. Enzymatic digestions of glycopeptides were performed in a total volume of 50 µl in 0.7 ml Eppendorf tubes in the same buffer as mentioned above. The glycosidases PNGase-F, β1-2,3,4,6-N-acetylglucosaminidase from recombinant *E. coli*, α1-2,3-mannosidase from recombinant *E. coli,* α1-2,3,6-mannosidase from recombinant *E. coli and* β1-3,4,6-galactosidase from

bovine testes were used (Calbiochem) in sequence, and the reactions were started with the addition of 5 µl of these enzymes. After a 24 h incubation at 37℃, the samples were analyzed by electrospray ionization mass spectrometry (ESI-MS).

3.2.12 MALDI-MS analysis of glycopeptides 1 and 2 of functional unit RvH1-a and glycopeptide 3 of functional unit RvH1-f

The glyco- and deglycosylated peptides were analysed by MALDI-MS by means of a Kratos MALDI III equipment (Shimadzu). The glycopeptides were dissolved in 0.1% TFA (v/v) and applied onto the target. As matrix α-cyano-4-hydroxycinnamic acid in 70% acetonitrile/H_2O (70:30, v/v) was used.

3.2.13 Electrospray ionization mass spectrometry on glycopeptides 1 and 2 of functional unit RvH1-a and glycopeptide 3 of functional unit RvH1-f

ESI-MS was performed with a triple quadrupole mass spectrometer (TSQ700, Finnigan MAT, Bremen, Germany), equipped with an ESI-Finnigan electrospray ion source. The targeted fractions were dried at room temperature, using a speed vacuum evaporator (Savant, New York, N.Y.) and the remaining substances were dissolved in 50 % water/methanol (v/v). After centrifugation (2 min, 2,000 xg), the supernatant was infused into the ESI-MS *via* a Harvard syringe pump (5 µl/min). Mass spectra were acquired in positive-ion mode. Q1 was scanned over a mass range of m/z 400-2000 for 3 s or m/z 400-3000 for 3.5 s.

3.2.14 Capillary electrophoresis on glycopeptides 1 and 2 of functional unit RvH1-a and glycopeptide 3 of functional unit RvH1-f

All separations were performed on a BioFocus 3000 CE instrument (Bio-Rad, Munich, Germany). Separations were performed on a 50 cm x 50 µm (I.D.) fused silica capillary (Grom, Herrenberg, Germany). The samples were dissolved in 50 µl running buffer (50 mM phosphate pH 2.5), diluted with water (10:1, v/v) and introduced by pressure injection. All electrophoretic separations were carried out at 25 kV constant

voltage and the capillary temperature was maintained at 25℃. The peptides were detected by absorption at λ =214 nm.

3.2.15 Isolation of *Carcinus aestuarii* Hc and structural subunit 2 (CaeSS2)

Native Hc from the crab *Carcinus aestuarii* was prepared from the hemolymph obtained by injection into the dorsal lacuna of living animals collected in the lagoon of Venice. The protein was stored at -20℃ in the presence of 18% (w/v) sucrose. Before use, Hc was exhaustively dialysed against 20 mM phosphate buffer containing 10 mM EDTA and 5 mM hydroxylamine hydrochloride at pH 7.5. Protein concentration was determined using the absorption coefficient at 278 nm of $E_{278}0.1\%$ =1.24 $mg^{-1}.ml.cm^{-1}$ at pH 7.5 and 20℃. A molecular mass of 75 kDa was assumed for the structural subunit, containing one active site. The degree of oxygenation was determined by determining the absorbance ratio of A_{337}:A_{280} =0.21 for a preparation containing 100% oxy-Hc. The native protein was dissociated into its subunits by dialysis for 24 h against 100 mM sodium bicarbonate buffer, pH 9.5, containing 20 mM EDTA and 1 M urea. The subunits were isolated by FPLC ion exchange chromatography using a Resource column eluted with 50 mM Tris/HCl buffer, 1 M urea and a non-linear gradient of 0.0–0.5 M NaCl.

3.2.16 Modification of CaeSS2 by reduction and S-pyridylethylation

Before each enzymatic cleavage, portions of 5 mg of CaeSS2 were dissolved in 3.0 ml of 0.25 M Tris/HCl buffer, pH 8.5, 6 M guanidine-HCl, 1 mM EDTA. An ethanolic solution of 2-mercaptoethanol (10% v/v in water, at 100-fold molar excess over the cysteine residues) was added. The mixture was incubated under nitrogen for 2 h at room temperature in the dark. Neat 4-vinylpyridine (100-fold molar excess over the expected cysteine residues) was added and the mixture incubated under nitrogen for 2 h at room temperature in the dark. The reaction was stopped and the pyridylethylated protein desalted by reverse phase HPLC on an Aquapore RP-300 column (2.1x30 mm; Applied

Biosystems, Weiterstadt, Germany). The elution was performed using the following conditions: eluent A, 0.1% TFA in water; eluent B, 0.085% TFA, 80% acetonitrile and 20% water; gradient program: 0% B for 5 min, then 0-100% B in 10 min. A flow rate of 0.5 $ml.min^{-1}$ was used and the absorbance of the eluate recorded at 214 nm. The fraction containing the modified protein was collected and recovered by lyophilization.

3.2.17 Enzymatic hydrolysis of CaeSS2 structural subunit

Chymotryptic cleavage of the S-pyridylethylated protein was performed at 37℃ for 50 min by the addition of chymotrypsin to a final concentration ratio of 1:40 (w/w) in 100 mM ammonium hydrogen carbonate, pH 7.8. The chymotryptic digest was fractionated *via* HPLC on a LiChrospher 60 RP column (250x4 mm; Merck, Darmstadt, Germany) by elution with a mixture of water and acetonitrile (eluent A, 0.1% trifluoroacetic acid in water; eluent B, 80% acetonitrile in 0.1% trifluoroacetic acid/water), using a linear concentration gradient from 5 to 100% B in 100 min at a flow rate of 1.0 $ml.min^{-1}$. The UV absorbance of the eluate was monitored at 214 nm.

One milligram of modified CaeSS2 was dissolved in 1 ml of 5 mM ammonium bicarbonate buffer, pH 8.2, and incubated with 20 µl of trypsin solution (1 $mg.ml^{-1}$) at room temperature for 15 h, followed by a further addition of 20 µl of trypsin solution. Then the reaction mixture (enzyme: protein ratio of 1:30, w/w) was incubated overnight at 37℃. The generated peptides were separated by reverse phase HPLC on a Nucleosyl 100 RP-18 column (250x10 mm; Macherey-Nagel, Germany) by applying the following gradient: from 5% buffer B to 90% buffer B for 110 min and a flow rate of 1.0 $ml.min^{-1}$ (eluent A, 0.1% trifluoroacetic acid in water; eluent B, 80% acetonitrile in 0.1% trifluoroacetic acid/water).

3.2.18 Mass spectrometric analysis of glycopeptides

Mass spectrometric analysis of the HPLC fractions containing the peptide fragments resulting from the cleavage was done by MALDI-MS (Voyager, PerSeptive Biosystems, Wiesbaden, Germany). Peptides (10-50 pmol) were dissolved in 0.1% (v/v) TFA and applied to the target. Analysis was carried out using α-cyano-4-hydroxycinnamic acid or 2,5-dihydroxybenzoic acid as a matrix. Solutions of human substance P (1347.7 Da) and bovine insulin (5733.6 Da) were used to calibrate the mass scale. The mass values assigned to the amino acid residues are the average masses.

3.2.19 Amino acid sequence determination of glycopeptides

Peak fractions were dried and after dissolving in 40% methanol, 1% formic acid they were subjected to automated Edman N-terminal sequencing (Procise 494A Pulsed Liquid Protein Sequencer, Applied Biosystems GmbH, Weiterstadt, Germany).

3.2.20 Fluorescence spectroscopy of glycopeptides

The apo-form (copper-deprived) of native protein and dissociation products was obtained by overnight dialysis against 25 mM KCN in 100 mM Tris/HCl, pH 8.0, at 4℃. The proteins were then dialyzed against the same buffer without KCN containing 10 mM EDTA, and finally against 100 mM Tris/HCl, pH 7.0.

Fluorescence spectra were recorded with a Perkin Elmer LS 5 spectrofluorimeter. Protein solutions had an absorbance at excitation wavelengths lower than 0.05 to minimize the inner filter or self-absorption effects. The relative quantum yields (Q) were measured by comparing the integrated corrected fluorescence emission spectra of Hcs with those of N-acetyltryptophanamide, normalized to the same absorbance at the excitation wavelength (295 nm). The quantum yield of the standard was 0.13 at 21℃ [Lehrer, 1971].

Fluorescence quenching experiments were performed with copper complex ($Cu^{II}(PuPhPy)^2$) [Lange et al., 2000] as external quenchers, in the concentration range from $1x10^{-7}$ to $20x10^{-7}$. Fluorescence quenching data were analyzed according to the Stern-Volmer relationship. Emission spectra were recorded at a speed of 60 $nm.min^{-1}$ and emission slit widths were adjusted to 5.0 nm band pass.

3.2.21 Purification of the native proteins and the structural subunits

Hcs were prepared from the hemolymph of the crab *Carcinus aestuarii* [Hristova et al., 1997], crab *Maia squinado* [Dolashka-Angelova et al., 2000], lobster *Homarus americanus* [Dolashka-Angelova et al., 1999] and scorpion *Buthus sindicus* [Abbasi et al., 2000] by the methods as described in the given references and of the adult *Limulus polyphemus* and spiny lobster *Palinurus vulgaris*. Before use, the *Limulus* and *Palinurus* Hcs, previously stored at -20℃ in the presence of 18% sucrose, was dialyzed at 4℃ against the 0.1 M sodium bicarbonate buffer, pH 9.5. The native Hc was dissociated by 24 h dialysis at the same buffer in the presence of 10 mM EDTA and 1 M urea. The protein was then loaded onto an ion exchange FPLC Resource 6 ml column (Pharmacia, Sweden), equilibrated with 0.1 M $NaHCO_3$, pH 9.5, containing 10 mM EDTA and 1 M urea (Eluent A). Elution was performed with a non-linear NaCl gradient made by using a 1 M NaCl solution in the buffer mentioned above as eluent (Eluent B). The purity and molecular masses of structural subunits were determined by SDS-PAGE [Laemmli, 1970].

3.2.22 UV spectroscopy of arthropodan hemocyanin *Limulus polyphemus* (LpH)

Hc concentrations of the proteins were determined spectrophotometrically (UVIKON spectrophotometer, model 930) at 278 nm using the following absorption coefficients (A_{280}): A =1.35 ml $(cm.mg)^{-1}$ for *M. squinado* [Dolashka-Angelova et al., 2000], A = 1.17 ml $(cm.mg)^{-1}$ for *L. polyphemus*, A = 1.34 ml $(cm.mg)^{-1}$ for *H. americanus* [Dolashka-Angelova et al., 1999] and A = 1.34 ml $(cm.mg)^{-1}$ for *P. vulgaris*, all in 50 mM

Tris/HCl buffer, pH 8.0. Molar concentrations were referred to 75 kDa as molecular mass for the species containing one dinuclear copper site [Bubacco et al., 1992]. The fraction of oxy-Hc was determined spectrophotometrically by measuring the absorbance ratio at 340 and 278 nm and assuming the values A_{340}/A_{278} = 0.21 for native fully oxygenated protein [Bubacco et al., 1992].

3.2.23 Fluorescence spectroscopy of arthropodan hemocyanin *L. polyphemus*

Fluorescence emission spectra were recorded with a Perkin Elmer Model LS5 spectrofluorimeter, equipped with a thermostatically controlled sample holder and a Model 3600 data station. Protein solutions had an absorbance at the excitation wavelength < 0.05 to minimize the inner filter or self-absorption effects. Excitation at 295 nm was used for predominant measuring the fluorescence of tryptophyl residues. Spectra were corrected for background due to the solvent.

Fluorescence quantum yields were calculated using N-acetyltryptophan amide (Ac-Trp-NH_2) with a quantum yield of 0.13 (λ_{ex}= 295 nm at 25℃) as a standard. The spectra of the protein and of the standard solutions were normalised for their absorbance at the excitation wavelengths.

Fluorescence lifetime measurements were carried out at 20℃ using a System PRA 2000 nanosecond single photon counting spectrofluorimeter and a nitrogen-filled flash lamp with full width at half-maximum (FWHM) of about 2.5 ns. The data were analyzed by convoluting the instrument response function *Y(t')* with an assumed decay function *P(t),* using the following relationship:

$$R_c(t) = \int Y(t')P(t-t')\,dt' \qquad (10)$$

The $R_c(t)$ value obtained, was compared with the experimental time dependence $R_m(t)$. The accuracy in the excited state lifetime (τ) determination was ± 0.1 ns. The decay

curves contained 10^4 counts at the maxima. The time interval for these curves was 100 ps per channel.

3.2.23.1 pH stability of arthropodan hemocyanin *Limulus polyphemus*

Different species of Hcs were kept for 24 hours in different buffers of the pH range 2-11.5; 0.05 M sodium citrate (pH 3.0-5.0); 0.05 M sodium phosphate (pH 5.0-7.0); 0.05 M Tris/HCl (pH 7.0-9.0); 0.05 M carbonate/bicarbonate (pH 9.0-10.5) and 5 M NaOH (pH 11-12).

3.2.23.2 Denaturation in Gdn.HCl-water solutions of arthropodan LpH

Fluorescence measurements were performed in 50 mM Tris/HCl buffer, pH 8.2, in the presence of 5 mM $CaCl_2$ and 5 mM $MgCl_2$ using a 10 mm quartz optical cell. The Gdn.HCl concentrations were stepwise (discrete) increased from 0 to 8 M denaturant. The tryptophan emission spectra were measured after equilibration for 24 hours from 300 to 420 nm at an excitation wavelength of 295.

3.2.23.3 Quenching of the tryptophan emission of arthropodan LpH

The results of the quenching reactions between the excited indole rings of tryptophans and copper complex 1,8-bis(2-pyridyl)-2,7-diazaoctadiene-1,7) Cu $^{II}(PuPhPy)^{2+}$ were analyzed according to the Stern-Volmer equation.

$$\frac{F_0}{F} = 1 + K_{sv}[X] \qquad (11)$$

where Fo and F are the fluorescence intensities at an appropriate emission wavelength in the absence and in the presence of quencher; K_{sv} is the collisional quenching constant, and [X] is the quencher concentration.

3.2.24 CD spectroscopy of arthropodan hemocyanin *Limulus polyphemus*

3.2.24.1 Temperature and pH stability of arthropodan Hc *Limulus polyphemus*

Circular dichroism spectra were recorded in a J-720 spectropolarimeter (Jasco, Tokyo, Japan). Cylindrical temperature-controlled quartz cells with a path length of 10 mm were used in all experiments. CD spectra were recorded in the range between 200 and 250 nm at 0.2 nm intervals with a bandwidth of 1 nm, a scan speed of 50 nm/min, and a time constant of 8.0 s. Protein solutions in 50 mM Tris/HCl buffer, pH 8.0 were thermostatically controlled using a NESLAB thermostat model RTE-110, connected with a digital programming controller, and a thermocouple placed inside the cuvette. Temperature denaturation studies were performed at a temperature increase rate of 2℃ per min up to 95℃ and the $[\theta]_{222}$ was measured each 5 deg. Thereafter, temperature was decreased at the same rate down to 25℃. The attain ment of thermal equilibrium of samples was confirmed by the constancy of their ellipticity. Each experimental spectrum derived by averaging two or three separate scans and was corrected for baseline recorded with buffer as blank. The computer program, using the method of Yang calculated the α-helix content of the protein. The CD spectrum of a protein can be considered as the sum of the CD spectra of each secondary structure comprising the protein, In another series of experiments the complete CD spectra in the range measured at 25℃ but in solutions with pH (2-11,5); 0.05 M s odium citrate (pH 3.0-5.0); 0.05 M sodium phosphate (pH 5.0-7.0); 0.05 M Tris/HCl (pH 7.0-9.0); 0.05 M carbonate/ bicarbonate (9.0-10.5) and NaOH for pH 11-12). CD spectra were measured at various times up to 24 hours.

3.2.24.2 Denaturation by guanidine hydrochloride (Gdn.HCl) of arthropodan hemocyanin *Limulus polyphemus*

Gdn.HCl denaturation was followed by recording the 200-260 nm CD spectra of Hc (0.4 mg/ml in 50 mM M Tris/HCl buffer, pH 7.0 and 8.2, 5 mM $CaCl_2$ and 5 mm $MgCl_2$) in

the presence of different concentrations of denaturant (0-8.0 M Gdn.HCl) at 25℃. Quartz cylindrical cells with 0.05 cm path length were used throughout. The free energy of Gdn.HCl denaturation, ΔG_D, was estimated from the equation:

$$\Delta G_D = -RT \ln K \qquad (12)$$

where R is the gas constant (8.31 J℀K.mol $^{-1}$), T - the absolute temperature (℀K). K is the constant of the conformational equilibrium between the folded and denaturated state, whose value changes as a function concentration of denaturant. The value of K was experimentally calculated at the different concentrations of Gdn.HCl as:

$$K = \frac{\left([\theta]_{Obs} - [\theta]_N\right)}{\left([\theta]_D - [\theta]_{Obs}\right)} \qquad (13)$$

In this equation, $[\theta]_{Obs}$ is the observed ellipticity at 221 nm at different concentrations of the denaturant, and $[\theta]_N$ and $[\theta]_D$ are the ellipticities at the same wavelength for the folded and unfolded conformations of the proteins. Equation 10 can be expressed also as a linear function of ΔG_D *versus* the concentration of the denaturant where the intercept at zero concentration of denaturant gives $\Delta G_D^{H_2 0}$, or the free energy of denaturation in water, and the slope gives the cooperativity index of the conformational transition**.**

3.2.25 Preparation and analysis of glycopeptides of *Carcinus aestuarii* hemocyanin

3.2.25.1 Enzymatic digestion of CaeSS2

5 milligrams of subunit Ca2 was dissolved in 2 ml of 0.25 M Tris/HCl buffer, pH 8.5, 6 M guanidine–HCl, 1 mM EDTA. An ethanolic solution of 2-mercaptoethanol (10% (v/v) in water, at 100-fold molar excess with respect to the cysteinyl residues) was added. The mixture was incubated under nitrogen for 2 h at room temperature in the dark. Neat 4-vinylpyridine (100-fold molar excess to the expected cysteinyl residues) was added and the mixture was incubated under nitrogen for 2 h at room temperature in the dark. The reaction was stopped and the pyridylethylated protein was desalted by dialyses with

$(NH_4)HCO_3$ buffer. Three milligrams of modified Ca2 was dissolved in 1 ml of 5 mM ammonium bicarbonate buffer, pH 8.2, and incubated with 50 µl of trypsin solution (1 mg. ml^{-1}) at room temperature for 15 h, followed by a further addition of 50 µl of trypsin solution. Then the reaction mixture (enzyme: protein ratio of 1:30, w/w) was incubated overnight at 37℃. The generated peptides were sepa rated by gel filtration on a Superdex 300 column (Pharmacia, Freiburg, Germany) at a flow rate of 2 $ml.min^{-1}$ using water as eluent. The fractions were analyzed for carbohydrates with the orcinol/H_2SO_4 test [Francois et al., 1998)] and only the fraction that gave positive reaction was further purified by reverse-phase HPLC on a Nucleosyl 100 RP-18 column (250x10 mm; 7 mm; Macherey-Nagel, Germany). The glycopeptides were eluted (detection at 214 nm) at a flow rate of 1 $ml.min^{-1}$ by applying the following gradient: 90% Buffer A, 10% Buffer B for 10 min, then 10–100% Buffer B in 70 min (Buffer A, 0.1% TFA in H_2O; Buffer B, 0.085% TFA, 80% acetonitrile, and 20% H_2O). The collected fractions were lyophilized and those identified as glycopeptides, again identified by the orcinol/H_2SO_4 test, were further subjected to MALDI-MS and amino acid sequence analysis.

3.2.25.2 Automated amino acid sequence analysis of CaeSS2

Glycopeptides were dissolved in 0.1% (v/v) TFA and spotted onto filters. Automated Edman degradation was performed using a pulsed liquid sequencer Model 473 A (Applied Biosystems) with one-line analysis of the phenylthiohydantion derivatives (Weiterstadt, Germany).

3.2.25.3 Treatment of glycopeptides with α-N-acetylgalactosaminidase and Peptide N Glycosidase F (PNGase-F).

The lyophilized purified glycopeptides were dissolved in 100 ml of 20 mM sodium acetate buffer, pH 5.0. Five microliters of neuraminidase (*Arthbacter nocotianae* 1 U/100 ml) [Abrashev et al., 1998] was added and the mixture was incubated overnight at 37℃

[Settineri et al., 1997]. The sample was dissolved in 30 ml of 20 mM acetate buffer, pH 5.0, and incubated overnight with 20 ml of β-galactosidase from bovine testes (1.0 U/ml) and α-*N*-acetylgalactosaminidase from *Acromonium* sp. (13 U/ml) at room temperature. Alternatively, the glycopeptidic fraction having an amino acid sequence Asn-X-Ser/Thr was dissolved in 50 mM Tris–HCl buffer, pH 7.0, and the N-deglycosylated by treatment with 5 ml of PNGase-F (1.5 U in 1 ml) for 24 h at room temperature [Settineri et al., 1997]. The released carbohydrate chains were separated from the peptides by gel filtration on a Superdex 300 column, using water as eluent, and after lyophilization, the molecular masses of the glycopeptides and deglycosylated peptides were determined by MALDI-MS.

3.2.26 Culture conditions of fungal strain *Humicola lutea* 103

The fungal strain, *H. lutea* 103, from the Mycological Collection of the Institute of Microbiology, Sofia, was used throughout and maintained at 4°C on beer agar, pH 6.3. To monitor Cu resistance of the fungal strain, conidiospores were cultivated in Petri dishes (d=10 mm) with beer agar, supplemented with various concentrations of $CuSO_4$ during 10 days at a temperature of 30°C.

For the submerged cultivation, both, seed and productive media were used [Angelova et al., 1996]. For the inoculum, 80 ml of seed medium was inoculated with 5 ml of spore suspension at a concentration of $2x10^8$ spores ml^{-1} in 500 ml Erlenmeyer flasks. The cultivation was performed on a shaker (220 rpm) at 30°C for 24 h. Then, 6 ml of seed culture were transferred to 500 ml Erlenmeyer flasks, containing 74 ml of production medium. The cultures were grown at 30°C for 72 h. For the investigation of the effect of different Cu concentrations, cultures were incubated with various concentrations (70-500 μg/ml) of $CuSO_4$. Results were evaluated from repeated experiments using three or five parallel runs.

3.2.27 Analytical methods for measurement the activity of superoxide dismutase

SOD activity was measured by the nitro blue tetrazolium (NBT) reduction method of Beauchamp and Fridovich [Beauchamp and Fridovich, 1971]. One unit of SOD activity was defined as the amount of SOD required for inhibition of the reduction of NBT by 50% (A_{560}) and was expressed as units per mg protein [U $(mg.protein)^{-1}$]. Cyanide (2 mM) was used to distinguish between the cyanide-sensitive isoenzyme Cu/ZnSOD and the cyanide-resistant MnSOD. The Cu/Zn-SOD activity was obtained as total activity minus the activity in the presence of 2 mM cyanide. Catalase was assayed by the method of Beers and Sizer (Beers and Sizer, 1952). Glucose 6-phosphate dehydrogenase (G6PD) activity was measured by the glucose 6-phosphate-dependent reduction of $NADP^+$ [Bergmeyer, 1983]. One unit equals 1 μmol of substrate reduced per min. Specific activity is given as U/mg protein. Protein was estimated by the Lowry procedure [Lowry et al., 1951] using crystalline bovine albumin as standard. The dry weight determination was performed on samples of mycelia harvested throughout the culture period. The culture fluid was filtered through a Whatman (Clifton, USA) № 4 filter. The separated mycelia were washed twice with distilled water and dried to a constant weight at 105°C.

3.2.28 SOD antibodies against *Humicola lutea* Cu/Zn-superoxide dismutase

Antibodies were raised in white rabbits (2.5 kg and 6 weeks old) against the Cu/Zn-SOD from *Humicola lutea* 103. The primary injection in complete Freund's adjuvant (day 0) and the second and third in incomplete Freund's adjuvant (days 7 and 42) were given intramuscularly (1 mg of antigen for each injection per rabbit). Bleeding occurred at days 87 and 164 after immunization.

3.2.29 Western-blotting analysis of *Humicola lutea* Cu/Zn-superoxide dismutase

Proteins separated by 10% SDS-PAGE gels were transferred (18 h at 12 V at room temperature) to nitrocellulose membranes (0.45 mm, Millipore) with a semidry electroblotter (Jancos, Denmark) as described by Towbin et al. [Towbin et al., 1979]. As transfer buffer 30 mM Tris, 240 mM glycine, 20% methanol (v/v) was used. Immobilized proteins were stained with 0.2% Ponceau dye in 3% glacial acetic acid and destained with water. The non-specific remaining binding sites were blocked with phosphate-buffered saline (PBS; 80 g/l NaCl, 2 g/l KCl, 14.4 g/l $Na_2HPO_4.7H_2O$, 2.4 g/l KH_2PO_4, pH 7.4) containing 3% bovine serum albumin and 0.05% Tween for 1 h at 20°C. The primary antibodies were used for the first test at a 1:400 dilution. Reacting proteins were visualized by staining with horseradish peroxidase-conjugated goat anti-rabbit immunoglobulin G (IgG) (1:2000) as secondary antibody.

3.2.30 Measurement of protein carbonyl content

Protein oxidative damage was measured spectrophotometrically as protein carbonyl content using the 2,4-dinitrophenylhydrazine (DNPH) binding assay [Hart et al., 1999], slightly modified by Adachi Ishii [Adachi et al., 2000]. Following Cu treatment, the cell-free extracts were incubated with DNPH for 1 h at 37°C, proteins were precipitated in 10% cold TCA, washed with ethanol: ethylacetate (1:1), to remove excess of DNPH, and finally dissolved in 6 M guanidine-HCl, pH 2. Optical density was measured at 380 nm, and the carbonyl content was calculated using a molar extinction coefficient of 21 $mM^{-1}.cm^{-1}$, as nanomoles of DNPH incorporated (protein carbonyls) per mg of protein.

3.2.31 Purification of *Humicola lutea* Cu/Zn-superoxide dismutase

The enzyme was isolated from fungal strain *H. lutea* 103 as described [Angelova et al., 2001]. Further purification was achieved by ion exchange chromatography on a DEAE

cellulose - 52 column (3.5x10 cm, Serva, Heidelberg, Germany), eluted with a 50 mM KH_2PO_4 buffer, pH 7.8, NaCl gradient (0-0.1 M). Active fractions were further purified by a FPLC system, equipped with a 10/10 Mono Q anion exchange column, and pure HL-SOD was eluted with 50 mM phosphate buffer, pH 7.8, employing stepwise increases in sodium chloride (0-0.1 M NaCl).

3.2.32 Pyridylethylation of *Humicola lutea* Cu/Zn-superoxide dismutase

Five mg of SOD were dissolved in 3.0 ml of 0.25 M Tris/HCl, pH 8.5, 6 M guanidine-HCl, 1 mM EDTA. An ethanolic solution of 2-mercaptoethanol (10% v/v in water, at 100-fold molar excess to the cysteinyl residues) was added. The mixture was incubated under nitrogen for 2 h at room temperature in the dark. Neat 4-vinylpyridine (100-fold molar excess to the expected cysteinyl residues) was added and the mixture incubated under nitrogen for 2 h at room temperature in the dark. The reaction was stopped and the pyridylethylated protein desalted by reverse phase HPLC on an Aquapore RP-300 column (2.1x30 mm; Applied Biosystems, Weiterstadt, Germany). Elution was performed using the following conditions: eluent A, 0.1% TFA in water; eluent B, 0.085% TFA, 80% acetonitrile and 20% water; gradient program: 0% B for 5 min, then 0-100% B in 10 min. A flow rate of 0.5 ml/min was used and the absorbance of the eluate recorded at 214 nm. The fraction containing the modified protein was collected and recovered by lyophilization.

3.2.33 Enzymatic digestions of *Humicola lutea* Cu/Zn-superoxide dismutase

Cleavage of SOD with lysyl endopeptidase, specifically hydrolyzing bonds located C-terminal to lysine, was performed in 25 mM Tris/HCl, pH 8.3, containing 1 mM EDTA and 1 M urea (the molar ratio of substrate to enzyme was 50) for 24 h at 37℃ and the generated peptide fragments were separated by a reverse phase HPLC Nucleosil 100 RP-18 column (250x10 mm; 7 μm; Macherey-Nagel, Germany), eluted with eluent A,

(0.1% TFA in water), eluent B, (80% acetonitrile in A), using as gradient program 0% B for 5 min and then 0-100% B in 110 min and a flow rate of 1.2 ml/min. The UV absorbance of the eluate was monitored at 214 nm. 50 µl of the trypsin solution (enzyme to substrate 1:50) was added to 2.0 ml 25 mM Tris/HCl, pH 9.0, containing 3 mg carboxymethylated SOD and the reaction mixture was incubated at room temperature overnight (20 h). The sample was applied to a Nucleosyl 100 RP-18 column (250x10 mm; 7 µm; Macherey-Nagel, Germany) and eluted with a linear gradient of solvent A (0.1% TFA in water) and B (0.085% TFA in acetonitrile) within 70 min and a flow rate of 1ml.min^{-1}.

3.2.34 Mass spectrometric analysis of *H. lutea* Cu/Zn-superoxide dismutase

Mass spectra of the native and deglycosylated SOD were obtained by MALDI mass spectrometry (Voyager, PerSeptive Biosystems, Wiesbaden, Germany). The sample (10-50 pmol), obtained using anion-exchange chromatography, was dissolved in 0.1% (v/v) TFA, dialyzed against water and applied to the target. Analysis was carried using α-cyano-4-hydroxycinnamic acid as a matrix. Chicken egg ovalbumin (44400 Da) and bovine serum albumin (66430 Da) were used for mass scale calibration. Mass spectrometric analysis of the HPLC fractions containing the peptide fragments resulting from the cleavage was also done by MALDI-MS (Voyager, PerSeptive Biosystems, Wiesbaden, Germany). Peptides (10-50 pmol) were dissolved in 0.1% (v/v) TFA and applied to the target. Analysis was carried out using α-cyano-4-hydroxycinnamic acid or 2,5-dihydroxybenzoic acid. Solutions of human substance P (1347.7 Da) and bovine insulin (5733.6 Da) were used to calibrate the mass scale. The mass values assigned to the amino acid residues are the average masses.

3.2.35 Amino acid sequence determination of *Humicola lutea* Cu/Zn-SOD

Peak fractions were dried and after dissolving in 40% methanol, 1% formic acid they were subjected to automated Edman degradation (Procise 494A Pulsed Liquid Protein Sequencer, Applied Biosystems GmbH, Weiterstadt, Germany).

3.2.36 Glycoprotein/peptide staining of *H. lutea* Cu/Zn-SOD on a silica-gel plates

The lyophilised peptides were dissolved in water and 2-4 µl solutions were applied to the plate and air-dried, taking care to restrict the size of the spot to 2-3 mm in diameter. The plate was sprayed with orcinol/H_2SO_4 and heated for 20 min at 100℃.

3.2.37 Enzymatic deglycosylation of *Humicola lutea* Cu/Zn-superoxide dismutase

HL-SOD and the peak fraction giving a positive test for carbohydrates and containing an Asn-X-Ser/Thr sequence were N-deglycosylated by PNGase-F of *Flavobacterium meningosepticum* (Roche GmH). Digests were performed in 0.7 ml Eppendorf tubes in a total volume of 50 µl 50 mM Tris/HCl buffer, pH 7.0. Then 5 µl PNGase-F (1.5 U in 1 ml) was added. After 24 h incubation at room temperature the samples were applied to MALDI-MS.

3.2.38 Dithiothreitol (DTT) titration of *Humicola lutea* Cu/Zn-superoxide dismutase

For reduction of disulfide bonds, HL-SOD samples were incubated (in the dark) for 30 min at 25℃ with varying concentrations of DTT (0 to 30 mM) in 50 mM Tris/HCl buffer, pH 7.5, containing 50 mM NaCl. Using a Jasco J-720 dichrograph and a cuvette of 0.2 cm, circular dichroism (CD) spectra were measured on protein samples (0.20 mg/ml) before and after treatment with DTT. Each spectrum, used for further calculations, represents an average of three measurements in the range of 195-250 nm, collected at 0.2 nm intervals, with a spectral band width of 0.5 nm and 4 s integration time. The CD

spectra are expressed in molar ellipticity (deg.cm^2.dmol^{-1}) using 110 as a mean residue molecular mass.

3.2.39 Effect of glycosylated and non-glycosylated SODs on influenza-induced pneumonitis in mice

Male and female (16-18 g) inbred ICR mice were obtained from the Experimental Animal Station, BAS, Sofia. They were quarantined 24 h prior to use and maintained on standard laboratory chow and tap water *ad libitum* for the duration of the studies. After the end of the experiments, surviving mice were sacrificed by cervical dislocation.

3.2.40 Ethical aspects

Experiments with animals were indispensable in investigations concerning the treatment of influenza infection. The number of experimental animals was reduced as much as possible, depending on statistical significance. Refinement of the tests with animals was achieved by careful planning of multifactor experiments. The animals were bred under standard conditions, accepted by the Bulgarian Veterinary Health Service. Specialists took care of the welfare of the animals.

3.2.41 Virus infection and effect of glycosylated and non-glycosylated SODs

The infection was induced under light ether anaesthesia by intranasal (i.n.) inoculation of A/Aichi, adapted to mouse lungs. This virus causes haemorrhagic pneumonia in mice. The strain is from the collection of the Institute of Microbiology, BAS, Sofia. To induce a lethal infection, mice were infected with 10 LD_{50} of the virus in the volume of 0.05 ml buffered physiological saline (PBS)/mice. The virus was maintained by passages in mice lungs and virus stock was kept at –70°C.

3.2.42 Experimental design to study the effect of glycosylated and non-glycosylated SOD to influenza-induced pneumonitis

Viability of mice was checked daily for 21 days after viral challenge. All experimental groups consisted of 10 animals each. HL-SOD and bovine SOD were inoculated intravenously (i.v.) 4 times from day 4 to day 7 post infection (p.i.). Ribavirin was applied intraperitoneally (i.p.) according to the same schedule. The protective effect was evaluated as described by Serkedjieva and Ivanova [Serkedjieva et al., 1997]. Additional three animals from each experimental group were killed on day 7 and their lungs were weighed and assayed for virus titre and lung score as described before [Serkedjieva et al., 1997]. The results are mean values from 2-3 independent experiments.

4. Results and Discussion

4.1. Isolation, structure and investigations on selected hemocyanins

4.1.1 Oligomeric stability of *Rapana venosa* hemocyanin (RvH) and its structural subunits

4.1.1.1 Isolation of *Rapana venosa* molluscan hemocyanins and separation of structural subunits

Native Hc was purified from the hemolymph of *Rapana venosa* Hc as described previously [Boteva et al., 1991]. The dissociation of the native Hc was obtained dialyzing the native protein for 24 hours against 0.13 M glycine/NaOH, pH 9.6. The dissociated fractions were loaded on an ion-exchange chromatography HiLoad 26/10 Sepharose Q column, equilibrated with 50 mM Tris/HCl buffer, 10 mM EDTA, pH 8.2, using an FPLC system **(Figure 30a)** [Dolashka-Angelova et al., 2003].

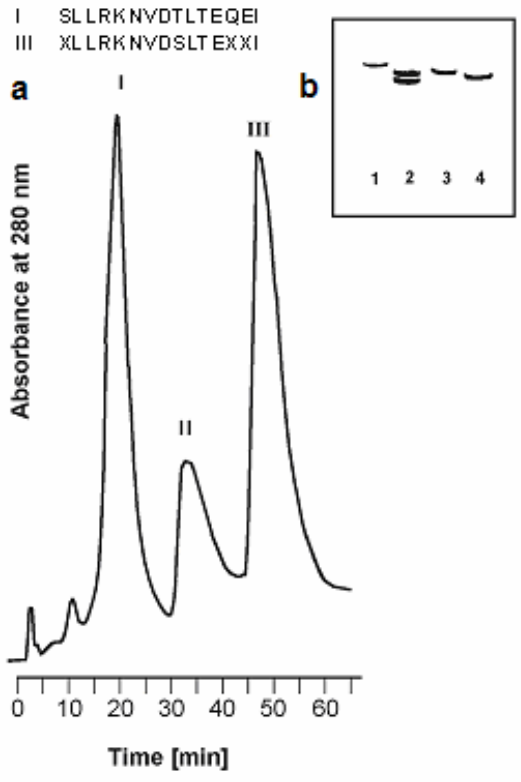

***Figure 30. a) Fast performance liquid chromatogram (FPLC) of dissociated structural subunits**, performed on a HiLoad 26/10 Sepharose Q column (3.4×100 mm), equilibrated with 50 mM Tris/HCl buffer, 10 mM EDTA, pH 8.2. Subunits were separated with a step gradient of NaCl (0.15 – 1.0 M) at a flow rate of 7.0 ml.min^{-1} for elution. The first fraction (I) contained pure RtH1, the second one (II), both, RtH1 and RtH2 and the third one (III) pure RtH2; **b) Native PAGE (7.5 % gel) of Rapana Hc and its structural subunits RvH1 and RvH2**. Lane 1: Standard sample of ferritin (M_W= 440 kDa); lane 2: dissociated hemocyanin; lanes 3,4: protein composition after FPL ion exchange chromatography on a HiLoad 26/10 Sepharose Q column; lane 3: RtH1 (peak I, Fig. 30a) and lane 4: RtH2 (peak III, Fig. 30a). Results of N-terminal sequencing for peak fraction I: SLLRKNVDTLTEQEI and peak fraction III: XLLRKNVDSLTEXXI.*

The subunits were separated by elution with a non-linear sodium chloride gradient (0.15-1.0 M NaCl) at a flow rate of 7.0 ml.min^{-1}. Electrophoretic analysis confirmed the separation of the two subunits. Two fractions, indicated in **Figure 30a** as RvH1 (peak I)

and RvH2 (peak III), were separated as major components, PAGE separations of fractions I and III **(Figure 30b, lanes 3 and 4)** yielded single major protein bands; fraction I was identified as RvH1 (420 kDa) and fraction III as RvH2 (400 kDa), respectively. Each subunit was further purified on a HPLC Nucleosil RP C18 column using 0.1% TFA in H_2O as loading buffer and 0.085%TFA (eluent A), 80% acetonitrile in H_2O and 0.05 % TFA as eluting solution (eluent B). The following conditions were used: 10% B for 10 min followed by 10-100% B within 70 min at a flow rate of 1 $ml.min^{-1}$. Peak fractions were dried and after dissolving in 40% methanol, 1% formic acid, they were subjected to automated Edman N-terminal sequencing. N-terminal amino acid sequencing confirmed structural identification of peak fractions I, II and III [Stoeva et al., 1997] **(Figure 30)**. Two isoforms were identified in fraction II. Unfractionated RvH was obtained directly from the hemolymph by centrifugation and dialysis against the different buffers for electron microscopic analysis.

4.1.1.2 Gallery of electron micrographs of native, dissociated and reassociated *Rapana venosa* hemocyanin

The multimeric/higher oligomeric states of the two isoforms of Rapana hemocyanin and its two subunits RvH1 and RvH2 were investigated by transmission electron microscopy (TEM) and compared with previously published structural data of keyhole limpet Hc (KLH1 and KLH2) [Harris et al., 1997a, Harris et al., 1997b], *Haliotis tuberculata* (HtH1 and HtH2) [Harris et al., 2000] and *Helix pomatia* [van Breemen et al., 1979]. For EM studies, samples of native RvH were dialyzed against 50 mM Tris/HCl stabilizing buffer (SB), pH 7.0, containing different concentrations (10 and 100 mM) of, both, $CaCl_2$ and $MgCl_2$ **(Figure 31).** The dissociation of the native molecule into its structural subunits RvH1 and RvH2 was performed by overnight dialysis at 4^oC against 0.13 M Gly/NaOH buffer, pH 9.6. Reassociation of the isoforms from the fully dissociated state at pH 9.6 was achieved by dialysis against the stabilizing buffer (50 mM Tris, pH 7.0, containing either

10 or 100 mM of, both, $CaCl_2$ and $MgCl_2$) at 4^oC. After several days or weeks, the samples were taken for negative staining for EM studies.

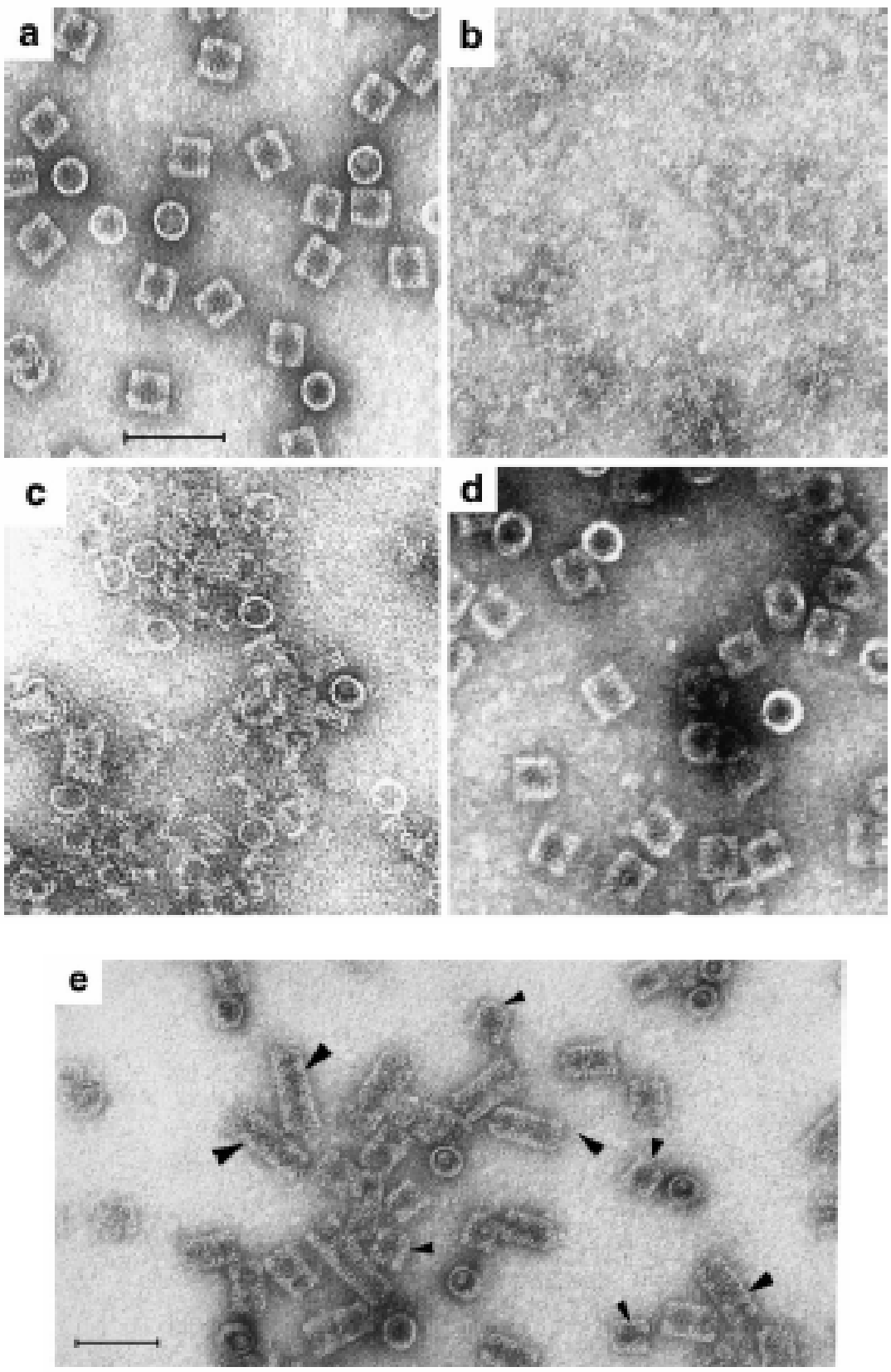

Figure 31. Legend see following page

Figure 31. Gallery of electron micrographs of Rapana venosa hemocyanin. a) Native Hc (RvH) in 50 mM Tris/HCl buffer*, pH 7.0, containing 20 mM $CaCl_2$ and 5 mM $MgCl_2$;* ***b) dissociated protein in 0.13 M Gly/NaOH buffer*** *at pH 9.6;* ***c) reassociated RvH after dialysis for 2 days against SB****, pH 7.0, containing 20 mM $CaCl_2$ and $MgCl_2$;* ***d) reassociation after dialysis for 2 days against SB****, containing 50 mM $CaCl_2$ and $MgCl_2$;* ***e) reassociation of RvH after dialysis for 2 days against SB*** *with higher concentration of $CaCl_2$ and $MgCl_2$ (100 mM each). By increasing the concentrations of both divalent ions, Ca^{2+} and Mg^{2+}, the reassociation is increased, and not only didecamers (small arrowheads), but also multidecamers (larger arrowheads) are observed. Staining with 1% uranyl acetate was performed as described in Materials and methods. The scale bar indicates 100 nm.*

Figure 31 shows a gallery of electron micrographs of the native, dissociated and reassociated Rapana Hc. **Figure 31a** reveals that the native material appears as homogeneous hollow cylindrical didecameric structure in 50 mM Tris/HCl buffer, pH 7.0, containing 20 mM $CaCl_2$ and 5 mM $MgCl_2$ (stabilizing buffer). No dissociated forms can be seen in the electron micrographs. After 24 h dialysis against 0.13 M Gly/NaOH buffer, pH 9.6, the protein appears to be fully dissociated into structural subunits RvH1 and RvH2**,** and the cylindrical form, typical for the native Hc, is not seen **(Figure 31b)**. The reassociation behaviour of these structural subunits was studied in SB, pH 7.0, in the presence of different concentrations of Ca^{2+} and Mg^{2+} ions. After reassociation of the fully dissociated protein, the sample is more heterogeneous than to the native protein. Some subunits are still present after dialysis for 2 days against stabilizing buffer (SB), pH 7.0, containing 20 or 50 mM $CaCl_2$ and $MgCl_2$, respectively **(Figure 31c,d),** and the circles show an empty central hole. After reassociation for two days in stabilizing buffer, containing 100 mM $CaCl_2$ and $MgCl_2$, the samples show good reassociation, slightly more complete than after dialysis against SB, containing 20 or 50 mM of the same divalent ions **(Figure 31e)**. The reassociated sample is different compared to the native protein **(Figure 31a)** after one week of reassociation of the fully dissociated RvH in SB, containing 100 mM $CaCl_2$ and $MgCl_2$, pH 7.0; only RvH didecamers and multidecamers of varying length are present in **Figure 31e**. Reassociation in the presence of 100 mM of $CaCl_2$ and $MgCl_2$ is considered to be most satisfactory.

4.1.1.3 Gallery of electron micrographs of the oligomerization dynamics of structural subunit RvH1

The ionic manipulation of the RvH1 subunit was achieved by adding calcium and magnesium ions and the samples were studied after two to three days and one or two weeks by TEM. **Figure 32a** shows an example of RvH1 taken after chromatographic elution with 50 mM Tris/HCl buffer, pH 8.5, containing 10 mM EDTA **(Figure 30 peak I)**.

The RvH1 sample contains predominantly didecamers, but with a few decamers. After dialysis of the dissociated structural subunit RvH1 against the stabilizing buffer at pH 9.6, containing 2 mM $CaCl_2$ and $MgCl_2$, some subunits, didecamers and mostly decamers can be identified **(Figure 32b)**. At higher concentrations of Ca^{2+} and Mg^{2+} ions, up to 100 mM, and at pH 7.0, incomplete reassociation of RvH1 into helical tubular structures of short lengths and of ca 25 nm diameter with occasional didecamers, elongated multidecamers and residual subunits were observed after overnight dialysis.

The tubular polymer of RvH1 is of significant smaller diameter compared to the multidecamers (ca. 25 nm versus 33 nm). Most of the free subunits are utilized for the formation of tubular polymers and multidecamers which become progressively longer after three days of dialysis **(Figure 32c)**. Individual tubules occasionally link end-to-end, but mostly they remain separate over an extended period of time and are not as long as the multidecamers. Tubular polymers were produced with KLH1 [Harris et al., 1997a], HtH1 subunits [Dolashka et al., 1999] and *Helix pomatia* Hc [van Breemen et al., 1979] after dialysis against SB, containing 100 mM $CaCl_2$ and $MgCl_2$. With increasing time of dialysis against SB containing 100 mM $CaCl_2$ and $MgCl_2$, KLH1 forms a mixture of oligomeric forms and polymeric tubules, which have a tendency of parallel alignment and progressive elongation. The speed of reformation for KLH and HtH subunits was more rapid at 100 mM $CaCl_2$ and $MgCl_2$ [Harris et al., 1997b; Dolashka et al., 1996] than at 10 mM. The same tendency was observed for RvH1, faster reassociation in SB containing 100 mM $CaCl_2$ and $MgCl_2$ occurred in comparison with the presence of 10 mM $CaCl_2$ and $MgCl_2$.

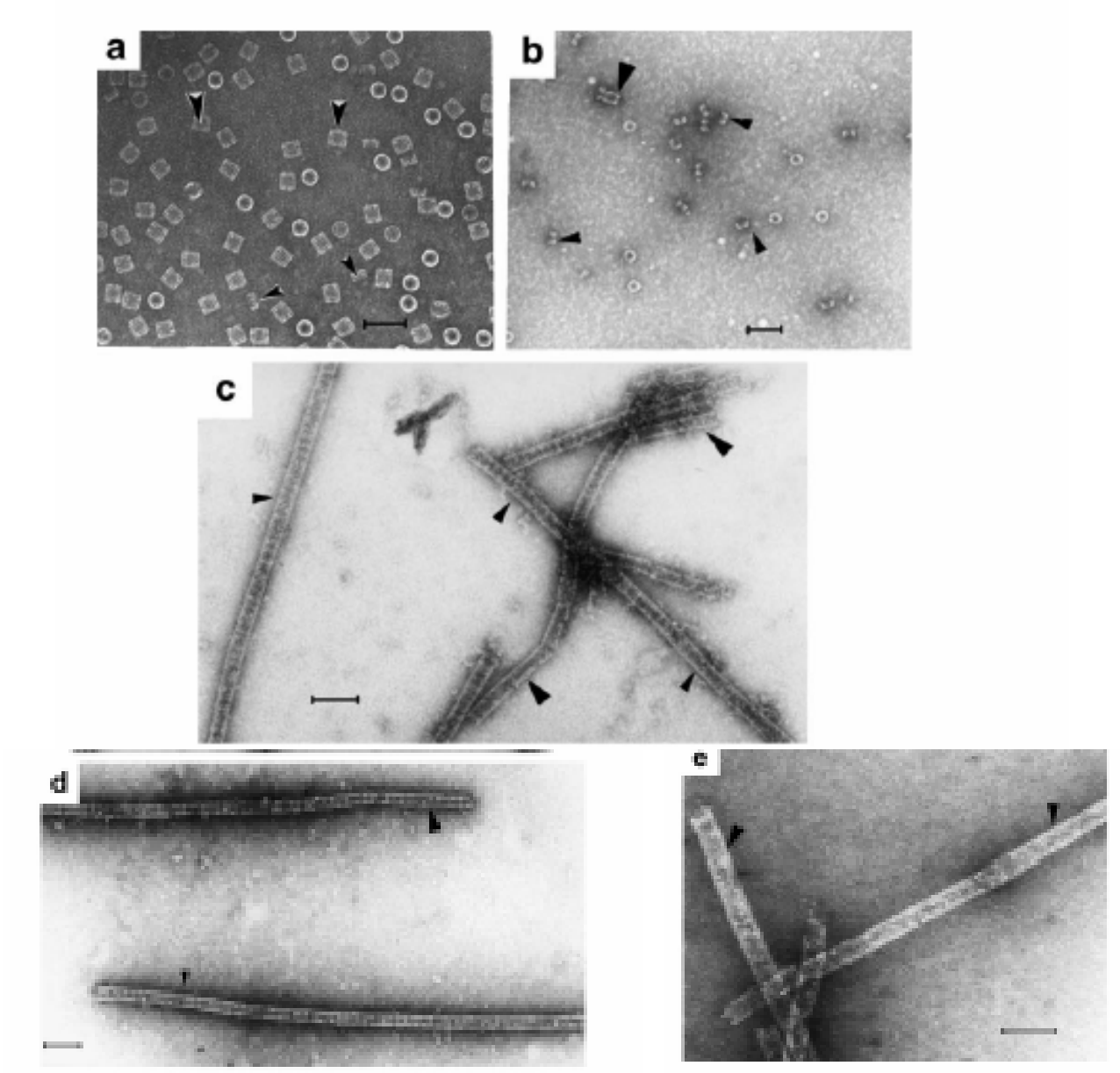

***Figure 32. Gallery of electron micrographs of the oligomerization dynamics of RvH1**. **a) Purified RvH1**, obtained by ion exchange chromatography, contains predominantly didecamers (large arrowheads) and decamers (small arrowheads); **b) RvH1 decamers (small arrowheads) produced by overnight dialysis** against 50 mM Tris/HCl buffer, pH 9.6, containing 2 mM $CaCl_2$ and $MgCl_2$. Complete reassociation of the monomers into stable decamers did not occur and some didecamers (large arrowheads) are still present; **c) Formation of a mixture of short helical tubules** (large arrowheads) and multidecamers (small arrowheads) after dialysis of RvH1 for three days in 50 mM Tris/HCl buffer, pH 7.0, containing 100 mM $CaCl_2$ and $MgCl_2$; **d) Reassociation of RvH1, after a period of one week** into multidecamers (small arrowhead) and helical tubules (large arrowhead) in the presence of 100 mM $CaCl_2$ and $MgCl_2$. Residual subunits are not present; **e) RvH1 multidecamers and helical tubules** (no didacemers) were elongated after dialysis of two weeks against the same buffer as in d.*

After dialysis of RvH1 for one week against SB, containing 100 mM $CaCl_2$ and $MgCl_2$, only

long multidecamers and tubules can be observed **(Figure 32d)**. For the RvH1 subunits the situation after reassociation in the presence of calcium and magnesium ions parallels more closely to KLH2 and HtH2 than to KLH1 and HtH1.

4.1.1.4 Studies on the stability of RvH1 multidecamers and tubules at different pH values

The stability of the multidecameric forms of RvH1 and RvH2 were investigated after dialysis of the proteins against the same buffer, but with different pH values (pH 7.0, 8.6, 9.2 and 9.6) **(Figure 33).**

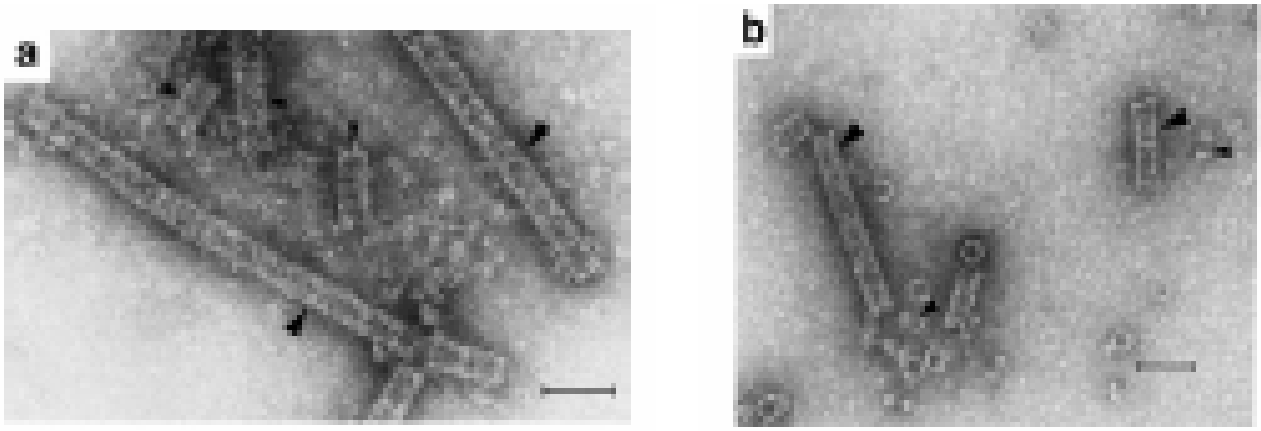

Figure 33. Study of stability of RvH1 multidecamers and tubules with incresing pH of the buffer. a) After dialysis for 2 days *against 50 mM Tris buffer, containing 100 mM $CaCl_2$ and $MgCl_2$, pH 8.6, stable multidecamers (large arrowheads) and some shorter multidecamers (small arrowheads) are present;* ***b) Stable RvH1 multidecamers dissociated to shorter multidecamers*** *(large arrowheads), didecamers and many decamers (small arrowheads) after one week of dialysis against 50 mM Tris buffer, containing 100 mM $CaCl_2$ and $MgCl_2$, pH 9.2.*

The stability of the RvH1 multidecamers **(Figure 32e)** was found to be pH – dependent. After dialysis for 2-3 days against 50 mM Tris/HCl buffer, pH 8.6, containing 100 mM $CaCl_2$ and $MgCl_2$, the length of the multidecamers and helical tubules decreased.

Figure 33a shows long multidecamers and tubular polymers, but also the presence of shorter multidecamers and dissociated subunits. Only few long, but mostly short multidecamers, didecamers, decamers and subunits were observed after increasing the pH to 9.2 **(Figure 33b)**.

4.1.1.5 Gallery of electron micrographs on the oligomerization dynamics of structural subunit RvH2

The situation after reassociation of the second isoform RvH2 **(peak III in Figure 30)** is different to RvH1, but also depends on pH and the concentration of Ca^{2+} and Mg^{2+} ions. After dissociation in 0.13 M Gly/NaOH buffer, pH 9.6**,** the RvH2 subunit was reassociated by dialysis against SB in the presence of 2 mM Ca^{2+} and Mg^{2+} ions into decamers and some didecamers **(Figure 34a)**. These forms are, however, not stable and they reassociate into stable didecamers after dialysis against stabilizing buffer, pH 7.0, in the presence of 100 mM Ca^{2+} and Mg^{2+} **(Figure 34b)**. Although the speed of reformation was more rapid with 100 mM divalent cation concentrations, efficient production of RvH2 didecamers also occurred with a 10 mM calcium and magnesium concentration. Ionic manipulation of RvH2 subunit by dialysis against stabilizing buffer containing a higher (100 mM) concentration of $CaCl_2$ and $MgCl_2$ after three days **(Figure 34c)**, one week **(Figure 34d)** and two weeks **(Figure 34e)** increases the number and length of the multidecamers. However, the length of the multidecamers appears to be rather constant after two weeks and no extremely long multidecamers of RvH2 have been detected **(Figure 34e)** contrary to RvH1 **(Figure 32e)**. At higher concentrations of calcium and magnesium ions a tendency of the subunit RvH2 to form helical tubules was also observed, but these are shorter compared to the isoform RvH1. In **Figure 34d** and **e**, after one and two weeks of dialysis against SB with 100 mM of divalent ions, in addition to didecamers, short and long multidecamers, are present and short helical tubules. The length of the multidecamers is considerably larger than that of the tubular polymers. Also a different stability was observed for RvH2 at higher pH values compared to RvH1.

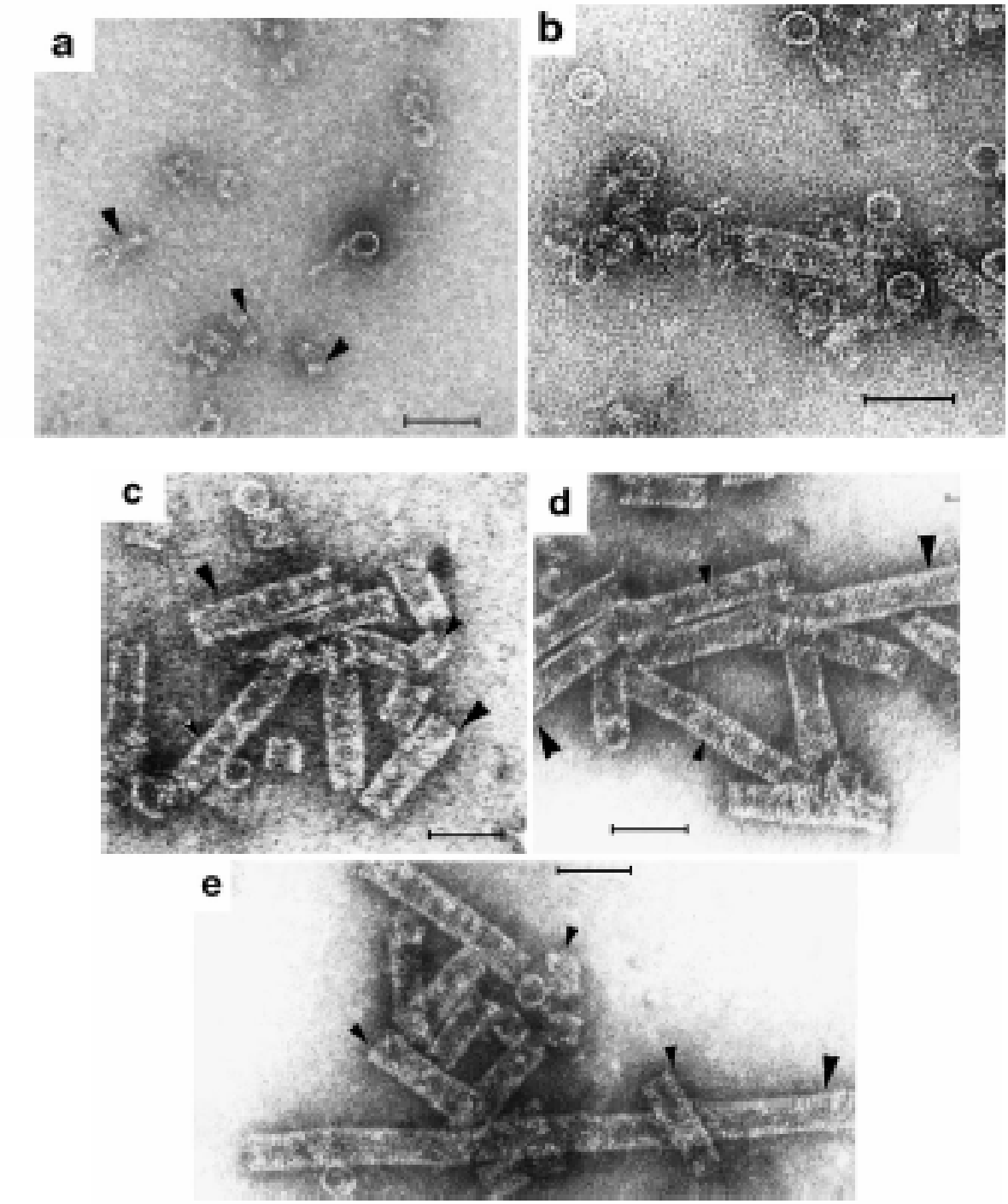

Figure 34. Gallery of electron micrographs of the oligomerization dynamics of RvH2. a) Purified RvH2*, dissociated into structural subunits, producing decamers (arrowheads) by overnight dialysis against stabilizing buffer, pH 9.6, containing 2 mM $CaCl_2$, 2 mM $MgCl_2$. Complete reassociation of the subunit of RvH2 into stable decamers does not occur;* ***b) Partial reassociation of RvH2 subunit*** *following overnight dialysis against 50 mM Tris/HCl buffer, pH 7.0, containing 100 mM $CaCl_2$ and $MgCl_2$, into free subunits, multidecamers and didecamers;* ***c) After three days, reassociation*** *under the conditions as in b is observed into, longer multidecamers (large arrowheads), tubules (small arrowheads) and some didecamers;* ***d) RvH2 aggregated to longer*** *(large arrowheads) and shorter multidecamers and tubular polymers (small arrowheads) after one week of dialysis under conditions as in b;* ***e) RvH2 multidecamers (large arrowheads) became elongated*** *after two weeks of dialysis.*

4.1.1.6 Studies on the stability of RvH2 multidecamers and tubules at different pH values

By increasing the pH of the SB, RvH2 multidecamers are less stable than those of RvH1, In the presence of high concentrations (100 mM) of Ca^{2+} and Mg^{2+} ions and increasing the pH of SB to 8.6, only few multidecameric forms of RvH2 are detected **(Figure 35a)** which dissociate at pH 9.2 into short multidecamers and mainly didecameric RvH2 forms and subunits are detected **(Figure 35b)**.

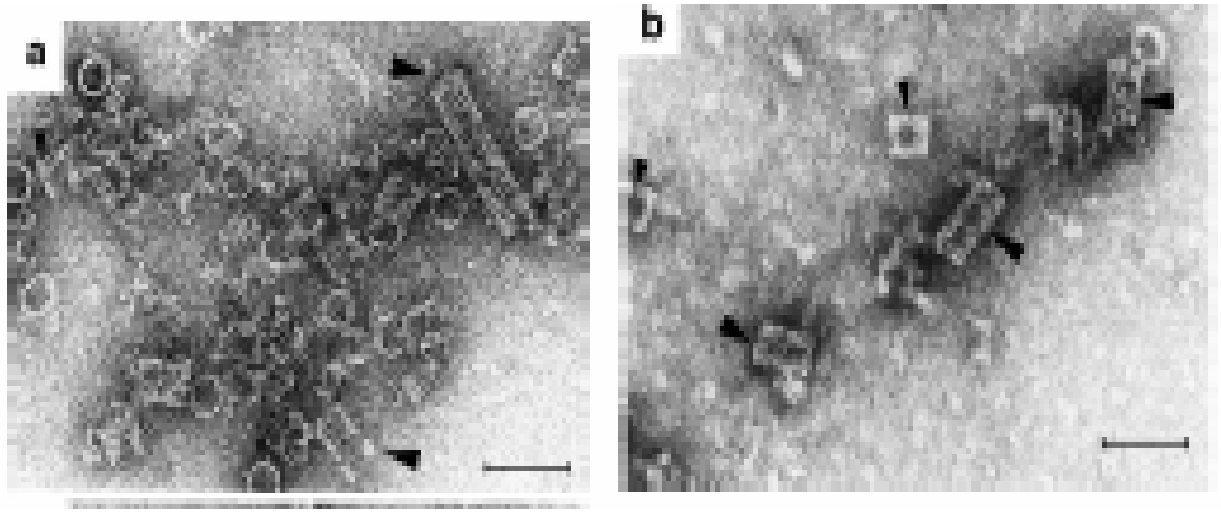

Figure 35. Study of stability of RvH2 multidecamers and tubules with increasing pH of the buffer. a) Dissociation of RvH2 multidecamers into short multidecamers *(larger arrowheads) and didecamers (smaller arrowheads) is observed after two days of dialysis against SB, pH 8.6;* ***b) Complete dissociation of RvH2 multidecamers into didecamers*** *(large arrowheads) is observed after two days of dialysis against SB, pH 9.2, containing 100 mM $CaCl_2$ and $MgCl_2$.*

The somewhat reduced ability of the RvH2, HtH1 and KLH1 subunits compared to those of RvH1, HtH2 and KLH2 to reassociate into long multidecamers and tubular helical polymers, [Harris et al., 2000; Söhngen et al., 1997] could be explained by the higher stability of these isoforms. Our preliminary studies have shown that RvH2 is more stable than RvH1. Its melting temperature (T_m=59℃) is also higher compared to that of RvH1 (T_m=53℃), KLH1 (T_m=56℃), and KLH2 (T_m=49℃) [Dolashka et al., 1996].

Reformation of RvH1 and RvH2 subunits is closer to the reformation process of keyhole limpet subunits, than to that of *Haliotis tuberculata* subunits [Harris et al., 2000].

4.1.1.7 Fluorescence intensity at 600 nm of purified RvH1 and RvH2 didecamers in stabilizing buffer.

The process of reassociation of RvH isoforms was also studied by fluorescence spectroscopy. The fluorescence intensity at 600 nm decreased stronger after reassociation of the structural subunit RvH1 **(Figure 36a)** compared to that of RvH2 **(Figure 36b)**.

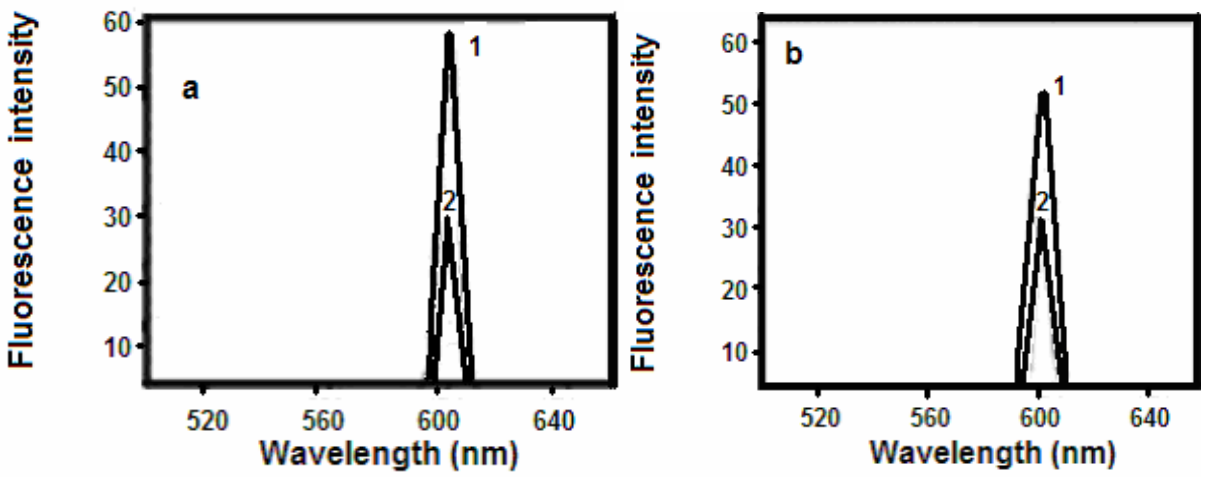

Figure 36. a). Fluorescence intensity at 600 nm of the purified RvH1 didecamers in stabilizing buffer, pH 8.2 (spectrum 1)*. Fluorescence intensity at 600 nm of the reassociated RvH1 subunit after two weeks of dialysis against 50 mM Tris/HCl buffer, pH 7.0, containing 100 mM $CaCl_2$ and 100 mM $MgCl_2$ (spectrum 2);* ***b) Fluorescence intensity at 600 nm of the purified RvH2 didecamers in stabilizing buffer, pH 8.2 (spectrum 1)*** *and reassociated RvH2 subunit, after two weeks of dialysis against 50 mM Tris/HCl buffer, pH 7.0, containing 100 mM $CaCl_2$ and 100 mM $MgCl_2$ (spectum 2).*

These fluorescence studies during the process of reassociation of Rapana hemocyanin isoforms confirms our conclusion from EM studies that the behaviour of the structural subunits RvH1 and RvH2 during reassociation at a 100 mM concentration of calcium and magnesium ions is different.

4.1.2 Oligomeric stability of *Helix vulgaris* hemocyanin (HvH)

Two isoforms have been isolated after dialysis of *Helix vulgaris* Hc against 0.13 M Gly/NaOH buffer, pH 9,6, overnight. They are α- and β- hemocyanin with molecular masses about 400 kDa as calculate from 8% SDS electrophoresis. After dissociation in

0.13 M Gly/NaOH buffer the protein was completely dissociated in subunits. Reassociation in 50 mM $CaCl_2$ and $MgCl_2$ buffer, pH 7.0, was not complete, and only decamers, didecamers and multidecamers were observed. The subunit of *Helix vulgaris* Hc appears to be more intact than the subunit of RvH and the reassociation is rather poor **(Figure 37 a and b)**.

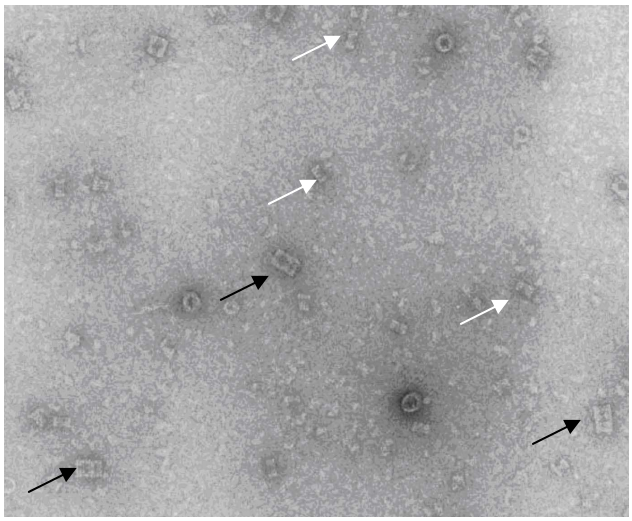

Figure 37. a) Partial reassociation of structural subunits of Helix vulgaris hemocyanin *following overnight dialysis against 50 mM Tris/HCl buffer, pH 7.0, containing 50 mM $CaCl_2$ and 20 mM $MgCl_2$ into free subunits, multidecamers (black arrowheads) and didecamers (white arrowheads). Native staining with 1% uranyl acetate was performed. The scale bar indicates 100 nm.*

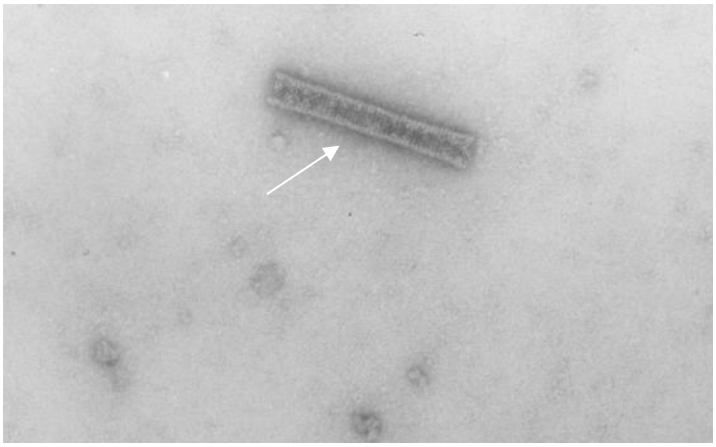

Figure 37. b) Gallery of electron micrographs of the oligomerization dynamics of HvH*. After three days**,** reassociation of HvH subunit following dialysis against 50 mM Tris/HCl buffer, pH 7.0, containing 100 mM $CaCl_2$ and $MgCl_2$**,** into, longer multidecamers (large white arrowhead).*

4.1.3. Isolation of functional units of the structural subunits RvH1 and RvH2 and N-terminal sequence determination after depolymerisation with $ZnCl_2$ and proteolytic enzymes.

Various FUs have been obtained by limited proteolysis of the structural subunits using suitable proteolytic enzymes, but different N-terminal sequences have been determined [Gebauer et al., 1999; Idakieva et al., 2000; Stoeva et al., 1998]. After depolymerisation of the structural subunits RvH1 and RvH2 with $ZnCl_2$, several FUs have

been isolated which showed identical sequences with FUs purified from trypsin- treated RvH1 and RvH2 (RvH1-a, RvH1-f, RvH2-a and RvH-e)**.**

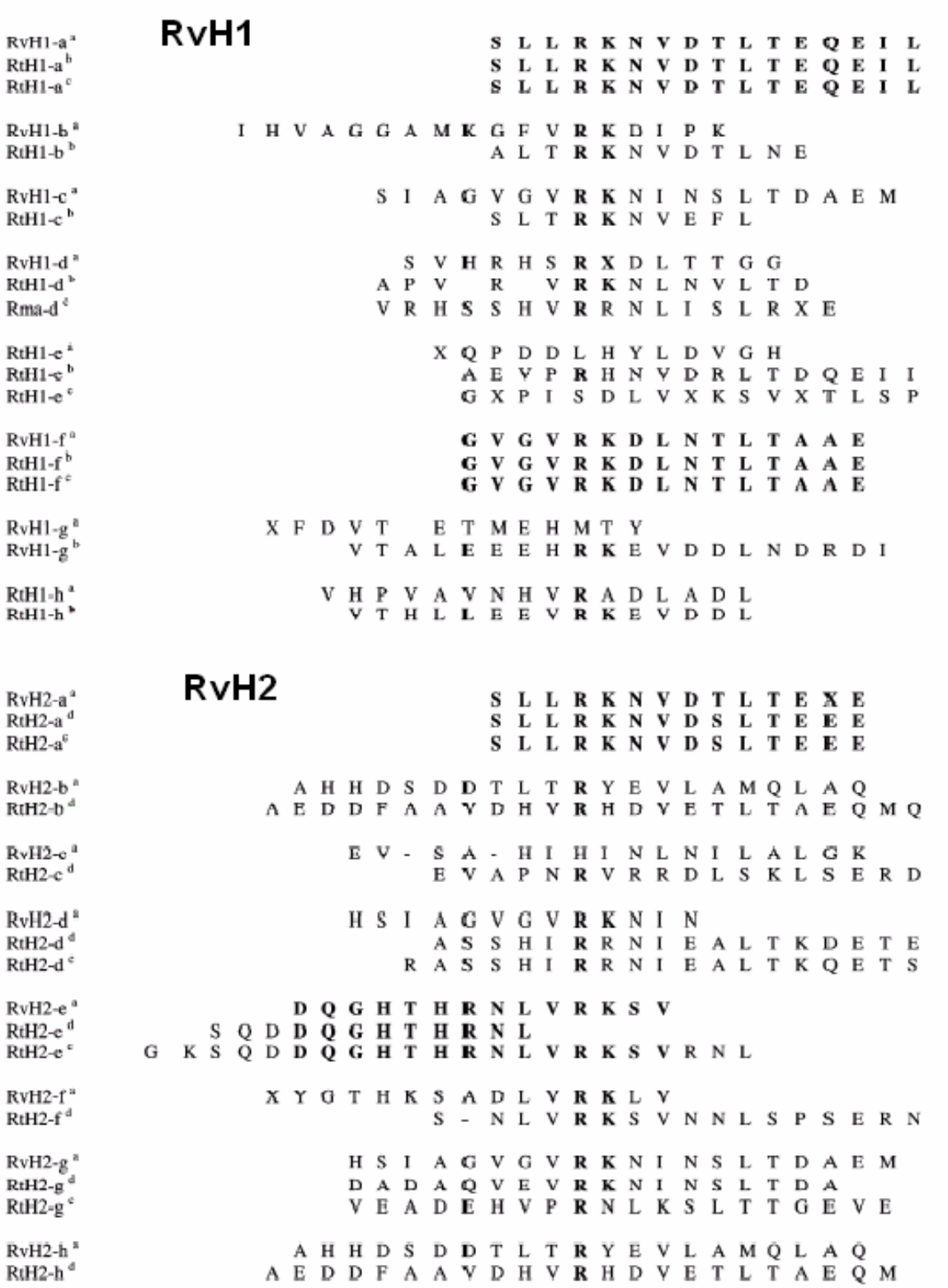

Figure 38. Comparison of the N-terminal sequences of various FUs obtained after treatment with Zn^{++} or limited proteolysis of structural subunits RvH1 and RvH2 using suitable proteolytic enzymes. *[a]- after depolymerisation with Zn; [b,c,d]- after treatment with enzymes [[b] Gebauer, et al., 1999; [c] Idakieva, et al., 2000; [d] Stoeva, et al., 1998].*

4.1.4 Characterization of the carbohydrate moieties of *Rapana venosa* hemocyanin using HPLC/electrospray ionization mass spectrometry and glycosidase digestions

4.1.4.1 Isolation of glycopeptides from the functional unit RvH1-a

Most hemocyanins (Hcs) are glycoproteins and there are large differences in their carbohydrate content and their monosaccharide composition. The carbohydrate moiety of molluscan Hcs has recently received particular interest for its immunostimulatory property. *Rapana* Hc is a glycoprotein, with a total carbohydrate content of 8.9% for the native molecule; 12.8 and 4.4%, were determined for the structural subunits RvH1 and RvH2 respectively [Stoeva et al., 1995]. The oligosaccharide content is more abundant in the N-terminal FU RvH1-a (7%) of the structural subunit RvH1 than in N-terminal FU RvH2-a (5.1%) of the structural subunit RvH2. The sugar content of the marine snail *Rapana venosa* Hc is similar to that of the protein from *Helix pomatia* (8.25%) [Lommerse et al., 1997], and about three times higher as compared with *Lymnaea stagnalis* (3.01%) Hc [Hall et al., 1977].

To confirm that the RvH1-a is indeed glycosylated, a screen on its carbohydrate content was performed using the orcinol method. The strategy used to analyze the carbohydrate portion of RvH1-a was to prepare a tryptic hydrolysate of the FU and separate its fragments, first by gel filtration and then by HPLC. Fractions giving a positive orcinol color reaction were further subjected to their amino acid and carbohydrate sequence determination.

Figure 39 shows the separation profile of the tryptic digestion products of FU RvH1-a using a Superdex 300 column. Gel filtration of the tryptic digest was separated on Superdex 300 column (2x30 cm) at a flow rate 1 ml.min^{-1} with bidistilled water. Faction peak № 1 gave a positive reaction in the orcinol/H_2SO_4 test and was further processed.

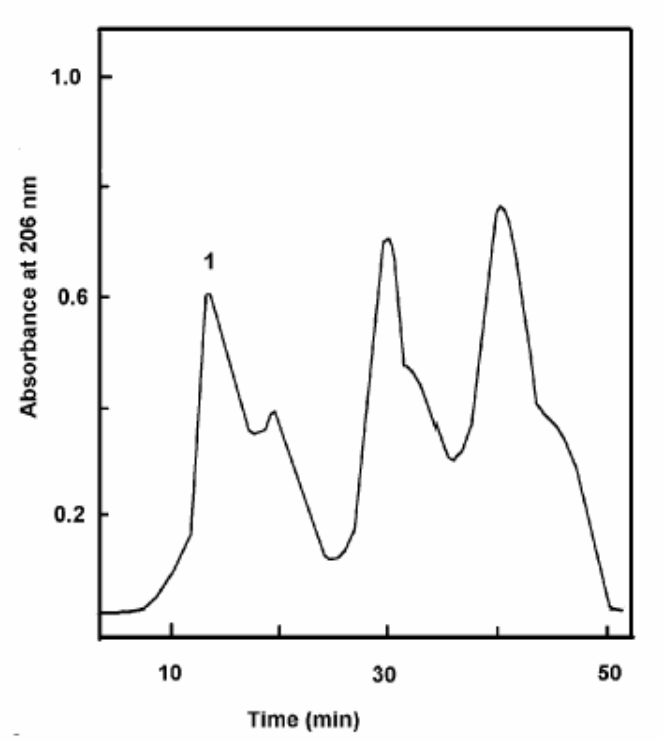

Figure 39. Separation profile of the tryptic digestion products of FU RvH1-a using a Superdex 300 column. *Gel filtration of the tryptic digest (50 µl of the trypsin solution bovine pancreas, Hc-trypsin ratio 50:1) was separated on Superdex 300 column (2x30 cm) at a flow rate 1 ml. min^{-1} with bidistilled water. Faction peak № 1 gave a positive reaction in the orcinol/H_2SO_4 test.*

The material eluted by fraction 1 of **Figure 39** was pooled and peptides were separated by reverse phase HPLC.

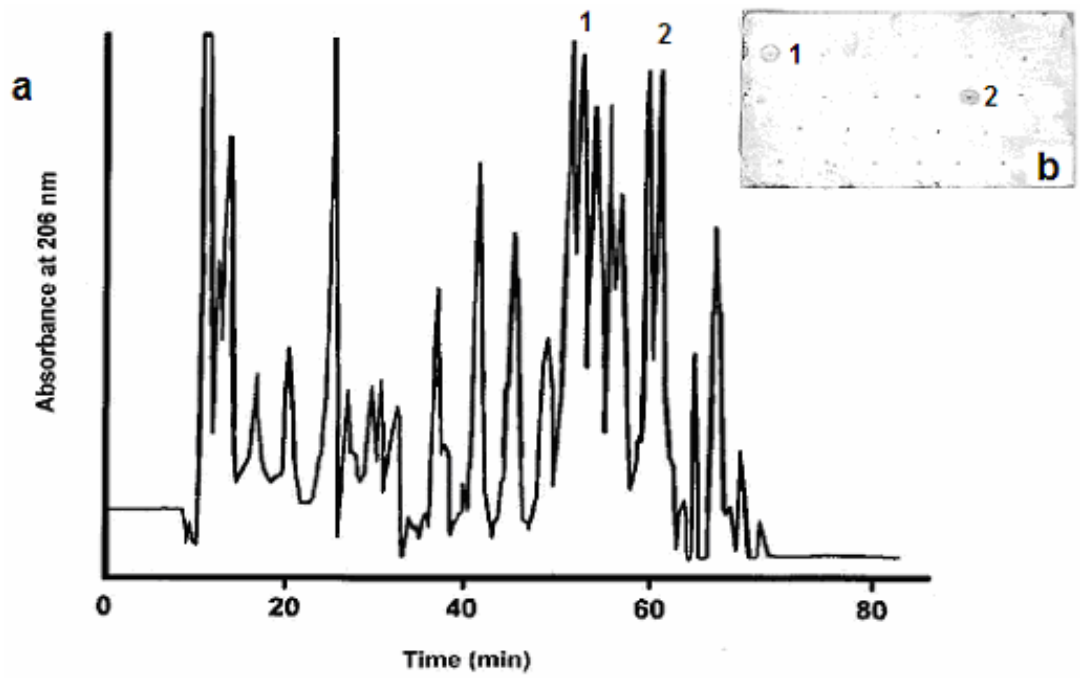

Figure 40. a) HPLC profile of fraction peak 1 (Figure 39) separated on a Nucleosil RP18 (C18, 100 mm length x 2.1 mm diameter) column *and eluted with a linear gradient of solvent A (0.1% TFA in water) and solvent B (0.085% TFA in acetonitrile) within 70 min at a flow rate of 1ml.min^{-1}. Peptide peak fractions were detected at a wavelength of 206 nm;* ***b) Insert, orcinol/H_2SO_4 test of eluted (glyco)peptides using a silica gel plate.*** *Fractions, 1 and 2 gave a positive reaction for carbohydrates.*

Each fraction was collected, vacuum-concentrated and tested for carbohydrates on a silica-gel plate with orcinol/H_2SO_4. Two fractions, 1 and 2 **(Figure 40a)**, gave a positive reaction for carbohydrates **(Figure 40b, insert)** and were further studied using ESI-MS [Harvey, 1998; Harvey, 1996] and MALDI-MS [Sutton et al., 1994].

4.1.4.2 Sequencing of glycopeptides from the functional unit RvH1-a

The two glycopeptides were automatically sequenced after removal of the carbohydrate chains with PNGase-F and their sequences are shown in **Figure 41** (Glp 1 and Glp 2). In the same figure these structures are compared with specific sequences of other molluscan Hcs containing carbohydrate linkages.

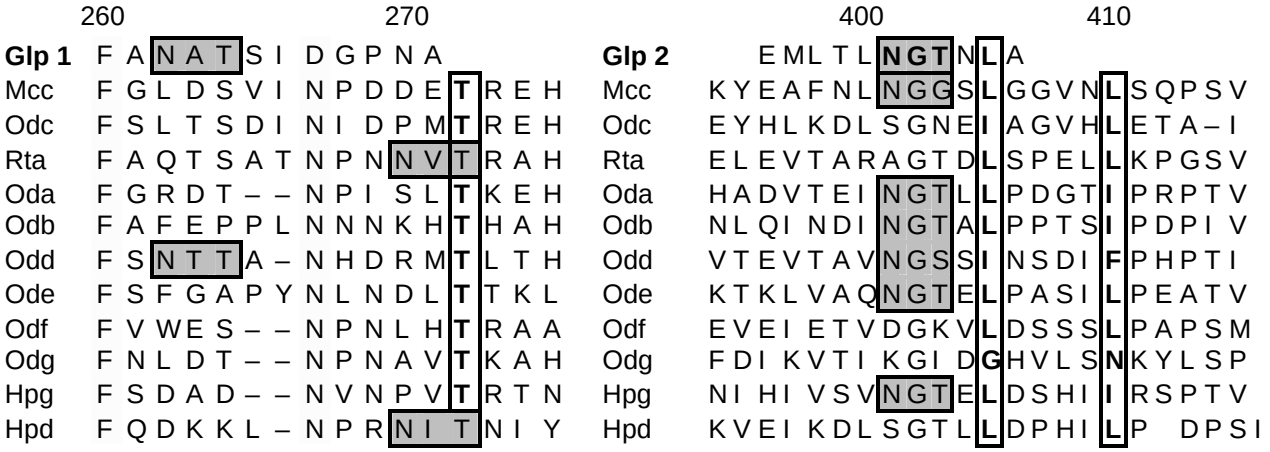

Figure 41. Sequence alignments of the regions with suggested N-linked sites of FUs from different molluscan Hcs*: Keyhole limpet M. crenulata (Mcc) [Stoeva et al., 1999], O. dofleini (Oda Odb, Odd, Ode, Odf and Odg) [Cuff et al., 1998], R. thomasiana (Rta) [Stoeva et al., 1997], H. pomatia (Hpd and Hpg) [Gielens et al., 1997]*

Glycopeptide 1 (Glp 1 in **Figure 41**) consists of 12 amino acid residues with a molecular mass of 1177.5 Da, as calculated from the sequence. LALIGN and Fasta programmes were used to analyse the alignment of Glp 1 and Glp 2 with the amino acid sequences of other molluscan Hcs. The amino acid sequence of Glp 1 (FA**NAT**SIDGPNA) well overlaps with positions 260-271 of the FUs of molluscan Hcs from *Megathura crenulata* (Mcc) [Stoeva et al., 1999], *Octopus dofleini* (Oda-Odg) [Cuff et al., 1998], *Rapana thomasiana* (Rta) [Stoeva et al., 1997] and *Helix pomacia* (Hpd and Hpg) [Gielens

et. al., 1997]. The presence of a fully conserved Phe residue at position 260 and Asn/Asp residue at position 267 allows the alignment with the other reported sequences in spite of the rather high variability in this region. From all the listed sequences in **Figure 41,** only for the Odd Hc fragment a glycosylation site is observed. Similar considerations apply for glycopeptide 2 (Glp 2, EMLTL**NGT**NL, **Figure 41)** where Gly 402, Leu 405 and Leu 410 are conserved residues. A sequence containing 11 amino acid residues with a calculated molecular mass of 1175.6 Da was found for Glp 2. This glycopeptide contains a N-G-T sequence that is strongly conserved among molluscan Hcs: *M. crenulata* (Mcc) [Stoeva et al., 1999], *O. dofleini* (Oda-Ode) [Cuff at al., 1998] and *H. pomatia* (Hpd) [Gielens et. al., 1997] in the 401-403 sequence region (N-G-T/S), and the Glu residue at position 396 is found in 6 out of 12 residues and the Leu residue at position 405 is found in 9 out of 12 cases. Thus, two putative glycosylation sites are found in the sequence of RvH1-a with consensus sequences for N-linked carbohydrate oligosaccharides.

4.1.4.3 Composition of the carbohydrate portion of glycopeptide 1 (Glp 1) of functional unit RvH1-a

Glycopeptide 1 was analyzed by MALDI-MS before and after treatment with PNGase-F **(Table 3, Figure 42a, b)**. The glycopeptides were dissolved in 0.1% TFA (v/v) and applied onto the target. As matrix α-cyano-4-hydroxycinnamic acid in 70% acetonitrile/H_2O (70:30, v/v) was used.

In the MALDI mass spectrum, acquired before PNGase-F treatment only one molecular ion at m/z 2786 could be detected, caused by the intact Glp 1 sodium adduct ion $[Glp\ 1+Na]^+$ **(Figure 42a)**. In contrast, after PNGase-F treatment three signals could be observed in the MALDI mass spectrum **(Figure 42b)**. The signal at m/z 2786 is related to the intact Glp 1 **(see Figure 42a)**, whereas the signal at m/z 1609 $[M+Na]^+$ is attributed to the oligosaccharide.

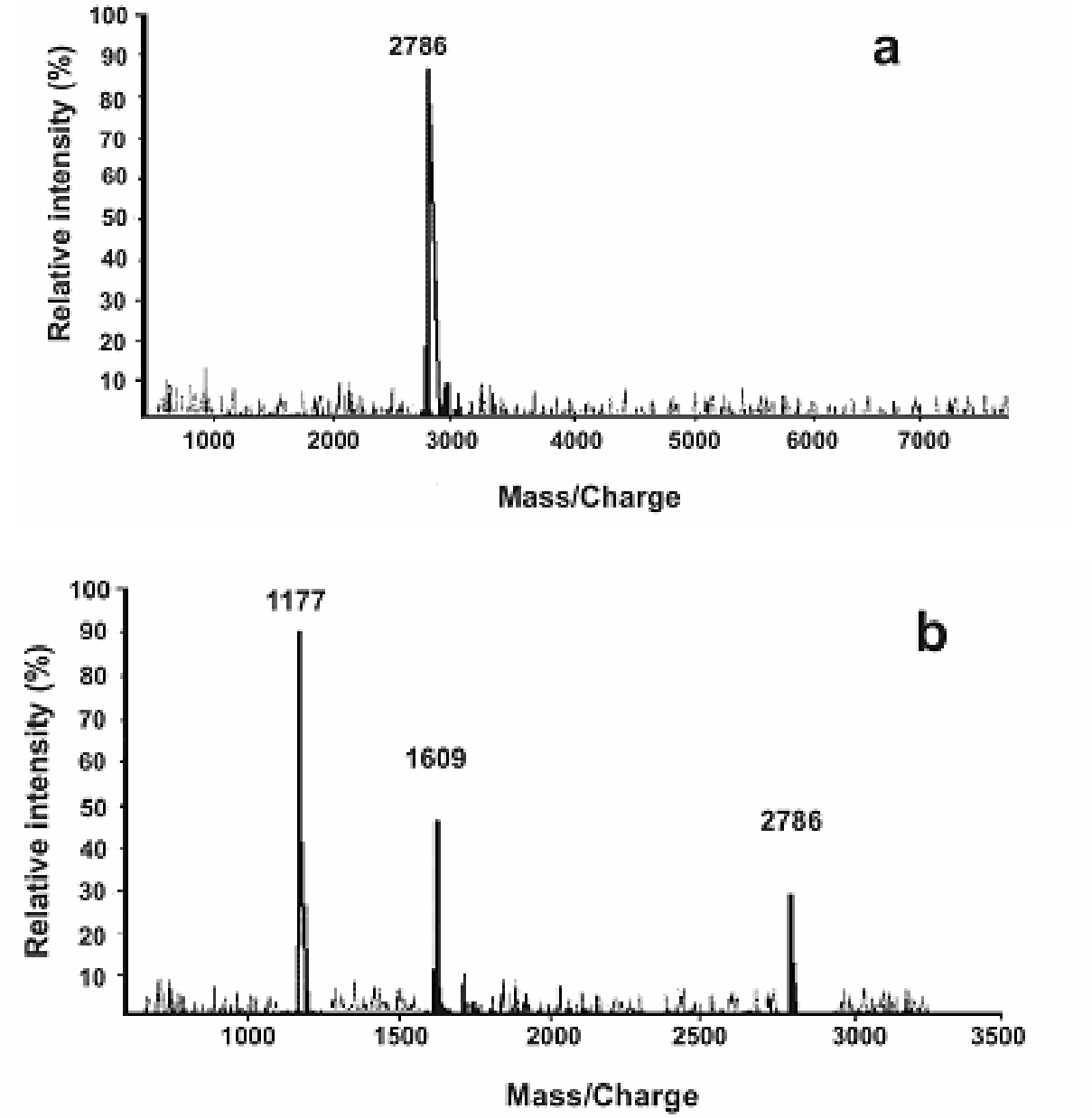

Figure 42 a) MALDI mass spectrum of Glp 1 from FU RvH1-a, *isolated via HPLC as illustrated in Figure 40, before treatment with PNGase-F and only one molecular ion at m/z 2786 was detected;* ***b) MALDI mass spectrum of Glp 1 after treatment with PNGase-F*** *with three molecular ions at m/z 2786, 1609 and at 1177 were observed related to the intact Glp 1, oligosaccharide and deglycosylated peptide, respectivelly. As matrix α-cyano-4-hydroxycinnamic acid in 70% acetonitrile/H_2O (70:30, v/v) was used.*

The first signal (m/z 1177) corresponds to the deglycosylated peptide, as demonstrated by the mass value calculated from the amino acid sequence (1177.5 Da, **Table 3)**.

To determine the oligosaccharide sequence, different specific glycolytic enzymes were added to glycopeptide 1: β1-2,3,4,6-GlcNAcase; α1-2,3-mannosidase, α1-2,3,6-mannosidase, β1-3,4,6-galactosidase. The mass (1586 Da, **Table 3**) of this carbohydrate

Table 3. Monosaccharide masses of FUs RvH1-a and RvH1-f from R. venosa Hc determined after treatment with PNGase-F and measured by MALDI-MS.

Fraction	Amino acid sequence of the peptide	Glycopeptide Mw (Da)	Peptide Mw (Da)	Oligosaccharide Mw (Da)
Glp 1	FA**NAT**SIDGPNA	2786 $[2763 + Na]^+$	1177.0[a] 1177.5[b]	1609 $[1586 + Na]^+$
Glp 2	EMLTL**NGT**NLA	2846.2 $[2828 + H]^+$	1175.7[a] 1175.6[b]	1653 $[1652 + H]^+$
Glp 3	IHSYSGSYINASLLHGPSII	3848 $[3847+H]^+$	2940[a]	907

[a] Molecular mass measured by MALDI.
[b] Molecular mass calculated by amino acid sequence.

moiety would account for an oligosaccharidic chain containing (SO_4) MeGal $GlcNAc_4$ Man_3 connected to the peptide. Depending on the specificity of the individual enzymes, the different linkages can be identified by recording the pattern of molecular weights resulting from the digestion with the pool of glycosidases. After 24 h incubation at 37℃, the sample was first analyzed by capillary electrophoresis **(Figure 43b, insert)**. Four different peaks were detected, indicating that the treatment causes heterogenity resulting from different cleavage sites.

In parallel, Glp 1 treated with the different glycolytic enzymes was analyzed by ESI-MS **(Figure 43)**. The mass spectrum was interpreted on the basis of the data obtained from MALDI-MS **(Figures 42)**, amino acid sequence **(Figure 41)** and the known specificity of the glycosidases.

The signal observed at m/z 1747.0 can be attributed to the peptide FANATSIDGPNA (1177,5 Da) bearing two GlcNAc and one (β1-4) Man residues (568 Da), as expected from the specifity of α1-2,3,6-, α1-2,3-mannosidases and β1-2,3,4,6-GlcNAcase removing the carbohydrates attached to (α1-6)Man and (α1-3)Man, connected to (β1-4) Man **(Table 4, A)**

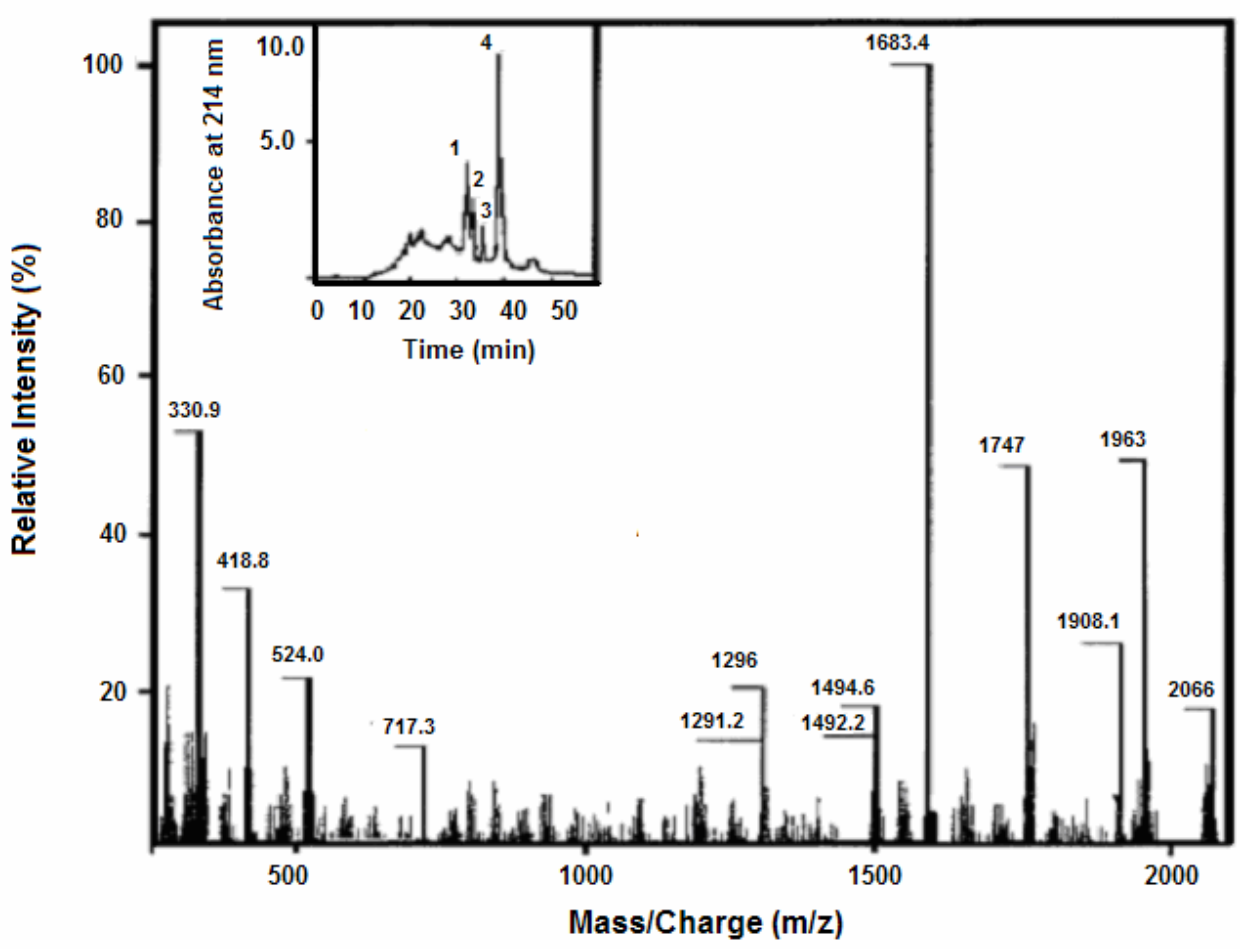

Figure 43. a)(Main diagram): Positive ion ESI-MS of Glp 1 after enzymatic cleavage *with specific glycosidases: β1-2,3,4,6-GlcNAcase, α1-2,3,6-mannosidase and α1-2,3-mannosidase.* ***b) (Insert)****: Capillary electrophorogram of the Glp 1 after treatment with different glycosidases indicated several fragments separations. Conditions: Glp 1 was dissolved in 50 µl running buffer (50 mM phosphate buffer, pH 2.5), diluted with water (10:1, v/v) and introduced by pressure injection (5 µl.min^{-1}).*

The signal at m/z 1908.1 results from the peptide bearing two GlcNAc, one (β1-4) Man and one (α1-6) Man residue (730 Da), as expected from the specifity of α1-2,3-mannosidase, cleaving only (α1-3) Man and β1-2,3,4,6- GlcNAcase removing 3MeGal and GlcNAc(β1-2) from (α1-6) Man (**Table 4, B**). This loss of 856 Da compared to the intact glycopeptide indicates that suggestively, the following residues were removed: MeGal, GlcNAc, Man, MeGlcNAc, and SO_4^{2+}.

The peak at m/z 1953 corresponds to the carbohydrate fragment containing two GlcNAc, one (β1-4) Man and suggestively 3MeGlcNAc(β1-2) resulting from the activity of α1-2,3,6- and α1-2,3-mannosidases removing carbohydrates attached to (α1-6) Man and

(α1-3) Man connected to (β1-4) Man (**Table 4,C**). The signal observed at m/z 1583.4 can be attributed to the peptide FANATSIDGPNA (1177.5 Da) bearing two GlcNAc groups (**Table 4,D**).

Table 4. Suggested structures of the carbohydrate chains, calculated on basis of observed [M+H]$^+$ signals in the ESI-MS (Figures 43 and 45). *P represents the peptide with the sequence FANATSIDGPNA (1177 Da).*

№	*Enzymes*	[M+H]$^+$ (m/z)	*Structure*
	Glycopeptide 1		
A	α1-2,3- and α1-2,3,6-mannosidase and β1-2,3,4,6-N-GlcNAcase	1747	← Man(β1-4) GlcNAc(β1-4) GlcNAc ¬**P**
B	α1-2,3-mannosidase and β1-2,3,4,6-N-GlcNAcase	1908	Man(α1-6) ↖ ← Man(β1-4) GlcNAc(β1-4) GlcNAc ¬**P**
C	α1-2,3,6-mannosidase and α1-2,3-mannosidase	1953	3MeGlcNAc(β1-2) ←Man(β1-4) GlcNAc(β1-4) GlcNAc¬**P**
D	β1-2,3,4,6-N-GlcNAcase	1583	-GlcNAc(β1-4) GlcNAc¬**P**
	Glycopeptide 2		
E	α1-2,3-mannosidase, β1-2,3,4,6-N-GlcNAcase and PNGase F	731	Man(α1-6) ↖ ← Man(β1-4) GlcNAc(β1-4) GlcNAc

Based on these data the carbohydrate structure for glycopeptide 1 from FU RvH1-a is proposed as shown below:

glycopeptide 1 SO_4 Man(α1-6) ↖

3MeGlcNAc(β1-2) ← Man(β1-4) GlcNAc(β1-4) GlcNAc-ol

3MeGal(β1-3) GlcNAc(β1-2) Man(α1-3) ↙

4.1.4.4 Carbohydrate content of glycopeptide 2 (Glp 2) of functional unit RvH1-a and glycopeptide 3 (Glp 3) of functional unit RvH1-f

The use of specific glycosidases, as described above, and the combination of changes in glycopeptide mass after each digestion step allows to suggest a sequence also for glycopeptide 2 (Glp 2). Only one peak at 2846 Da $[M+2H]^{2+}$ was observed in the MALDI mass spectrum (**Figure 44a**).

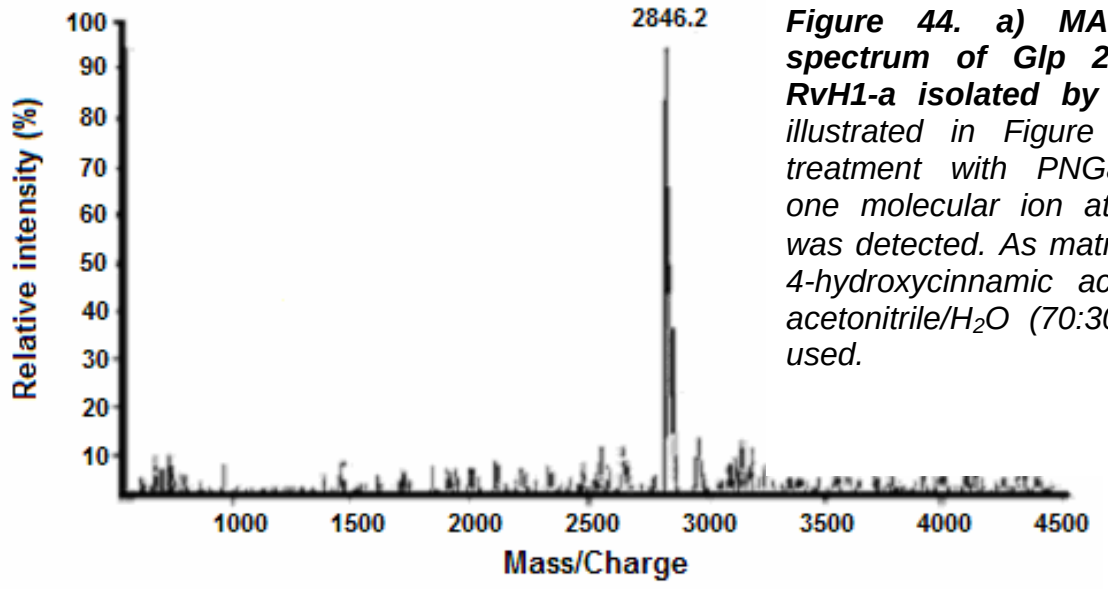

Figure 44. a) MALDI mass spectrum of Glp 2 from FU RvH1-a isolated by HPLC. *As illustrated in Figure 40 before treatment with PNGase-F only one molecular ion at m/z 2846 was detected. As matrix α-cyano-4-hydroxycinnamic acid in 70% acetonitrile/H_2O (70:30, v/v) was used.*

As reported in **Figure 44b**, two peaks characterize the MALDI-MS spectrum of the oligopeptide after cleavage with PNGase-F.

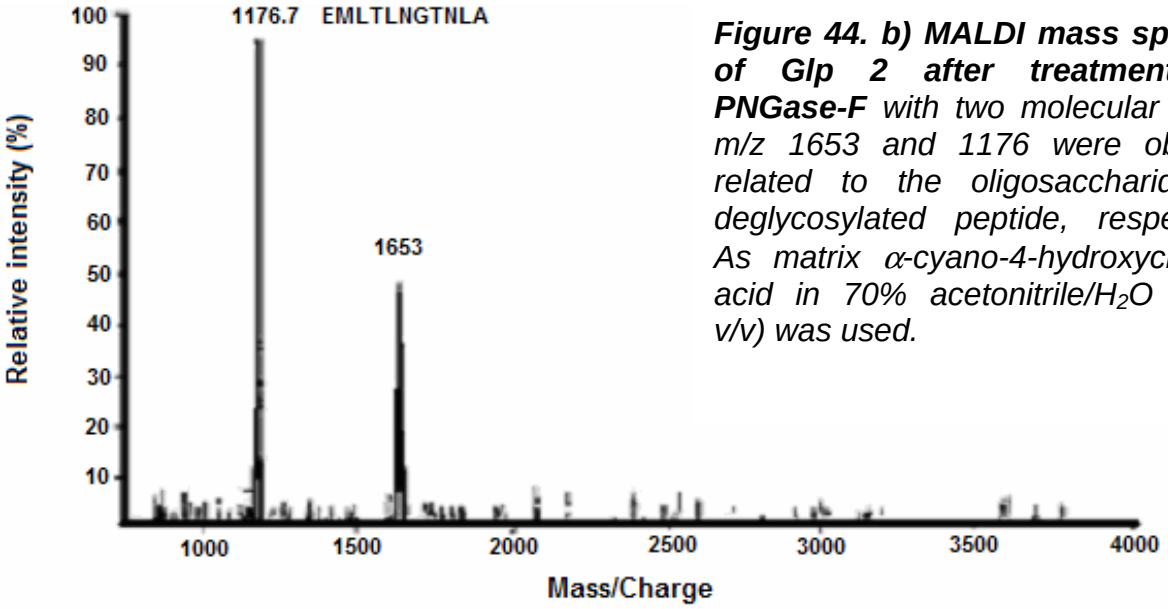

Figure 44. b) MALDI mass spectrum of Glp 2 after treatment with PNGase-F *with two molecular ions at m/z 1653 and 1176 were observed related to the oligosaccharide and deglycosylated peptide, respectively. As matrix α-cyano-4-hydroxycinnamic acid in 70% acetonitrile/H_2O (70:30, v/v) was used.*

The signal observed at m/z 1175 can be attributed to the peptide FANATSIDGPNA with the molecular weight 1177.5 Da, calculated on basis of its amino acid sequence (Table 3). Thus, the 1653 peak can be suggestively assigned to an oligosaccharide with the structure $3MeGal_2\ GlcNAc_4\ Man_3$.

The presence of a consensus sequence for one N-linked glycosylation site (-N-G-T) of the peptide chain indicates that the oligosaccharide is connected to Asp 401 *via*

GlcNAc. Two peaks were separated also by capillary electrophoresis after treatment of glycopeptide 2 with PNGase-F only, corresponding to the peptide and the carbohydrate chain (Figure 45b insert). Glp 2 was treated with β1-3,4,6-galactosidases, β1-2,3,4,6-GlcNAcase, α1-2,3-mannosidase and subsequently analyzed by ESI-MS (Figure 45). Because Glp 2 was cleaved with PNGase-F before glycosidic treatment, the N-linked carbohydrate was removed from the glycopeptide. Therefore, the signal at m/z 731 in the ESI mass spectrum is tentatively assigned to $Man_2GlcNAc_2$. (**Table 4, E**).

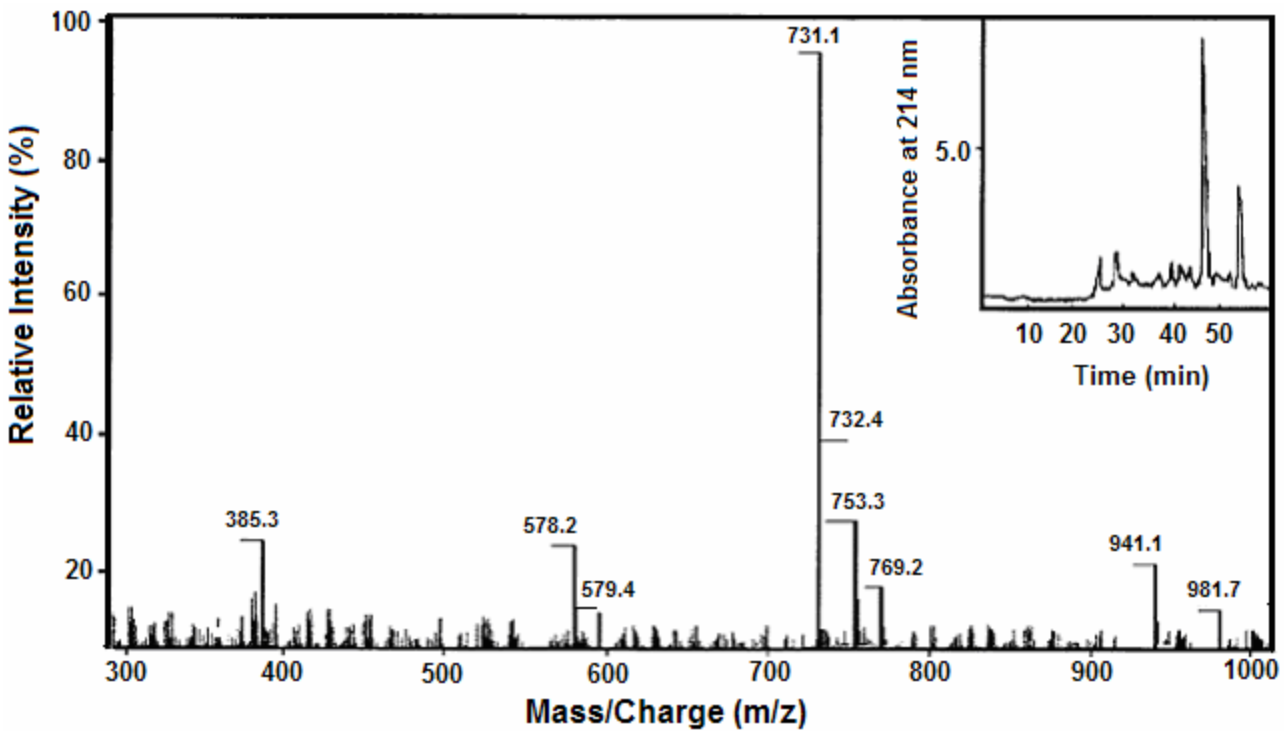

Figure 45. a) (Main diagram): Positive ion ESI mass spectrum of Glp 2 after enzymatic cleavage *with PNGase-F, β1-2,3,4,6-GlcNAcase and α1-2,3- mannosidase.* ***b) (Insert)****:* ***Capillary electropherogram of glycopeptide 2 after treatment with PNGase-F*** *shows two main fragments separation. Conditions: Glp 2 was dissolved in 50 µl running buffer (50 mM phosphate buffer, pH 2.5), diluted with water (10:1, v/v) and introduced by pressure injection (5 µl.min^{-1}).*

Based on cleavage with specific glycosidases followed by observed mass spectrometric data we suggest that the carbohydrate structure of glycopeptide 2 from FU RvH1-a could be assigned as follows:

glycopeptide 2

3MeGal(β1-3) GlcNac(β1-2) Man(α1-6) ↖
Man(β1-4) GlcNAc(β1-4) GlcNAc-ol
3MeGal(β1-3) GlcNAc(β1-2) Man(α1-3) ↙

Our results are in line with the presence of a common trimannosyl-N,N'-diacetylchitobiose core Man(α1-6) [Man(α1-3)]Man(β1-4)GlcNAc(β1-4)GlcNAc-ol and different antennae are attached to the α-Man residues [Lommerse et al., 1997, Hall et al., 1977]. This structural principle applies also to Hcs of different molluscs as well as to the FUs RvH1-a (this study) and RvH2-e [Stoeva et al., 1997]. The recent characterization carried out on the carbohydrate chains of all FUs of *Helix pomatia* Hc [Lommerse et al., 1997] identified primary structures of 21 novel monoantennary and diantennary N-glycans of the glycoprotein besides its core element. The oligosaccharide fragments (antennae) were released from the glycoprotein by Smith degradation of an Hc pronase digest and the major antennae were characterized using ^{1}H NMR spectroscopy and fast atom bombardment mass spectrometry. In this study, however, the number of carbohydrate chains for each FU was not defined, because the whole Hc was used, and also the linkage sites were not identified. In the present study we show that two N-linkage sites are present within one functional unit and that the two different chains differ in their branching characteristics. From the sequence alignment we suggest that the presence of two N-linkage sites are characteristic for the FUs of other Hcs as well. As far as the N-terminal FUs a of *Rapana venosa* Hc RvH1-a and RvH2-a are concerned, the sequence of the former shows the presence of two consensus sequences: one is found in the same region as Glp 1 **(Figure 41)** while a second one is located upstream close to the N-terminus (-N-D-S-; res. 32-34 [Stoeva et al., 1997, data not reported in **Figure 41**]. As it is obvious from **Table 3,** the glycosidic linkage site at position 401-403 well overlaps with several other Hcs. These results are in agreement with the X-ray study of the RvH2-e, identifying two olygosaccharide side chains connected to Asn 127 and Asn 17, although only one

glycopeptide has been so far isolated but not identified from the same source [Stoeva et al., 2002].

The same method was applied and for study of carbohydrate properties of FU RvH1-f. After trypsin treatment only one glycopeptide was identified with a Mw 3845, which was reduced to 2940 after PNGase-F treatment. Based on cleavage with specific glycosidases followed by observed mass spectrometric data we suggest that the carbohydrate structure of glycopeptide 3 from RvH1-f could be assigned as follows:

glycopeptide 3 Man(α1-6) ↖
Man(β1-4) GlcNAc(β1-4) GlcNAc-ol
3MeMan(α1-3) ↙

4.1.5 Structure and stability of arthropodan hemocyanin *Limulus polyphemus*

4.1.5.1. Isolation of structural subunits of *Limulus polyphemus* hemocyanin

The electron microscopic observations of native *M. squinado* [Dolashka-Angelova et al., 2000], *H. americanus* [Dolashka-Angelova et al., 1999], *B. sindicus* [Abbasi et al., 2000] Hcs reveal that these proteins exist as a mixture of four-, di- and mono-hexameric aggregates. The same results were observed for Hcs of *L. polyphemus* and *P. vulgaris*. The native molecule was dissociated at 0.1 M $NaHCO_3$, pH 9.5, containing 10 mM EDTA and 1 M urea, then chromatographically separated on a Resource 6 ml column, equilibrated with 0.1 M $NaHCO_3$ buffer, containing 10 mM EDTA and 1 M urea, pH 9.5, into five major bands with molecular masses of about 75 kDa **(Figure 46a, b)**.

The undissociated protein, eluting in the front of the chromatogram, accounts for 5% of total protein. Five fractions, indicated in **Figure 46a** as L1–L5, can be separated as major components present to 90% as the oxygenated form, as indicated by A_{340}:A_{278} values at 0.20.

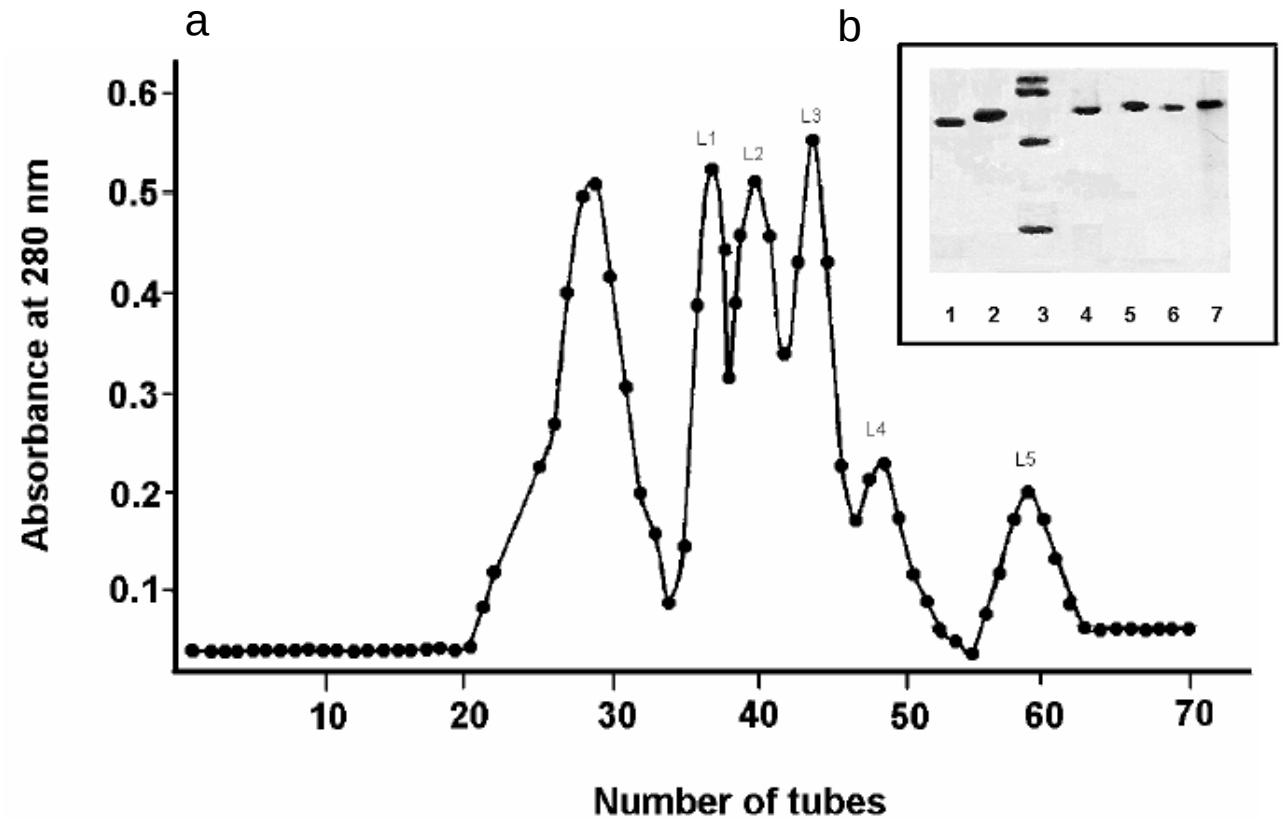

Figure 46. a) Fast protein liquid chromatography (FPLC) of dissociated subunits of Limulus polyphemus *on a Resource 6 ml column, equilibrated with 0.1 M $NaHCO_3$ buffer, containing 10 mM EDTA and 1 M urea, pH 9.5. Subunits were separated with a linear NaCl gradient (0–1 M) at a flow rate of 2.0 ml.min $^{-1}$. The first peak (without number) is non-dissociated protein;* ***b) SDS PAGE of fractions L1-L5 on a 10% gel*** *represented as lanes 2,4,5,6,7; lane 1- bovine serum albumin – (66 kDa), lane 2 – structural subunit L5, lane 3- standards (protein mixture (a) egg albumin (45 kDa); (b) bovine serum albumin (66 kDa); and (c) phosphorylase b (97.4 kDa) and lanes 4-7 - structural subunits L1, L2, L3, L4, respectivelly.*

The high overall sequence similarity between these proteins is particularly pronounced at their CuA and CuB sites. Two well-separated copper-binding regions, the CuA site close to the N-terminus and the CuB site, near to the C-terminus have high sequence identity **(Figure 47).**

According to the X-ray crystal structure, subunit II of the *Limulus* Hc is composed of three domains [Magnus et al., 1994], and a dinuclear copper centre that reversibly binds oxygen is located in domain 2. Each copper ion is buried in the core of this domain and is coordinated by three histidine side chains **(Figure 47)**.

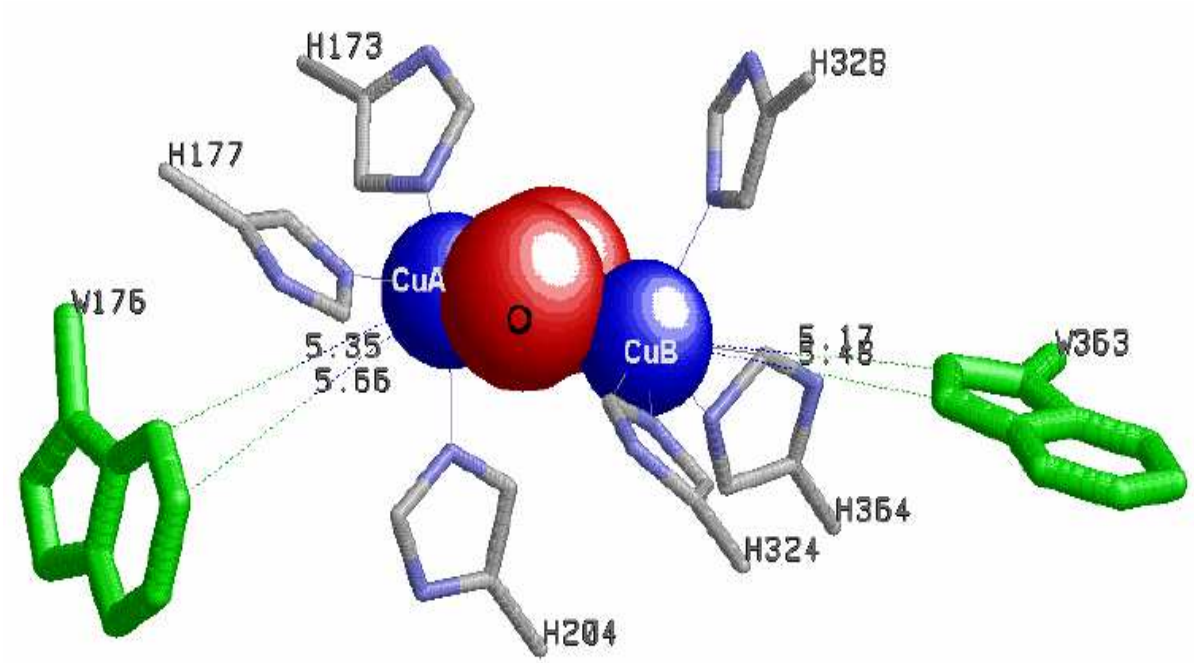

Figure 47. X-ray structure of active sites "A" and "B" of structural subunit of arthropodan Hc Limulus polyphemus [*Dolashka-Angelova et al., 2005b*]***.*** *Three histidine residues 173, 177 and 204 bind to CuA and three histidine residues 324, 328 and 364 bind to CuB. Tryptophan residues W176 and W363 are located near to the copper ions.*

The distances between Trp residues and Cu ions in the active site of structural subunit of arthropodan hemocyanin *Limulus polyphemus* are shown in **Table 5**.

Table 5. Distances between Trp residues and Cu ions in the active site of structural subunit of arthropodan hemocyanin Limulus polyphemus calculated from X-ray crystal structure.

	CuA	CuB	W65	W174	W176	W184	W326	W363	W538	W563
CuB (Å)	3.59	0.00	25.24	14.99	11.8.	18.89	13.36	5.17	16.16	30.88
CuA (Å)	0.00	3.59	22.80	12.02	5.36	17.09	15.82	9.08	13.88	28.54
Accessibility (%)			58.6	2.0	0.0	8.0	19.1	36.3	0.1	51.0

Alignment of partial sequences of CuA and CuB sites from structural subunit Ca2 from *C. aestuarii* (Ca2) and different structural subunits from other Crustacea (*Cancer magister* subunit Cm6, *Panulirus interruptus* subunit Pic, *Panulirus vulgaris* subunit Pv1) and

second order Chelicerata (*Limulus polyphemus* subunit Lp1; *Euripelma californica* subunit Ece, *Androctonus australis* subunit Aa6) show considerable homology. Sixteen positions are conserved around the CuA site (Tyr162, Asn166, Gly168, Asp170, His172, His173, Trp176, His177, Pro181, Trp184, Asn194, Arg195, Lys196, Gly197, Glu198, His205, marked bold in **Figure 48** with even higher homology, observed for the first above mentioned three subunits Ca2, Cm6, and Pic and the last three subunits (Lp1, Ece and Aa6).

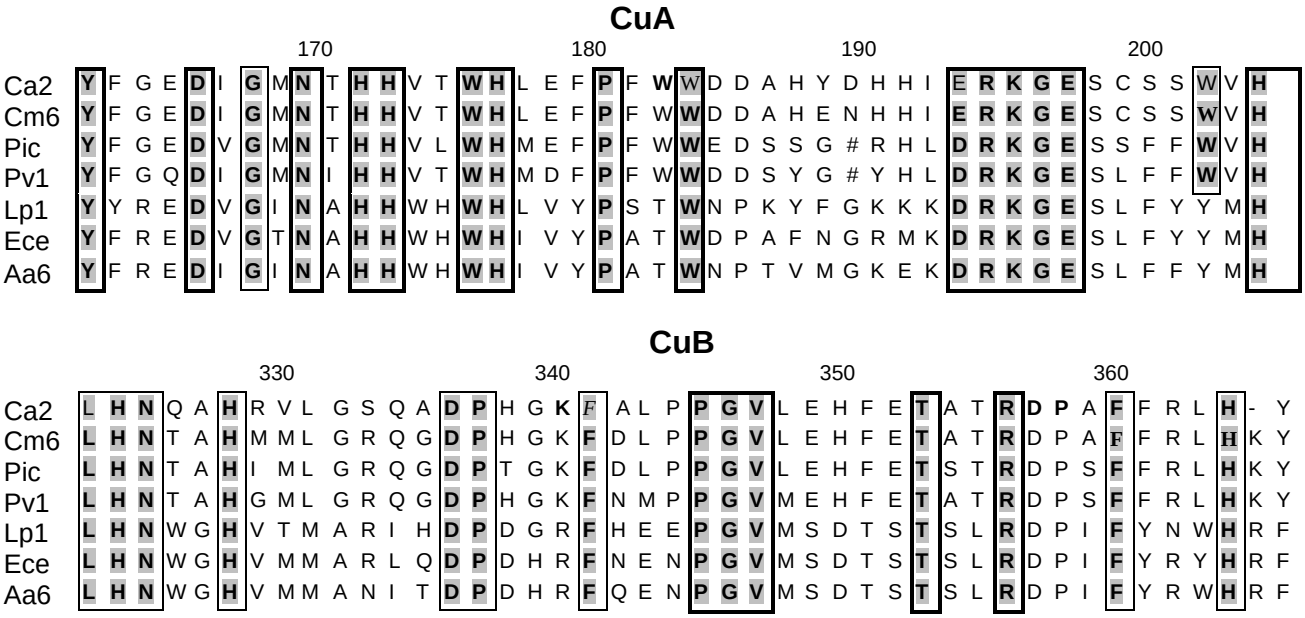

Figure 48. Alignment of partial sequences around CuA and CuB sites from different structural subunits from the order of Crustacea*: Carcinus aestuarii subunit Ca2, Cancer magister subunit Cm6 (GB AF091261), Panulirus interruptus subunit Pic (SP P80096), Panulirus vulgaris subunit Pv1 (SP P80888) and from second order of Chelicerata Limulus polyphemus subunit Lp1 (SP P04253), Euripelma californica subunit Ece (GB X16650) and Androctonus australis subunit Aa6 (SP P80476). SP -SwissProt. accession no., GB: Gen Bank accession no.*

In each subunit the residues in the copper-binding domain A, are conserved at positions 172, 173, 177, and 205 and at positions 324, 328, and 364 in the copper-binding domain B. Seven or eight Trp residues are present in one structural subunit of arthropodan Hcs, whereby 3 or 4 of them are located in Cu active sites at positions 174, 176, 183, 184 or 203. One or two Trp residues are located near to the CuB site in Lp1,

Ece, Aa6 while in Crustacea Hcs no Trp residue is found in the CuB site. Location of Trp residues in the active sites near to the Cu ions influences fluorescence emission, which is statically quenched by Cu ions.

4.1.5.2 Fluorescence properties of native molecule and structural subunits of LpH

The fluorescence properties (quantum yield Q and λ_{max}) of these two orders of Crustacea and Chelicerata Hcs are expected to be similar for both orders of Hcs, as a large numbers of tyrosine (about 720) and tryptophan residues (about 140) are found in the native molecule, corresponding to about 18 tyrosine and 7-8 tryptophan residues in one structural subunit. The emission spectra of *L. polyphemus* Hc from the order of Chelicerata are characterized by an emission band with a maximum at 333 nm upon excitation at 295 nm, where the tryptophan residues are almost exclusively excited which are similar to those found for other Hcs from this order **(Table 6)**. *P. vulgaris* has a λ_{max} of 326 nm as other crustacean Hcs. The quantum yields for both *P. vulgaris* Hc and *Limulus polyphemus* Hc are similar because they contain the same number of Trp residues. The shift of the emission maximum towards shorter wavelengths is diagnostic for tryptophyl side chains in a non-polar environment, since λ_{max} for Trp in water is 355-360 nm [Tabak et al., 1990]. Comparison of the emissive properties of the oxy- and apo-forms under the same experimental conditions (50 mM Tris/HCl buffer, pH 8.2) shows that the quantum yield strongly increases for both, *Limulus* (Q_{oxy}= 0.025; $Q_{apo\text{-}}$= 0.078) and *P. vulgaris* (Q_{oxy}= 0.012; $Q_{apo\text{-}}$= 0.082) Hcs upon removal of copper from the active site. This effect is accompanied by a 10 nm shift of the emission maximum from 333 nm (oxy-Hc) to 343 nm (apo-Hc) **(Table 6)**.

Table 6. N-terminal sequences of different species of arthtropodan hemocyanins *of the Order Crustacia, infraorders Palinura: Palinurus vulgaris (Pv); Panulirus interruptus (Pi),[Neuteboom et al., 1992], Panulirus japonicus (Pj) [Makino and Kimura, 1988]; Astacidea: Homarus americanus (Ha). [Dolashka et al., 1996]; Brachyura: Carcinus aestuarii (Ca), [Schütz et al., 2001], Maia squinado (Ms). [Abbasi et al., 2000]; order Chelicerate, infraorders Xiphosura: Limulus polyphemus (Lp); Buthidae: Buthus sindicus (Bs). [Laemmli, 1970]; Araneae: Euyrypelma californicum (Ec), [Voit et al., 2000] and their fluorescence properties: λ_{max} – maximum wavelenght and quantum yield-Q.*

Order: Crustacea																						λ_{max}		Q	
Infraorder Palinura																						oxy-	apo-	oxy-	apo-
	1					5					10						15				20				
Pv native																						326±1	335±1	0.012	0.082
Pva			D	V	H	S	S	D	N	**A**	H	**K**	**Q**	Q	D	V	**N**	H	L	L	D	K	333±1	338±1	0.024	0.096
Pvb			D	V	H	S	S	D	N	**A**	H	**K**	**Q**	H	D	V	**N**	H	L	L	D	K				
Pia			D	A	L	G	T	G	N	**A**	Q	**K**	**Q**	Q	D	I	**N**	H	L	L	D	K				
Pib			D	A	L	G	T	G	N	**A**	N	**K**	**Q**	Q	D	F	**N**	H	L	L	D	K				
Pic		G	D	S	A	D	K	L	L	**A**	Q	**K**	**Q**	H	D	V	**N**	Y	L	V	Y	K				
Pjla		G	D	S	T	D	K	L	L	**A**	Q	**K**	**Q**	D	D	V										
Infraorder Astacidea																									
Ha1					G	T	T	V	V	**A**	H	**K**	**Q**	Q	S	V	**N**	R	L	L	Y	K	336±1	338±1	0.053	0.120
Ha2					G		A	D	V	**A**	H	**K**	**Q**	Q	S	V	**N**	H	L	L	Y	L	335±1	337±1	0.058	0.110
Ha3		P	S	V	S	T	V	N	V	**A**	Q	**K**	**Q**	H	D	V	**N**	F	L	L	F	K	335±1	336±1	0.058	0.100
Ha4		G	A	Y	G		Q	G	Q	N	I	G	**Q**	L	F	V	**N**	I	L	I	F	L	334±1	338±1	0.056	0.110
Ha5			G	A	G	E	A	L	N	**A**	K	R	**Q**	Q	D	V	**N**	H	L	L	D	L	333±1	336±1	0.030	0.100
Ha6					S	P	A	F	Q	**A**	Q	**K**	**Q**	A	K	V	**N**	D	V	L	D	K	336±1	338±1	0.038	0.110
Infraorder Brachyura																									
Ca1		X	D	P	A	S	V	S	D	**A**	X	**K**	**Q**										336±1	336±1		0.106
Ca2							T	C	L	**A**	H	**K**	**Q**	Q	A	V	M	R	L	L	Y	R	335±1	338±1		0.093
Ca3		D	S	P	G	G	A	S	D	**A**	Q	**K**	**Q**	H	D	V	**N**	S	I	L	X	K	332±1	334±1		0.090
Ca4			D	Q	P	G	D	V	K	**T**	H	**K**	**Q**	**Y**	**D**	**V**	**N**	**Y**	**L**	**F**	**F**	**K**				
Ms1			D	Q	P	G	D	V	K	T	H	**K**	**Q**	Y	D	V	**N**	Y	L	F	F	K	336±1	337±1	0.028	0.082
Ms2							G	Q	L	**A**	L	**K**	**Q**	Q	T	V	**N**	R	L	L	N	K	333±1	337±1	0.030	0.080
Ms3							G	G	P	**A**	G	**K**	**Q**	N	A	V	**N**	Q	L	L	V	L	336±1	338±1	0.026	0.085
Ms4							D	G	P	**A**	Q	**K**	**Q**	N	T	V	**N**	Q	L	L	V	L	334±1	336±1	0.024	0.087
Ms5		D	H	A	G	T	V	S	K	**A**	H	**K**	**Q**	H	D	V	**N**	S	V	L	Y	K	333±1	335±1	0.025	0.085
Ms6					G	G	P	S	Q	K	Q	**K**	**Q**	H	K	V	**N**	L	V	N	I	K				
Order Chelicerate																									
Infraorder Xiphosura																									
Lp native																						333±1	343±1	0.025	0.078
Lp1							**T**		L	H	**D**	**K**	**Q**	I	**R**	V	C	H	L	F	E	Q	340±1	347±1	0.043	0.109
Lp2							**T**		I	K	**E**	**K**	**Q**	K	**R**	X	N							346±1		0.098
Lp3								H	I	K	**E**	**K**	**X**	D	**R**	**I**	**L**							343±1		0.113
Lp4							**T**		I	K	**E**	**K**	**Q**	D	**R**	**I**	**L**							347±1		0.102
Lp5								X	L	Q	**E**	**L**	**Q**	A	H	**I**	**L**									
Infraorder Buthidal																									
Bs							**T**		V	L	**E**	K	**Q**	G	**R**	I	**L**	S	L	F			335±1	336±1	0.024	0.070
Infraorder Araneae																									
Eca					M		**T**	I	L	H	**D**	**K**	**Q**	V	Q	A	**L**	K	L	F	E	K	335±1	345±1	0.006	0.092
Ecb					M	P	**S**		T	A	**E**	**K**	**Q**	R	**R**	**I**	**L**	P	F	F	Q	F				
Ecc					M	P	**S**	D	A	N	**E**	M	**Q**	A	**R**	**L**	**L**	Q	L	F	E	H				
Ecd					M		**T**		I	A	**D**	H	**Q**	A	**R**	**I**	**L**	P	L	F	K	K				
Ece					M	P			D	K	Q	**K**	**Q**	L	**R**	V	**I**	S	L	F	E	H				
Ecf					M		**T**		V	Q	**D**	**K**	**Q**	R	Q	**I**	**L**	P	L	F	E	H				
Ecg					M	A	**S**		I	P	**E**	**K**	**Q**	A	L	**I**	**L**	P	L	F	E	K				

Figure 47 shows in detail the environment around the active site of *Limulus* Hc, where the positions of neighboured Trp residues are evidenced. Subunit II contains eight Trp residues: Trp65, Trp174, Trp176, Trp184, Trp326, Trp363, Trp538 and Trp563, however, not all of them are present in the various subunits of other hemocyanins. All Trp

residues, with the exception of Trp563, are located in the second domain of *Limulus* Hc. Two of them (Trp176 and Trp363) are located within a small distance below 6 Å from CuA and/or CuB, respectively **(Table 5)**; Trp176 5.36 Å from CuA site and Trp363 5.17 from the CuB site). Trp174 (12.02 Å) and Trp538 (13.88 Å) are located also in the neighbourhood at the CuA site. The emission of these Trp residues in the oxy-form is strongly quenched by the Cu ions. Removal of O_2 and copper ions drastically increases the tryptophan fluorescence (343 nm for the whole molecule and about 347 nm for the structural subunits). **Figure 47** shows that, connections Trp176...CuA=O_2=CuB-His328 and Trp363…CuB=O_2=CuA-His177 are "parallel" to each of the "conjugated chains" [Dolashka-Angelova et al., 2005b]. The distance of Trp176...CuA (5.36 Å) is somewhat larger than Trp363...CuB (5,17 Å), but the first is "in touch" with the negative dipole side (CE3) of Cu^{2+}(A) and the second Trp363 is "in touch" with Cu^{2+}(B) with its positive dipole side (near CD1) and thus, both polarize CuA=O_2=CuB in a way that CuA could be more positively and CuB more negatively charged. The fluorescence of both Trp residues has to be strongly quenched by cupric ions in oxy-Hc and by their environment [Terwilliger et al., 1999]. In the oxy state, the distance between both Cu ions is 4.6 Å (CuA….4.6…CuB) and this is very understandable from an electrostatic point of view (repulsion). The Trp distribution around the active site is a strict peculiarity of *Eurypelma* Hc, actually, only 50% of the Trp residues in other Chelicerata Hcs are located near the copper ions and are distributed only in the vicinity of one metal centre [Hodgson et al., 2000]. The access to Trp174, Trp176 and Trp538 for the quenchers is very low 2.0%, 0.0% and 0.1 %, respectively. These features of *Limulus* Hc explain the exceptionally strong quenching of the Trp fluorescence in the oxy-form, in comparison with other Hcs [Dolashka-Angelova et al., 1999; Dolashka-Angelova et al., 2000; Abbasi et al., 2000], **Figure 48** shows that 4 Trp residues are located in the CuA site of Crustacea Hcs and 3 in Chelicerata Hcs, while only 1 or 2 Trp are present in the CuB site near to His residues. No Trp residue is observed in the CuB site in Crustacea Hcs.

4.1.5.2.1 Fluorescence lifetime of native molecule of *Limulus polyphemus* Hc

Three classes of Trps are represented in native arthropodan Hcs. Some of them are located on the subunit surface, in a protein region involved in intersubunit contacts, as Trp563 in *Limulus* and Trp292 in *Euripelma* Hcs. The exposure of these residues to the solvent is connected with short-life time and the access to them, which is 58.6 and 36.3 %, respectively. The distances between these two Trp residues and Cu ions are 4 times higher then that between Cu and the Trp176 and Trp363 **(Figure 47)**, and their emission can not be quenched by Cu ions. The emission of whole molecule is quenched by the microenvironment of the Trp residues and by the interaction of the subunits. Evidence for this is that the fluorescence quantum yield of the whole molecule is less than that for its structural subunits **(Table 6)**. The isolated subunits in the oxy-form exhibit quantum yields approx. 20-40% higher as compared to the whole Hc, while the quantum yields for their corresponding apo-forms are only about 10% higher.

Moreover, the lifetime values of Hc remain almost constant upon O_2 and copper removal, changes being observed only in the normalized pre-exponentials A; this supports a mechanism of static quenching by copper ions of the active site [Burmester, 2001]. Removing quenching Cu ions from the active site of the molecule is connected with an increase of the quantum yield but not with τ_1. Thus, the increase of fluorescence quantum yield in apo-Hc must be attributed to the demasking of Trp fluorophores which are fluorimetrically almost silent in the native protein. The fluorescence decay curve for Trp residues has been found to be multiexponential in single as well as multiple Trp-containing proteins. The multiexponential decay arises due to the conformational isomers of the Trp residues, where the local environment of the indole chromophore differs substantially. The time-resolved fluorescence decay of *Limulus* Hc gave two lifetime components which indicate conformational changes of the proteins **(Figure 49).**

The fluorescence decays of the parent molecule, the two subunits, and N-Ac-Trp-NH_2, excited at 295 nm, well fitted to two exponentials. The theoretical fluorescence

intensity is given by the function $P(\tau) = A_1e^{-t/\tau1} + A_2e^{-t/\tau2}$, where A_1 and A_2 are amplitudes. This function was used for the determination of the excited state lifetimes. Analysis of the data in terms of biexponential models give a good fit between the experimental and theoretical curves. The values show that the environment of these chromophores significantly influences their dynamic fluorescence characteristics. The lifetimes for the native molecule of arthropodan LpH are very short (τ_1 = 0.3 ns, τ_2 = 3.3 ns), but higher than for molluscan keyhole limpet Hc (τ_1 = 0.17 ns, τ_2 = 2.56 ns) [Schutzt et al.,2001].

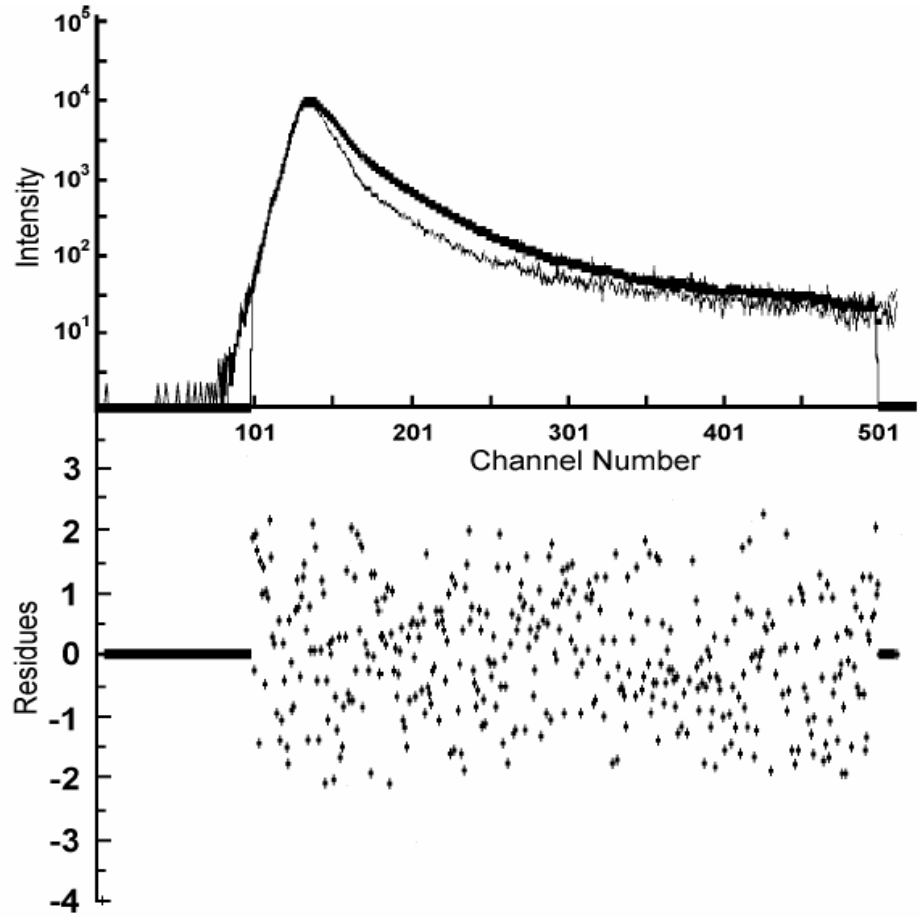

Figure 49. Fluorescence decay of native Limulus polyphemus Hc *in 50 mM Tris/HCl buffer with 5 mM $CaCl_2$ and $MgCl_2$, pH 8.2 after excitation at 295 nm. Fluorescence lifetime measurements were carried out at 20℃ usin g a System PRA 2000 nanosecond single photon counting spectrofluorimeter and a nitrogen-filled flash lamp with full width at half-maximum (FWHM) of about 2.5 ns.*

Our experimental data as well as the data from similar structures gives us the reason to suggest that Trp563 and Trp65 seems to be short-lived (τ_1 = 0.3 ns) and their

emission (81%) is almost completely quenched and Trp197 and Trp346 are long-lived (τ_1 = 2.56 ns) with emission of about 18%.

The fluorescence decay properties clearly differ between the whole molecule and the subunits which suggests that the respective tryptophans are affected differently by the local tertiary structure. The specific environment of the indole groups in *Limulus* Hc decreases the excited state lifetime by a factor of 2 in comparison with the value, determined for its subunits.

4.1.5.2.2 Denaturation with Gdn.HCl of native molecule of *L. polyphemus* Hc

The unfolding of proteins in denaturing compounds has been widely investigated. In the case of oligomeric proteins, inactivation, dissociation and unfolding have been described as the structural events that occur subsequently during the denaturation process. We studied the changes in conformation and aggregation of tetrameric Hcs during unfolding in guanidine hydrochloride. The denaturation of these proteins takes place in several stages. **Figure 50** shows the fluorescence spectra of the whole molecule of *Limulus polyphemus* Hc at different concentrations of Gdn.HCl. The addition of denaturant concentrations between 0 and 1.5 M produced a slight increase of the fluorescence intensity, but at 2 M Gdn.HCl, the emission is higher, and the quenching of Cu ions is eliminated. At 2.0 M guanidine buffer, the whole molecule is fully dissociated into its structural subunits. The results are consistent with an aggregation occurring at 0.5 M guanidine, followed by a similarly drastic dissociation to give a monomeric protein unfolding at 1.5-2 M guanidine.

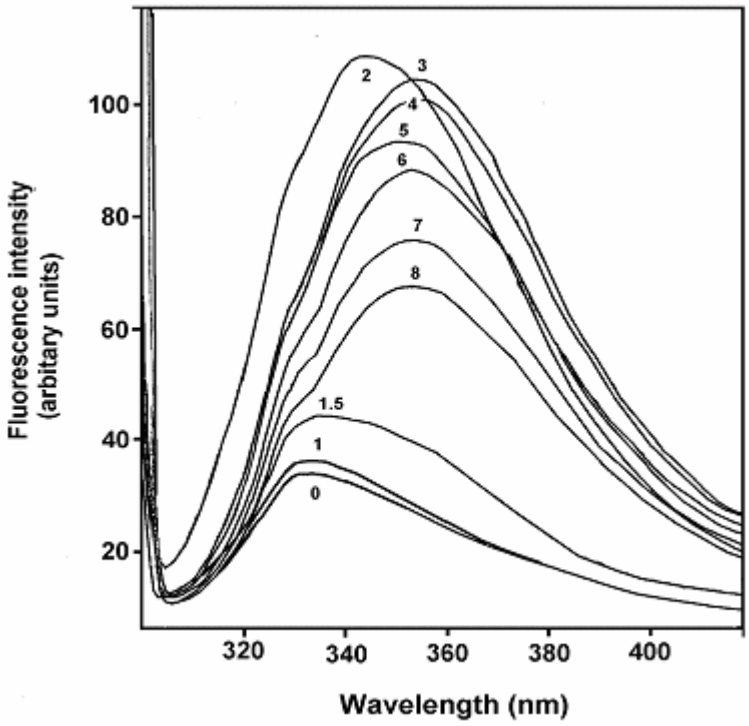

Figure 50. Fluorescence emission spectra of oxy- LpH at different concentrations (0-8 M) of Gdn.HCl. *Protein solutions had an absorbance at the excitation wavelength < 0.05 to minimize the inner filter or self-absorption effects. Excitation at 295 nm was used for predominant measuring the fluorescence of tryptophyl residues. Spectra were corrected for background due to the solvent.*

Further increase of denaturant concentration decreases the intensity and is connected with a shift of λ_{max} towards 355 nm (red shift) as shown in **Figure 50**, which can be explained, by protein unfolding. The curves in the insert of **Figure 51**, expressing the unfolding of oxy-Hc at different concentrations of Gdn.HCl is analogous to the curve in **Figure 52** (expressing the unfolding of apo-Hc), but with specific changes in quaternary structure fluorescent properties **(Figure 51 insert, limb-a)** which seems to contain two transitions. The first transition has a similar “position" (C_m= 0.52) and amplitude (dQ) typical for very quenched total Trp fluorescence. Obviously, this observation is due to quencher, the effect of which is removed at the followed unfolding step at C_m*= 1.77 and with very big amplitude and sharpness of the transition (within 1.6 M interval). The only explanation is that in this step the Cu=O_2=Cu...Trp(s) native structure is destroyed causing a rise of Trp fluorescence.

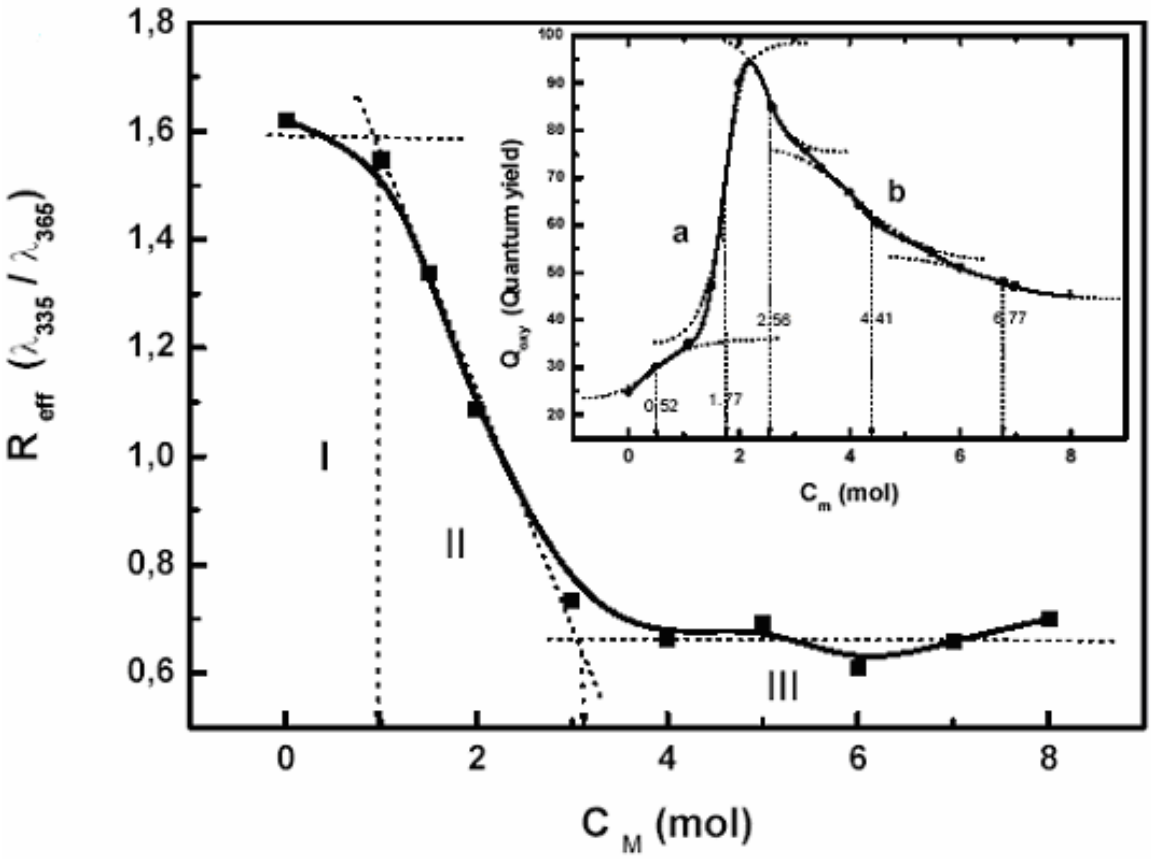

Figure 51. Effective ratio of fluorescent intensities (R_{eff}) at different concentrations of Gdn.HCl of Limulus polyphemus; Insert: Effect of guanidine hydrochloride (0-8 M) on the fluorescence intensity of L. polyphemus native oxy-Hc molecule. *The protein concentrations are about 0.05 mg.ml^{-1} in 0.05 M Tris/HCl buffer with 5 mM $CaCl_2$ and $MgCl_2$, pH 8.2. The fluorescence quantum yield (Q) was determined using N-Ac-Trp.NH_2 as a standard. Different concentration of Gdn.HCl were used (0-8 M). Fluorescent intensities at two arbitrary wavelengths (335 and 365 nm) were selected.*

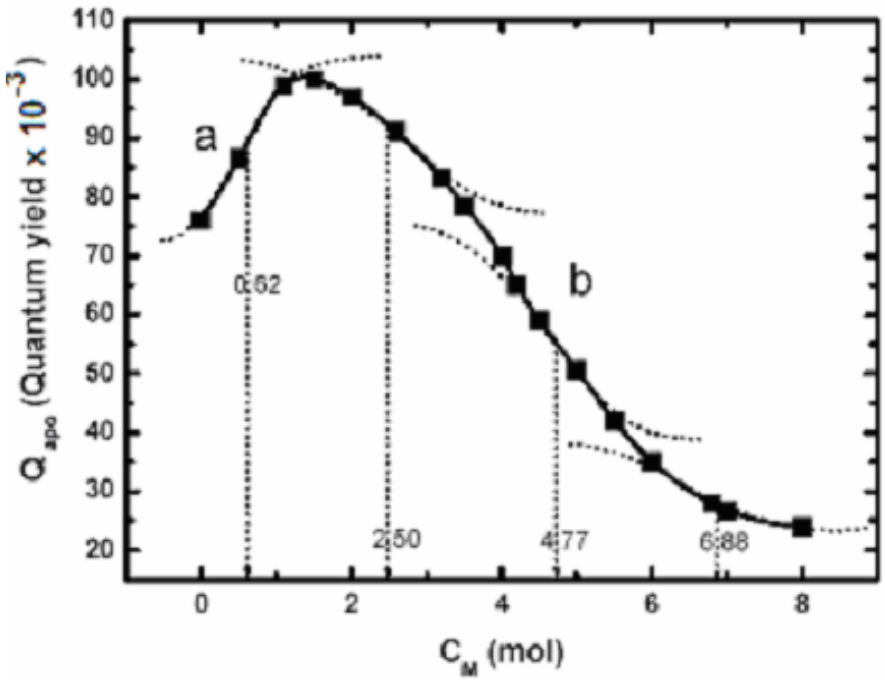

Figure 52. Effect of guanidine hydrochloride (0-8 M) on the quantum yield of apo-Hc of L. polyphemus. *The protein concentrations are about 0.05 mg.ml^{-1} in 0.05 M Tris/HCl buffer with 5 mM $CaCl_2$ and $MgCl_2$, pH 8.2. The fluorescence quantum yield (Q) was determined using N-Ac-Trp.NH_2 as a standard. Different concentration of Gdn.HCl were used (0-8 M). Four denaturating steps were identified with C_m 0.62; 2.50; 4.77, and 6.88, respectively.*

After this apparent "peak" of the amplitude (Q) and C_m in the curve for oxy-Hc, the following limb-b has analogous (but not the same) behavior as in the apo-Hc case. Three unfolding steps with apparent C_m* at 2.56, 4.41 and 6.77 M, respectively, could be identified in the **insert of Figure 51, limb-b**. The first of them (at the same amplitude) with ΔC_m= 1.2 is much sharper not only than the other two steps, but also in comparison with the first transition step with ΔC_m= 3.5 in case of the apo-Hc **(Figure 52)**. The C_m* of the next two transitions are at slightly lower Gdn.HCl concentrations, but with analogous small cooperativity. This behaviour can be explained assuming non-symmetric interactions between structural domains in the holoprotein, i.e. at the Cu=O_2=Cu site, formation of intra-subunit and chain-chain interactions are changed and the active site formation is coupled with structural alterations. Because the first (less-stable) domain is Cu site-dependent it can be selected from the known 3D-structure, and the rest of two domains should be easily assigned in terms of their stabilities. For a better understanding of the unfolding process of oxy-Hc we have compared the Q(C_m) curve **(Figure 51 insert)** with the R_{eff}(C_m) curve shown in **Figure 51**. The "velocity" of R_{eff} changes are different for the first two processes, showing their different nature (mark in figure in regions I and II). Notably, the first domain (at the active site) transition falls in the same region II as previous ones and all of them are definitely cooperative. The other two transitions are without drastic changes of Trp environment after the unfolding. **Figure 52** shows the fluorescence intensity of apo-Hc at different concentrations of guanidine. Quenching by Cu ions is eliminated and the intensity at 0 M Gdn.HCl is higher than for the oxy-form, but less than for structural subunits. In case of whole apo- multichain Hc, ("all apo-Hc"), the unfolding curve is more complex, but logically altered. It contains two limbs: a) at low Gdn.HCl concentrations (0.0-2.4 M) and b) at higher concentrations of denaturant (2.5-8.0 M). The last limb b (b) exhibits also a three-step process as described above, but only the effective C_m* values for oxy-Hc **(Figure 51 insert)** are 0.6-0.7 higher than those for the

apo-Hc **(Figure 52)**. This means, the formation of the quaternary structure increases the stability in each of the three domains and this alteration is approximately equal and independent for each of the domains. The presence of limb a confirms the presence of a quaternary structure which is most sensible and easily destroyed at very low concentrations of denaturant. From these results follows that multichain complex decomposition leads to an increase of apparent Trp fluorescence and we have to conclude that chain-chain interactions function as a moderate quencher of Trp fluorescence. This can be done by introduction of quenching groups to the given Trp residue(s) and/or by structural changes in the vicinity of the Trp residue(s) after polypeptide complex formation. In **Figure 53** the influence on one structural subunit a is shown expressing the conformational stability only for this protein.

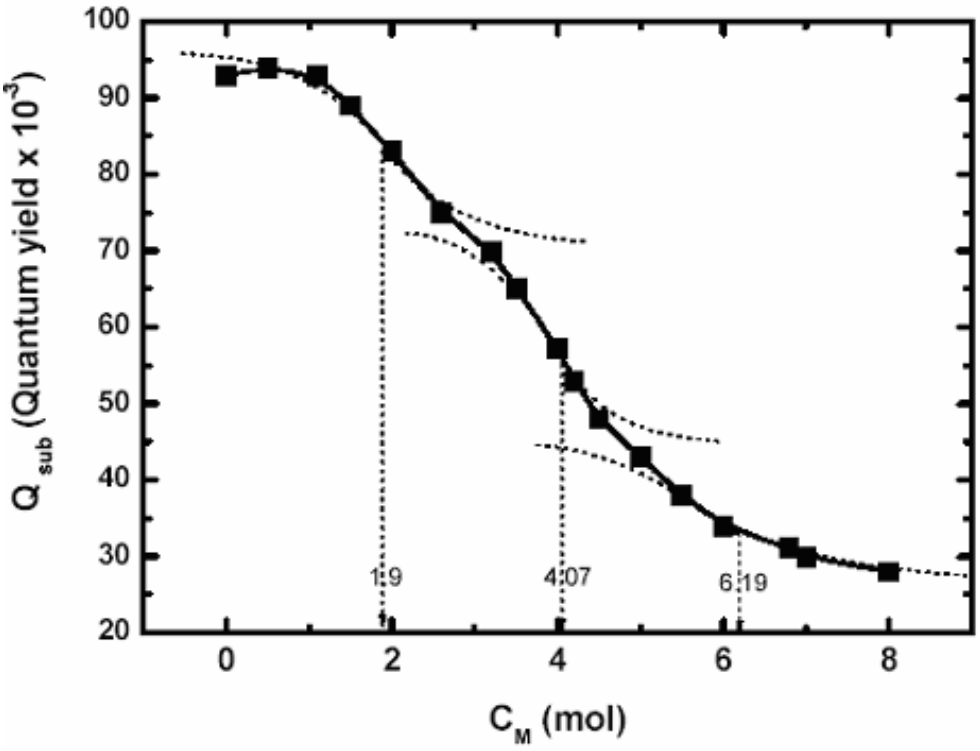

Figure 53. Effect of guanidine hydrochloride on the quantum yield of Limulus polyphemus oxy-subunit. *The protein concentrations are about 0.05 mg.ml^{-1} in 0.05 M Tris/HCl buffer with 5 mM $CaCl_2$ and $MgCl_2$, pH 8.2. The fluorescence quantum yield (Q) was determined using N-Ac-Trp.NH_2 as a standard. Different concentration of Gdn.HCl were used (0-8 M).*

The single polypeptide Hc subunit undergoes unfolding in water-Gdn.HCl solutions as a multistep process. Because the interval of the Q-change is very wide (from 1 to 8 M Gdn.HCl) and using the present shape the curve was deconvoluted into three sigmoid curves with apparent midpoints (Cm*) at 1.90, 4.07 and 6.19 M, respectively. It is known from 3D X-ray analysis that this subunit contains 3 structural domains and we can speculate to assign each of the processes to each of these domains. This hypothesis requires domains to differ considerable in stability at a ratio of approximately 1:2:3. We hope to prove this suggestion from specially designed experiments, now in progress. On the basis of the above discussion, a model is given summarizing the results as follows:

$$Tn \Leftrightarrow Tn' \Leftrightarrow A \Leftrightarrow Mn' \Leftrightarrow Mu \qquad (14)$$

In this model, Tn represents the native tetrameric protein that, at low guanidine concentrations, forms a fully active intermediate (Tn') with more hydrophobic surfaces exposed to the solvent. As the guanidine concentration increases, further exposure of hydrophobic interaction area lead to the formation of aggregated species (A). Finally, at concentrations higher than 2.0 M guanidine-HCl, the highly aggregated species dissociate into partly unfolded monomers (Mn') that are eventually completely unfolded (Mu), accompanied by a further increasing maximum fluorescence emission.

4.1.5.2.3 Effect of pH on the stability of native molecule of *L. polyphemus* Hc

Finally, we also measured the effect of pH in the range from 2.0 to 12.0 on the tryptophan fluorescence of *L. polyphemus* and *P. vulgaris* Hcs and their structural subunits. **Figure 54a** and **b** show the fluorescence spectra on *L. polyphemus* oxy-Hc recorded at different values pH intervals (8-11.4 and 8-2.5).

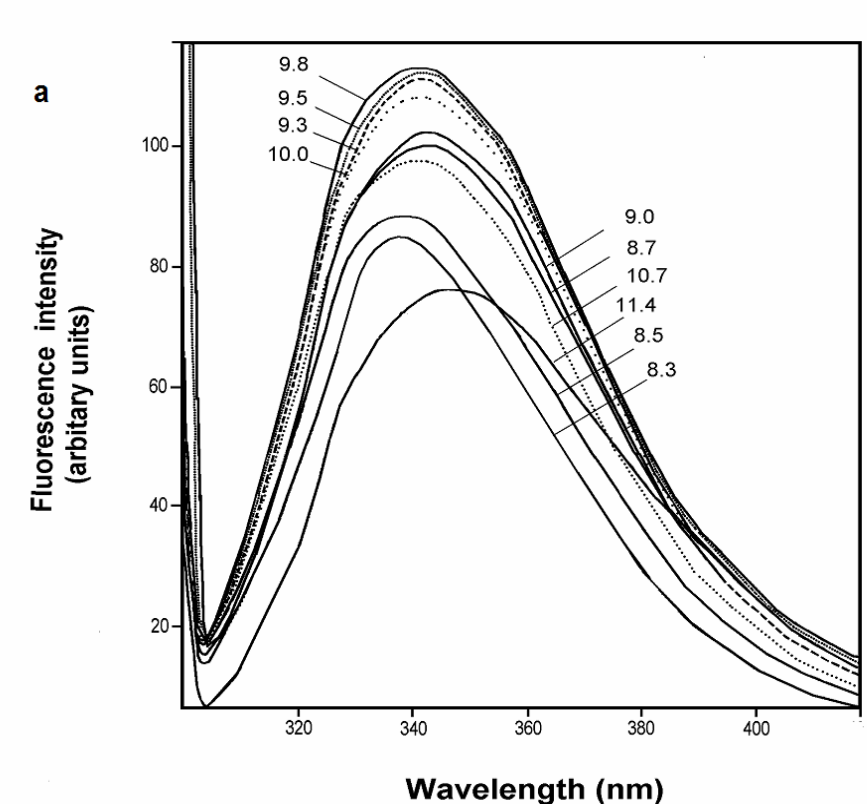

Figure 54. a) Fluorescence emission spectra of native L. polyphemus oxy Hc in the pH region 8.3-11.4. *Hc was kept for 24 hours in different buffers: 0.05 M Tris/HCl (pH 8.3-9.0) and 0.05 M carbonate/bicarbonate (pH 9.0-10.5). The tryptophan emission spectra were measured after equilibration for 24 hours from 300 to 420 nm at an excitation wavelength of 295.*

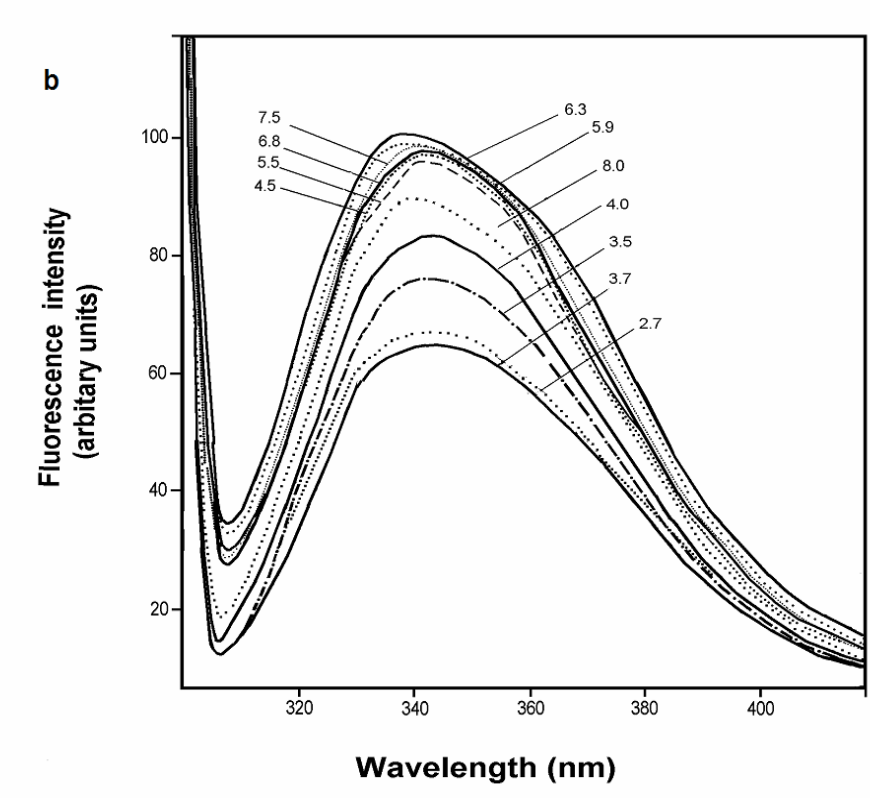

Figure 54. b) Fluorescence emission spectra of native L. polyphemus oxy Hc in the pH region 2-8.5. *Hc was kept for 24 hours in different buffers: 0.05 M sodium citrate (pH 2.0-5.0), 0.05 M sodium phosphate (pH 5.0-7.0), and 0.05 M Tris/HCl (pH 7.0-9.0). The tryptophan emission spectra were measured after equilibration for 24 hours from 300 to 420 nm at an excitation wavelength of 295.*

The pH-dependence of Trp-fluorescence quantum yield of native oxy-Hc *Limulus polyphemus* is shown in **Figure 55**.

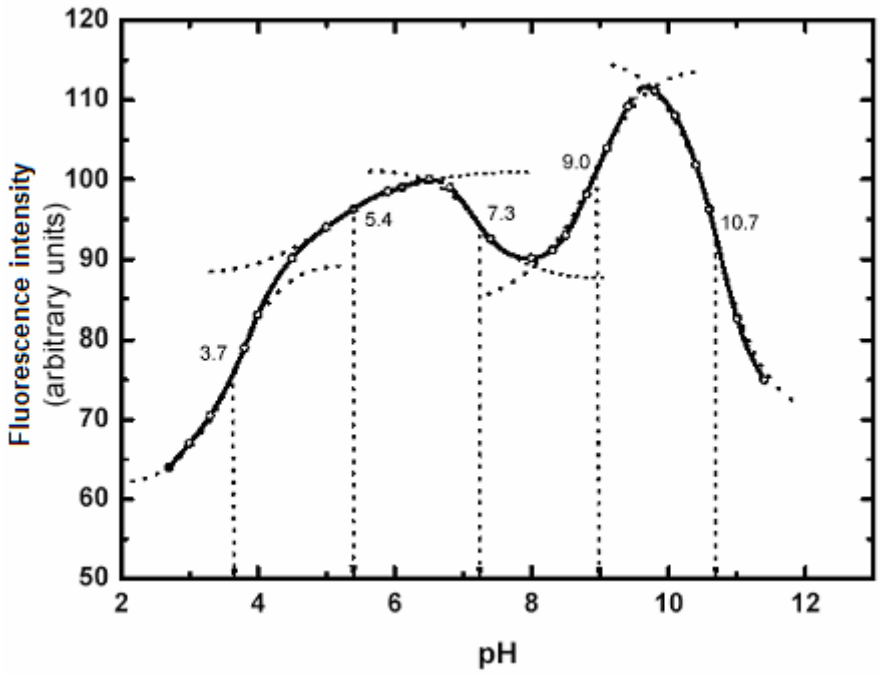

Figure 55. Effect of pH on the fluorescence intensity of native L. polyphemus oxy-Hc. *Hc was kept for 24 hours in different buffers of the pH range 2-11.5: 0.05 M sodium citrate (pH 3.0-5.0) 0.05 M sodium phosphate (pH 5.0-7.0), 0.05 M Tris/HCl (pH 7.0-9.0), 0.05 M carbonate /bicarbonate (pH 9.0-10.5), and 5 M NaOH (pH 11-12). The fluorescence intensity of tryptophan emission was measured after equilibration for 24 hours from 300 to 420 nm at an excitation wavelength of 295.*

In the acidic pH-region (3.5-6.5), two proton bindings, influencing the quantum yield, were observed with crude resolved pK_s at 3.7 and 5.4. The first is tentatively addressed to Asp (pK= 3.7) or Glu ionization(s) and exhibits cooperative behaviour (it involves more than one proton uptake within the pH interval, i.e. the sharpness of Q(pH)-transition is larger than one). Based on cooperative behaviour, this transition can also be caused by acid denaturation and its nature will be proven later based on CD measurements. The second acidic pH-dependent Q-change is three times smaller in amplitude, with a crude effective pK=5.4 and not cooperative. Again this may be a single carboxyl group ionization being in a negative electrostatic potential field. However, and more probably, it is due to a single His ionization located close to a positively charged $Cu^{(2+)}$ ion and near to Trp, the deprotonation of which partially removes its quenching effect. Most interesting is the Q(pH) behaviour at the neutral pH region (6.5-9.5) with two contrary processes: deprotonation of first site(s) increase Trp quenching (diminish Q) with a crude pK of 7.3 and obvious cooperativity and a second one with a crude pK of 9.0 causing decoupling of Trp fluorescence quenching. Probable candidates for both sites should be His residues in the Cu^{2+} vicinity or coupled ionisations of α-amino groups at the N-terminus.

Since the equilibrium constant of Hc for oxygen is expected to change as a function of pH, the experiments have been carried out on the apo-proteins **(Figure 56)** in order to avoid the complications due to the change in fluorescence intensity depending on the shift in the position of the oxygen-binding equilibrium and compared with pH denaturation of oxy-Hc. Disappearance of the first transition (pK=7.3) in apo-Hc leads to the conclusion for O_2-binding-dependent ionization (in analogy to the Bohr effect). The last "alkaline ionization" at pK=10.7 is obviously connected with the loss of the Cu^{2+} ion and followed by alkaline denaturation. Removal of the oxygen from Cu^{2+}-binding centre of Hc leads to the characteristic change to its pH-dependent intrinsic (Trps) fluorescence.

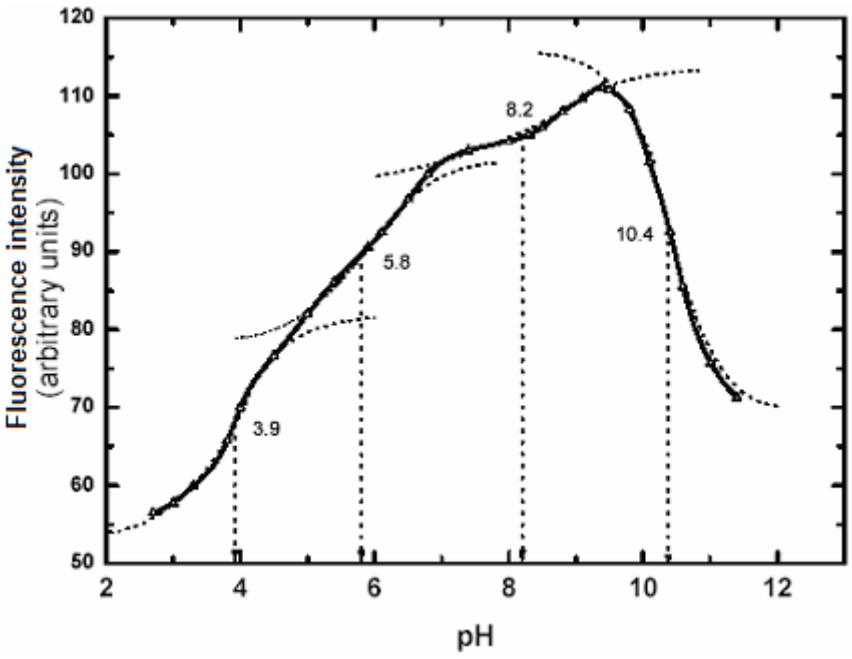

Figure 56. Effect of pH on the fluorescence intensity of L. polyphemus apo-Hc. *Hc was kept for 24 hours in different buffers of the pH range 2-11.5: 0.05 M sodium citrate (pH 3.0-5.0), 0.05 M sodium phosphate (pH 5.0-7.0), 0.05 M Tris/ HCl (pH 7.0-9.0), 0.05 M carbonate/ bicarbonate (pH 9.0-10.5), and 5 M NaOH (pH 11-12). The fluorescence intensity of tryptophan residues was measured after equilibration for 24 h from 300 to 420 nm at an excitation wavelength of 295.*

The Q(pH) shape is quite new in the pH region of 6.5-9.5 in comparison to that for oxy-Hc **(Figure 55)**. Both "processes", observed for oxy-Hc (with pK 7.3 and 9.0, respectively), are substituted by a one “process” in apo-Hc with positive tangent and apparent pK=8.2, leading to Trp fluorescence increase. This single process can be addressed to the "second" one in the oxy-Hc, but with pK shifted from 9.0 to 8.2 (ΔpK=0.8). The effect could be complex: omitting O_2 (a biradical particle, Trp fluorescence quencher) should increase

both, the Trp quantum yield and the "amplitude" of the Q(pH) transition with an effective pK of 5.8 which is shifted by 0.4 pH units compared to a pK of 5.4 in oxy-Hc. This is connected to small conformational changes of His and Trp residues in the O_2-binding site. Two types of Trp-His couplings by non-contact coplanar π-π interactions were identified. One is located within the Cu centre (W176...H173 and W363...H324) and the second one through the Cu-O_2-Cu bridge (W176...H328 and W363...H177). Removal of O_2 in deoxy-Hc will change the distances between Trp and His and Trp...Cu(O_2), and especially their orientations. Both transitions in oxy-Hc (with pK 7.3 and 9.0, respectively) are cooperative (see above), while the single transition in apo-Hc (with pK 8.2) is a non-cooperative one and is addressed to a single group ionization. Both, the acidic and alkaline limbs (pK 3.9 and 10.4, respectively) in **Figure 56** are slightly drawn together. The calculated values from the curves in **Figure 55** and **56** for the oxy- and apo-Hcs (dpK = pK_{al} - pK_{ac}) are 7.0 and 6.5, respectively, i.e. they differ in 0.5 pH units, which qualitatively is in agreement that O_2-binding to the active site stabilizes the Hc structure.

The spectral position of the apparent Trp fluorescence band which is a sum of individual contributions of each emitted single Trp residue, is also pH sensitive and defines their summary position and shape by the ratio of fluorescent intensities (R_{eff}) at two arbitrary wavelengths (335 and 365 nm were selected).

$$\frac{\lambda(335)}{\lambda(365)} = R(eff) = f(pH) \qquad (15)$$

Both limbs with pK 3.7 and 10.7 shown in Figure 57 overlap the regions of changeable pH /R_{eff} values, i.e. the structure is "in transition". The same could be said for the transition with a pK= 9.0, but at this pH the protein is native what allows to speculate that this transition is coupled with change in Trp orientation(s). It seems that the both other transitions with pK values of 5.4 and 7.0, respectively, proceed without structural changes altering Trp fluorescence.

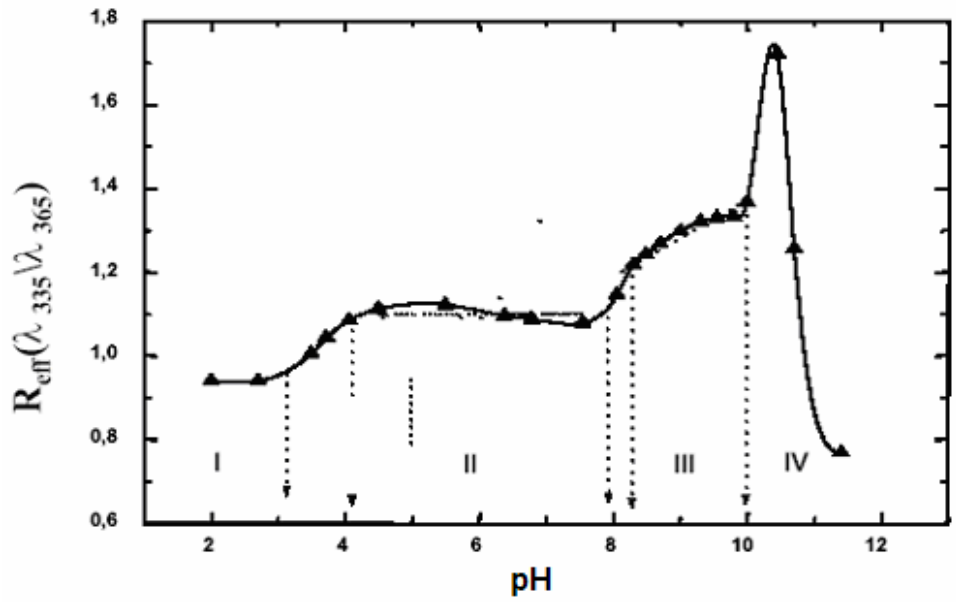

Figure 57. Effective ratio of fluorescent intensities (R_{eff}) of Limulus polyphemus at different pH. *The protein concentrations are about 0.05 mg.ml^{-1} in 0.05 M Tris/HCl buffer with 5 mM $CaCl_2$ and $MgCl_2$, pH 8.2. The fluorescence quantum yield was determined using N-Ac-Trp.NH_2 as a standard. Fluorescent intensities at two arbitrary wavelengths (335 and 365 nm) were selected.*

4.1.5.3 Circular dichroism properties of native molecule of *L. polyphemus* Hc

4.1.5.3.1 Temperature denaturation of native molecule of *L. polyphemus* Hc

Thermostability and stability in the presence of chemical denaturants is an important property of biomolecules, especially regarding their practical application. Thermal denaturation of different species of arthropodan Hcs was studied by circular dichroism (CD) spectroscopy. The far-UV CD spectrum of the native protein in 50 mM Tris/HCl, pH 8.2, is dominated by the negative dichroic band between 250 and 202 nm with a minimum at 210 nm and a shoulder around 220 nm, since α-helices display negative ellipticity at this wavelength range. β-sheet also displays negative ellipticities down to approximately 205 nm. Only minor changes in the far-UV CD spectrum are observed upon removing of copper and upon dissociation. This spectroscopic property, therefore, can be conveniently used for conformational studies without the complications arising from the presence of the metal ions in the active site or from the aggregation state of the starting material. CD spectra of the oxy-forms of the whole Hc have been recorded

in the temperature interval 20-90℃ at different pH in the acid and basic regions **(Figure 58 and 59)**. The melting temperatures T_m are determined at the temperatures corresponding to the mid-point of the transition and their values for all investigated species, both in the oxy- and in the apo-forms. Sigmoidal curves for *L. polyphemus* Hc are obtained when the ellipticity at 221 nm is plotted as a function of the temperature at different pH values. Melting temperatures (T_m), the midpoint in the sigmoidal denaturation curves for the whole oxy-Hc at acid **(Figure 58)** and basic **(Figure 59)** pH are in the region from 48 to 60℃. The SSs are less thermostab le than the whole molecule of *Limulus* Hc with T_m values of 49–55℃. Removing of the copper dioxygen system from the active site led to a decrease of the melting temperature by 4–6℃, which can be explained by a stabilizing effect of the binding metal ion.

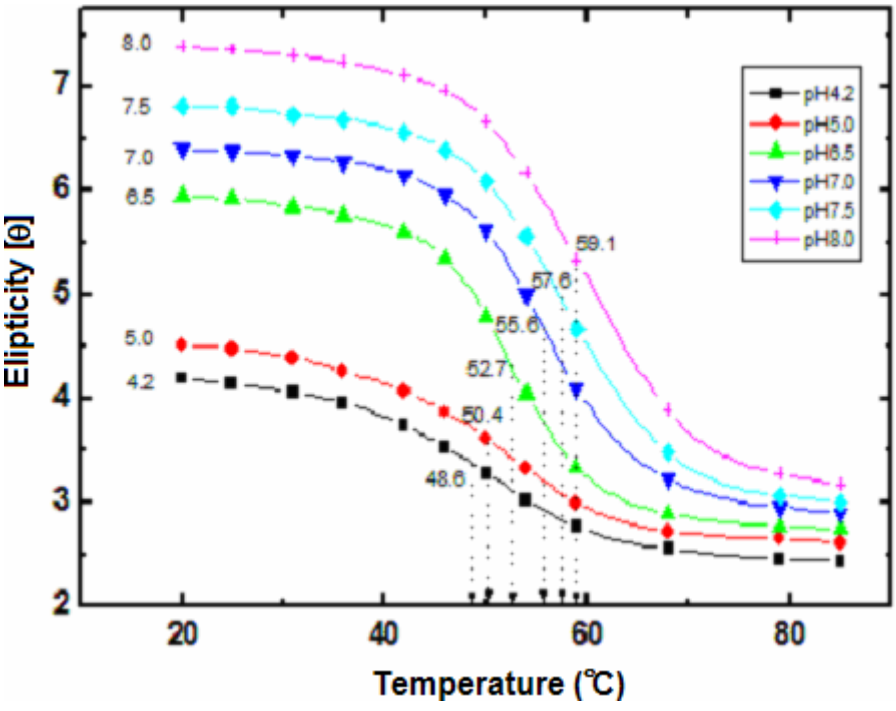

Figure 58. pH dependence (acid region) of the 222 nm intensity of Cotton effect of oxy-hemocyanin from LpH. *Temperature denaturation studies were performed at a temperature increase rate of 2℃ per min up to 95℃ in each buffer and the $[\theta]_{222}$ was measured each 5 deg. Hc was kept for 20 min in different buffers of the pH range 2-11.5: 0.05 M sodium citrate (pH 6.5-7.0), 0.05 M sodium phosphate (pH 7.0-7.5), and 0.05 M Tris/HCl (pH 7.5-8.0). pH denaturation was followed by recording the CD spectra of Hc (0.4 mg/ml) from 200-260 nm. Protein shows a characteristic strong negative Cotton effect at 221 nm. Quartz cylindrical cells with 0.05 cm path length were used throughout.*

The sygmoidal curve in **Figure 59** shows the temperature of denaturation of *Limulus* oxy-hemocyanin at different basic pH values. Reversibility of the folding/unfolding transition of

the protein was observed at low protein concentrations (< 0.2 mg/ml) in the pH range 6<pH>9. Thus, for the native molecule the investigation of the thermal unfolding was limited. Unfolding experiments, carried out close to the isoelectric point of the protein, showed only limited reversibility. A two-state nature unfolding transition was observed. Comparing melting temperatures (T_{ms}) at basic and acid pH regions is seen that at acid pH region T_{ms} are from 48.6 to 59.1°C while in basic region are from 55.0 to 60.1°C.

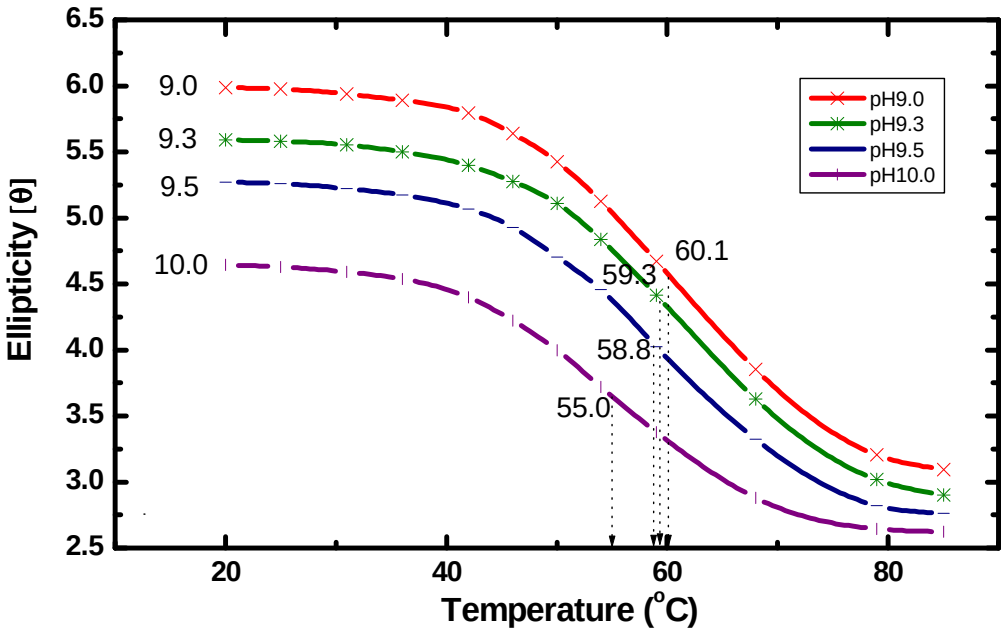

Figure 59. Influence of pH (basic region) and temperature on the intensity of the Cotton effect at 222 nm of Limulus polyphemus oxy-hemocyanin. *Temperature denaturation studies were performed at a temperature increase rate of 2℃ per min from 25 to 95℃ in each buffer and the [θ]$_{222}$ was recorded each 5℃. The Hc solution was kept for 20 min in buffers (0.05 M carbonate/bicarbonat) of the pH range 9.0-10.0. pH and temperature denaturation was followed by recording the 200-260 nm CD spectra of Hc (0.4 mg/ml). Quartz cylindrical cells with 0.05 cm path length were used throughout.*

The dependence of the melting temperature, calculated from Figures 58 and 59 from the pH (3.0 to 12.0) is represented by a pH-phase diagram (Figure 60). At pH values 5.0<pH<6.5 and 7.2<pH<9.5 T_m is independent of pH and in this region the unfolding process of the protein depends on ionization of different groups but not on temperature denaturation (Td). Td (ΔG)- pH phase diagram shows that the temperature of denaturation

decreases rapidly at pH values lower than 5.0 to 3.6 and higher than 10.0 to 12.2. In these regions the unfolding process is connected with temperature unfolding, but not with ionization of different groups.

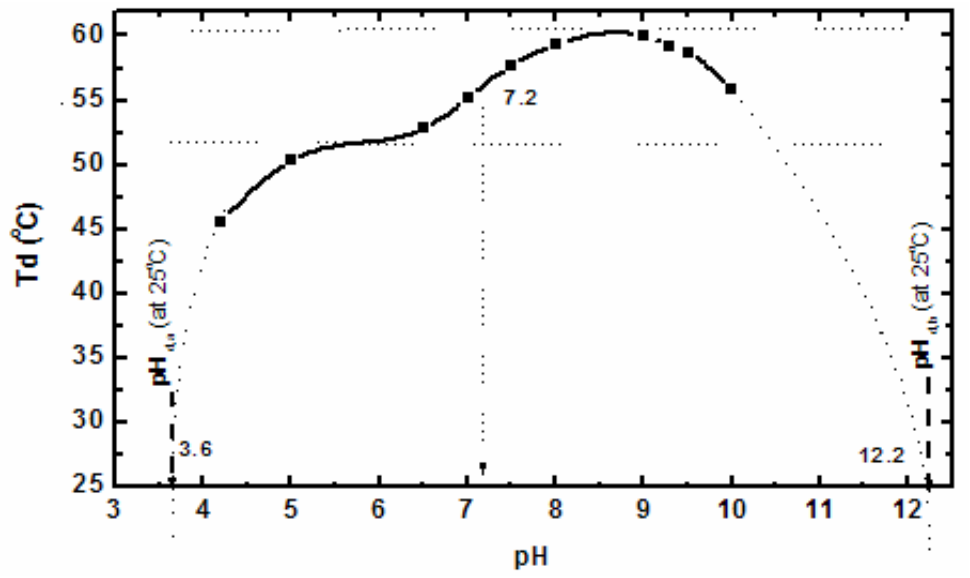

Figure 60. Td(ΔG)-pH phase diagram of oxy-hemocyanin from Limulus polyphemus. *pH (pH 3-12) dependence of the temperatures of denaturation (Td). Tm- melting temperature. The protein is completely denaturated at pH 3.6 and pH 12.2 at 25°C. The native protein at pH 7.2 is stable.*

The pH dependence of the melting temperatures is quite similar for the native molecule and structural subunit. They reach their maximum melting temperature around pH 9.

4.1.5.3.2 Effect of pH on the stability of native molecule of *L. polyphemus* Hc

The near-UV CD spectrum of *L. polyphemus* apo-hemocyanin appears to be less structured than that of holo-protein. The unfolding process was monitored in the far UV. The far-UV CD spectra of *L. polyphemus* hemocyanin in Tris buffer and in pH region (pH 3-12) are shown in **Figure 61** and **62**

We also measured the effect of pH in the range from 2.0 to 12.0 on the ellipticity at 222 nm, caused mainly with the α-helix content. Each spectrum was recorded by averaging two or three separate scans and was base line-corrected based on the buffer solution as blank. By the computer program of Yang, the α-helix content of the protein

was calculated. The CD spectra of a *L. polyphemus* protein were measured at various times up to 24 hours at 25°C in solutions of pH 2 to 11.5, using different buffers: 0.05 M sodium citrate (pH 3.0-5.0); 0.05 M sodium phosphate (pH 5.0-7.0); 0.05 M Tris/HCl (pH 7.0-9.0); 0.05 M carbonate/ bicarbonate (pH 9.0-10.5) and NaOH (pH 11-12).

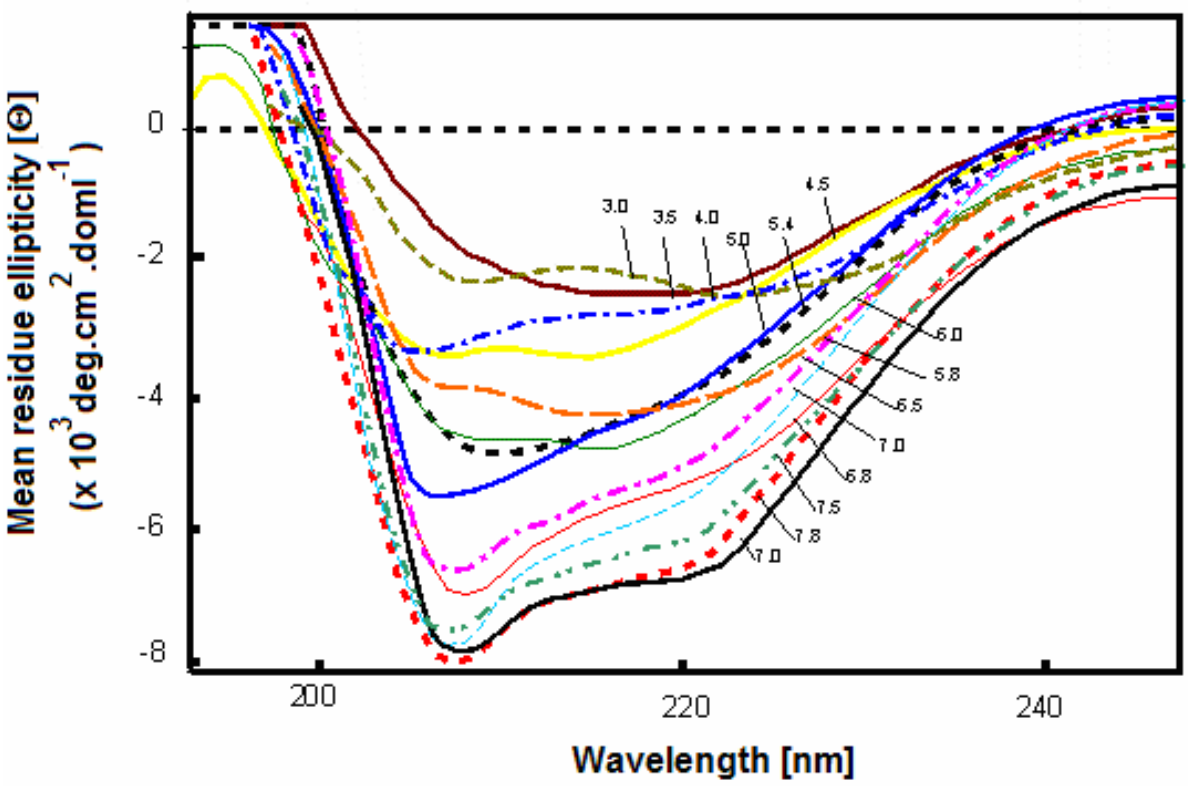

Figure 61. CD spectra of native of L. polyphemus Hc in the acid pH region (3.0-7.8). *Hc was kept for 24 hours in different buffers of the pH range 3.0-8.0: 0.05 M sodium citrate (pH 3.0-5.0) and 0.05 M sodium phosphate (pH 5.0-7.0). pH denaturation was followed by recording the 200-260 nm CD spectra of Hc (0.4 mg/ml). Quartz cylindrical cells with 0.05 cm path length were used throughout.*

There are only minor changes of the ellipticity in pH range 6-10. **(Figure 61, 62)** These results correlate with the fluorescence emission maximum position and confirm the conclusion that the structure of the native molecule and its structural subunits is stable over the pH range 6-9.

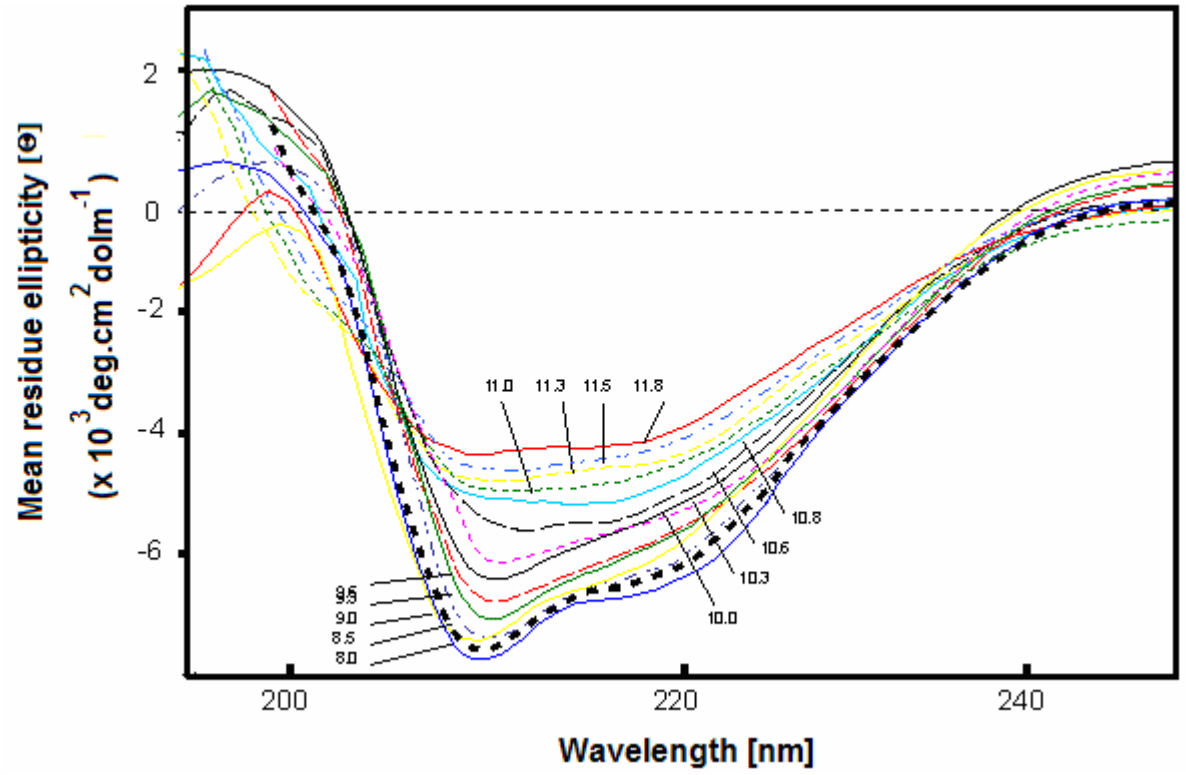

Figure 62. CD spectra of native L. polyphemus Hc in the basic region of pH (8.0-11.8). *Hc was kept for 24 hours in different buffers of the pH range 7.0-12.0: 0.05 M Tris/HCl (pH 7.0-9.0), 0.05 M carbonate/bicarbonate (pH 9.0-10.5) and NaOH (pH 11-12). pH denaturation was followed by recording the 200-260 nm CD spectra of Hc (0.4 mg/ml). Quartz cylindrical cells with 0.05 cm path length were used throughout.*

4.1.5.3.3 Denaturation of native LpH with guanidine hydrochloride (Gnd.HCl)

The effect of Gdn.HCl on the Hc conformation was studied by CD spectroscopy. *L. polyphemus* Hc and one structural subunit were pre-equilibrated at several concentrations of Gnd.HCl in the 0 to 8.0 M range (protein was 1 mM in Tris throughout). The Guanidine-induced unfolding of Hc *L. polyphemus* subunit is shown in **Figure 63**. Changes of CD signals at 222 nm were simultaneously monitored. Upon increasing the denaturant concentration, the CD signal decreased considerably, as shown in **Figure 63.** The effect was already observed at very low denaturant concentration with a threshold near 0.5 M, followed by a monotonic decrease of Cotton effect intensity. This implies that an aggregation-prone intermediate was soon formed in the presence of Gdn.HCl.

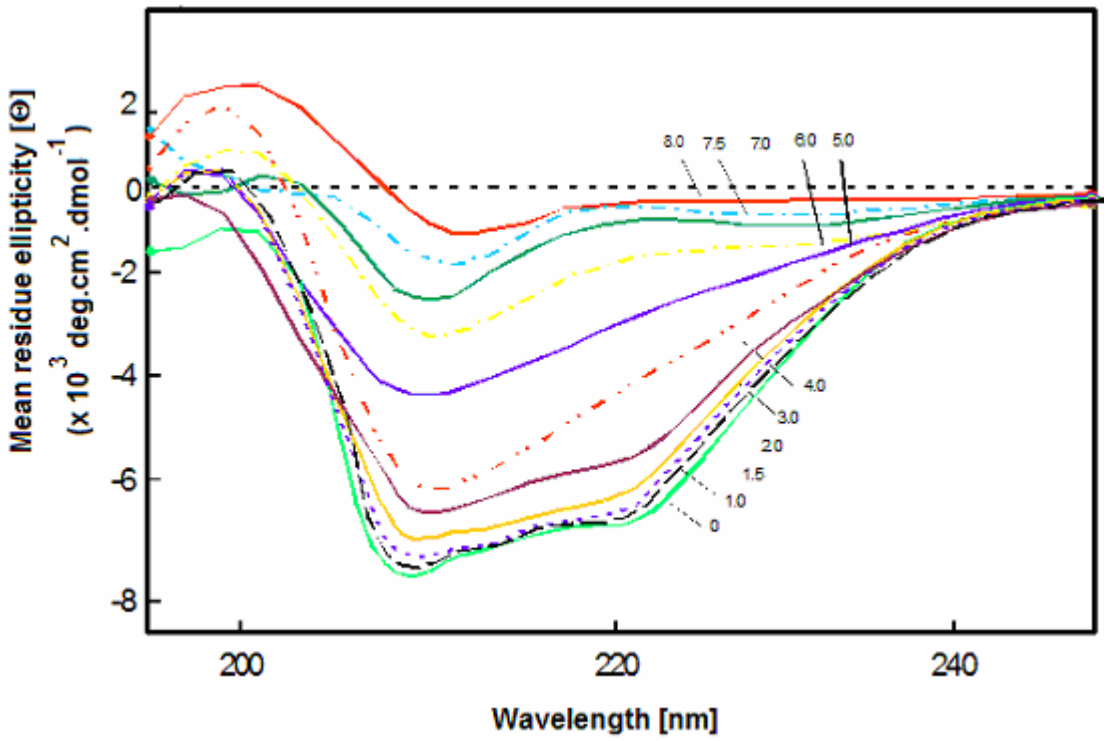

Figure 63. CD spectra of structural subunit 1 of Limulus polyphemus (LpH1) at different concentrations of Gdn.HCl. *Gdn.HCl denaturation was followed by recording the 200-260 nm CD spectra of LpH1 (0.4 mg/ml protein in 50 mM Tris/HCl buffer, pH 8.2, containing 5 mM $CaCl_2$ and 5 mm $MgCl_2$) in the presence of different concentrations of denaturant (0-8.0 M Gdn.HCl) at 25℃. Quartz cylind rical cells with 0.05 cm path length were used throughout.*

At higher concentrations of denaturant hydrophobic residues are better solvated, and the protein turned completely soluble again above 1.2 M Gnd.HCl, i.e. well before denaturation. Gel filtration chromatography experiments showed that *L. polyphemus* Hc in 1.2 M Gdn.HCl had the same elution volume as in 0 M Gdn.HCl, suggesting that it turns back to the monomeric state above this denaturant threshold concentration. The aggregation threshold increased with final protein concentration above 1 mM, but remained approximately constant below it. Therefore, the protein concentration was always kept at 0.4 mg/ml to have spectroscopic signals as intense as possible.

Unfolding kinetics of *L. polyphemus* apo-hemocyanin, induced by Gdn.HCl, was also followed by means of CD measurements. Again, due to protein aggregation at lower concentration of denaturant, data could be collected only above 1.2 M Gdn.HCl. The molar ellipticity data at 225 nm, plotted as a function of Gdn.HCl concentration, are not

shown. Since the intensity of Cotton effect strongly decreased upon unfolding, its time dependence, after mixing the protein with Gdn.HCl, was expected to report on the unfolding kinetics. All experimental traces were best fitted by a sum of two exponentials for the whole Gdn.HCl concentration range investigated (3.0–5.0 M), suggesting the transient formation of an intermediate.

Both phases were found to be affected by the denaturant since both rate constants increased more or less steadily over the entire Gdn.HCl concentration range. The relative amplitudes of the two phases followed an opposite trend: that of the faster phase increased, whereas that of the slower one decreased steadily with Gdn.HCl concentration. Furthermore, since the denaturation process remains biphasic even at very high denaturant concentration, with the slow phase still accounting for about 30% of the total amplitude, this points to a relatively high stability of the intermediate.

Stability of *L. polyphemus* Hc towards the denaturation with Gdn.HCl was compared with the stability of other Crustacea Hcs, i.e. *C. aestuarii* and *P. vulgaris* (**Figure 64)**. The extensive decrease of the ellipticity occurring between 2.5- 6.0 M Gdn.HCl is observed with all so far investigated Hcs.

By increasing the concentration of denaturant, typical spectra for unfolded proteins are observed in 6 M Gdn.HCl for the *L. polyphemus* oxy-hemocyanin **(see Figure 64)**. The denaturated proteins do not reverse to the original conformation upon removal of the reagent of denaturation. Two transitions were observed with Gdn.HCl, when the whole (hexamers and didecamers) form of *L. polyphemus* oxy-hemocyanin was studied. Such a difference can be attributed to complications related to the quaternary structure and the molecular heterogeneity of the whole Hc with respect to the single L1 subunit.

Gdn.HCl-induced equilibrium denaturation of Hcs yielded a structural, partially unfolding state and a rapid conformational transition that occurred between 4 and 5 M Gdn.HCl for native molecules and 3.5-4 M Gdn.HCl for their structural subunits. The

apparent monophasic denaturation curve observed at very low concentration of 0.5 M Gdn.HCl is connected with dissociation of the native molecule.

Comparison of the stability of several arthropodan Hcs: *L. polyphemus, C. aestuarii* and *P. vulgaris* are shown in **Figure 64**. These data confirm that the native LpH is more stable to the Gdn.HCl denaturation as compared to the other Hcs. This interpretation is in

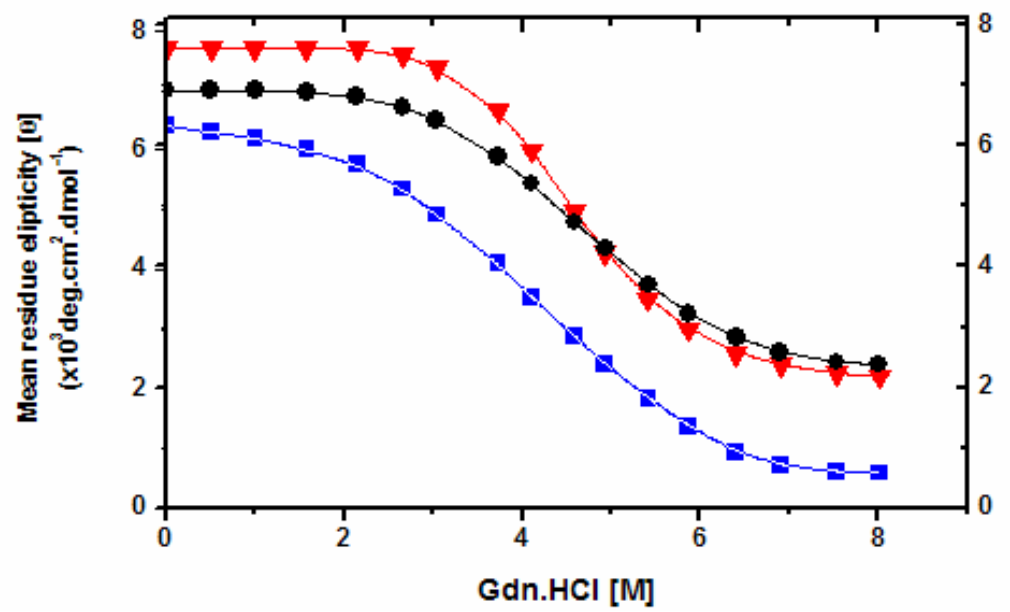

Figure 64. Effect of guanidinium chloride on the intensity of the Cotton effect at 221 nm of native L. poliphemus (red), C. aestuarii (blue) and P. vulgaris (black) Hcs. *Gdn.HCl denaturation was followed by recording the 200-260 nm CD spectra of Hcs (0.4 mg/ml protein in 50 mM M Tris/HCl buffer, pH 7.0, containing 5 mM $CaCl_2$ and 5 mm $MgCl_2$) in the presence of different concentrations of denaturant (0-8.0 M Gdn.HCl) at 25℃. Protein shows a characteristic strong negativ e Cotton effect at 221 nm. Quartz cylindrical cells with 0.05 cm path length were used.*

agreement with the results by [Huebler et al.,2000] who also found that the various subunits of *Eurypelma* Hc exhibited a different stability towards Gdn.HCl and also with results for *Carcinus* Hc [Favilla et al., 2002]. Moreover, native *Carcinus* Hc is composed of two different hexamers which can therefore be expected to have a different stability towards different denaturants. The change in free energy, associated with the transition from the globular to the random coil conformation in the absence of denaturant ($\Delta G_D^{H_2O}$), are calculated for the various Hc species by extrapolating to zero concentration of

denaturant from the plots of ΔG_D *versus* Gdn.HCl concentration. For the glycosylated subunit Ca1 (renamed to CaeSS1) and other SSs, it was found to be 1.2 and 1.3 times higher than the subunits Ca3 and Ca2, respectively. These results correlate well with the temperature denaturation experiments, since the species exhibiting higher stability to Gdn.HCl denaturation also exhibit a higher temperature of melting (Tm). The three subunit types of *C*. *aestuarii* show differences in their stability toward denaturation with Gdn.HCl, which could be expected on the basis of their heterogeneous primary structures. According to previous studies [Dolashka-Angelova et al, 1999], the denaturation effect of 3 M urea is higher for *C*. *aestuarii* compared to molluscan *Octopus vulgaris* Hc and arthropodan *Limulus polyphemus* Hc.

4.1.6 Structure of *Carcinus aestuarii* structural subunit 2 (CaeSS2)

Hemocyanin (Hc) of *Carcinus aestuarii* contains three major and two minor electrophoretically separable polypeptide chains with different N-terminal amino acid sequences [Dolashka-Angelova et al., 1999]. Usually, the reconstitution of the native aggregates requires the full complement of subunits. However, in some instances (i. e. *Carcinus aestuarii* Hc) the higher aggregation forms (24S dodecamer or above) are scarcely populated in reassociation experiments [Dainese et al., 1998]. Studies of the stability of the native *Carcinus aestuarii* Hc dodecamer towards various denaturants (temperature and guanidine hydrochloride), using different techniques, indicate that the quaternary structure is stabilized by oligomerization between structural subunits, and that the possibility of a structural role of the sugar moieties cannot be excluded [Hristova et al., 2000; Favilla et al., 2002; Hazes et al., 1993]. Under appropriate experimental conditions CaeSS1 and CaeSS3 are able to reassociate to the hexameric form [Dainese et al., 1998] while CaeSS2, which has been found to be glycosylated, is unable to reassociate after its separation from the subunit's pool. It retains its monomeric state also at neutral pH and in the presence of Ca^{2+}.

4.1.6.1 Fragmentation and purification of peptides from subunit CaeSS2

The amino acid sequence of CaeSS2 was determined by automated Edman degradation and MALDI-MS analysis of protein fragments obtained by cleavage with chymotrypsin and trypsin. After reduction with 2-mercaptoethanol, modification with 4-vinylpyridine and cleavage with chymotrypsin, the generated peptides/glycopeptides were fractionated on a Superdex peptide HR 10/30 column, yielding two fractions. After fractionation of the peptide mixture in these two fractions *via* RP-HPLC **(Figure 65)**, the peptides were analyzed by mass spectrometry followed by sequencing.

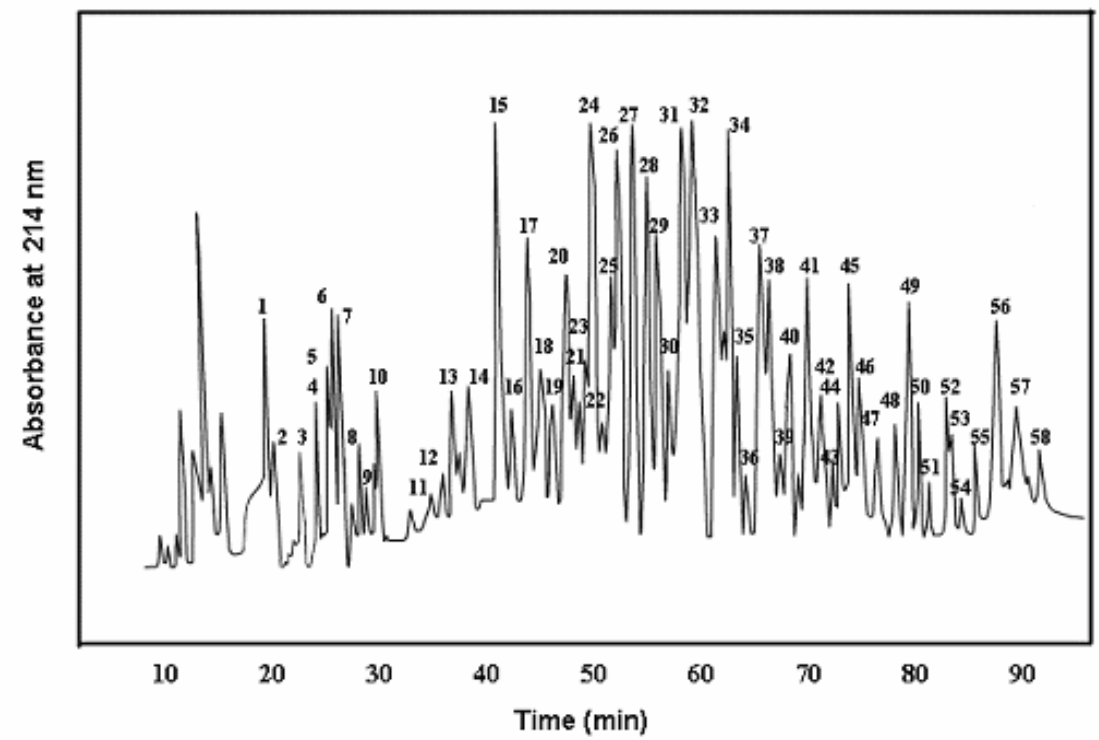

Figure 65. HPLC separation of tryptic fragments of CaeSS2. *Column: Nucleosyl 100 RP-18 (250x10 mm). Solvents: A, 0.1% trifluoroacetic acid in water and B, 80% acetonitrile in 0.1% trifluoroacetic acid/water; linear gradient: from 5% B to 90% B in 110 min; flow rate: of 1.0 ml.min^{-1}; detection: UV, λ=206 nm.*

Similarly, the enzymatic cleavage of subunit CaeSS2 was performed by TPCK-trypsin **(Table 7)**. The resulting peptides were separated by RP-HPLC, providing a well-resolved typical peptide map of this subunit. Although most of the isolated fractions contained pure individual peptides, mixtures of peptides were obtained in a few cases.

About 40–45 HPLC fractions per digest were sequenced and used for alignment and overlap. Approximately 95% of the amino acid residues in the CaeSS2 structure were identified at least twice by sequencing of different fragments. Occasionally, non-specific cleavages were observed **(Table 7)**.

Table 7. Edman degradation and mass spectrometric analysis (MALDI-MS) of peptides generated by tryptic cleavage of the Carcinus aestuarii subunit Hc CaeSS2. Potential O- and N-linked glycosylation sites are indicated in bold.

Peak №	Sequence determination	Position	MW (Da)
4	DSPGGASDAQK	1-11	1032.0
32	TFDVNSLMPVK	12-22	1250.5
49	YEEIRDPHLK	23-32	1299.4
6	ELSLSFDPLSGHYDDDGVSAKR	33-54	2408.5
47	LMKELNEHRLLQQSHWF	55-71	2209.5
11	SLFNPR	72-77	732.8
54	TREEDLMLYNV	78-88	1382.5
42	DEHSGNWDTF	89-98	1207.2
57	AGNAAFFR	99-106	852.9
56	VHVNEGFFVYA**SYS**	107-120	1618.7
16	VVIHSK	121-126	681.8
34	LTQHVVLPPLYEVTPH	127-142	1843.1
53	LF**TNS**EVIQK AYAAK	143-157	1682.9
2	M**TQT**PTK	158-164	805.9
5	IFAHF**TGS**K	165-173	1007.1
1	SNPEQR	174-179	729.7
33	VAYFGEDIGMNTHHVTWH	180-197	2114.3
40	HLEFPFWWDDAHYD	197-210	2511.7
10	AHYDHHIER	207-215	1177.2
51	GESCSS	217-222	568.5
38	VHHQLTVR FDAER	224-236	1607.8
35	LSNYLDPVR	237-245	1076.2
22	ELHWDDV	246-252	912.9
15	IHEGFAPHTSYK	253-264	1386.5
17	YGGYFPDRPDNVNFEDVDGVARVR	265-288	2757.9
12	VRDMLLFEER	287-296	1780.1
20	IQDAIAHGYLR	297-307	1256.4
18	Y**NGS**TINIR	308-316	1037.1
27	DNHGIDVLGDVFESSMYSPRQDYY	317-340	2808.0
7	GALHNQAHR	341-349	1003.1
9	VLGSQADPHGK	350-360	1108.2
13	FALPPGVLEHFETATR	361-376	1785.0
30	DPAFFRLHK	377-385	1130.3
31	YMDNIFRKHK	386-395	1351.6

Table 7 continued

Peak №	Sequence determination	Position	MW (Da)
19	DSLTPYTKNELK	396-407	1408.6
37	FEGVNIDSIYEK	408-419	1413.5
36	GNLETYF	420-426	842.9
44	TYFESFMYTGVNI	425-437	1571.7
48	MLLTNDVDDVDI	438-449	1362.5
8	ATYITDLAHK	450-459	1132.3
55	ELSFQEDVTNEGDIGVLETVR	460-480	2350.5
39	IFAWP	481-485	632.7
28	IDDDHVEFSFNEGR	486-499	1679.7
45	WDVIEMDKFWVM	500-511	1598.9
58	LEHGHHSIDR	512-521	1200.3
41	SSFDSTVTIPDR	522-533	1324.4
52	SFHDIEDRT	535-543	1119.1
46	SEAIPHGK	544-551	837.9
3	ELHIEEFE**SVT**GLPNR	552-567	1870.0
23	FLIPK	568-572	616.8
29	GLVKGKDMDVMV	573-584	1291.6
50	AVTSGEGLA	585-593	803.9
21	AVEGLHR	594-600	780.9
14	SANFAHHGCPEVR	601-613	1424.5
24	YPDKRPHGYPLYR	614-626	1638.8
43	PVDDER	627-632	729.7
25	IITGVTNFK	633-641	992.2
26	HIQVKVFHH	642-650	1144.3

The results of the sequences of tryptic peptides obtained by a combination of Edman degradation and mass spectrometry, in comparison with sequences of known Hcs, are summarized in **Figure 66**.

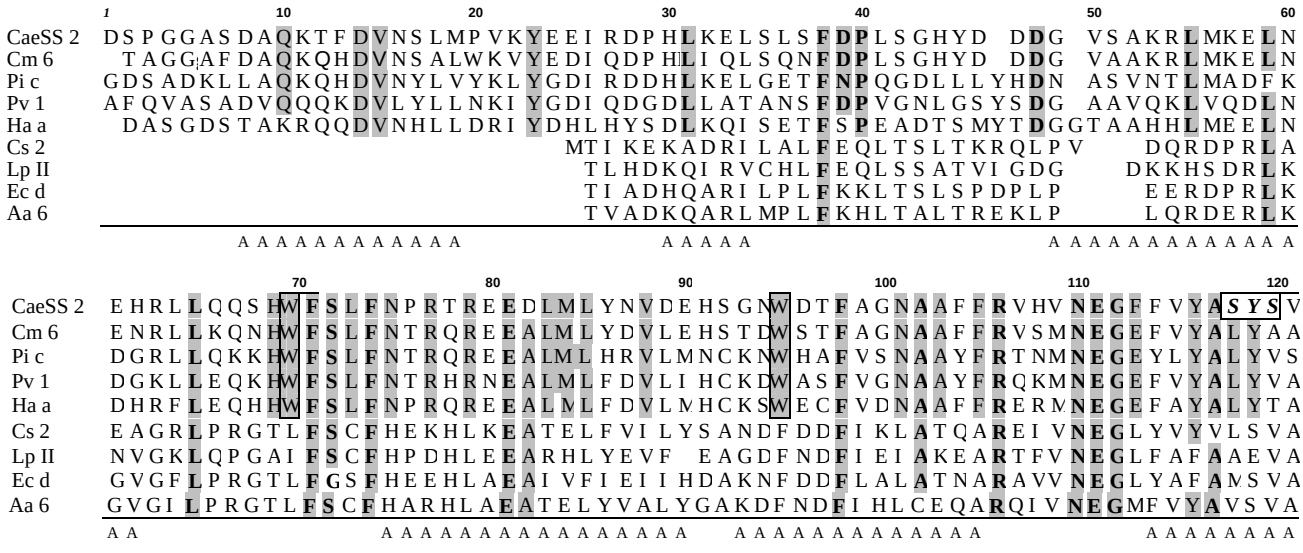

Figure 66 continued

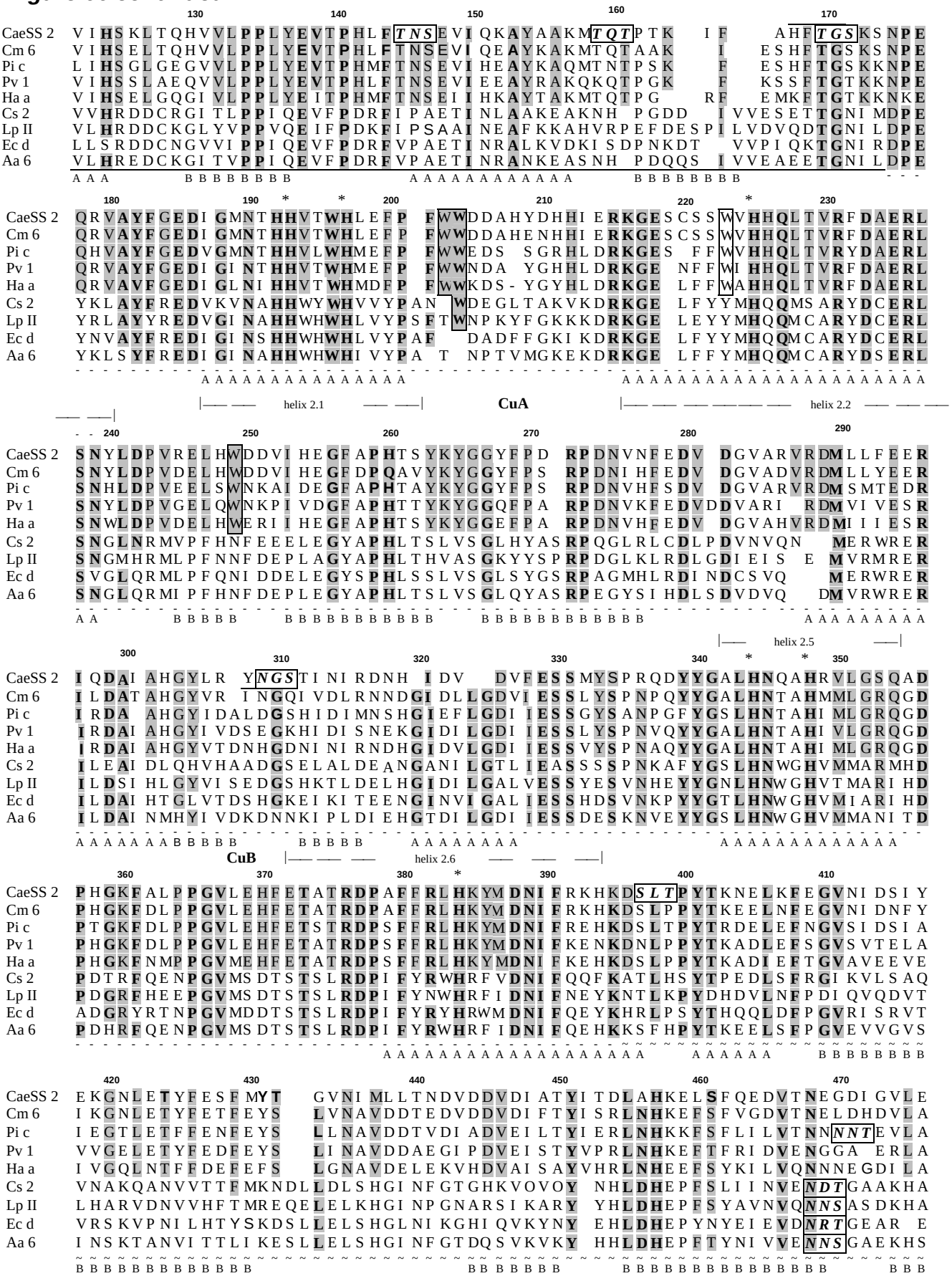

Figure 66 continued

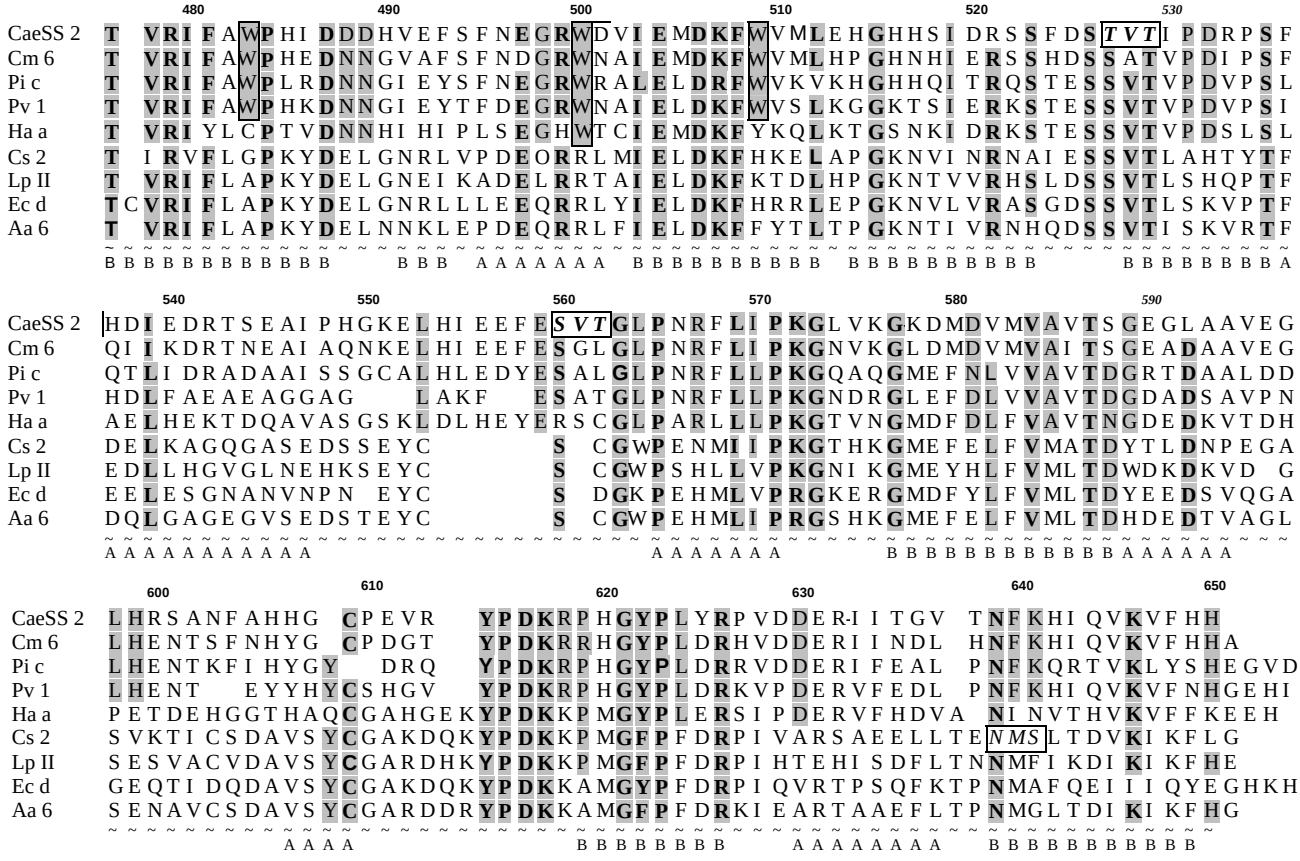

Figure 66. Alignment of the amino acid sequences of subunit CaeSS2 of C. aestuarii hemocyanin with selected crustacea hemocyanins: *γ–type subunits of C. magister subunit 6 (Cma, AAA96966); P. vulgaris subunit 1 (Pv1, P80888); P. interruptus subunit c (Pic, P80096); α–type subunit of H. americanus (Ham, AJ272095) and cheliceratan Hcs: C. salei subunit 2 (Cs2, AJ307904); L. polyphemus subunit II (LpII, P04253); A. australis subunit 6 (Aa 6, P80476), E. californicum subunit d (Ecd, P02241). Structural elements are related to P. interruptus Hc: domain I (—), domain II (- - -) and domain III (~ ~ ~). The putative O- and N-glycosylation sites are boxed and in italics, conserved residues are shaded; copper-binding histidine residues (*), disulfide bridges (**c**), α–helix (A) and β-sheets (B) are marked correspondingly.*

4.1.6.2 Primary structure of *Carcinus aestuarii* structural subunit 2 (CaeSS2)

The primary structure including all structurally and functionally important sites of crab *Carcinus aestuarii* Hc subunit CaeSS2 was established by comparison with peptide sequences of the phylogenetically-related *Cancer magister* Hc subunit 6 [Durstewitz and Terwilliger, 1997] **(Figure 66)**. The subunit is a protein of 650 amino acids with a calculated molecular mass of 74 870 Da what agrees with the results obtained by SDS-PAGE. The subunit was calculated to be acidic, with an isoelectric point [pI] of 5.59. The

amino acid sequence shows the presence of high amounts of aromatic amino acids (tryptophan, phenylalanine and tyrosine) and of a low methionine content.

The complete hemocyanin sequence of subunit CaeSS2 was aligned with other crustacean hemocyanins: dungeness crab *Cancer magister* subunit 6 (Cm a, Accession No. AAA96966; 73.2% homology) [Durstewitz and Terwilliger, 1997], *Palinurus vulgaris* subunit 1 (Pv1, P80888; 53.2%) [Jekel et al., 1996], *Palinurus interruptus* subunit c (Pic, P80096; 56%) [Neuteboom et al., 1992], *Homarus americanus* (Ham, AJ272095; 46.8%) [Burmester, 1999], and cheliceratan Hcs: *Cupiennius salei* subunit 2 (Cs2, AJ307904; 31.1%) [Ballweber et al., 2002], *Limulus polyphemus* subunit II (LpII, P04253; 30%) [Hazes et al., 1993], *Androctonus australis* subunit 6 (Aa6, P80476; 32%) [Buzy et al., 1995] and *Eurypelma californicum* subunit d (Ec d, P02241; 32%) [Voit et al., 2000].

Multiple sequence alignment of these primary structures reveals that the protein chain lengths of crustacean Hcs are roughly the same: CaeSS2 (650 aa), *H. americanus* -a (654 aa), *C. magister* 6 (650 aa), *P. vulgaris* 1 (657 aa) and *P. interruptus* -c (661 aa), except for the cheliceratan Hcs spider *E*. *californicum* subunit Ecal-a, the scorpion *A*. *australis* subunit 6 and the horseshoe crab *L*. *polyphemus* subunit LpII which have amino acid chains of 630, 626 and 628 residues, respectively [Hazes et al., 1993; Voit et al., 2000; Beintema et al., 1994]. Furthermore, the high degree of sequence similarity among arthropodan hemocyanins (30%-70% sequence identity) suggests that the proteins have a common tertiary structure.

As expected, we observe the highest degree of sequence identity to other crustacean hemocyanins, in particular to *P. vulgaris* subunit 1 (52.5% identity) and *P. interruptus* subunit c (56% identity). These three subunits belong to the γ-type hemocyanins according to the definition of Markl [Markl and Decker, 1992]. CaeSS2 and *Cancer magister* subunit 6 seem to be more homologous to each other (73% identity) **(Figure 66)**. This value is very close to the homology reported between the subunits of *H.*

americanus -a and the hemocyanin subunits a and b of spiny lobster *P. interruptus* (70.2 and 70.4% identity respectively) and that of *P. vulgaris* (69% identity).

Crystallographic studies of hemocyanin from *Panulirus* and *Limulus* [Gaykema et al., 1986; Volbeda and Hol, 1989; Hazes et al., 1993; Nakashima et al., 1986] have shown that arthropodan hemocyanins consist of three structural domains. A structure-based sequence alignment of the CaeSS2 amino acid sequence against homologous hemocyanins for which structural information is known suggests a rather strict conservation of structural features **(Figure 66)**. Domain 1 (residues 1-175 in CaeSS2) is mainly α-helical and is quite variable in sequence. Domain 2 (residues 175-395*)* is the most conserved one and is sandwiched between domains 1 and 3. It is also mostly α-helical and contains the oxygen-binding CuA and CuB sites. Each copper ion is buried in the core of this domain and is ligated to three histidine side chains. The six histidines marked by an asterisk in **Figure 66** are implicated in Cu binding according to their highly conserved character among arthropodan hemocyanin subunits [Markl and Decker, 1992; Voit et al., 2000]. The CuA helix pair in CaeSS2 extends from residue 187 to residue 201 (helix 2.1) and from residue 216 to 240 (helix 2.2). The Cu binding histidines are located at positions 193, 197, and 225. The CuB helix pair extends in the region from 342 to 354 aa (helix 2.5) and 375 to 397 aa (helix 2.6). Histidine residues binding the copper ion at the CuB site are located at positions 344, 348, and 384. Domain 3 is rich in β-sheets and forms a β-barrel structure: it also contains a seven-stranded Greek-key motif with two long loops. One of these loops contains a disulfide bond that bridges and interacts with domain 2 and a Ca^{2+} binding site.

Two cysteine residues were identified in the crustacean Hcs: CaeSS2, Cm6, Pic, and Pv1, while 4 or 6 of these residues were observed in cheliceratan Hcs: Cs2, LpII, Ecd, Aa6. The cysteines forming the disulfide bridge and stabilizing domain 3 are conserved in CaeSS2 and in *C. magister* subunit 6 at positions 220 and 609, respectively, but are

different from the cysteines forming disulfide bridges in LpII and in *E. californicum* subunits. There are about 8 Cys residues in each subunit of *C. salei* hemocyanin, where four strictly conserved cysteine residues are in domain 3. They most likely form two disulfide bridges that make up a flexible hinge stabilizing the three-dimensional structure of the subunit, as deduced from other hemocyanins [Ballweber et al., 2002].

As the amino acid sequence of CaeSS2 shows a rather high content of aromatic amino acids (tryptophan, phenylalanine and tyrosine) fluorescence spectroscopy is a useful tool to study the stability of this protein.

4.1.6.3 Fluorescence properties of *Carcinus aestuarii* subunit 2 (CaeSS2)

Our determination of the amino acid sequence of CaeSS2 identified 10 Trp and 27 Tyr residues. Upon excitation at 295 nm, the native oxy-Hc and oxy-SSs upon excitation at 295 nm show an emission band with λ_{max} at 310–336 nm **(Table 8)**, indicating the presence of “buried“ tryptophan side chains.

Table 8. Quenching constants (K_{sv}) of the indole emission of monomeric CaeSS and native Carcinus aestuarii Hc in presence of acrylamide, potassium iodide and copper complex ($Cu^{II}(PuPhPy)^{2+}$).

Sample	KI (K_{SV}^-) ($dm^3.mol^{-1}$)		Acrylamide (K_{SV}) ($dm^3.mol^{-1}$)		Copper complex (K_{SV}) ($dm^3.mol^{-1}$)		Emission λ_{max} (nm) Excitation at 295 nm	
	oxy-	oxy-	oxy-	apo-	oxy-	apo-	oxy-	apo-
Native Hc	-	-	-	3.64[a]			310±1[a]	322±1[a]
CaeSS1	1.0[b]	1.0[b]	2.2[b]	4.0[b]			329±1[a]	331±1[a]
CaeSS2	1.0[b]	1.0[b]	2.4[b]	3.5[b]	$0.9x10^6$	$1.4x10^6$	336±1[a]	339±1[a]
CaeSS3	1.0[b]	1.0[b]	0.9[b]	10.0[b]			332±1[a]	335±1[a]

[a] [Dolashka-Angelova et al., 1999]**; [b]** [Di Muro et al., 2002]

Indeed, analysis of the fluorescence decay [Di Muro et al., 2002] reveals that Trp residues of the CaeSS2 subunit can be classified into three classes with fluorescence lifetimes of around 0.11-0.15, 0.33, and 3.1-3.5 ns, respectively. The short-lived component is mainly responsible for the decay of the holo-form. Its contribution to the overall fluorescence (around 70%) corresponds to that calculated as the most acrylamide-accessible

fluorescence. The second class of Trp residues, with an intermediate lifetime value (0.33 ns) is present only after copper removal. It can be identified with residues localized in the close surrounding of the active site whose fluorescence is fully quenched by copper-related heavy atom and paramagnetic ion effects in the oxygenated form [Ricchelli et al., 1987; Boteva et al., 1993].

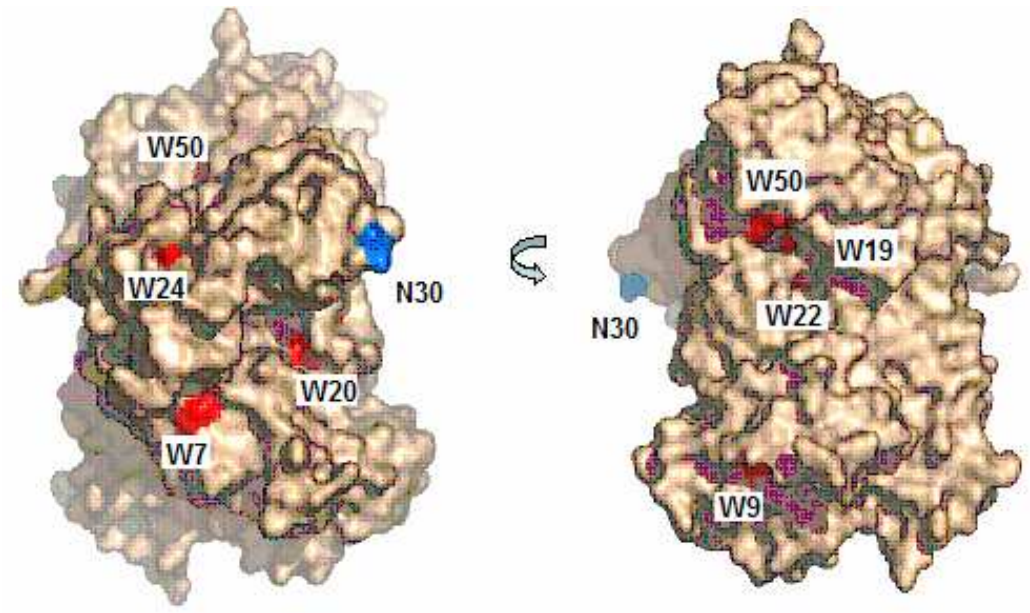

Figure 67. Putative localization of tryptophan residues and N-linked glycosylation site of CaeSS2. *Tryptophan residues are indicated in red. Trp483 is not shown because it is predicted to be completely buried in the structure. The N-linked glycosylation site (Asn309) is shown in blue. The model was generated using the structure of subunit 1 of P. interruptus hemocyanin (PDB code 1HC1) following a structure-based sequence alignment of the sequence of CaeSS2 against the sequence and crystal structure of P. interruptus hemocyanin. This figure was prepared and rendered with program PyMol 0.95.*

To identify the contribution of Trp residues in CaeSS2, the structure of the *P. interruptus* subunit a was used to construct a tentative model of the structural subunit of *C. aestuarii* hemocyanin. **Figure 67** shows the Trp distribution in subunit CaeSS2, based on this model. The Trp positions, together with the decay parameters, can give useful information on the fluorescence properties of these residues individually. The quenching of tryptophan fluorescence by copper ions (see above) is a very short-range process involving quenching interactions within chromophore-quencher distances of about 14 Å [Strambini, and Gabellieri, 1991].

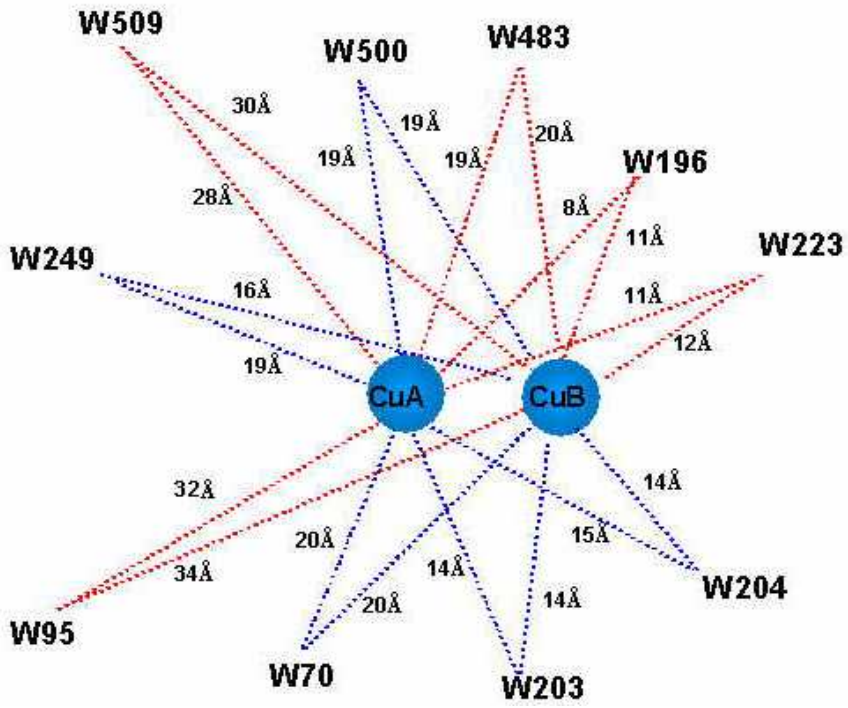

Figure 68. Approximate distances between tryptophan residues in C. aestuarii and the di-copper center. *The distances indicated are $Trp_{C\alpha}$-Cu values observed in the homology model that was used. This Figure was prepared and rendered with program PyMol 0.95.*

As calculated from the model, the distances of Trp196, 203, 223 and 249 are within this range **(Figure 68)** and they should constitute the class of fluorophores, characterized by a τ value of about 0.3 which become fluorimetrically active only after copper removal. Most of the tryptophans located near the active site are conserved in Hcs from other arthropods such as *Cancer magister* Hc subunit Cm6, *Palinurus vulgaris* subunit 1, *Palinurus interruptus* subunit c and *Homarus americanus* **(Figure 66)**. The third class of Trp residues with high τ values (3.0-3.5 ns) represents amino acids close to the active site. Trp196, with a distance to the active site of 8-11 Å, most probably belongs to this class. In most arthropodan Hcs only 50% of Trp residues are located in the vicinity of the metal centres. Most of the indole residues of structural subunit a of *E. californicum* Hc are located within a short distance (less than 1.1 nm) from copper A and B, which explains the exceptionally strong fluorescence quenching in the oxy-form.

As is seen from the model of CaeSS2 **(Figure 67)** the emission of holo-CaeSS2 mainly arises from Trp70, 95, 500, and Trp509 which are exposed or are near the surface of the molecule. They belong to the first class of Trp residues having a very short

fluorescence lifetime of 0.15 ns. Trp483 is about 19-20 Å removed from the copper ions, but is buried by the Cys residues and cannot be observed at the surface of the molecule.

The static fluorescence parameters agreed fairly well with the data obtained by quenching experiments. The quenching of the indole fluorescence of CaeSS1, CaeSS2, CaeSS3 and 16 S hexamer of *C. aestuarii* Hc is shown in **Table 8**. The decrease in fluorescence emission is a linear function of the concentration of quenching agent, i.e. the quenching process follows the unmodified Stern-Volmer equation and can be described using single K_{sv} constants. The quenching efficiency K_{sv} of the oxy-form is lower compared to the apo-form. Removal of the copper ions from the active site increases the fluorescence intensity. This conclusion is further confirmed by the values of the respective Stern-Volmer constants **(Table 8)**. Considerable increase in the quenching efficiency is observed, when iodide (I^-) is exposed to different concentrations of acrylamide; K_{sv} values of 3.64, 4.0, 3.5, and 10.0 were calculated for the whole molecule and the structural subunits [Dolashka-Angelova et al., 1999; Di Muro et al., 2002] **(Table 8)** and for the copper complex ($Cu^{II}(PuPhPy)^2$) **(Figure 69)**.

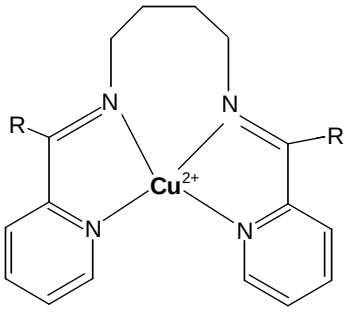

R= phenyl: Cu^{II} $(PuPhPy)^{2+}$

Figure 69. Copper complex ($Cu^{II}(PuPhPy)^{2+}$) including one Cu ion.

The copper complex ($Cu^{II}(PuPhPy)^{2+}$) which, as in hemocyanins, includes one Cu ion in its center, shows very high values of Stern-Volmer constants: $0.90x10^6$ for oxy and $1.45x10^6$ for apo-CaeSS2 **(Figure 70, Table 8)**. The difference of K_{sv} values calculated from holo- and apo-forms relates to the quenching effect on the indole emission of copper ions in the active site.

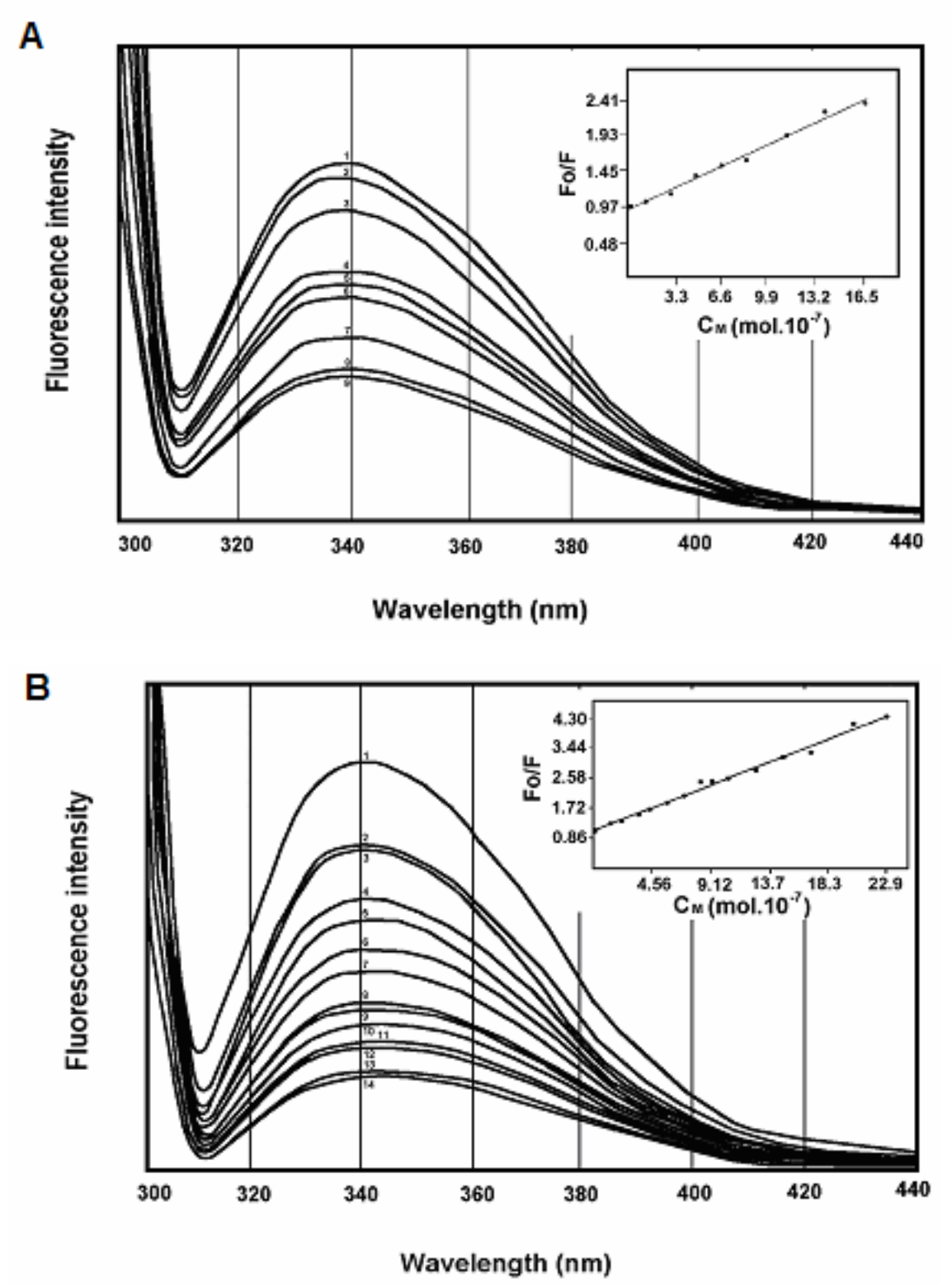

Figure 70. Fluorescence quenching of structural subunit 2 of Carcinus aestuarii Hc. *Stern-Volmer plots describing the quenching of oxygenated* ***(A)*** *and apo-form* ***(B)*** *of CaeSS2 by the copper complex ($Cu^{II}(PuPhPy)^{2+}$). The monomer was dissolved in 50 mM Tris/HCl buffer, pH 8.2. The relative quantum yields (Q) were measured by comparing the integrated corrected fluorescence emission spectra of Hcs with those of N-acetyltryptophanamide, normalized to the same absorbance at the excitation wavelength (295 nm). The quantum yield of the standard was 0.13 at 21℃ [Lehrer, 1971]. F_0/F: fluorescence intensity of protein without quencher to fluorescence intensity at different concentrations of the quencher.*

4.1.7 Carbohydrate composition of *Carcinus aestuarii* (Ca) hemocyanin

4.1.7.1 Carbohydrate content of *Carcinus aestuarii* structural subunit 2 (CaeSS2)

The carbohydrate content of oligomeric native Hc of CaeSS2 is 1.6% (w/w), as determined with the orcinol/H_2SO_4 assay [Abrashev et al., 1998]. This glycosylated fraction, however, is present specifically in subunit Ca2, according to the nomenclature of subunits introduced in [Dolashka-Angelova et al., 1999], where 6.3% (w/w) of carbohydrates are found. The sugar content of *Carcinus aestuarii* Hc and subunit Ca2 is compared in **Table 9** with that of other arthropod Hcs: *Limulus polyphemus* [Van Kuik et al., 1990], *Eurypelma californicum* [Markl et al., 1976], *Scutigera coleoptrata* [Van Kuik et al., 1990], *Astacus leptodactylus* [Tseneklidou-Stoeter et al., 1995], *Homarus americanus* [Waxman, 1975], *Panulirus interruptus* [Van Kuik et al., 1987], and *Androctonus australis* [Debeire et al., 1986].

Table 9. Monosaccharide composition (nmol sugar/mg protein) and carbohydrate content (%, w/w) of arthropodan hemocyanins.

		Monosaccharide composition *nmol sugar/mg protein*		
Species	Subunits	Man (Gal)	GlcNAc (GalNAc)	Carbohydrate content *%, w/w*
Limulus polyphemus (Lp)	Native molecule			<0.1
Androctorius australis (Aa)	Native molecule	34.8	7.9	0.8
Eurypelma californicum (Ec)	Native molecule			<0.1
Panulirus interruptus (Pi)	Native molecule	29.6	11.3	0.8
		39.7	16.1	1.0
		35.9	15.2	1.0
Astacus leptodactylus (Al)	Hexamer	31.9	22.0	1.1
Scutigera coleoptrata (Sc)	Native molecule	182.0	78.0	4.9
Homarus americanus (Ha)	Native molecule			0.9
Carcinus aestuarii (Ca)	Native molecule	31.7	39.1	1.6

The 6.3% (w/w) carbohydrate content of CaeSS2 is unusually high for an arthropod Hc, where the carbohydrate content is usually about 1%, with the exception of Hc *S. coleoptrata,* where 4.9% (w/w) carbohydrates are found [Van Kuik et al., 1990]. As far as

the site of glycosylation is concerned, there are differences between the crustacean species investigated so far. In contrast to *P. interruptus* and *H. americanus,* where all subunits are glycosylated, one subunit is glycosylated only in *Carcinus aestuarii* hemocyanin and *A. leptodactylus* [Tseneklidou-Stoeter et al., 1995].

4.1.7.2 Tryptic digestion of *Carcinus aestuarii* structural subunit 2 (CaeSS2)

To study the glycosylation sites of CaeSS2, the purified subunit was subjected to tryptic digestion followed by fractionation on a Superdex 300 column. **Figure 71** shows the elution profile of the lysate. Peak fraction 1 gave a positive reaction with the orcinol/ H_2SO_4 assay **(Figure 71)** and was further fractionated by reverse phase HPLC **(Figure 72)**.

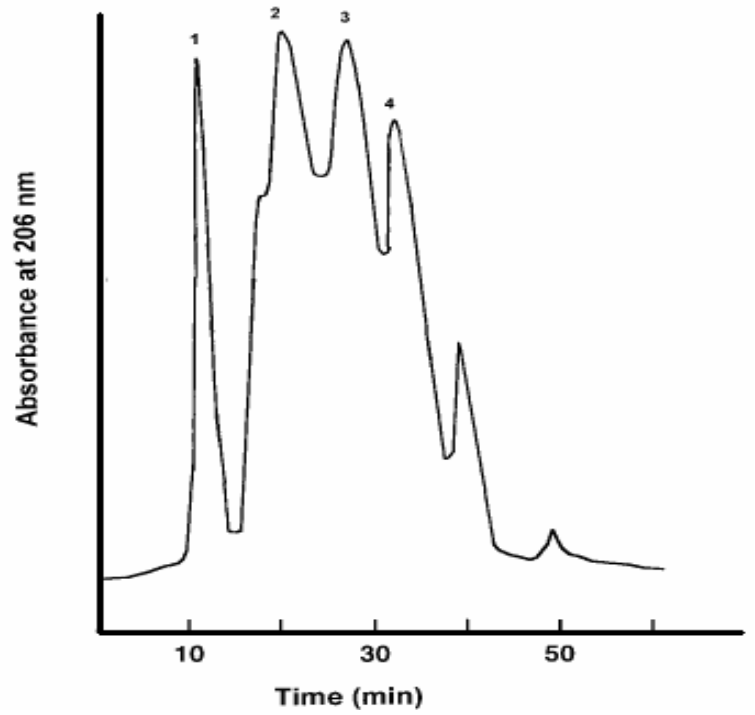

Figure 71. Gel filtration elution profile of subunit Ca2 of Carcinus aestuarii hemocyanin, after tryptic digestion. *The glycopeptide mixture was separated on a Superdex 300 gel filtration column (2x30 cm), and the fractions were eluted with water at a flow rate of 1 ml.min^{-1}.*

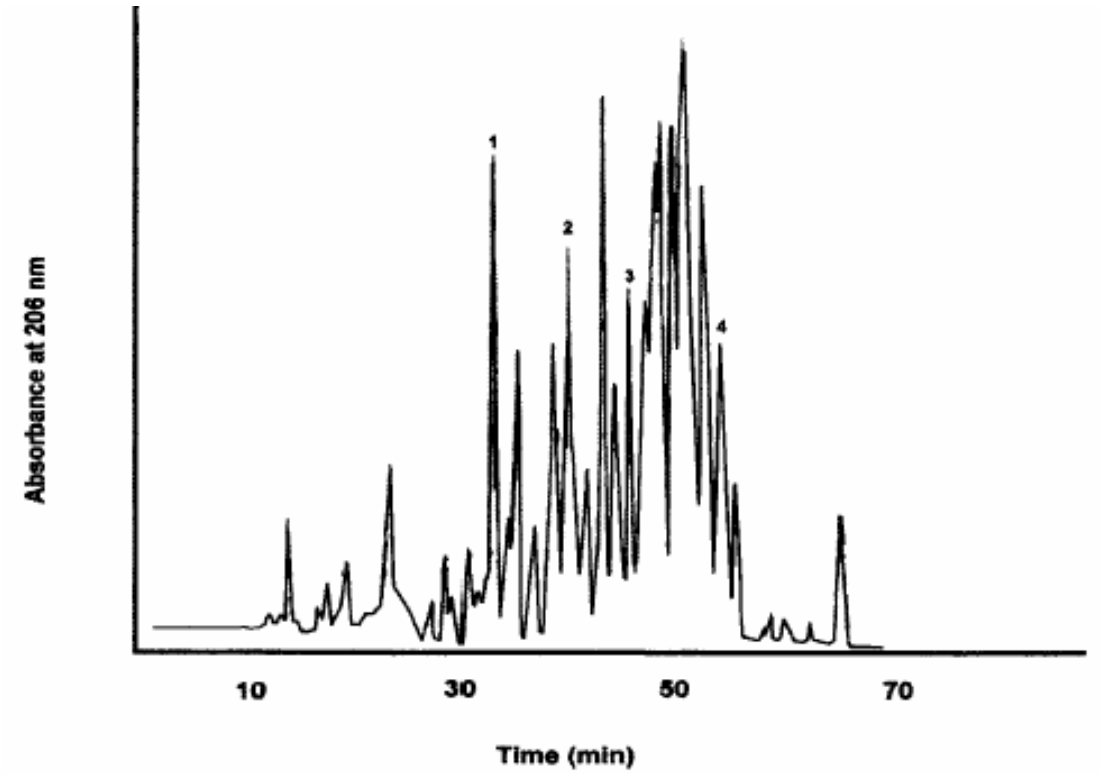

Figure 72. HPLC separation profile of the Carcinus aestuarii glycopeptide fragments obtained from peak 1 of Figure 71. *The peak fraction giving a positive reaction was further fractionated by reverse phase HPLC using a Nucleosil 7 C18 column (250x10 mm). For elution, a linear gradient of 5% A (0.1% TFA in water) and 100% B (0.085% TFA in acetonitrile) within 70 min at a flow rate of 1ml.min^{-1} was used*.

Four fractions were found to contain carbohydrates **(identified by the numbers 1–4 in Figure 72)**. Fractions 1–3 contain Ser/Thr which are sites for O-glycosylation, whereas fraction 4 presents the consensus sequence Asn-Xxx-Ser/Thr, typical for N-glycosylation.

4.1.7.3 MALDI-MS of glycopeptides 1, 2, 3 and 4 of CaeSS2 before and after treatment with specific glycosidases

The various glycopeptides were further characterized by MALDI-MS to determine their molecular weights before and after removal of the carbohydrate chains **(Table 10).** To this aim, we used specific glycosidases, which proved to give positive reactions with other arthropod Hcs. For interpretation of the glycopeptide results, the digest can be considered in two steps: digestion with neuraminidase, and followed by digestion with α-*N*- acetylgalactosaminidase or β-galactosidase.

Table 10. Properties of the glycopeptides isolated from subunit Ca2 of Carcinus aestuarii hemocyanin.

Fraction[a]	Glycopeptide mass[b]	Glycopeptide mass after treatment with neuraminidase [b]	Peptide mass[c]	Oligosaccharide mass[d]	Sugar composition[e]	Linkage site
1	1399	1399	995 (993.6)	404	$GalNAc_2$	The-Gln-Ser
2	2496	1762	1030 (1071)	1466	N-Acetyl-O-di-$NeuAc_2Gal_3GalNAc_2$	Ser-Pro-Ser
3	2855	2222	1330 (1330)	1525	N-Acetyl-O-$NeuAc_2Gal_3GalNAc_2$	Ser-Tyr-Ser
4	2498	2498	1150 (1158)	1348	$SO_4Man_4GlcNAc_3$	Asn-Asn-Ser

a) The numbering of glycopeptide corresponds to that of the HPLC peaks of **Figure 69.**
b) Determined by MALDI-MS
c) Determined by MALDI-MS (the values in parentheses are predicted on the basis of the peptide sequence).
d) Calculated from the difference between the glycopeptide mass and the peptide mass.
e) Based on enzymatic cleavage and MALDI-MS.

Glycopeptide **1**, having Mw of 1399 Da, was first treated with neuraminidase to remove sialic acid. By this treatment no reduction in molecular mass was observed by MALDI-MS **(Figure 73a).** Further treatment with α-*N*-acetylgalactosaminidase to hydrolyze the bonds between Ser and *N*-acetyl-D-galactosamine results in a decrease of molecular mass of the glycopeptide to 995 Da **(Figure 73a, Table 10)**, a value in excellent agreement with that expected on the basis of the amino acid sequence (993.6 Da). Thus, it is concluded that the mass of the oligosaccharide moiety is 404 Da, corresponding to the presence of two GalNAc groups **(GalNAc2, Table 10)**. The same procedure was applied to peptides 2 and 3, where treatment with neuraminidase decreases the molecular mass as shown in **Figures 73b, 73c and Table 10**, indicating the presence sialic acid residues of 734 and 633Da, corresponding to (*N*-acetyl- *O*-di-NeuAc)$_2$ and (*N*-acetyl-*O*-NeuAc)$_2$, respectively [Settineri et al., 1997]. Again, further treatment with α-*N*-acetylgalactosa-minidase results in a decrease of molecular mass **(Figures 73b, 73c)** to 1030 and 1330 Da in the case of peptides 2 and 3, respectively **(Table 10)**, as expected on the basis of the peptide sequence.

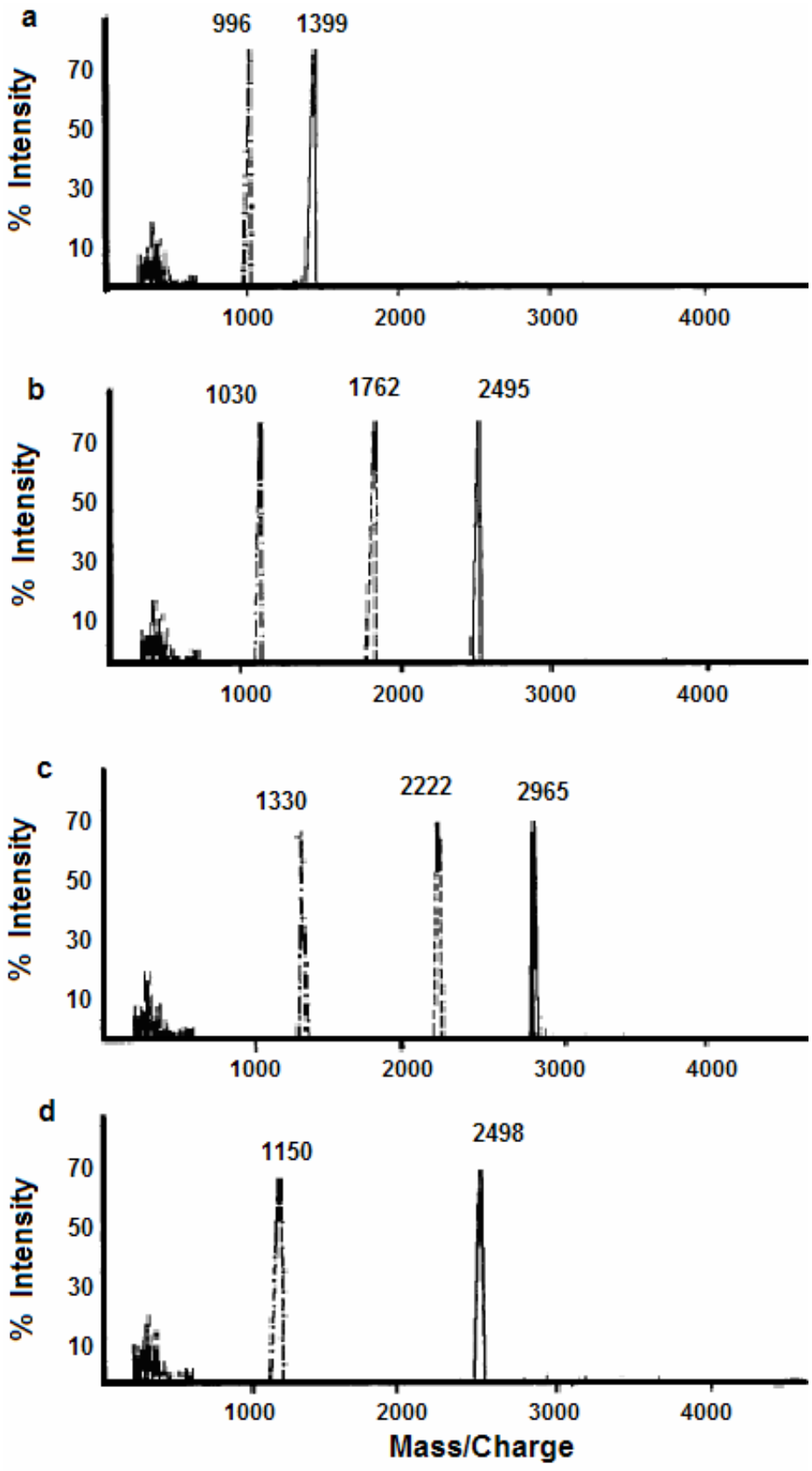

Figure 73. MALDI mass spectra of glycopeptides 1–4 isolated by HPLC from subunit Ca2 of Carcinus aestuarii hemocyanin (Figure 72) a) *glycopeptide 1;* ***b)*** *glycopeptide 2;* ***c)*** *glycopeptide 3 and* ***d)*** *glycopeptide 4. The solid lines refer to glycopeptide peaks before treatment with specific glycosidases. The dashed lines refer to glycopeptide peaks after treatment with neuraminidase; the dashed–dotted lines refer to glycopeptides after treatment with α-N-acetylgalactosaminidase.*

In the case of peptide 4, no sialic acid is found **Figure 73d, Table 10)** and a decrease of molecular mass from 2498 to 1150 results after treatment with PNGase-F, indicating the presence of an N-linked carbohydrate chain with 1348 Da molecular mass. The carbohydrate compositions of the various glycopeptides are inferred from the reactivity toward the various enzymes (presence or absence of sialic acid and O- or N-linked carbohydrates) and from the estimated molecular masses. The suggested compositions are reported in **Table 10**, whereas in **Table 11** the putative sequences of the glycopeptides are shown.

The carbohydrate content of arthropod Hcs is usually low and only D-Man and D-GlcNAc are detected [Van Kuik et al., 1990]. Structural analysis of the glycan chains of Hcs of *An. australis* [Debeire et al., 1986], *P. interruptus* [Van Kuik et al., 1987], and *As. Leptodactylus* [Tseneklidou-Stoeter et al., 1987] revealed N-linked glycans, while in *C. aestuarii* Hc three O-linkage glycopeptides and one Nlinked glycopeptide were isolated.

4.1.7.4 Suggested structure of carbohydrate chains of glycopeptides 1, 2, 3 and 4 of CaeSS2

Glycopeptide 1 could be assigned to the subunits e and a of *Eurypelma* Hc. The presence of two putative O-linkage sites (T and S) suggests that each GalNAc present in the peptide is linked to a distinct amino acid as reported in **Table 11**. Glycopeptide 2 bears an O-linkage glycosylation site and the carbohydrates that are found in peptide 2 are typical for O-linked carbohydrate chains with the sequence shown in **Table 11**. Glycopeptide 3 with an O-linkage site was so far found to be present only in subunit e of *Eurypelma* Hc. The carbohydrate sequence, proposed on the basis of the same considerations as above, is presented in **Table 11**. Glycopeptide 4 is different from the other peptides since it contains the asparagine group in the typical consensus sequence -N-X-S(T)- for N-linkages.

Table 11. Suggested compositions of the glycopeptides identified in subunit Ca2 of Carcinus aestuarii Hc. *TGS, SPS, SYS and NNS-amino acids sequences of CaeSS2.*

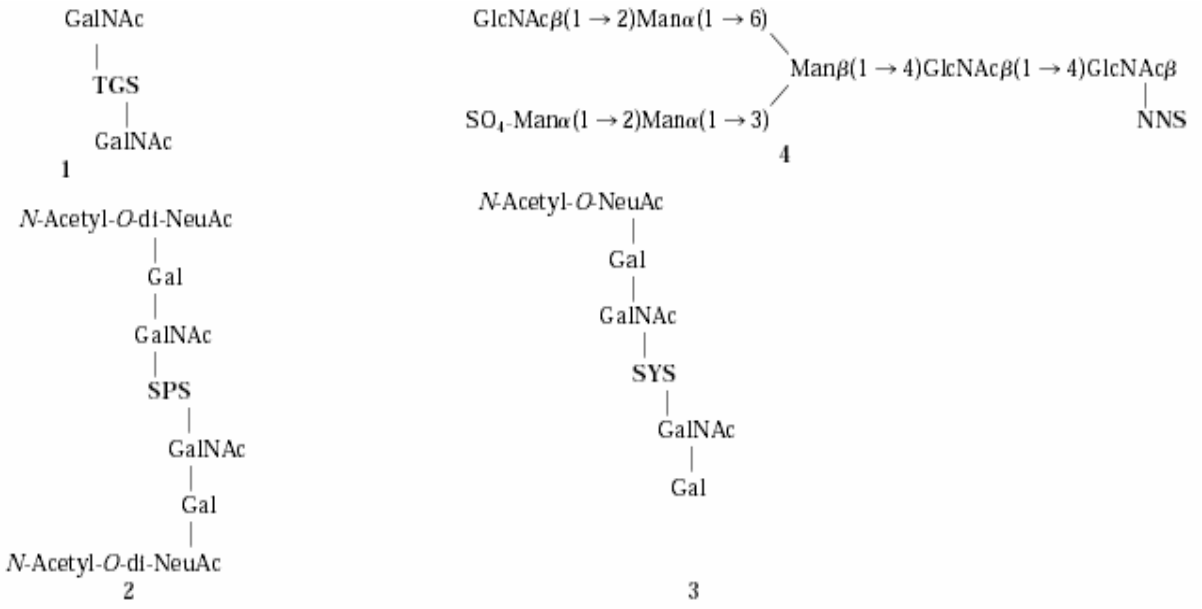

Note. Each structure was based on the mass signal shifts identified by MALDI MS before and after treatment with neuraminidase and α-N-acetylgalactosaminidase or PNGase-F. The numbers identify the different glycopeptides as described in ***Figure 72*** *(Dolashka-Angelova et al., 2004).*

Our sequence results show three consensus sequences for O-glycosylation and one for N-glycosylation. The putative N-linked site is observed at position 309 with a consensus sequence Asn-Gly-Ser, typical for N-glycosylation. We found that a carbohydrate chain with a molecular mass of 1348 Da and a potential $SO_4Man_4GlcNAc_3$ structure is connected to this site. One potential N-glycosylation site (-Asp-Val-Thr-) was observed at the C-terminal position 639 in *Cupiennius salei* subunit 2, which is, however, not conserved in other crustacean hemocyanin subunits. Four potential N-glycosylation sites are present in each of the *H. americanus* pseudohemocyanins [Burmester, 1999]. One N-linkage site was identified at position 166 in the α-type subunits of *P. elephas* subunits 1, 2 and 3 [Meissner et al., 2003], in *P. interruptus* subunits a and b, and at position 470 in β-type subunit c of *P. interruptus*. The presence of several putative *N*-glycosylation sites (-Asn-X(Thr/Ser-)) were observed in the primary structure of all seven subunits of *E. californicus* Hc, but it does not pass through the Golgi apparatus and no carbohydrate moiety was detected in the native tarantula hemocyanin [Voit et al., 2000].

There are several putative sites but the sequence -Thr-Gly-Ser- from the glycopeptide 1 fits position 170-173 of the protein sequence. Thereby the carbohydrate chain 1 with a molecular mass of 404 Da and suggested structure $GalNAc_2$, is connected to this O-linked site. The sequence –Ser-Tyr-Ser- of the second peptide, binding an oligosaccharade, with the suggested structure *N*-Acetyl-*O*-$NeuAc_2Gal_3GalNAc_2$ and a Mw of 1525 Da, fits the position 118-120. The position of the third O-linkage carbohydrate chain with the sequence *N*-Acetyl-*O*-di-$NeuAc_2Gal_2GalNAc_2$ and a molecular mass of 1466 Da could not been identified. The potential linkage site -Ser-Pro-Ser- which was sequenced from the glycopeptide [Dolashka-Angelova et al. 2004] is not present in the sequence of CaeSS2. Maybe it is connected to positions 145-147 (-Thr-Asn-Ser-), 159-161 (-Thr-Gln-Thr-) or 527-529 (-Thr-Val-Thr) which are conserved in the crustacean Hcs.

4.2 Isolation, structure and biological investigations on fungal Cu/Zn superoxide dismutase

4.2.1 Structural and functional analysis of glycosylated Cu/Zn-superoxide dismutase from the fungal strain Humicola lutea 103 (HL-SOD) cultivited under copper stress conditions

Copper is a typical redox metal ion with an important physiological role as a prosthetic group of many enzymes, but it also is able to catalyze the production of cytotoxic ROS. The influence of copper stress on antioxidant defense is studied intensively [Avery et al., 2001]. Filamentous fungi are suitable models to examine the effects of Cu concentrations because of several potential advantages, i.e., high resistance to heavy metals and high levels of antioxidant enzyme activities. The Cu-resistant fungal strain Humicola lutea was found to be a convenient producer of Cu/Zn-SOD. The fungal strain *Humicola lutea* 103 produces a naturally glycosylated Cu/Zn-superoxide dismutase (Cu/Zn-SOD) (HL-SOD). To improve its yield, the effect of increased concentration of Cu^{2+} (from 1 to 750 μg/ml) on growth and enzyme biosynthesis was studied.

4.2.1.1 Response of *Humicola lutea* cells to Cu^{2+} stress

Increasing Cu^{2+} concentrations did hardly affect fungal growth up to 70 μg/ml, the highest concentration compatible with mycelium production in the standard medium **(Figure 74)**. At concentrations between 150 and 350 μg/ml a progressive reduction of biomass (from 20 to 80%) was observed. Growth was completely inhibited by Cu^{2+} concentrations above 750 μg/ml. These results demonstrate a high resistance of the model strain to Cu^{2+} toxicity. Protein synthesis in the cells appeared to be more sensitive to copper treatment than culture growth. In the medium with enhanced Cu^{2+} concentration a gradually decrease in intracellular protein content was determined. Simultaneously with significant biomass reduction, the total protein in the biomass grown in presence of high Cu^{2+} concentrations (above 150 μg/ml) sharply decreased. Moreover, our results show that heavy metal stress caused oxidation of intracellular proteins, as indicated by a dose-dependent increase in carbonyl content **(Figure 74)**.

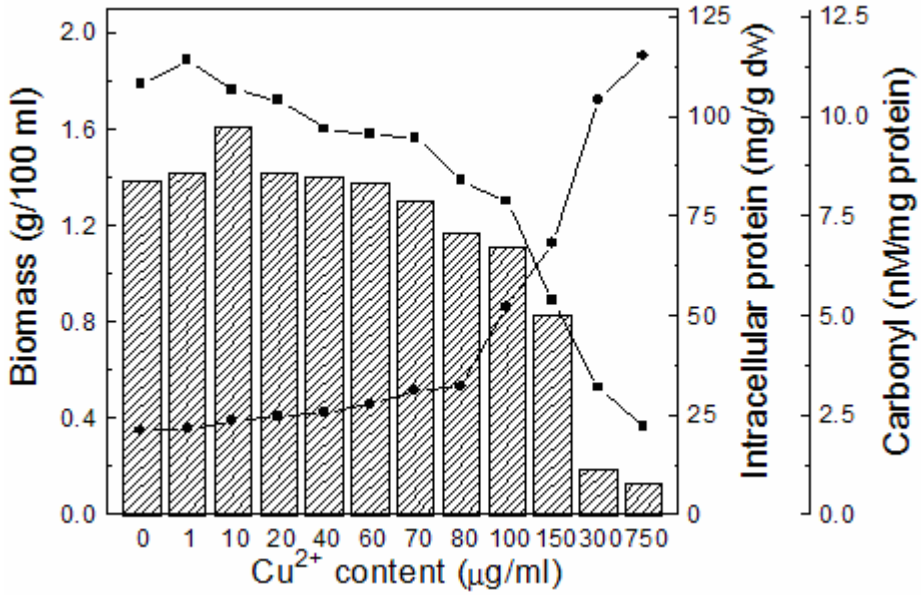

Figure 74. Effect of elevated Cu^{2+} concentrations on biomass production (bars), intracellular protein content (■) and protein carbonyl accumulation (●) in Humicola lutea cultures. *The cultivation was performed on a shaker (220 rpm) at 30°C for 24 h. Then, 6 ml of seed culture were transferred to 500 ml erlenmeyer flasks, containing 74 ml of production medium. The cultures were grown with 0-750 μg/ml Cu^{2+} at 30°C for 72 h (Dolashka-Angelova et al., 2004b).*

The curve of protein carbonyl accumulation shows a mirror image to the growth curve. A similar relationship was reported under conditions of oxidative stress [Bai et al., 2003].

Cultivation of the fungal strain in media with increasing amounts of Cu^{2+} (0 - 750 μg/ml) significantly affected antioxidant defense **(Figure 75)**. Enhanced Cu^{2+} contents drastically induced SOD activity up to 70 μg/ml. Higher metal ion concentrations, between 80 and 150 μg/ml, caused a decreased induction of SOD compared to the maximum activity at 70 μg/ml. However, in the presence of 300 - 750 μg/ml Cu^{2+} the SOD activity decreased markedly. The enhanced SOD amount was accompanied by the induction of catalase, and G6PD. It is worthwhile mentioning that even in the presence of extremely high Cu concentrations (300 - 750 μg/ml) there remains considerable G6PD activity. Probably, G6PD compensates for reduction of SOD in these variants.

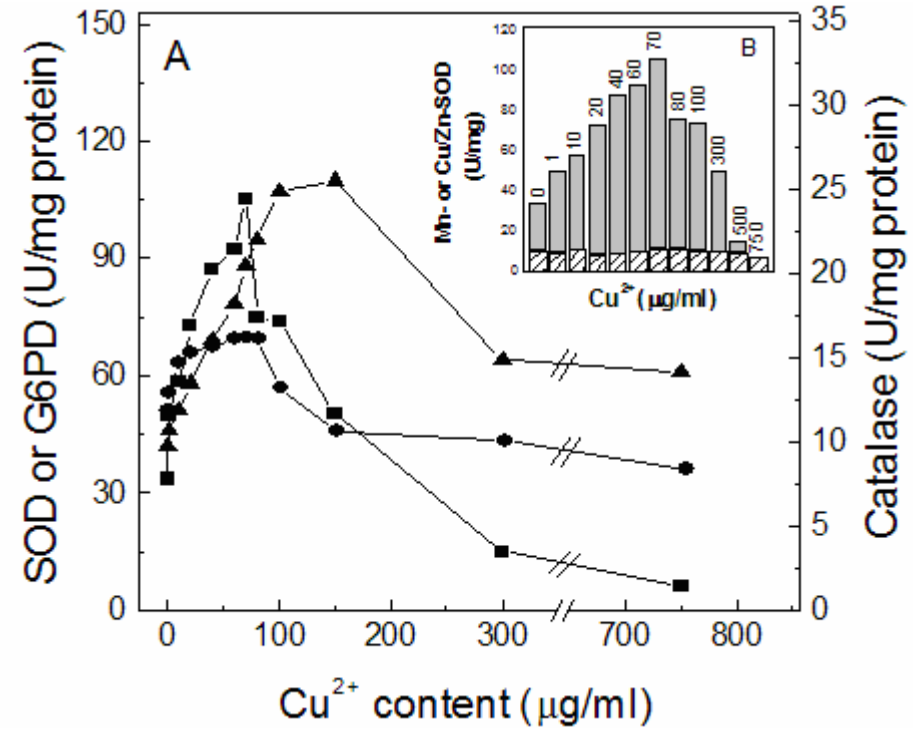

Figure 75. Effect of Cu^{2+} concentrations on the biosynthesis of antioxidant enzymes in Humicola lutea cultures. *The fungal strain was grown as in* **Fig. 74***. **A)** cell-free extracts were assayed for SOD (▲), catalase (●) and G6PD (■) activity. **B)** isoenzyme profile of H. lutea SOD. Cyanide (2 mM) was used to distinguish between the cyanide-sensitive isoenzyme Cu/Zn-SOD (gray bars) and the cyanide-resistant Mn-SOD (hatched bars)* (*Dolashka-Angelova et al., 2004b).*

The fungal strain *H. lutea* 103 produces Mn- and Cu/Zn-containing SOD **(Figure 75)**. There was no significant alteration in Mn-SOD activity, whereas Cu/Zn-SOD increased about 3-fold by an enhanced Cu content up to 70 μg/ml.

Induction of Cu/Zn-SOD by Cu^{2+} supplementation of the fungal cultures was confirmed by PAGE electrophoresis (10% gel) **(Figure 76a)**.

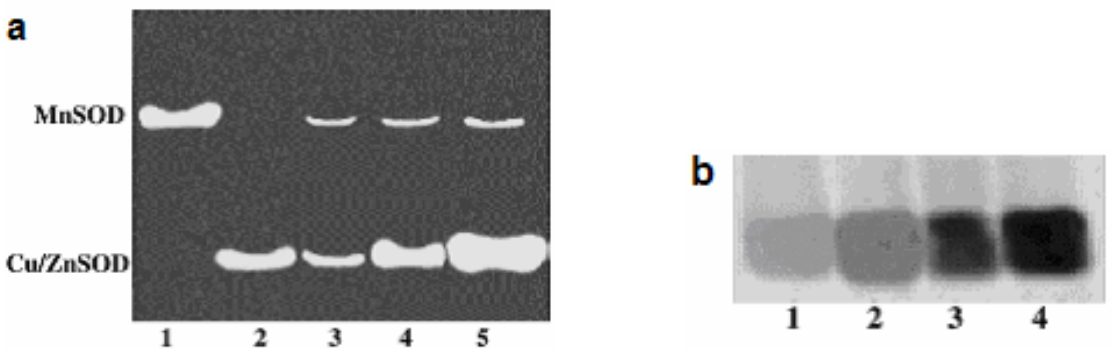

***Figure 76. Cu-induced SOD biosynthesis in H. lutea cells. a)**, **Polyacrylamide gel electrophoresis** (10% gel) of free-cell extracts from fungal culture grown under conditions of Cu^{2+}-stress, stained for enzymatic activity; lane 1, Mn-SOD standard from Escherichia coli; lane 2, Cu/Zn-SOD standard from bovine erythrocyte; lanes 3, 4, and 5, Mn- and Cu/Zn-SOD in the cells cultivated in presence of 20, 70 and 100 μg/ml Cu^{2+}, respectively; **b) Western blot analysis of extracts from identical cultures**. Lane 1, control, cells grown in the productive medium without Cu^{2+}; lanes 2, 3, and 4, cells grown in presence of 20, 70 and 100 μg/ml Cu^{2+}, respectively. The separated proteins were transferred to nintrocellulose membranes and probed with anti-H. lutea polyclonal antibodies.*

In order to relate the Cu^{2+} concentration in the medium to Cu/Zn-SOD production, a Western blot analysis was performed using anti-*H. lutea* Cu/Zn-SOD rabbit antibodies **(Figure 76b)**. The results show that there is an increase in Cu/Zn-SOD production in the presence of Cu^{2+}, confirming the inductive effect of the metal. The results demonstrate that Cu stress accelerates new enzyme synthesis (data not shown).

4.2.1.2 Amino acid sequence determination of HL Cu/Zn-superoxide dismutase

The primary structure of HL-SOD was elucidated by N-terminal sequencing of the intact protein and the determination of the amino acid sequences of a set of overlapping peptides generated by cleavage at different peptide bonds. HPLC-separated protein fragments were used for analysis. **Figure 77a** presents the reverse phase HPLC isolation

profile of the tryptic fractions which were collected and subsequently analyzed by MALDI-MS and amino acid sequencing.

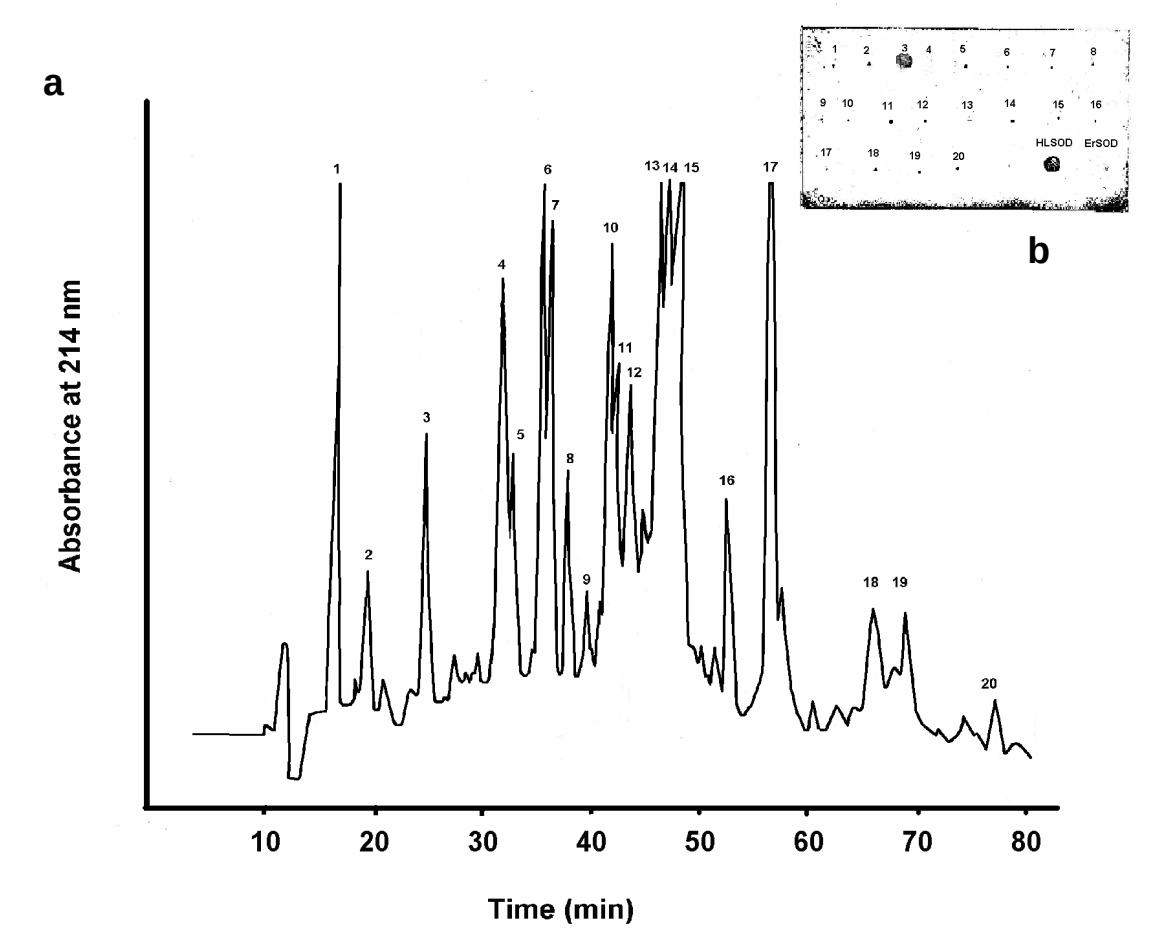

Figure 77. a) HPLC profile on trypsin-digested HL-SOD, applied to a Nucleosyl RP18 (C18, 100 mm length x 2.1 mm diameter) column *and eluted with a linear gradient of solvent A (0.1% TFA in water) and solvent B (0.085% TFA in acetonitrile) in 70 min at a flow rate of 1ml.min^{-1}. Peptide peak fractions were detected at a wavelength of 206 nm;* ***b)*** *Orcinol/H_2SO_4 test of peptides eluted by HPLC and applied on a silica gel plate.*

Experimentally determined peptide masses were in good agreement with the theoretical molecular weights calculated from the sequences. The complete amino acid sequence of HL-SOD, determined by a combination of automated Edman degradation, MALDI-TOF analysis, and sequence alignment, is shown in **Figure 78** in comparison with SODs from other species: *Aspergillus fumigatus* (Q9Y8D9), *Emericella nidulans* (Q9HEY7), *Claviceps purpurea* (Q96VL0), *Neurospora crassa* (P07509), *Colletotrichum gloeosporioides* (094178) and *Saccharomyces cerevisiae* (P00445), *Homo sapiens* (P00441), bovine (P00442) and *Oryctolagus cuniculus* (P09212) Cu/Zn-SODs. Two

programmes, LALIGN and Fasta, were used to analyse the alignment of HL-SOD to fungal SODs and other eukaryotic organisms.

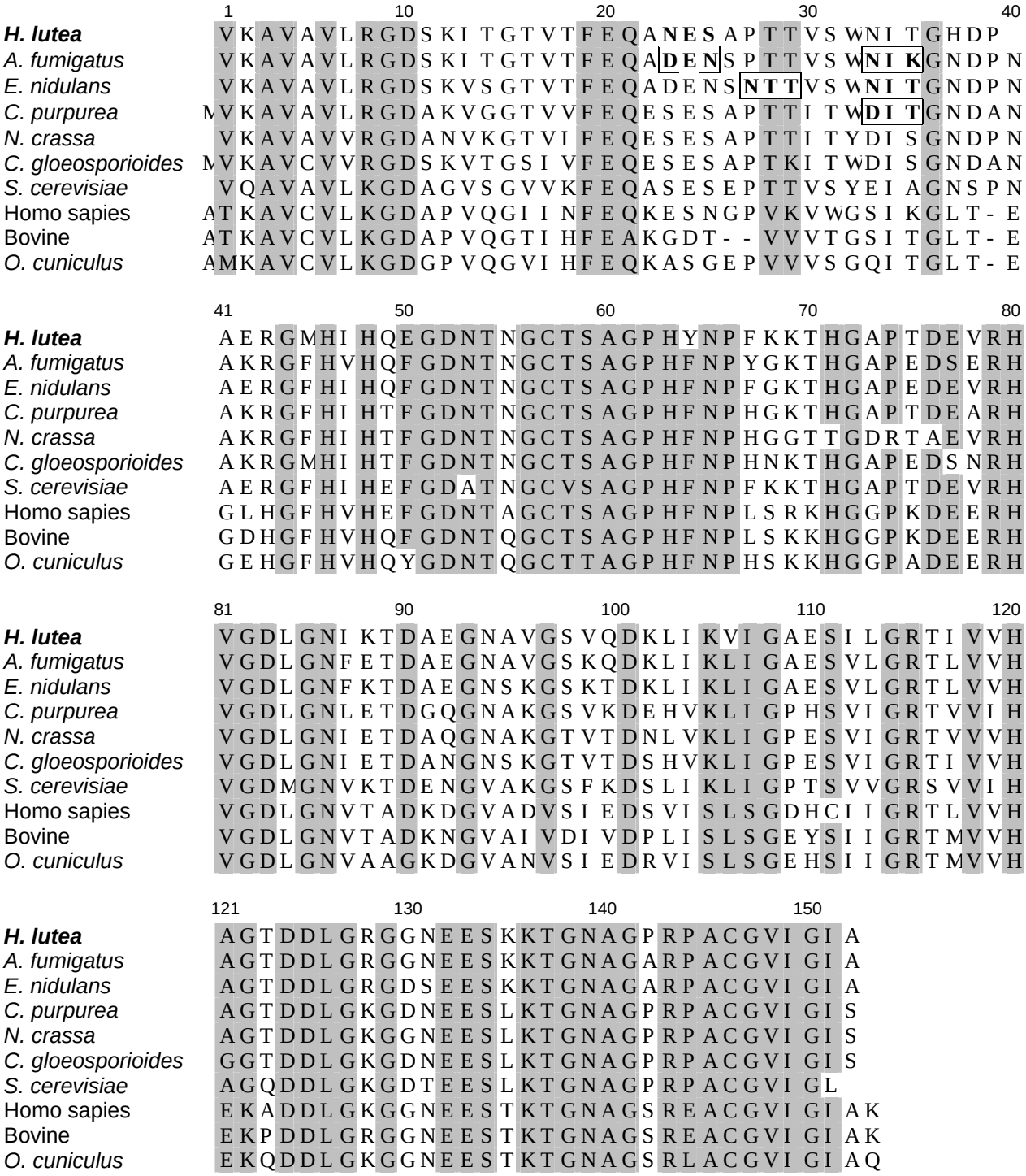

Figure 78. Alignment of the amino acid sequence of HL-SOD (P83684) with SODs from other surces: *Aspergillus fumigatus (Q9Y8D9), Emericella nidulans (Q9HEY7), Claviceps purpurea (Q96VL0), Neurospora crassa (P07509), Colletotrichum gloeosporioides (094178) and Saccharomyces cerevisiae (P00445), Homo sapiens (P00441), bovine (P00442) and Oryctolagus cuniculus (P09212) and Cu/Zn-SODs. The protein sequence data are reported from SWISS-PROT and TrEMBL knowledge base.*

At acidic pH of 0.1% (v/v) TFA, the homodimer SOD dissociated into monomers with 152 amino acid residues and a Mw of 15716 Da. Two Cys residues at positions 56 and 146 were identified by amino acid analysis of HLSOD which may form disulfide bonds and have been reported to be cross-linked in various Cu/Zn-SODs [Bordo et al., 1994]. Our suggestion was proven using DTT as a reducing agent for -S-S- bridges and applying CD spectroscopy. The CD spectrum of native SOD shows a typical negative Cotton effect at 208 nm, caused by mainly β-sheet regions. Using the software of Yang [Yang et al., 1986], 39% β-sheet and only 1.4% α-helix content were calculated **(Figure 79, curve 1).**

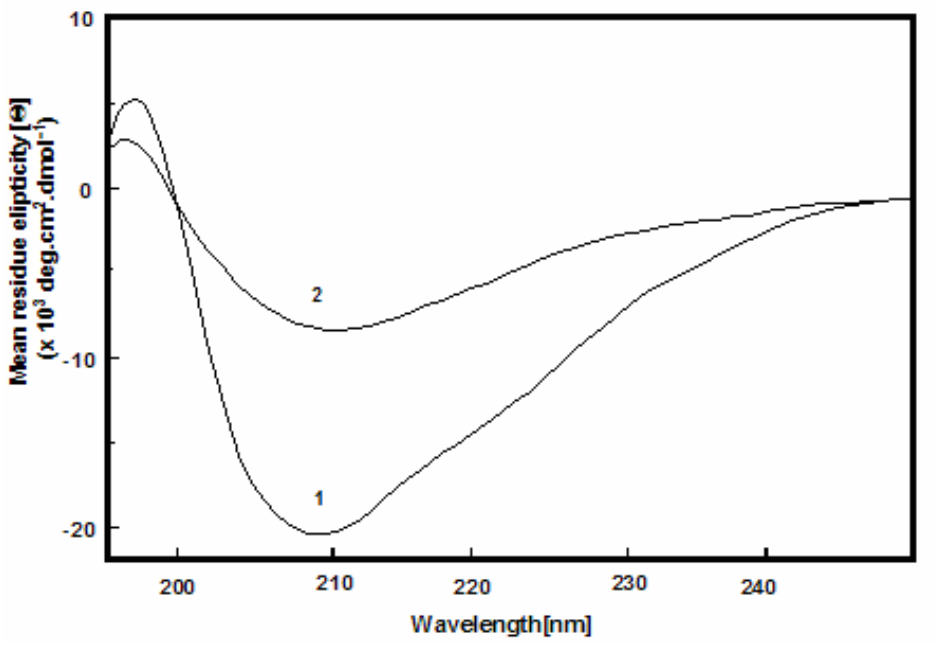

Figure 79. CD spectra of HL-SOD were recorded in the range of 195-250 nm before (1) and after (2) treatment with 30 mM DTT *in 50 mM Tris/HCl buffer, 50 mM NaCl, pH 7.5. HL-SOD samples of 0.20 mg/ml were incubated (in the dark) for 30 min at 25 ℃ and a cuvette of 0.2 cm was used for the measure-ments.*

Loss of the native conformation occurred after disulfide reduction by DTT **(Figure 79, curve 2)** indicating that potential disulfide bridges indeed exist in SOD and contribute to its conformational stability.

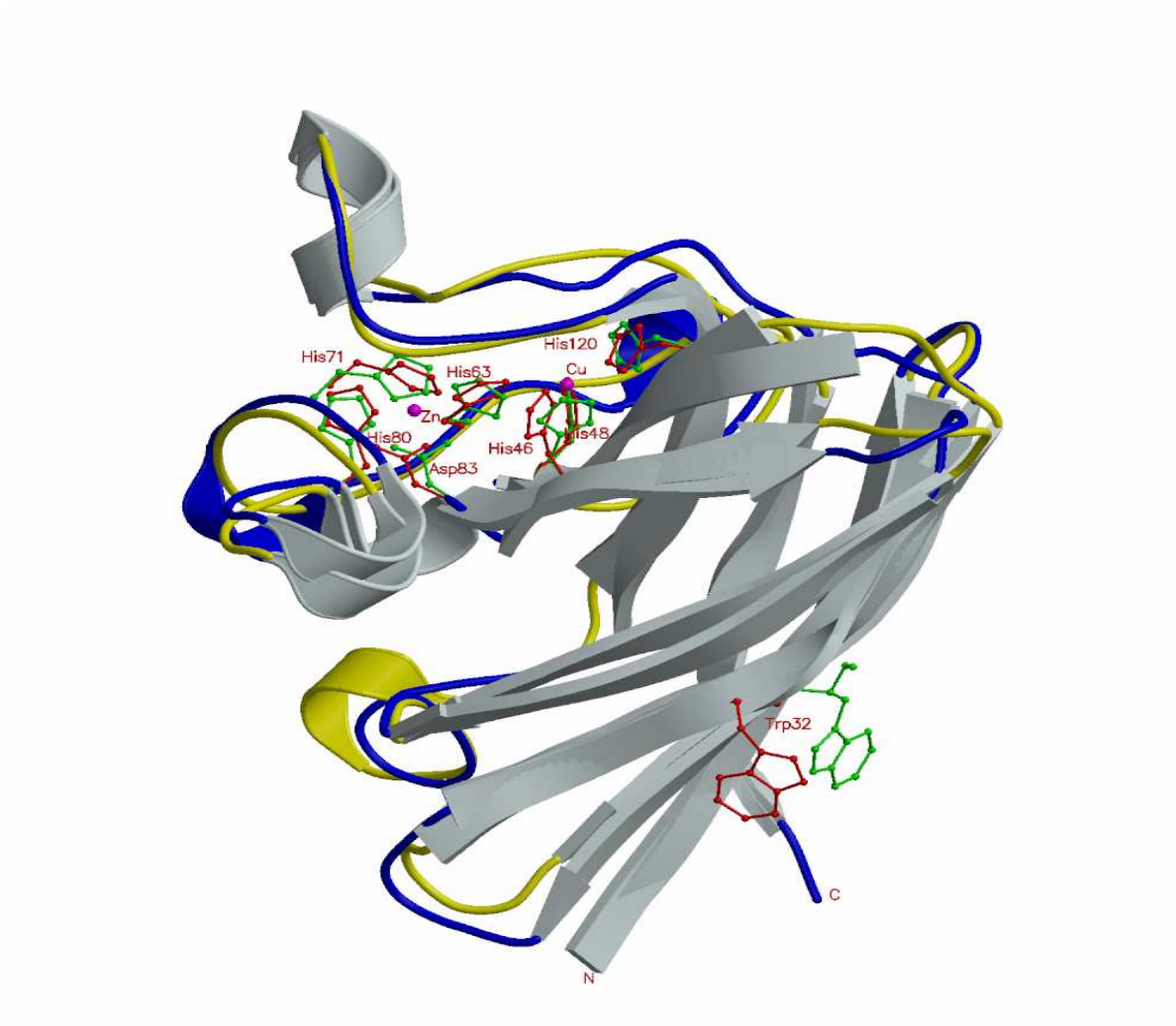

Figure 80. X-ray structural model of HL-SOD. *The modeling was done on a Silicon Graphics O_2 workstation using the SYBYL6.81 (Tripos Inc.) molecular modeling software. The PDB file (ID 1HLS) was read in and all water molecules except the four bound waters at the active site were removed. A close-up of the environment of Trp residues within a sphere of a radius of 6Å surrounding the Trp is shown for human holo SOD in red and HLSOD in green. The figure was drawn using MOLSCRIPT and Raster3D.*

Only one tryptophan residue at position 32 **(Figure 80)** was identified at the same position as in *A. fumigatus*, *E. nidulans*, *C. purpurea* and *C. gloeosporioides* which is substituted in the polypeptide chains of *N. crassa, S. cerevisiae*, Homo sapiens, bovine and *O. cuniculus* by a tyrosine residue.

The native protein of Cu/Zn-SOD was then subjected to MALDI-MS analysis, and the mass spectrum obtained is presented in **Figure 81a.**

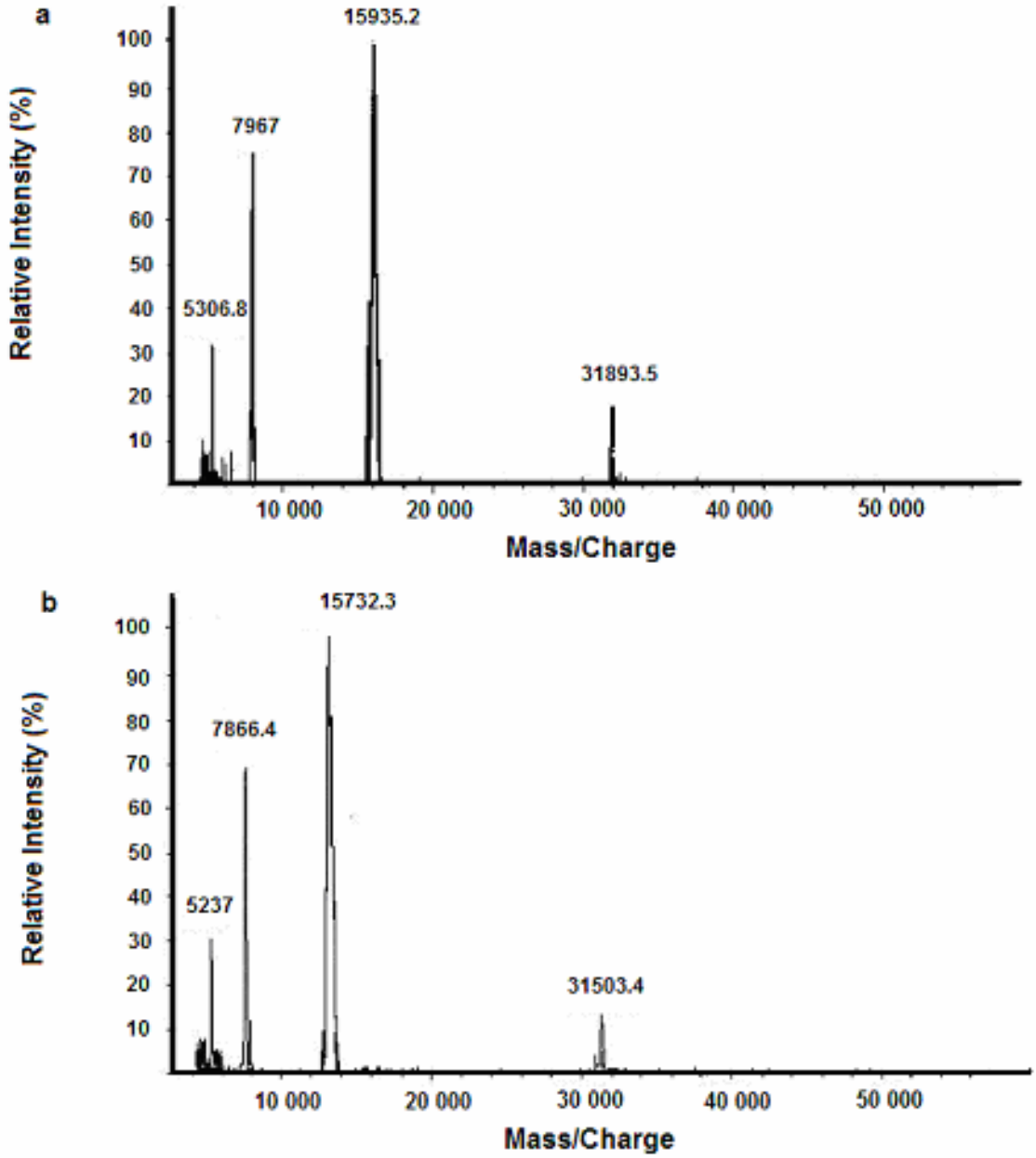

Figure 81. a) Matrix-assisted laser desorption ionization mass spectrum of the subunit of Cu/Zn-SOD. *The sample (10 pmol) was dissolved in 0.1% (v/v) TFA and applied onto the target. Analysis was carried out in α-cyano-4-hydroxycinnamic acid. Solutions of chicken egg ovalbumin (M= 44400 Da) and bovine serum albumin (M= 66430 Da) were used to calibrate the mass scale****; b) MALDI-MS spectrum of subunit of HL-SOD after treatment with PNGase-F.***

The observed highest mass peak at 15935 Da corresponds to monomeric SOD. In addition a low abundant peak at 31893 Da ($M+Na^+$) was detected which is in excellent agreement with the value of 32 kDa, also deduced from 10% PAG electrophoresis. However, the molecular mass as calculated from the complete amino acid sequence of SOD (Fig. 78) is 15716 Da. This leads to a difference of 219 Da (1.4%) between the

determined mass (15935 Da) and the mass calculated from the amino acid sequence, which might be attributed to oxygenated Met44 plus an olygosaccharide side chain (16+203).

4.2.1.3 MALDI-TOF analysis of the glycopeptide of HL-SOD and yeast SOD

The carbohydrate content of HL-SOD was estimated applying the orcinol/H_2SO_4 acid assay [Dolashka-Angelova et al., 2001], HPLC and MALDI-TOF MS analysis. To confirm the glycosylation of the protein, two different SODs**,** HL-SOD and yeast SOD, were subjected to the orcinol/H_2SO_4 method **(Figure 73b)**. For comparison, the arthropodan and molluscan hemocyanins from *Carcinus aestuarii* and *Rapana venosa*, which are known to contain oligosaccharides [Dolashka-Angelova et al., 2001, Dolashka-Angelova et al., 2003] were used. Adding orcinol/H_2SO_4 to the spotted *H. lutea* SOD **(Figure. 73b)** it changed its colour, providing initial information that HL-SOD is glycosylated**,** while the test was negative for yeast SOD. To identify the carbohydrate linkage site, the enzyme was treated with different glycosidases. For cleavage of serine/threonine-linked or asparagine-linked oligosaccharides, fungal SOD was incubated with endo-α-N-acetylgalactosaminidase and PNGase-F, respectively. The glyco- and deglycosylated HL-SODs were then analysed by MALDI-MS. A difference of 203 Da was observed after treatment with PNGase-F, confirming our suggestion that the carbohydrate chain is N-linked, e.g. to Asn23. This value agrees well with the mass of a single N-acetyl-glucosamine moiety. In **Figures 81a and b** two peaks with masses of 15935 and 15740 Da ($M+Na^+$) can be interpreted to represent mono-glycated and free HL-SOD, respectively. To locate and identify the specific glycosylation site of the protein, a tryptic digest was performed. Peak fractions from HPLC chromatography, **(Figure 76a)** were manually collected, vacuum concentrated and an aliquot of each fraction was spotted on a silicagel plate **(Figure 76b)**. Only one fraction gives a positive reaction after treated with orsinol/H_2SO_4. Amino acid analysis demonstrated that the carbohydrate-containing

fragment consists of 7 amino acid residues (-FQA**NES**APT-) with a calculated molecular mass of 945.5 Da and one putative linkage site at Asn23.

4.2.1.4 Protective effect of HL-SOD

The preliminary results from toxicity studies showed that HL-SOD caused neither acute nor chronic toxicity in experimental animals, applied 4 times in doses up to 1000 U/mouse/day. The protective effects of HL-SOD, bovine SOD and ribavirin treatment during the critical period of influenza-induced pneumonitis are presented in **Table12**.

Table 12. Protective effect of HL-SOD, bovine SOD and ribavirin in the murine experimental influenza A/Aichi/2/68 (H3N2) virus infection.

Lung parameters (7^{th} day)							
Treatment group[a]	Dosage (U/mouse/day)	Virus titer (log_{10} $TCID_{50}$/ml)	Weight (mg)	Score[b]	Mortality (%)	Protective index[c] (%)	MST (days)
Virus (control)		5.5	276.0	4.0	74.1		14.5
HL-SOD	500	5.0*	134.0	0.0	10.3	86.1	19.7
Bovine SOD	500	5.0*	237.0	3.0	50.0	32.0	16.6
Ribavarin	6.25 mg/kg/day	2.5	121.0	1.0	10.1	86.3	19.7

[a] Experimental groups were of 10 animals each. The results are the mean of 2-3 experiments.
[b] Scores 0-4, assigned to % visible consolidation.
[c] Protective index =(PR-1)/PRx100, where PR(protective ratio) is $M_{control}$/ $M_{experiment}$ and M is mortality.
[*] The difference between virus control and experiment is not significant

The protective effect was compared with that of the selective antiviral drug ribavirin, which increased the survival rate by 86.3% and the survival time by 5.2 days. Bovine SOD, applied according to the same schedule, conferred lower protection; the protective index was 32.0%, mean survival time was prolonged by 2.1 days. Using HL-SOD the survival rates were increased by 66% (protective index= 86.1%) and survival times were prolonged by 5.2 days. Lung weights as well as lung scores decreased significantly in all experimental groups. Lung scores and lung weights, used as measures for lung pneumonitis lesions, were not reduced dramatically in HL-SOD and ribavirin-treated mice. Bovine SOD reduced these parameters only to a limited extent. Treatment with both kinds of SOD did not affect infectious virus titers in the lung.

5. Conclusions

1. The oligomeric stability of gastropodan hemocyanins *Rapana venosa* (RvH) and *Helix vulgaris* and their structural subunits has been investigated. Two structural subunits RvH1 and RvH2 were separated of *Rapana venosa* Hc on an ion exchange column Hiload 26/10 Sepharose Q using a fast performance liquid chromatography (FPLC). The reassociation of these two RvH isoforms and the native molecule was characterized in buffers with different pH values and concentrations of Ca^{2+} and Mg^{2+} chloride. Mixed RvH subunits reassociate into didecamers and multidecamers over a period of 2 days of dialysis using a stabilizing buffer (SB) of pH 7.0 in the presence of 100 mM $CaCl_2$ and $MgCl_2$.

RvH1 and RvH2 are biochemically and immunologically different and have also different dissociation properties. The reassociation, performed at pH 9.6 with 2 mM $CaCl_2$ and $MgCl_2$ at 4℃ over a period of one to several weeks, led to the formation of decameric oligomers, while didecamers formed predominately in the stabilizing buffer (SB) at pH 7.0. Higher concentrations of calcium and magnesium ions led to a more rapid reassociation of RvH1 resulting in long stable multidecamers and helical tubules which were stable and slowly dissociated into shorter multidecamers and decamers at higher pH values. The reassociation of the RvH2 structural subunit in the same buffers processed slowly and yielded didecamers, shorter tubule polymers and long multidecamers which are less stable at higher pH values. It was found that the reformation of RvH1 and RvH2 subunits is closer to the reformation process of keyhole limpet subunits, than to that of *Haliotis tuberculata* subunits.

2. Using Zn^{2+} ions as new method, several FUs have been isolated from molluscan Hc *Rapana venosa* without formation of non-functional proteolytic side products. N-terminal sequences of these fragments in comparison with FUs from other gastropodan Hcs show a very high degree of structural identity. Only four FUs, purified from enzyme-treated structural subunits RvH1 and RvH2 (RvH1-a, RvH1-f, RvH2-a and RvH2-e) show identical

N-terminal sequences compared to fragments isolated after treatment with Zn^{2+} ions. In some cases trypsin cleaves RvH chains at different positions if compared to the Zn^{2+} treatment.

3. Two isoforms α-hemocyanin and β-hemocyanin of the garden snail *Helix vulgaris* with molecular masses about 400 kDa have been isolated from the hemocyanin which do not reassociate completely in 50 mM $CaCl_2$ and $MgCl_2$ buffer, pH 7.0 and only decamers, didecamers and multidecamers were observed. The subunit appears to be more intact than with the *Rapana venosa* Hc and the reassociation is rather poor.

4. It is generally accepted that the sugar constituents of the hemocyanin are likely to be implicated in their antigenicity. Carbohydrate moieties of molluscan *Rapana venosa* and arthropodan *Carcinus aestuarii* hemocyanins have been determined using several techniques: capillary electrophoresis, MALDI-MS, ESI-MS in combination with glycosidase digestions. Oligosaccharide composition of two FUs from the first structural subunit of *Rapana venosa* Hc, RvH1-a and RvH1-f, have been analysed and two N-linkage sites were identified in the FU RvH1-a, but only one in the FU RvH1-f.

5. The native subunit 2 of *Carcinus aestuarii* is a polypeptide of 650 amino acid residues with a molecular weight determined to be 75036 Da which agrees with the SDS-PAGE results. The subunit is acidic (isoelectric point [pI] = 5.37). The primary structure of CaeSS2 of crab *Carcinus aestuarii* Hc shows a high degree of sequence similarity with the other crustacean hemocyanins, in particular with *P. vulgaris* subunit 1 (52.5%) and *P. interuptus* subunit c (56.0%). Furthermore CaeSS2 and *Cancer magister* subunit 6 seem to be more homologous with each other (73%).

10 Trp and 28 Tyr residues were identified in CaeSS2 and classified into three classes with fluorescence lifetimes around 0.11-0.15, 0.33 and 3.1-3.5 ns, respectively. The static fluorescence parameters agreed fairly well with the data obtained by quenching experiments. Removal of the copper ions from the active site increases the fluorescence intensity.

6. The conformation stability of arthropodan Hc *Limulus polyphemus* has been studied by CD and fluorescence spectroscopy. Five major electrophoretically separable protein chains (structural subunits), indicated as L1–L5, were separated as major components. The conformational stabilities of the native dodecameric aggregates and their isolated structural subunits towards various denaturants (pH and guanidine hydrochloride) indicate that the quaternary structure is stabilized by hydrophilic and polar forces, whereby both, the oxy- and apo-forms of the proteins are considered. The structural subunits (SSs) are less thermostable than the native molecule of *Limulus* Hc with T_m values of 49–55 ℃. Removing of the copper dioxygen system from the active site led to a decrease of the melting temperature, which can be explained by a stabilizing effect of the binding metal ion. Gnd.HCl-induced equilibrium denaturation of Hcs yielded a structural, partially unfolded state and a rapid conformational transition that occurred between 4 and 5 M Gnd.HCl for the native molecules and about 3.5-4 M for their structural subunits.

7. The enzyme was isolated from fungal strain *Humicola lutea* 103 as described [Angelova et al., 2001]. The primary structure of glycosylated Cu/Zn-superoxide dismutase from the fungal strain *Humicola lutea* was determined by Edman degradation. A single chain of the protein, consisting of 152 amino acid residues, reveals a very high degree (74–85%) of structural homology in comparison to the amino acid sequences of other fungal Cu/Zn-SODs. The difference of the molecular masses of *H. lutea* Cu/Zn-SOD, measured by MALDI-MS (15,935 Da) and calculated by its amino acid sequence (15,716 Da), is attributed to the carbohydrate chain of one mole of N-acetylglucosamine, attached to the N-glycosylation site Asn23-Glu-Ser.

HL-SOD protected mice from mortality after experimental influenza A/Aichi/2/68 (H3N2) virus infection. Using the glycosylated HL-SOD, the survival rate is increased by 66% (protective index = 86.1%) and the survival time prolonged by 5 days, similar to the application of ribavarin, while non-glycosylated bovine SOD conferred lower protection.

The results of this thesis are a further contribution to the structure, function and phylogenetic evolution of two clones of copper-containing proteins, the hemocyanins and superoxide dismutases.

6. References

Abbasi, Ali, A., Stoeva, S., Kayed, R., Dolashka-Angelova, P., Schwarz, H. and Voelter, W. (2000) Oxygen transport proteins: III. Structural studies of the scorpion (*Buthus sindicus*) hemocyanin, partial primary structure of its subunit Bsin1. Comp. Biochim. Physiol. Part B 126, 361-376.

Abrashev, R., Genova, V. E., Sotirova, A. V., and Ilieva, K. Z. (1998) Purification and partial characterization of neuraminidase from the non-pathogenic *Arthrobacter nicotianae*. Enzyme Microb. Technol. 22, 142–146.

Adachi, H. and Ishii, N. (2000) Effects of tokotrienols on life span and protein carbonylation in *Caenorhabditis elegans*. J. Gerontol. BioL. Med. Sci. 55, B280-B285.

Altenhein, B., Markl, J., Lieb, B., (2002) Gene structure and hemocyanin isoform HtH2 from the mollusc *Haliotis tuberculata* indicate early and late intron hot spots. Gene 301, 53–60.

Angelova, M., Dolashka-Angelova, P., Ivanova, E., Serkedjieva, J., Slokoska, L., Pashova, S., Toshkova, R., Vassilev, S., Simeonov, I., Hartman, H.-J., Stoeva, S., Weser, U. and Voelter, W. (2001) A novel glycosylated Cu/Zn-containing superoxide dismutase: production and potential therapeutic effect. Microbiology (UK) 147, 1641-1650.

Angelova, M., Genova, L., Pashova, S., Slokoska, L., and Dolashka, P. (1996) Effect of cultural conditions on the synthesis of superoxide dismutase by *Humicola lutea* 110. J. Ferm. Bioeng. 82, 464-468.

Arai, K., Iizuka, S., Tada, Y., Oikawa, K. and Taniguchi, N. (1987) Increase in the glucosylated form of erythrocyte Cu-Zn-superoxide dismutase in diabetes and close association of the nonenzymatic glucosylation with the enzyme activity. Biochim. Biophys. Acta. 924, 292-296.

Averdam, A., Markl, J., and Burmester, T. (2003) Subunit sequences of the 4x6-mer hemocyanin from the golden orb-web spider *Nephila inaurata*: Intramolecular evolution of the chelicerate hemocyanin subunits. Eur. J. Biochem. 270, 3432-3439

Avissar, I., Daniel, E., Daniel, V., (1986) Haemocyanin mRNA from arthropod and mollusc origin. Evidence for a multi-unit structure in mollusc hemocyanin mRNA. Biochem. J. 233, 253–257.

Bai, Z., Harvey, L.M. and McNeil, B. (2003) Physiological responses of chemostat cultures of *Aspergillus niger* (B1-D) to simulated and actual oxidative stress. Biotechnol. Bioeng. 82, 691-701.

Bak, H. J., and Beintema, J. J. (1987) *Panulirus interruptus* hemocyanin. The elucidation of the complete amino acid sequence of subunit a. Eur. J. Biochem. 169, 333–348.

Ballweber, P., Markl, J. and Burmester, T. (2002) Complete hemocyanin subunit sequences of the hunting spider *Cupiennius salei*: recent hemocyanin-remodelling in entelegyne spiders. J. Biol. Chem. 277, 14451-14457.

Beauchamp, C., and Fridovich, I. (1971) Superoxide dismutase: Improved assay and an assay applicable to polyacrylamide gels. Anal Biochem 44, 276-287.

Beavis, R. and Chait, B. (1994) Matrix-assisted laser desorption mass spectrometry of proteins.

Beers, R. F. and Sizer, I. W. (1952) A spectrophotometric method for measuring the breakdown of hydrogen peroxide by catalase. J. Biol. Chem. 195, 133-140.

Beintema, J.J, Stam, W.T, Hazes, B., Smidt, M.P. (1994) Evolution of arthropod hemocyanins and insect storage proteins (hexamerins). Mol. Biol. Evol. 11, 493-503.

Berg, J., Tymoczko, J. and Stryer, L. (2002) Biochemistry Fifth edition.

Bergmann, S., Gebauer, W., Ruth, P., Markl, J., Lieb, B., (2003) The hemocyanin of two living fossils: *Nucula nucleus* and *Nautilus pompilius*. 95th Annual Meeting of the DZG, Berlin, Germany.

Beuerlein, K., Springer, J., Scholz, F.R., Ruth, P., 2003. Cloning of the oxygen carrier hemocyanin from the common cuttlefish, *Sepia officinalis*. acc. # AF401231.

Bergmeyer, H. U. (1983) Glucose-6-phosphate dehydrogenase. In: Methods of Enzymatic Analysis, Third Edition vol III, Ed. D. W. Moss, pp 191-197, Verlag Chemie, Weinheim; Deerfield Beach, Florida; Basel.

Bevelaqua, F.A., Kim, K.S., Kumarasiri, M.H., Schwartz, J.H. (1975) Isolation and characterization of acetylcholinesterase and other particulate proteins in the hemolymph of *Aplysia californica*. J Biol Chem. 250(2):731-8.

Bilodeau, J.F., Blanchette, S., Cormier, N. and Sirard, M.A. (2002) Reactive oxygen species-mediated loss of bovine sperm motility in egg yolk Tris extender: protection by pyruvate, metal chelators and bovine liver or oviductal fluid catalase. Theriogenology 57: 1105-1122.

Boisguerin, V., Lieb, B., Gebauer, W., Markl, J., (2003) The complete cDNA of an opisthobranch gastropod (*Aplysia californica*). 95th Annual Meeting of the DZG, Berlin, Germany.

Boisset, N. and Mouche, F. (2000) Sepia officinalis hemocyanin: A refined 3D structure from field emission gun cryoelectron microscopy, J. Mol. Biol. 296, 459-472.

Bordo, D., Djinovic, K. and Bolognesi, M. (1994) Conserved patterns in the Cu,Zn-superoxide dismutase family. J. Mol. Biol. 238, 366-386.

Boteva, R., Severov, S., Genov, N., Beltramini, M., Filippi, B., Ricchelli, F., Tallandini, L., Pallhuber, M.M., Tognon, G. and Salvato, B. (1991) Biochemical and functional characterization of *Rapana thomasiana* hemocyanin, Comp. Comp. Biochem. Physiol. 100B, 493-501

Boteva, R., Ricchelli, F., Sartor, G. and Decker, H. (1993) Fluorescence properties of hemocyanin from taran- Tistula (*Eurypelma californicum*): a comparison between the whole molecule and isolated subunits. J. Photochem. Photobiol. B, 17, 145-153.

Bubacco, L., Magliozzo, R. S., Beltramini, M., Salvato, B. and Peisach, J. (1992) Preparation and spectroscopic characterisation of a coupled binuclear center in cobalt(II)-substituted hemocyanin. Biochemistry 31, 9294-9303.

Burmester, T. (1999) Identification, molecular cloning and phylogenetic analysis of a non-respiratory pseudo-hemocyanin of *Homarus americanus*. J. Biol. Chem,. 274, 3217–13222.

Burmester, T. (2001) Molecular evolution of the arthropod hemocyanin superfamily. Mol. Biol. Evol. 18, 184-195.

Burmester, T. (2002) Origin and evolution of arthropod hemocyanins and related proteins. J. Comp. Physiol. B 172, 95-117.

Buzy, A., Gagnon, J., Lamy, J., Thibault, P., Forest, E. and Hudry-Clergeon, G. (1995) Complete amino acid sequence of the Aa6 subunit of the scorpion *Androctonus australis* hemocyanin determined by Edman degradation and mass spectrometry. Eur. J. Biochem. 233:93-101.

Cervantes, C. and Gutierrez-Corona, F. (1994) Copper resistance mechanism in bacteria and fungi. FEMS Microbiol. Rev. 14, 121-37.

Clijsters, H., Cuypers, A. and Vangronsveld, J. (1999) Physiological responses to heavy metals in higher plants; defense against oxidative stress. Z. Naturfor. 54C, 730-734.

Creel, H., (1993) Trends in Polym. Sci., 1(11), 336-342.

Cuff, M.E., Miller, K.I., van Holde, K.E., Hendrickson, W.A. J. (1998) Crystal structure of a functional unit from *Octopus hemocyanin*. Mol. Biol. 278, 855-870.

Dainese, E., Di Muro, P., Beltramini, M., Salvato, B., and Decker, E. (1998) Subunits composition and allosteric control in *Carcinus aestuarii* hemocyaninEur. J. Biochem. 256, 350–358.

D'Agnillo, F. and Chang, T. M. (1998) Polyhemoglobin-superoxide dismutase-catalase as a blood substitute with antioxidant properties. Nat Biotechnol. 16, 667-671.

Debeire, P., Montreuil, J., Goyffon, M., van Kuik, A. J., van Halbeek, H., and Vliegenthart, J. F. G. (1986) Primary structure of the oligosaccharide moiety of hemocyanin for the scorpion *Androctonus australis*. Carbohydr. Res. 151, 305–310.

Decker, H., Markl, J., Loewe, R., Linzen, B. (1979) Hemocyanins in spiders, VIII. Oxygen affinity of the individual subunits isolated from *Eurypelma californicum* hemocyanin. Hoppe-Seyler's Z. Physiol. Chem. 360:1505-1507.

Declerq, L., Witters, R. and Preaux, G. (1990) Partial sequence determination of *Sepia officialis* hemocyanin via cDNA. In: Preaux, G., Lontie, R. (eds.) Invertebrate Dioxygen Carriers, Leuven University Press, Leuven, 131-134.

De Haas, F., van Breemen, J.F., Boekema, E.J., Keegstra, W., van Bruggen, E.F.J., (1993) Comparative electron microscopy and image analysis of oxy- and deoxy-hemocyanin from the spiny lobster *Panulirus interruptus*. Ultramicroscopy 49, 426–435.

Dimitrova, P., Toshkova, R., Ivanova, E., Stefanova, Z., Angelova, M., Dolashka, P. and Voelter ,W. (2000) Superoxide production by phagocytes in myeloid Graffi tumor-bearing hamsters. Z. Naturforsch. 55c, 788-805.

Dolashka, P. (2003) Evolution and diversity of the arthropod hemocyanin superfamily. XIII International Conference on Invertebrate Dioxygen Binding Proteins. Mainz 2003.

Dolashka-Angelova, P., Beck, A., Dolashki, A., Beltramini, M., Stevanovic, S., Salvato, B. and Voelter, W. (2003a) Characterization of the carbohydrate moieties of the functional unit RvH_1-a of *Rapana venosa* haemocyanin using HPLC/electrospray ionization MS and glycosidase digestion. Biochem. J. 374, 185-192.

Dolashka-Angelova, P., Beck, A., Dolashki, A., Beltramini, M., Stevanovic, S., Salvato, B., Hristova, R., Velkova, L., Voelter, W. (2004a) Carbohydrate moieties of molluscan *Rapana venosa* hemocyanin. Micron 35 101–104.

Dolashka-Angelova, P., Beltramini, M., Dolashki, A., Salvato, B., Hristova, R., Voelter, W. (2001) Carbohydrate composition of *Carcinus aestuarii* hemocyanin. Arch. Bioch. Biophys. 389, 153-158

Dolashka-Angelova, P., Dolashki, A., Stevanovic, S., Hristova, R., Atanasov, B., Nikolov, P. and Voelter, W. (2005a) Structure and stability of arthropodan hemocyanin *Limulus polyphemus*. Spectrochim. Acta Part A

Dolashka-Angelova, P., Dolashki, A., Savvides, S., Hristova, R., Van Beeumen, J., Voelter, W., Devreese, B., Weser, U., Di Muro, P., Salvato, B. and Stevanovic, S. (2005b) Structure of hemocyanin subunit CaeSS2 of the crustacean mediterranean crab *Carcinus aestuarii*. In print

Dolashka, P., Genov, N., Parvanova, K., Voelter, W., Geiger, M. and Stoeva, S. (1996) *Rapana thomasiana* grosse (gastropoda) haemocyanin: spectroscopic studies of the structure in solution and the conformational stability of the native protein and its structural subunits. Biochem. J. 315, 139-144.

Dolashka-Angelova, P., Hristova, R., Schuetz, J., Stoeva, S., Schwarz, H., and Voelter, W. (2000a) Structural and spectroscopic studies of the native hemocyanin from *Maia squinado* and its structural subunits. Spectrochim. Acta A Mol. Biomol Spectrosc. 56A, 1985-1999.

Dolashka-Angelova, P., Hristova, R., Stoeva, S., and Voelter, W. (1999a) Spectroscopic properties of *Carcinus aestuarii* hemocyanin and its structural subunits. Spectrochim. Acta Part A55, 2927-2934.

Dolashka, P., Genov, N., Parvanova, K., Voelter, W., Geiger, M., Stoeva, S. (1996) *Rapana thomasiana* grosse (gastropoda) haemocyanin: spectroscopic studies of the structure in solution and the conformational stability of the native protein and its structural subunits. Biochem. J. 315, 139-144

Dolashka-Angelova, P., Schick, M., Stoeva, S., Voelter, W. (2000b) Isolation and partial characterization of the N-terminal functional unit of subunit RtH1 from *Rapana thomasiana* grosse hemocyanin Int. J. Biochem. Cell Biology 32, 529-538

Dolashka-Angelova, P., Schwarz, H., Dolashki, A., Beltramini, M., Salvato, B., Schick, M., Saeed, M. and Voelter, W. (2003b) Oligomeric stability of *Rapana venosa* hemocyanin (RvH) and its structural subunits. Biochim. Biophys. Acta 1646 (1-2) 77-85.

Dolashka-Angelova, P., Stevanovic, S., Dolashki, A., Angelova, M., Serkedjieva, J., Krumova, E., Pashova, S., Zacharieva, S., and Voelter, W. (2004b) Structural and functional analysis of glycosylated Cu/Zn-superoxide dismutase from the fungal strain *Humicola lutea* 103. Biochem. Biophys. Res. Commun. 317 1006–1016.

Dolashka-Angelova, P., Stoeva, S., Hristova, R., Schuetz, J., Beltramini, M., Salvato, B. H. Schwartz and Voelter, W. (1999b) Structural organization of hemocyanin from lobster *Homarus americanus* and spectroscopic studies of the native protein and structural subunits. Curent Topics in Peptide & Prot. Res. 3, 19-36.

Dickerson, R.E. and Geis, I. (1983) Hemoglobin: Structure, Function, Evolution and Pathology. Benjamin Cummings Publishing Co. Inc. Menlo Park, CA, USA.

Di Muro, P., Beltramini, M., Nikolov, P., Petkova, I., Salvato, B. and Ricchelli, F. (2002) Fluorescence spectroscopy of the tryptophan microenvironment in *Carsinus aestuarii* Hemocyanin. Z. Naturforsch. 57c, 1084-1091.

Drexel, R., Siegmund, S., Schneider, H.J., Linzen, B., Gielens, C., Preaux, G., Lontie, R., Kellermann, J., Lottspeich, F. (1987) Complete aminoacid sequence of a functional unit from a molluscan hemocyanin (*Helix pomatia*). Biol. Chem. Hoppe Seyler 368, 617–635.

Durstewitz, G. and Terwilliger, N.B. (1997) cDNA cloning of a developmentally regulated hemocyanin subunit in the crustacean *Cancer magister* and phylogenetic analysis of the hemocyanin gene family. Mol. Biol. Evol., 14**,** 266-276

Edlund, A., Edlundm, T., Hjalmarssonm, K., Marklundn, S. L., Sandstrom, J., Stromqvist, M. and Tibell, L. (1992) A non-glycosylated extracellular superoxide dismutase variant. Biochem. J. 288, 451-456.

Ellerton, H. D., Ellerton, N. F. and Robinson, H. A. (1983) Hemocyanin - a current perspective. Prog. Biophys. Mol. Biol 41, 143–248.

Eriksson-Quensel, I.B., Svedberg, T. (1936) The molecular weights and pH-stability regions of the hemocyanins, Biol. Bull. 71, 498-547.

Favilla, R., Goldoni, M., Del Signore, F., Di Muro, P., Salvato, B., Beltramini, M. (2002) Guanidinium chloride induced unfolding of a hemocyanin subunit from *Carcinus aestuarii* II. Holo form. Biochim. Biophys. Acta, 1597, 51– 59.

Fink, R.C., and Scandalios, J.G. (2002) Molecular evolution and structure--function relationships of the superoxide dismutase gene families in angiosperms and their relationship to other eukaryotic and prokaryotic superoxide dismutases. Arch. Biochem. Biophys. 399, 19-36.

Francois, C., Marshall, R.D. and Neuberger, A. (1962) Carbohydrates in protein. Biochem. J. 83, 335-341

Fredericq, L. (1878) Sur l'hemocyanine, substance nouvelle du sang de Poulpe (*Octopus vulgaris*), Compt. Rend. Acad. Sci. 87, 996-998

Fridovich, I. (1983) Superoxide radical: An endogenous toxicant. Ann. Rev. Pharmacol. Toxicol. 23, 239-257.

Fridovich, I. (1995) Superoxide radical and superoxide dismutases. Annu. Rev. Biochem. 64, 97-112.

Fujita, T., Furitsu, H., Nishikawa, M., Takakura, Y., Sezaki, H., and Hashida, M. (1992) Therapeutic effects of superoxide dismutase derivatives modified with mono- or polysaccharides on hepatic injury induced by ischemia/reperfusion. Biophys Res Commun 189, 191-196.

Gaykema, W.P.J., Hol, W.G.J., Vereifken, J.M., Soeter, N.M., Bak, H.J. and Beintema, J.J. (1984) 3.2 Å structure of the copper-containing, oxygen-carrying protein *Panulirus interruptus* hemocyanin. Nature 309, 23-29.

Gaykema, W.P., Volbeda, A., Hol, W.G., 1986. Structure determination of *Panulirus interruptus* hemocyanin at 3.2 A ºesolution. Successful phase extension by sixfold density averaging. J. Mol. Biol. 187, 255–275.

Gebauer, W., Harris, J.R., Söhngen, S.M. and Markl, J. (1999) Keyhole limpet hemocyanin type 2 (KLH2): Detection and immunolocalization of a labile functional unit h, J. Struct. Biol. 128, 280-286.

Gebauer, W., Harris, J.R., Heid, H., Söling, M., Hillenbrand, R., Söhngen, S., Wegener-Strake, A. and Markl, J. (1994) Quarternary structure, subunits and domain patterns of two discrete forms of keyhole limpet hemocyanin: KLH1 and KLH2, Zoology Jena 98 51-68.

Gebauer, W., Stoeva, S., Voelter, W., Dainese, E., Salvato, B., Beltramini, M. and Markl, J. (1999). Hemocyanin subunit organization of the gastropod *Rapana thomasiana*. Arch. Biochem. Biophys. 372, 128–134.

Gielens, C., De Geest, N., Xin, X.-Q., Devreese, B., van Beeumen, J. and Préaux, G. (1997) Evidence for a cysteine-histidine thioether bridge in functional units of molluscan haemocyanins and location of the disulfide bridges in functional units d and g of the betaC-haemocyanin of *Helix pomatia*. Eur. J. Biochem. 248, 879-888

Guzman-Casado, M., Parody-Morreale, A., Mateo, P.L. and Sanchez-Ruiz, J.M. (1990) Differential scanning calorimetry of lobster haemocyanin. Eur. J. Biochem. 188, 181-185.

Hall, R.L., Kamerling, J.P., Gerwig, G.J. and Vliegenthart, J.F.G., (1977) 3-O-methyl sugars as constituents of glycoproteins. Identification of 3-O-methyl galactose and 3-O-methyl mannose in pulmonate gastropod hemocyanins. Biochem. J. 165, 173-176

Harris, J.R., Gebauer, W., Söhngen, S.M., Nermut, M.V. and Markl, J. (1997) Keyhole limpet hemocyanin (KLH), II: Characteristic reassociation properties of purified KLH1 and KLH2, Micron 28, 43-56.

Harris, J. R., Gebauer, W., Guderian, U F. and Markl, J. (1997) Keyhole limpet hemocyanin (KLH): Reassociation from Immucothel followed by separation of KLH1 and KLH2, Micron 28, 31-41.

Harris, J.R., Gebauer, W., Söhngen, S.M. and Markl, J. (1995) Keyhole limpet hemocyanin (KLH): Purification of intact KLH1 through selective dissociation of KLH2, Micron 26, 201-212.

Harris, J.R., Gebauer, W. and Markl, J. (1993) Immunoelectron microscopy of hemocyanin from the keyhole limpet (*Megathura crenulata*): a parallel subunit model, J. Struc. Biol. 111, 96-104.

Harris, J.R., Gebauer, W. and Markl, J. (1995) Keyhole limpet hemocyanin: Negative staining in the presence of trehalose, Micron 26, 25-33.

Harris, J.R., Gebauer, W., Adrian, M. and Markl, J. (1998) Keyhole limpet hemocyanin (KLH): Slow in vitro reassociation of KLH1 and KLH2 from Immucothel, Micron 29, 329-339.

Harris, J.R. and Markl, J. (1999) Keyhole limpet hemocyanin (KLH): a biomedical review, Micron 30, 597-623.

Harris, J.R. and Markl, J. (2000) Keyhole limpet hemocyanin: molecular structure of a potent marine immunoactivator. A review. Eur. Urol. 37, 3, 24-33

Harris, J.R., Meissner, U., Gebauer, W., Markl, J., 2003. 3D reconstruction of the hemocyanin subunit dimer from the chiton *Acanthochiton fascicularis*. Micron. doi:10.1016/j.micron.2003.10.008.

Harris, J.R., Scheffler, D., Gebauer, W., Lehnert, R. and Markl, J. (2000) *Haliotis tuberculata* hemocyanin (HtH): analysis of oligomeric stability of HtH1 and HtH2, and comparison with keyhole limpet hemocyanin KLH1 and KLH2, Micron 31, 613-622.

Hart, P. J., Belbirnie, M. M., Ogihara, N. L., Nersissian, A. M., Weiss, M. S., Valentine, J. S. and Eisenberg, D. (1999) A structure-base mechanism for copper-zinc superoxide dismutase. Biochemistry 38, 2167-2178.

Harvey, J.D. (1998) Identification of cleaved oligosaccharides by matrix-assisted laser desorption/ionozation. Methods in Mol. Biol. 61 (Chapman J.R., Humana Press Inc., Totowa, NJ)

Harvey, J.D. (1996) Matrix-assisted laser desorption/ionisation mass spectrometry of oligosaccharides and glycoconjugates, J. Chromatog. A 720, 429-446

Hazes, B., Magnus, K.A., Bonaventura, C., Bonaventura, J., Dauter, Z., Kalk, K.H. and Hol, W.G.J. (1993) Crystal structure of deoxygenated *Limulus polyphemus* subunit II hemocyanin at 2.18 A resolution: clues for a mechanism for allosteric regulation. Prot. Science 2, 597-619.

Herskovits, T.T. (1988) Recent aspects of the subunit organization and dissociation of hemocyanins. Comp. Biochem. Physiol. 91 B, 597-611

Herskovits, T.T. and Russell, M.W. (1984) Light-scattering investigation of the subunit structure and dissociation of *Helix pomatia* hemocyanin. Effects of salts and ureas, Biochemistry 23, 2812-2819.

Herskovits, T.T. and Hamilton, M.G. (1991) Higher order assemblies of molluscan hemocyanins. Comp. Biochem. Physiol. 99B, 19 34.

Hillenkamp, F., Karas, M., Beavis, R. and Chait, B., (1991) Anal. Chem. 63, 1193A.

Hodgson, E. and Spicer, J. I. (2001) Subunit compositions of crustacean haemocyanins are species-specific: Evidence from non-decapod speciesComp. Biochem. Physiol. Part A 128, 873-888.

Holmes, M., Trong, I., Turley, S., Sieker, L. and Stenkamp, R. (1991) Structures of deoxy and oxy hemerythrin at 2.0 Å resolution. J. Mol. Biol. 218:583-593.

Hong, Z., Lo Verde, P. T., Thakur, A., Hammarskjold, M. L. and Rekosh, D. (1993) Schistosoma mansoni: a Cu/Zn superoxide dismutase is glycosylated when expressed in mammalian cells and localizes to a subtegumental region in adult schistosomes. Exp. Parasitol. 76, 101-114.

Hough, M. A., Strange, R. W. and Hasnain, S. S. (2000) Conformational variability of the Cu site in one subunit of bovine Cu/Zn superoxide dismutase: the importance of mobility in the Glu119-Leu142 loop region for catalytic function. J. Mol. Biol. 304, 231-241.

Hsi. K.-L., Chen L., Hawke, D.H., Zieske, L.R. and Yuan, P.-M. (1991) A general approach for characterizing glycosylation sites of glycoproteins.Anal. Biochem. 198, 238-245.

Hristova, R., Dolashka, P., Stoeva, S., Voelter, W., Salvato, B. and. Genov, N. (1997) Spectroscopic properties and stability of hemocyanins. Spectrochim. Acta Part A 53, 471-478.

Hristova, R., Dolashka-Angelova, P., Gigova, M. and Voelter, W. (2000) Fluorescence properties of the arthropodan hemocyanin *Carcinus aestuarii*. Oxidation Commun., 23, 1, 145-152.

Hübler, R., Fertl, B., Hellmann, N. and Decker, H. (1998) On the stability of the hemocyanin from the tarantula *Eurypelma californicum*. Biochim. Biophys. Acta 1383, 327-339.

Jaenicke, E., Decker, H. (2003) The physico-chemical properties of the hexameric phenoloxidase may explain their role in the innate immunity of crustaceans. Protein Sci. 12 Supp. 1:93

Jaenicke, E., Decker, H. (2003) Tyrosinases from crustacean form hexamers. Biochem. J. 371:515-523

Jekel, P. A., Neuteboom, B., and Beintema, J. J. (1996) Primary structure of haemocyanin from *Palinurus vulgaris*. Comp. Biochem. Physiol. B 115, 243–246.

Jekel, P.A., Bak, H.J., Soeter, N.M., Verejken, J.M. & Beintema, J.J. (1988) *Panulirus interruptus* hemocyanin: the amino acid sequence of subunit b and anomalous behaviour of subunits a and b on polyacrylamide gel electrophoresis in the presence of SDS. Eur. J. Biochem. 178, 403-412.

Idakieva, K., Schwarz, H., Genov, N., Voelter, W. and Stoeva, S. (2002) *Rapana thomasiana* hemocyanin (RtH): dissociation and reassociation behaviour of two isoforms, RtH1 and RtH2, Micron 33, 7-14.

Idakieva, K., Stoeva, S., Pervanova, K., Genov, N., Voelter, W. (2000) Arrangement of functional units within the *Rapana thomasiana* hemocyanin subunit RtH2. Biochim. Biophys. Acta 1479, 175–184.

Ivanova, E., Angelova, M., Slokoska, L., Pashova, S., Toshkova, R., Dolashka-Angelova, P., Dimitrova, P. (2002) Effect of Cu/Zn-superoxide dismutase from the fungal strain *Humicola lutea* 103 on antioxidant defense of graffi tumor-bearing hamsters Z. Naturforsch. 57c,197-204.

Kakimoto, K., Kojima, Y., Ishii, K., Onone, K. & Maeda, H. (1993) The suppressive effect of gelatin-conjugated superoxide dismutase on disease development and severity of collagen induced arthritis in mice. Clin Exp Immunol 94, 241-246.

Karas, M. and Hillenkamp, F. (1988), Anal. Chem. 60, 2299.

Kehrer, J. P. (1993) Free radicals as mediators of tissue injury and disease. Crit Rev Toxicol 23: 21-48,.

Keller, H., Lieb, B., Altenhein, B., Gebauer, D., Richter, S., Stricker, S. and Markl, J. (1999) Abalone (*Haliotis tuberculata*) hemocyanin type 1 (HtH1): Organization of the ~ 400 kDa subunit, and amino acid sequence of its functional units f, g and h, Eur. J. Biochem. 264, 27-38.

Krantz, S., Lober, M. and Henschel, L. (1986) The nonenzymatic glycation of proteins and nucleic acids, their importance for the development of diabetic complications,

possible molecular basis of aging and autoimmunological processes. Exp. Clin. Endocrinol. 88, 257-269.

Krieg, J., Gläsner, W., Vicentini, A., Doucey, M. A., Löffler, A., Hess, D. and Hofsteenge, J. (1997) C-Mannosylation of human RNase 2 is an intracellular process performed by a variety of cultured cells. J. Biol. Chem. 272, 26687-26692.

Kubowitz, F. (1938) Spalting und Resynthese der Polyphenoloxydase und des Hämocyanins, Biochem. Z.299, 32-57

Kurtz, D.M Jr. (1999) Oxygen-carrying proteins: three solutions to a common problem Essays Biochem.,34:85-100

Kusche, K. and Burmester, T. (2001) Diplopod hemocyanin sequence and the phylogenetic position of the Myriapoda. Mol. Biol. Evol. 18, 1566-1573.

Kusche, K. and Burmester, T. (2001) Molecular cloning and evolution of lobster hemocyanins. Biochem. Biophys. Biochem. Biophys. Res. Commun. 282, 887-892.

Kusche, K., Hembach, A., Hagner-Holler, S., Gebauer, W. and Burmester, T. (2003) Complete subunit sequences, structure and evolution of the 6x6-mer hemocyanin from the common house centipede, *Scutigera coleoptrata*. Eur. J. Biochem. Volume 270 Issue 13 Page 2860

Kusche, K., Hembach, A., Milke, C., and Burmester, T. (2003) Molecular characterisation and evolution of the hemocyanin from the European spiny lobster, *Palinurus elephas*. J. Comp. Physiol. B. 173, 319–325

Laemmli, U.K. (1970) Cleavage of structural proteins during the assembly of the head of bacteriophage T_4. Nature 227, 680-685.

Lang, W.H. (1988) cDNA cloning of the Octopus dofleini hemocyanin: sequence of the carboxyl terminal domain, Biochemistry 27, 7276-7282.

Lang, W.H., van Hold, K.E. (1991) Cloning and sequencing of *Octopus dofleini* hemocyanin cDNA: derived sequences of functional units Ode and Odf. Proc. Natl. Acad. Sci. USA 88, 244-248

Lange, J., Elias, H., Paulus, H., Muller, J., Weser, U. (2000) Copper(II) and copper(I) complexes with an open-chain N4 Schiff base ligand modeling CuZn superoxide dismutase: structural and spectroscopic characterization and kinetics of electron transfer. Inorg. Chem. 39, 3342-3349.

Lamy, J., You, V., Taveau, J.-C., Boisset, N. and Lamy, J.N. (1998) Intramolecular localization of the functional units of *Sepia officinalis* hemocyanin by immunoelectron microscopy. J. Mol. Biol. 284, 1051-1074.

Lehrer, S. S. (1971) Solute perturbation of protein fluorescence. The quenching of the tryptophan fluorescence of model compounds and of lysozyme by iodide ion. Biochemistry, 10, 3254-3263.

Lieb, B., Altenhein, B., Markl, J., Vincent, A., van Olden, E., van Holde, K.E., Miller, K.I. (2001a) Structures of two molluscan hemocyanin genes: Significance for gene evolution. Proc. Natl Acad. Sci. USA 98, 4546–4551.

Lieb, B., Altenhein, B., Markl, J., (2000) The Sequence of a gastropod hemocyanin (HtH1 from *Haliotis tuberculata*). J. Biol. Chem. 275, 5675–5681.

Lieb, B., Boisguerin, V., Gebauer, W., Markl, J. (2004) cDNA sequence, protein structure, and evolution of the single hemocyanin from *Aplysia californica*, an opisthobranch gastropod. Mol Evol.;59(4):536-45

Lieb, B., Schmidt, M., Berg, S., Bergmann, S., Freibert, S., Markl, J., (2001b) Molluscan hemocyanin as a phylogenetic character. Zoology (Supplement IV). Proceedings of the 94th Annual Meeting Osnabru¨ck, Germany.

Ling, J.S., Nestor, L.P., Czernuszewicz, R.S., Spiro, T.G., Fraczkiewicz, R., Sharma, K.D., Loehr, T.M. and Sanders-Loehr, J. (1994) Common oxygen binding site in hemocyanins from arthropods and molluscs. Evidence from Raman spectroscopy and normal coordinate analysis. J. Am. Chem. Soc. 116, 7682–7691.

Liochev, S.I. and Fridovich, I. (1992) Effects of overproduction of superoxide dismutases in *Escherichia coli* on inhibition of growth and on induction of glucose-6-phosphate dehydrogenase by paraquat. Arch. Biochem. Biophys. 294, 138-143.

Lommerse, J.P.M., Thomas-Oates, J.E., Gielens, C., Preaux, G., Kamerling, J.P. and Vliegenthart, J.F.G. (1997) Primary structure of 21 novel monoantennary and diantennary N-linked carbohydrate chains from alpha D-hemocyanin of *Helix pomatia*. Eur. J. Biochem. 249, 195-222

Lowry, O. H., Rosenbrough, H. J., Faar, A. L. and Randall, R. J. (1951) Protein measurement with the Folin phenol reagent. J Biol Chem 193, 265-275.

Makino, N. (1985) An oxygenation-linked dye binding to *Limulus polyphemus* hemocyanin. Eur. J. Biochem. 146, 563-569.

Magnus, K.A., Ton-That, H. and Carpenter, J.E. (1994) Recent Structural Work on the Oxygen Transport Protein Hemocyanin. Chem. Rev. 94, 727-735.

Magnus, K.A., Hazes, B., Ton-That, H., Bonaventura, C., Bonaventura, J. and Hol, W.G.J. (1994) Crystallographic Analysis of Oxygenated R Deoxygenated States of Arthropod Hemocyanin Shows Unusual Differences. Proteins: Structure, Function, and Genetics 19, 302-309.

Makino N. and Kimura S. (1988) Subunits of *Panulirus japonicus* hemocyanin 1. Isolation and properties. Eur J Biochem., 173(2):423-30.

Maksimenko, A. V., Petrov, A. D., Caliceti, P., Konovalova, G. G., Schiavon, O., Grigoreva, E. L., Lankin, V. Z. and Veronese, F. M. (1993) The modification of Cu, Zn-superoxide dismutase by monomethoxypolyethylene glycol improves the indices of the experimental therapy of the ischemic myocardium in rats. Eksp. Klin. Farmakol. (In Russian) 56, 14-18.

Markl, J. (1986) Evolution and function of structurally diverse subunits in the respiratory protein hemocyanin from arthropods, Biol. Bull. 171, 90– 115

Markl, J., Decker, H., (1992) Molecular structure of the arthropod hemocyanins. In C.P. Mangum (Ed.), Advances in Comparative and Environmental Physiology (pp. 325–376). Berlin: Springer Verlag.

Markl, J., Decker, H., Savel, A., Linzen, B. (1981) Homogeneity, subunit heterogeneity, and quaternary structure of *Eurypelma* hemocyanin. In "Invertebrate oxygen binding proteins", Lamy J, Lamy J (eds.), Marcel Dekker Inc., N.Y., pp. 445-452

Markl, J., Decker, H., Stöcker, W., Savel, A., Linzen, B., Schutter, WG., van Bruggen, EFJ. (1981) On the role of dimeric subunits in the quaternary structure of arthropod hemocyanins. Hoppe-Seyler's Z. Physiol. Chem. 362:185-188

Markl, J., Savel, A., Knabe, B., Storz, H., Krabbe, T., Abel, S. and Markl, B. (1986) Mercury ions - a tool to study the specific role of individual subunits in the allosteric interaction of arthropod hemocyanins. In: Invertebrate oxygen carriers (Linzen B, ed). Springer, Heidelberg, 403-406

Markl, J., Schmid, R., Czichos-Tiedt, S. and Linzen, B. (1976) Haemocyanins in spiders, III. Chemical and physical properties of the proteins in Dugesiella and Cupiennius blood. Hoppe-Seyler’s Z. Physiol. Chem. 357, 1713-1725

Markl, J., Stöcker, W., Runzler, R. and Precht, E. (1986) Immunological correspondences between the hemocyanin subunits of 86 arthropods: evolution of a multigene protein family. In: Invertebrate oxygen carriers (Linzen B, ed). Springer, Heidelberg, pp 281-292

Matès, J. M. & Sánchez-Jimènez, F. (1999) Antioxidant enzymes and their implications in pathophysiologic processes. Front Biosci 4, D339-D345.

Maxwell, W. M., and Stojanov, T. (1996) Liquid storage of ram semen in the absence or presence of some antioxidant Reprod. Fertil. Dev. 8, 1013–20.

Meissner, U., Dube, P., Harris, J.R., Stark, H., Markl, J., (2000) Structure of a molluscan hemocyanin didecamer (HtH1 from *Haliotis tuberculata*) at 12A ° resolution by cryoelectron microscopy. J. Mol. Biol. 298, 21–34.

Meissner, U., Stohr, M., Kusche, K., Burmester, T., Stark, H., Orlova, E.V., Markl, J., (2003) Quaternary structure of the European spiny lobster (*Palinurus elephas*) 1 x 6-mer hemocyanin from cryoEM and amino acid sequence data. J. Mol. Biol. 325, 99–109.

Menze, M.A., Hellmann, N., Decker, H. and Grieshaber, K. (2000) Binding of urate and caffeine to haemocyanin of the lobster *Homarus vulgaris* (E.) studied by isothermal titration calorimetry. Biochemistry 39, 10806-10811.

Micetic, I. and Salvato, B. (2004) Model building of a molluscan hemocyanin from X-ray solution scattering. Micron.;35(1-2):17-20

Miller, K.I., Cuff, M.E., Lang,W.F.,Varga-Weisz, P., Field, K.G., van Holde, K.E., (1998) Sequence of the *Octopus dofleini* hemocyanin subunit: structural and evolutionary implications. J. Mol. Biol. 278, 827–842.

Muller, G., Ruppert, S., Schmid, E. and Schulz, G. (1988) Functional analysis of alternatively spliced tyrosinase gene transcripts. EMBO J. 7 2723- 2730.

Nakashima, H., Behrens, P.Q., Moore, M.D., Yokota, E. and Riggs, A.F. (1986) Structure of hemocyanin II from the horseshoe crab, *Limulus polyphemus*. Sequences of the overlapping peptides, ordering the CNBr fragments, and the complete amino acid sequence. J. Biol. Chem., Vol. 261, Issue 23, 10526-10533, 08

Nakauchi, K., Ikata, T., Katoh, S., Hamada, Y., Tsuchiya, K. and Fukuzawa, K. (1996) Effects of lecithinized superoxide dismutase on rat spinal cord injury. J. Neurotrauma 13, 573-582.

Neuteboom, B., Jekel, P.A. and Beintema, J. (1992) Primary structure of hemocyanin subunit c from *Panulirus interruptus*. Eur. J. Biochem. 206, 243-249

Orlova, E.V., Dube, P., Harris, J.R., Beckmann, E., Zmelin, F., Markl, J.,van Heel, M., (1997) Structure of keyhole limpet hemocyanin type 1(KLH1) at 15 A ?resolution by electron cryomicroscopy and angular reconstruction. J. Mol. Biol. 271 (3), 417–437.

Oury, T.D., Crapo, J. D., Valnickova, Z., and Enghild, J. J. (1996) Human extracellular superoxide dismutase is a tetramer composed of two disulfide linked dimers: A simplified high yield purification of EC-SOD. Biochem. J. 317, 51-57.

Ricchelli, F., Beltramini, M., Flamigni, L. and Salvato, B. (1987) Emission quenching mechanisms in *Octopus vulgaris* hemocyanin: Steady-state and time-resolved fluorescence studies. Biochemistry, 26, 6933-6939.

Rios, L., Cluzel, J., Vennat, J. C., Menerath, J. M. and Doly, M. (1999). Comparison of intraocular treatment of DMTU and SOD following retinal ischemia in rats. J Ocul Pharmacol Ther 15, 547-556.

Sabitha, K. E. & Shyamaladevi, C. S. (1999) Oxidant and antioxidant activity changes in patients with oral cancer and treated with radiotherapy. Oral Oncol 35, 273-277.

Salvato, B. and Beltramini, M. (1990) Hemocyanin: molecular architecture, structure and reactivity of the binuclear copper active site, Life Chem. Rep. 8, 1-47

Sancher, D., Gantornin, M. D., Gutierrer, G. and Bastiani, M. J. (1998) Mol. Biol. Evol. 15, 415- 426.

Saraswathi, M., Nakanishi, T. and Shimizu, A. (1999) Relative quantification of glycated Cu-Zn superoxide dismutase in erythrocytes by electrospray ionization mass spectrometry. Biochim Biophys Acta. 1426, 483-90.

Schartau, W., Eyerle, F., Geisert, H., Storz, H. and Linzen, B. (1983) Hemocyanins in Spiders,XIX. Complete amino acid sequence of subunit d from *Eurypelma californicum* hemocyanin and comparison to chain e. Biol. Chem.Hoppe-Seyler, 364, 1383-1409.

Schneider, H. J., Drexel, R., Feldmeier, G., Lottspeich, F. and Henschen, A. (1983) Hemocyanins in Spiders, XVIII. Complete amino acid sequence of subunit e from *Eurypelma californicum* hemocyanin. Biol. Chem Hoppe-Seyler, 364, 1357-1381.

Serkedjieva, J. and Ivanova, E. (1997) Combined protective effect of an immunostimulatory bacterial preparation and rimantadine hydrochloride in experimental influenza A virus infection. Acta virologica 41, 65-70.

Settineri, C.A. and Burlingame, A.L. (1997) Structural characterization of protein glycosylation using HPLC/electrospray ionization mass spectrometry and glycosidase digestion. Meth. in Mol. Biol. 61, 254-278

Shrive, A.K., Metcalf, A.M., Cartwright, J.R. and Greenhough, T.J. (1999) C-reactive proteins and SAP-like pentraxin are both present in *Limulus* haemolymph: Crystal structure of *Limulus* SAP. J. Mol. Biol. 290(5), 997-1008.

Schütz, J., Dolashka-Angelova, P., Abrashev, R., Nicolov, P. and Voelter, W. (2001) Isolation and spectroscopic characterization of the structural subunits of keyhole limpet hemocyanin, Bioch. Biophys. Acta 1546, 325-336.

Shen, T., Virgil, N., Zou, M., Green, B., Tam, M. and Ho, C., (1993) Production of unmodified human adult hemoglobin in *Escherichia coli*. Proceedings of the National Academy of Science *90, 8108-8112*.

Sidwell, R. W., Huffman, J. H., Bailey, K. W., Wong, M. H., Nimrod, A. & Panet, A. (1996) Inhibitory effects of recombinant manganese superoxide dismutase on influenza virus infection in mice. Antimicrob Agents Chemother 40, 2626-2631.

Siezen, R.J., van Bruggen, E.F.J., (1974) Structure and properties of hemocyanins. XII. Electron microscopy of dissociation products of *Helix pomatia* alpha-hemocyanin: quaternary structure. J. Mol. Biol. 90, 77–89.

Sikka SC. (2001) Relative impact of oxidative stress on male reproductive function. Curr Med Chem.;8:851–862.

Stadtman, E.R., and Levine, R.L. (2000) Protein Oxidation Ann. N.Y. Acad. Sci. 899, 191-208.

Semrau, F., Kuhl, R. J., Ritter, S. and Ritter, K. (1998) Manganese superoxide dismutase (MnSOD) and autoantibodies against MnSOD in acute viral infections. J. Med. Virol. 55, 161-167.

Simeonov, I., Corukova, K., Dolashka, P., Angelova, M., Voelter, W. (2000) A model of the kinetics of growth and biosynthesis of the enzyme superoxide dismutase in batch cultivation. Institute of Organic Chemistry, Bulgarian Academy of Sciences.

Söhngen, S.M., Stahlmann, A., Harris, J.R., Müller, S.A., Engel, A. and Markl, J. (1997) Mass determination, subunit organization and control of oligomerization states of keyhole limpet hemocyanin (KLH), Eur. J. Biochem. 248 602-613.

Solomon, E.I. and Spiro T.G (1978) Copper Proteins, Wiley, New York,.

Solomon, E.I., Baldwin, M.J. and Lowery, M.D., (1992) Electronic structures of active sites in copper proteins: contributions to reactivityChem. Rev. 92 521-542.

Sterner, R., Vogl, T., Hinz, H.-J., Penz, F., Hoff, R., Föll, R. and Decker, H. (1995) Extreme thermostability of tarantula hemocyanin. FEBS Letters 364, 9-12.

Stoeva, S., Dolashka, P., Pervanova, K., Genov, N. and Voelter W., (1998) Multidomain structure of the *Rapana thomasiana* (Gastropod) hemocyanin structural subunit RHSS1. Comp. Biochem. Biophys. B118 (4), 927–934.

Stoeva, S., Dolashka, P., Bankov, B., Voelter, W., Salvato, B. and Genov, N. (1995) Spectroscopic properties of *Callinectes sapidus* hemocyanin subunits. Spectrochim. Acta Part A 51, 1965-1974.

Stoeva, S., Idakieva, K., Betzel, C., Genov, N. and Voelter, W. (2002) Amino acid sequence and glycosylation of functional unit RtH2-e from *Rapana thomasiana* (Gastropod) hemocyanin. Arch. Biochem. Biophys. 15, 399,149-58

Stoeva, S., Rachev, R., Severov, S., Voelter, W. and Genov, N. (1995) Carbohydrate content and monosaccharide composition of *Rapana thomasiana* grosse (Gastropoda) hemocyanin and its structural subunits. Comparison with gastropodan hemocyanins. Comp. Biochem. Physiol. 110B, 761-765

Stoeva, S., Schutz, J., Gebauer, W., Hundsdorfer, T., Manz, C., Markl, J. and Voelter, W. (1999) Primary structure and unusual carbohydrate moiety of functional unit 2-c of keyhole limpet hemocyanin (KLH). Biochim. Biophys. Acta 1435 (1-2), 94-109

Stoeva, S., Idakieva, K., Genov, N. and Voelter W. (1997) Complete amino acid sequence of dioxygen-binding functional unit of the *Rapana thomasiana* hemocyanin. Biochem. Biophys. Res. Commun. 238, 2, 403-410

Strambini, G. B. and Gabellieri E. (1991) Quenching of indole luminescence by copper ions: A distance dependence study. J. Phys. Chem., 95, 4347-4352.

Streit, K., Lieb, B., Markl, J., (2003) Keyhole limpet hemocyanin: genes, cDNA and evolution. 95th Annual Meeting of the DZG, Berlin, Germany.

Strömqvist, M., Holgersson, J. and Samuelsson, B. (1991) Glycosylation of extracellular superoxide dismutase studied by high-performance liquid chromatography and mass spectrometry. J. Chromatogr. 548, 293-301.

Sutton, C.W., O'Neill J.A. and Cottrell J.S. (1994) Site-specific characterization of glycoprotein carbohydrates by exoglycosidase digestion and laser desorption mass spectrometry. Anal. Biochem. 218, 34-46

Svedberg, T., Hedernius, A. (1934) The sedimentation constants of the respiratory proteins, Biol. Bull. 66, 191-223.

Tabak, M., Sartor, G., Neyroz, P., Spisni, A. and Cavatorta, P. (1990) J. Luminesc. 46, 291-299.

Tainer, J. A., Getzoff, E. D., Beem, K. M., Richardson, J. S. and Richardson, D. C. (1982) Determination and analysis of the 2 A-structure of copper, zinc superoxide dismutase. J. Mol. Biol. 160, 2, 181-217.

Takata, I., Kawamura, N., Myint, T., Miyazawa, N., Suzuki, K., Maruyama, N., Mino, M. and Taniguchi, N. (1996) Glycated Cu,Zn-superoxide dismutase in rat lenses: evidence for the presence of fragmentation in vivo. Biochem. Biophys. Res. Commun. 219, 243-248.

Terwilliger, N.B. (1998) Functional adaptations of oxygen-transport proteins. J. exp. Biol. 201, 1085-1098.

Terwilliger, N.B., Dangott, L. and Ryan, M. (1999) Cryptocyanin, a crustacean molting protein: Evolutionary link with arthropod hemocyanins and insect hexamerins Proc Natl Acad Sci U S A 96, 2013-2018.

Top, A., Gielens, C., Witters, R., van Beeumen, J., Preaux, G. Partial amino-acid sequence and location of the carbohydrate chain in functional unit f of *Sepia officinalis* hemocyanin. In: Preaux, G., Lontie, R. (eds.) Invertebrate Dioxygen Carriers, Leuven University Press, Leuven 1990, 119-124

Topham, R., Tesh, S., Cole, G., Mercatante, D., Westcott, A. and Bonaventura, C. (1998) Active-site disruption in native Limulus hemocyanin and its subunits by disulfide-bond reductants. A chemical probe for the study of structure-function relationships in the hemocyanins. Arch. Biochem. Biophys. 352, 103-113.

Towbin, H., Staehelin, T. and Gordon, G. (1979) Electrophoretic transfer of proteins from polyacrylamide gels to nitrocellulose sheets: procedure and some applications. Proc. Natl. Acad. Sci. USA 76, 4350-4354.

Trotti, A. (1997) Toxicity antagonists in cancer therapy. Curr Opin Oncol 9, 569-578.

Tseneklidou-Stoeter, D., Gerwig, G. J., Kamerling, J. P., and Spindler, K.-D. (1995) Characterization of N-linked carbohydrate chains of the crayfish, *Astacus leptodactylus* hemocyanin. Biol. Chem. Hoppe-Seyler 376, 531–537.

van Breemen, J.F.L., Ploegman, J.H. and van Bruggen, E.F.J. (1979) Structure of *Helix pomatia* oxy- -hemocyanin and deoxy- -hemocyanin tubular polymers, Eur. J. Biochem. 100 61-65.

van Gelder, C. W. G., Flurkey, W. H. and Wicherts, H. J. (1997) Sequence and structural features of plant and fungal tyrosinases. Phytochem 45, 1309-.

van Holde, K.E. (1967) Physical studies of hemocyanins. III. Circular dichroism and absorption spectra, Biochemistry 6, 93-99

van Holde, K.E. and Miller, K.I. (1982) Hemocyanins. Q. Rev. Biophys. 15, 1-129.

van Holde, K.E. and Miller, K.I. (1995) Hemocyanins. Adv. Protein Chem. 47, 1-81

van Holde, K.E., Miller, K.I. and Decker, H. (2001) Hemocyanins and invertebrate evolution. J. Biol. Chem. 276, 19, 15563-15566

van Kuik, J. A., Breg, J., Kolsteeg, C. E. M., Kamerling, J. P., and Vliegenthart, J. F. G. (1987) Primary structure of the acidic carbohydrate chain of hemocyanin from *Panulirus interruptus*. FEBS Lett. 221, 150–154.

van Kuik, J.A., Kamerling, J.P. and Vliegenthart, J.F.G. (1990) Carbohydrate analysis of hemocyanins. In: Preaux, G., Lontie, R. (Eds.). Invertebrate Oxygen Carriers, Leuven University Press, Leuven, pp., 157-163

Vinogradov, S.N. (1985) The structure of invertebrate extracellular hemoglobins (erythrocruorins and chlorocruorins). Comp. Biochem. Physiol., 82B (1), 1-15.

Voit, R. and Schneider, H.J. (1986) *Tarantula hemocyanin* mRNA. In vitro translation, cDNA cloning and nucleotide sequence corresponding to subunit e. Eur. J. Biochem. 159: 23-29.

Voit, R., Feldmaier-Fuchs, G., Schweikardt, T., Decker, H., Burmester, T. (2000) Complete sequence of the 24-mer hemocyanin of the tarantula *Eurypelma californicum*. Structure and intramolecular evolution of the subunits. J. Biol. Chem. 275, 39339-39344.

Volbeda, A. and Hol, W.G.J. (1989) Pseudo-twofold symmetry in the copper-binding domain of arthropodan hemocyanins: possible implications for the evolution of oxygen transport proteins. J. Mol. Biol. 206, 531-546.

Volbeda, A. and Hol, W.G.J. (1989) Crystal structure of hexameric hemocyanin from *Panulirus interruptus* refined at 3.2 Å resolution. J. Mol. Biol. 209, 249-279.

Voll, W. and Voit, R. (1990) Characterization of the Gene Encoding the Hemocyanin Subunit e from the Tarantula *Eurypelma californicum*. Proceedings of the National Academy of Sciences, Vol 87, 5312-5316

Waxman, L. (1975) The structure of arthropod and mollusc hemocyanins. J. Biol. Chem. 250, 3796-3806

Weber, R.E. and Vinogradov, S.N. (2001) Nonvertebrate hemoglobins: functions and molecular adaptations. Physiol. Rev. 81:568-629.

Yang, Y. T., Wu, C.-S. C. and Martinez, H.M. (1986) Calculation of protein conformation from circular dichroism. Meth. Enzymol. 130, 208-269.

Yunoki, M., Kawauchi, M., Ukita, N. & 7 other authors (1997) Effect of lecithinized superoxide dismutase on traumatic brain injury in rats. J Neurotrauma 14, 739–746.

Xin, X.-Q., Gielens, C., Witters, R., Preaux, G. Amino acid sequence of the functional unit g from β_c–hemocyanin of *Helix pomatia*. In: Preaux, G., Lonite, R. (eds.) Invertebrate Dioxyge Carriers, Leuven University Press, Leuven 1990, 113-118.

In preparation:

Dolashki, A., Hristova R., Rao, G.S., Betzel, C., Atanasov, B., Voelter, W., Stevanovic, S. and Dolashka-Angelova P. Conformation Stability of *Humicola lutea* superoxide dismutase.

Dolashki, A., Stevanovic, S., Hristova R., Atanasov B., Voelter, W. and Dolashka-Angelova P. Conformation Stability of Arthropodan Hemocyanin *Limulus polyphemus*.

Velkova, L., Dolashki, A., Schwarz¸ H., Stevanovic, S., Hristova, R., Voelter, W. and Dolashka-Angelova, P. Structure and oligomeric stability of hemocyanin isolated of garden snail *Helix vulgaris*.

7. Appendix

Meine akademischen Lehrer waren:

Frau Prof. Dr. M. Angelova

Herr Prof. Dr. H. Decker

Herr Prof. Dr. B. Devreese

Herr Prof. Dr. I. Dobrev

Herr Prof. Dr. M. Hristov

Frau Dr. M. Kostova

Frau Prof. Dr. B. Koumanova

Herr Prof. Dr. J. Markl

Herr Prof. A. Minchev

Herr Prof. Dr. Dr. h. c. L. Mörl

Herr Prof. Dr. I. Pentchev

Herr Prof. Dr. H.-G. Rammensee

Frau Dr. J. Rangelova

Herr Prof. Dr. B. Salvato

Herr Prof. Dr. S. Stefanovic,

Herr Prof. Dr. J. Van Beeumen

Herr Prof. Dr. Dr. h. c. mult. W. Voelter

Herr Prof. Dr. U. Weser

Curriculum vitae

Name		Aleksandar Dolashki
Geburtsdatum/-ort		29.12.1977 in Sofia, Bulgaria
Eltern		Pavlina Dolashka Konstantin Dolashki
Schulbildung	09/1984-06/1992	Adalbert Malchika (Grundschule) Sofia
	09/1992-05/1995	Adam Mickevic- Gymnasium Sofia
Studium	09/1995-12/2000	Studium Verfahrenstechnik (Diplom) an der Universität für chemische Technologie und Metallurgie Sofia
	04/2000-09/2000	Diplomarbeit „Zerfallverhalten von Partikeln in Wirbelschichten“ unter der Anleitung von Prof. Dr. Dr. h. c. L. Mörl am Institut für Apparate- und Umwelttechnik der Universität Magdeburg
Promotion	02/2002-12/2004	Anfertigung der vorliegenden Dissertation „Structure, Function and Properties of Copper-containing Proteins: Hemocyanins and Superoxide Dismutase” bei Prof. Dr. Dr. h. c. mult. W. Voelter am Physiologisch-chemischen Institut der Universität Tübingen.